INFORMATION TO USERS

This manuscript has been reproduced from the microfilm master. UMI films the text directly from the original or copy submitted. Thus, some thesis and dissertation copies are in typewriter face, while others may be from any type of computer printer.

The quality of this reproduction is dependent upon the quality of the copy submitted. Broken or indistinct print, colored or poor quality illustrations and photographs, print bleedthrough, substandard margins, and improper alignment can adversely affect reproduction.

In the unlikely event that the author did not send UMI a complete manuscript and there are missing pages, these will be noted. Also, if unauthorized copyright material had to be removed, a note will indicate the deletion.

Oversize materials (e.g., maps, drawings, charts) are reproduced by sectioning the original, beginning at the upper left-hand corner and continuing from left to right in equal sections with small overlaps.

Photographs included in the original manuscript have been reproduced xerographically in this copy. Higher quality 6" x 9" black and white photographic prints are available for any photographs or illustrations appearing in this copy for an additional charge. Contact UMI directly to order.

Bell & Howell Information and Learning
300 North Zeeb Road, Ann Arbor, MI 48106-1346 USA
800-521-0600

UMI®

UNIVERSITY OF OKLAHOMA

GRADUATE COLLEGE

NOVEL Pt/KL CATALYSTS FOR THE AROMATIZATION OF N-HEXANE

A Dissertation

SUBMITTED TO THE GRADUATE FACULTY

in partial fulfillment of the requirements for the

degree of

Doctor of Philosophy

By

Gary Jacobs
Norman, Oklahoma
2000

NOVEL Pt/KL CATALYSTS FOR THE AROMATIZATION OF n-HEXANE

A Dissertation APPROVED FOR THE DEPARTMENT OF CHEMICAL ENGINEERING AND MATERIALS SCIENCE

BY

David Reyes

Brian Dodd

Robert L White

Lance Lobban

ACKNOWLEDGMENTS

First of all, I am indebted to my advisor, Dr. Daniel E. Resasco, especially for his guidance and encouragement. These last four years have been both enriching and exciting, and I will always treasure them. I have never met anyone with as much enthusiasm as Dr. Resasco has, and it was obvious to me the day I first walked into the lab that his enthusiasm was contagious. I thoroughly enjoyed both of his courses, and found them to be particularly useful in my studies. I also really appreciate the hospitality he and his family have shown me during my stay in Norman.

I would like to thank everyone in the OU Heterogeneous Catalysis Group for their help and friendship. Particularly, I would like to acknowledge Cristina L. Padro, Haiyang Liu, Armando Borgna, Firoz Ghadiali, Walter E. Alvarez, Fabio B. Noronha, and Adriana Pisanu – not only for their contributions to this project, but also for the fun times we shared together. Also, I would like to thank a number of staff at OU for their contributions, particularly Joel Young, who, along with Barry and Bob, expertly machined our XAFS cell, turning my drawings into something much better than I ever expected; Jim for his tenacious glassblowing work on the chemisorption system; Greg Strout for straining his eyes for many hours on the TEM; Ron Conlon for his XRD work; and Larry Isley and Daniel, for always being there when you need them. I also want to thank Syed Khalid at the National Synchrotron Light Source at Brookhaven National Laboratory for help with the EXAFS work.

Thanks are also due to the faculty in CEMS at the University of Oklahoma for the knowledge that they have passed along to me during my stay in Norman, especially to Dr. Richard Mallinson, Dr. Lance Lobban, Dr. John Scamehorn, and Dr. Brian Grady, who kindly served on my thesis committee. I appreciate the kindness and generosity that

Dr. Mallinson has shown to our group in the use of equipment and lab space. Certainly, much of this work would have been greatly limited without those commitments, and I am very grateful. I also would like to thank Dr. George Richter-Addo, both for serving on my thesis committee and for his course on surveying the elements, and Dr. Patrick McCann, for allowing me to stay in his super classes. I also want to thank Dr. Robert White and Dr. Brian Grady for willingly stepping in to serve on my committee.

I gratefully acknowledge the National Science Foundation for my GRT traineeship, the Oklahoma Center for Advancement of Science and Technology (OCAST), the Research Council, and Phillips Petroleum for generous support. Also, particularly helpful were correspondences with our industrial counterparts, Dr. T.T. Peter Cheung and Dr. Darin Tiedtke, at Phillips Petroleum in Bartlesville. I am also appreciative of the Richard J. Kokes Travel Grant that allowed me to attend the 16th North American Catalysis Society Meeting in Boston, Massachusetts in June 1999.

I would like to thank my parents for their advice, encouragement and moral support, especially when I left my job in Dallas to return to school. I would like to thank my brother Trevor and sister Elizabeth for being a constant source of inspiration for me throughout my life. I would like to especially thank Yahuei Chin (smartest person I know ... it's scary!) for always being there for me and uplifting my spirits again, and Greg (my other brother, music cohort, and running/hiking/camping buddy) and Shannon Davis, Soo Yin Chin, Boonyarach "Luke" Kitiyanan (hope to visit you in Thailand), Jose Herrera (hope to visit you in Peru), Lorena and Sebastian Torres, Susan (beamline card shark) and Michael Williams, Jeffrey and Jill Peterson (I'll never forget you), Humayun Qureshi, Matthew Stuckey, and all my friends in CEMS (you know who you are!).

TABLE OF CONTENTS

III. CATALYST SCREENING – Is Pt/KL unique?

IV. THE ROLE OF THE MORPHOLOGY OF Pt CLUSTERS

V. PREPARATION – Achieving desired Pt Cluster Morphology

LIST OF TABLES

LIST OF FIGURES

ABSTRACT

Pt/KL catalysts are important for the aromatization of n-hexane reaction, and have been the focus of study for the last 20 years. In this contribution, a number of studies were conducted to understand the underlying reasons for the uniqueness of Pt/KL for its high activity and selectivity for benzene production. Catalytic screening of basic supported Pt catalysts revealed that aromatization passes through dehydrogenated intermediates, including hexenes. Pt/KL was found to more efficiently convert hexenes to benzene than nonmicroporous basic supported Pt catalysts. The role of the L-zeolite was found to protect the Pt clusters from bimolecular pathways leading to the deposition of coke on the surface of the Pt. Coke production on nonmicroporous Pt catalysts was found to break up ensembles of Pt required for aromatization, leading to increased production of intermediate hexenes. Pt/KL catalysts are particularly sensitive to poisoning by sulfur. Studies indicated that sulfur deactivates Pt/KL by agglomeration of Pt clusters and the formation of Pt-S, which breaks up ensembles of Pt required for aromatization, again leading to increased production of hexenes.

The role of morphology of Pt inside the L-zeolite channels was found to play an important role in the stability of the catalysts. Catalysts were prepared with three different loadings by incipient wetness impregnation (IWI) and vapor phase impregnation (VPI) and characterized by a variety of techniques, including H_2 chemisorption, EXAFS, FTIR of adsorbed CO, pulse ring opening reaction of methylcyclopentane, and TEM and tested by both pulse and flow mode n-hexane reaction. While both catalysts exhibited small clusters inside the channels of the L-zeolite, the IWI catalysts had a fraction in the near surface region large enough to block or partially block the channels, as demonstrated by TEM and MCP-RO. Under reaction, the IWI catalysts deactivated to about half their initial activity. VPI catalysts were found by EXAFS to have clusters small enough to reside in the lobes of the ellipsoid cages making up the channels, and these catalysts were remarkably stable under reaction. The VPI catalysts had lower Pt-Pt coordination and higher coordination with the zeolite framework oxygen atoms than the IWI catalysts. Adsorption of CO was confirmed to cause disruption of the tiny Pt clusters, leading to the formation of platinum-carbonyl species that were stabilized by the L-zeolite.

The preparation parameters of Pt/KL catalysts prepared by ion exchange (IE), IWI, and VPI were studied in detail by catalyst characterization using FTIR of adsorbed CO and hydrogen chemisorption, as well as catalytic testing in a flow reactor. The standard IE method was found to lead to a fraction of clusters external to L-zeolite which deactivated rapidly by coke formation. However, a modified IE method from the patent literature was found to improve the morphology of the Pt clusters substantially. FTIR of adsorbed CO was conducted on samples reduced at two temperatures, 400°C and 500°C. VPI catalysts were found to retain bands in the FTIR spectra due to Pt-carbonyl formation after high temperature reduction, while IWI catalysts were more sensitive to loss of Pt-carbonyl formation due to Pt agglomeration. Two additional VPI preparation methods were studied, including a moderate vacuum method and a helium flow method, that would be more conducive

to industrial scale-up of the VPI method. Both were found to lead to very stable catalysts under flow reaction of n-hexane aromatization.

Addition of the lanthanide thulium to Pt/KL catalysts was studied in detail. While some preparation methods were found to lead to adverse Pt morphologies, one method, the sequential VPI of Tm and Pt acetylacetonates, lead to a catalyst with improved dispersion over the unpromoted VPI, as revealed by EXAFS. The addition of thulium also improved the sulfur tolerance of the catalyst. Using temperature programmed oxidation (TPO), the thulium was found to act a getter for sulfur, thus delaying the poisoning of Pt/KL under flow reaction. The thulium promoted catalyst was a marked improvement over the VPI catalyst under both clean and sulfur-poisoned conditions.

Electronic modification to Pt by exchanging the zeolite cation from potassium to lithium was studied by a combination of techniques, including a new shape resonance XANES method, microcalorimetry, pulse neopentane hydrogenolysis, and FTIR of adsorbed CO. The catalysts were also tested for n-hexane aromatization in both flow and pulse modes. Addition of lithium cation increased the acidity of L-zeolite lattice oxygen atoms, causing more rollover of the interatomic potential between Pt and O. The XANES method was based on the different information contained in the L_{III} and L_{II} white lines of the catalyst with and without chemisorbed hydrogen. Addition of lithium resulted in a shift of the Fermi level of Pt away from the antibonding state of Pt-H, strengthening the chemisorption bond of hydrogen. This increased chemisorption bond strength for lithium addition was confirmed by microcalorimetry, and increased hydrogenolysis rates were observed for both neopentane and n-hexane aromatization experiments at the expense of benzene production.

Finally, regeneration of Pt/KL catalysts was studied for sulfur poisoned catalysts. A combination of methods including EXAFS, FTIR of adsorbed CO, and pulse n-hexane aromatization were employed to study catalysts regenerated in air alone, and those regenerated sequentially by air and haloalcohol treatment. While air effectively burned off coke deposits, it lead to sintering of Pt clusters. The haloalcohol treatment effectively redispersed the Pt. The presence of thulium was found to aid in the redispersion of Pt clusters.

CHAPTER I: BACKGROUND AND INTRODUCTION

1.1 HISTORICAL PERSPECTIVE

In 1949, Universal Oil Products (UOP) developed the modern catalytic reforming process, and this process was further improved by Chevron in 1968. The catalysts used were effective for improving the octane number of heavy naphtha (C_8 to C_{10}). The catalysts employed were bifunctional, containing both active metal sites as well as acid sites. The typical catalyst reported was platinum or platinum-rhenium (metal function) supported on chlorided alumina (acid function). Unfortunately, the catalysts were much less effective for improving the octane rating of light naphtha (C_5 to C_8), due to their low selectivity to aromatics and their excessive irreversible hydrocracking over acid sites to light hydrocarbons. Also, the catalyst was particularly ineffective for conversion of paraffinic species in the light naphtha range. Therefore, for a time, the light naphtha species were not reformed. Instead, tetraethyl lead was added to gasoline in the amount of approximately 1.5 g per gallon to prevent knocking. Lead has since been phased out due to environmental regulations. For example, in January of 1988, the allowed level of lead was 0.1 g/gal. Therefore, refiners turned to isomerization as a means to convert light naphtha to branched isoparaffins. Unfortunately, still, the octane number feasible was only 80-90, and the greater the quantity of hexanes present, the more difficult it was to boost the octane number [1].

In 1980, Bernard [2] reported that Pt clusters supported on the potassium exchanged form of Linde Type L zeolite (i.e., Pt/KL catalysts) were highly effective

for the selective conversion of n-hexane to benzene. Commercialization of the process soon followed, with Chevron researchers announcing their Aromax catalytic reforming process [1]. Interestingly, the Pt/KL catalyst was monofunctional, relying only on the metal function to effect the dehydrocyclization. In fact, residual acid sites were found to be detrimental to catalyst performance, with the generation of coke deposits leading to rapid deactivation [3]. Chevron researchers showed that conversion of n-octane over Pt/KL was a 25% improvement in selectivity compared to the conventional bifunctional catalyst, while a remarkable 400% improvement in selectivity for conversion of n-hexane was found (150 psig, 495 °C, H_2/HC of 6, liquid hourly space velocity LHSV of 6) [1].

However, again environmental regulations were passed on reforming, and the new restrictions specified a reduction in the concentration of aromatics in gasoline. Shipping and transportation of aromatics were also closely regulated, and therefore, the on-site production of aromatics from the less hazardous paraffins was and remains highly in demand [4].

With these perspectives in mind, the goal of this project was to understand the structural-property relationships of Pt/KL catalysts, so that the catalyst could be optimally engineered. Since its discovery in 1980, there has been great controversy in the literature surrounding this catalyst. The background which follows addresses the scope of work contained in this thesis, which hopefully sheds some light (or at least reinforces correct hypotheses) on the understanding of Pt/KL catalysts. The next section underscores the importance of industrial Pt/KL catalysts from the standpoint of benzene production in the USA and worldwide.

1.2 MOTIVATION

Benzene is an important intermediate for the production of many other intermediates, including styrene (for making polystyrene and synthetic rubber), phenol (used to make phenolic resins), cyclohexane (used in nylon production), aniline (for dyes), alkylbenzenes (for making detergents), and chlorobenzenes. These intermediates are used as feedstocks to supply a number of branches of the chemical industry, producing specialty chemicals, plastics, resins, dyes, pesticides, and pharmaceuticals. Although the use of benzene, toluene, and xylenes in gasoline has been largely reduced in the United States, many countries still use them extensively for the production of commercial gasoline [5]. Since the 1950s, benzene production from petroleum feedstocks has been very successful and accounts for about 95% of all benzene obtained [5].

World benzene production was reported in 1988 to be 6×10^6 tons (1.8×10^9 gallons). The United States is the largest producer, accounting for 30% of world production. Table 1.1 shows the estimates of benzene for nonfuel related uses. Benzene consumption worldwide is dominated by the production of three main derivatives, styrene, cumene, and cyclohexane, which account for about 90% of total production [5].

Benzene is alkylated with ethylene to produce ethylbenzene, which is then dehydrogenated to styrene, the most important chemical intermediate derived from benzene. Styrene is a raw material for the production of polystyrene and styrene copolymers such as ABS and SAN. Ethylbenzene accounts for over one half of benzene consumption.

Benzene is alkylated with propylene to yield cumene. Cumene is catalytically oxidized in the presence of air to cumene hydroperoxide, which is decomposed into

Table 1.1: Use pattern for benzene in the U.S. [5].

Use	Total Consumption, %
Ethylbenzene	51.8
Cumene	21.7
Cyclohexane	14.4
Nitrobenzene	4.9
Chlorobenzene	2.1
Linear detergent alkylate	1.9
Other	3.2

phenol and acetone. Phenol is used to manufacture caprolactam (nylon) and phenolic resins such as bisphenol. A little over 20% of benzene is used to manufacture cumene.

Benzene is hydrogenated to cyclohexane. Cyclohexane is then oxidized to cyclohexanol, cyclohexanone, or adipic acid. Adipic acid is used to produce nylon. Cyclohexane manufacture is responsible for about 14% of benzene consumption.

Nitration of benzene yields nitrobenzene, which is reduced to aniline, an important intermediate for dyes and pharmaceuticals. Benzene is chlorinated to produce chlorobenzene, which is used to prepare pesticides, solvents, and dyes.

About 2% of benzene consumed is used for the manufacture of straight-chain or branched-chain detergent alkylate. Linear alkane sulfonates (LAS) are widely used

as household and laundry detergents. Finally, small amounts of benzene are used to make benzene-sulfonic acid and hydroquinone, which is a useful antioxidant.

The production of benzene is therefore of vital importance, and derivatives from benzene supply numerous sectors of the chemical and petrochemical industries. Before considering the scope of problems surrounding Pt/KL catalysts for the aromatization of n-hexane, it is helpful to first examine the structure of L-zeolite itself, as well as the n-hexane reaction pathways occurring on basic supported platinum catalysts, such as Pt/KL.

1.3 STRUCTURE OF LINDE TYPE L ZEOLITE

Natural zeolites have been known for centuries. However, it wasn't until the late 1940s that Milton et al. [6] from Union Carbide Corporation (UCC) hydrothermally synthesized a number of synthetic zeolites. Following this work, Breck and Acara hydrothermally synthesized L-zeolite [7] and patented the discovery in 1958. The crystallization kinetics of the Breck synthesis have been recently revisited by Shiralkar et al. [8].

As with Linde Type L-zeolite, all zeolites are aluminosilicates, with the primary building block being the MO_4 tetrahedron, where M is either Si or Al. Zeolites are formed by linking these units to give three-dimensional anionic networks where each oxygen of a given tetrahedron is shared between this tetrahedron and one of four others. Therefore, there are no unshared oxygen atoms in the framework and the ratio (Al + Si):O is equal to 1:2. For every Si^{IV} which is replaced in the framework by Al^{III}, a negative charge is created which must be counterbalanced by an

electrochemical equivalent of cations. The framework of zeolites are sufficiently open to accommodate H_2O molecules as well as cations, which can both move easily within the crystals. These ions undergo ready exchange with other cations, and the H_2O molecules can be removed or replaced in a continuous manner and often reversibly. Lowenstein's rule states that no Al-O-Al bonds are formed during hydrothermal synthesis of the zeolite [9].

Figure 1.1: Ellipsoid cages make up uniaxial channels of L-zeolite.

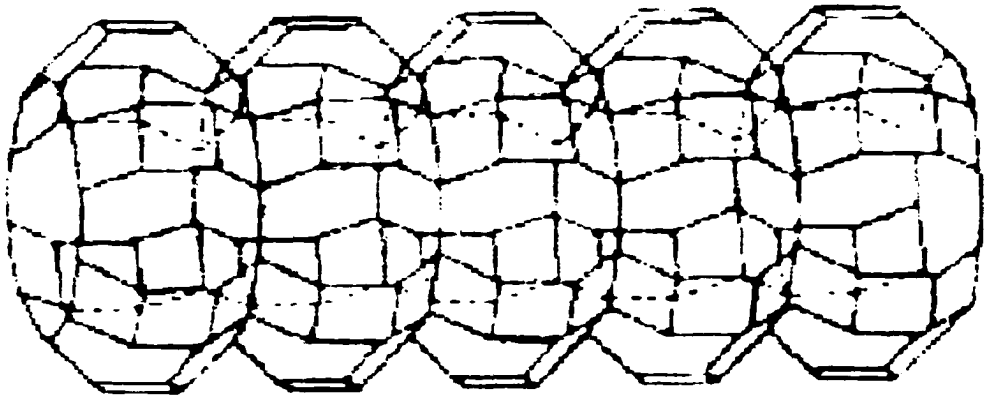

L-zeolite was characterized crystallographically in 1969 by Barrer and Villiger [10]. The crystal structure of L-zeolite (hexagonal, a = 18.4, c = 7.5) was found to be based on the 18 tetrahedra unit e-cage, which is also found in cancrinite. L-zeolite is classified as a Group 4 zeolite, because the main structural unit is the D6R unit, although additional oxygen bridges are also present [9]. In L-zeolite, e-cages are formed symmetrically across the D6R unit. L-zeolite consists of stacks of symmetrical e-D6R-e units crosslinked to others by single oxygen bridges. 12-membered rings produce wide channels parallel to the c-axis, as shown in Figure 1.1 [9]. Linked by small apertures of free diameter 0.74 nm, it is the ellipsoid cages that

make up these uniaxial channels of the L-zeolite which we are primarily interested in for loading of the catalytically active platinum metal. The ellipsoid cages have a maximum free diameter of 0.96 nm assuming K^+ cations are present, or 1.25 nm, not taking into account the presence of cations.

Fully hydrated (0.28 cm^3 liq. H_2O/cm^3 crystal), the structure of L-zeolite has four cation positions with occupancies as shown in Figure 1.2 and Table 1.2. During dehydration, a procedure which is usually carried out during catalyst preparation, cations in site D likely withdraw to a fifth site [9], which is located between the A sites. In site D, cations are coordinated with two H_2O molecules in the channels. The site D cations are readily exchangeable at 25°C [11], and can be replaced by other

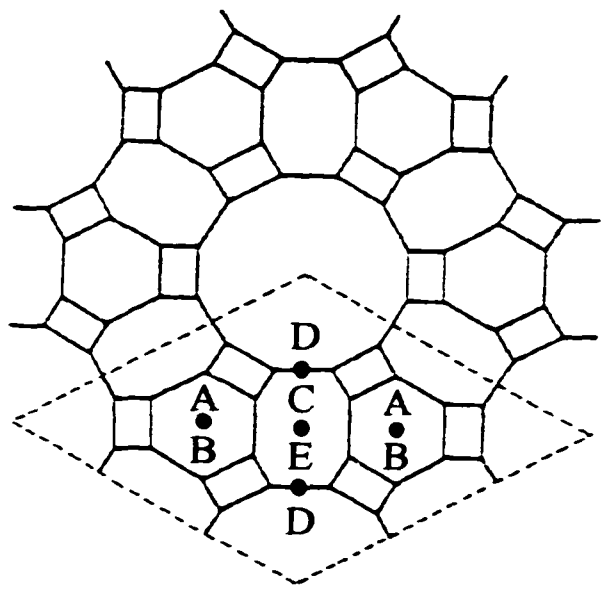

Figure 1.2: Cation positions in KL. Projection of L-Zeolite parallel to c showing main channels [9].

Table 1.2: Cation Position Occupancies [9].

Site	*Location*	*# Sites/uc*	*Occupancy*
A	Center of D6R	2	1.4
B	Center of e-cage	2	2.0
C	Between adjacent e-cages	3	2.7
D	Wall of Main Channel	6	3.6
	Total	**13**	**9.7**

group I cations, or cations from group II or III, including rare earths. L-zeolite is structurally stable after dehydration at high temperatures, as evidenced by XRD patterns after prolonged heating in air at 800°C [12]. The void volume in L-zeolite has been measured by a number of different adsorbates. The main channel calculated free volume of 614 A^3/uc is very close to the volume as measured by Ar and O_2 adsorption (619-642 A^3/uc). However, since the volume of zeolite occupied by H_2O molecules was found to be higher, H_2O must occupy space not available to other gases, and this additional available space must consist of the small voids in the e-cage units that form channel walls [9].

Now that we have a picture of the structure of L-zeolite, it is also instructive to consider the n-hexane reaction pathways occurring over basic supported Pt catalysts, such as Pt/KL.

1.4 REACTION MECHANISM

Flow reactor testing has suggested, and TAP reactor studies have confirmed [13], that the mechanism for n-hexane reforming over basic supported platinum catalysts, such as Pt/KL, follows the scheme depicted in Figure 1.3.

A Temporal Analysis of Products (TAP) reactor is one which operates under three important conditions: (1) the microreactor operates under a vacuum, (2) the catalyst is diluted by a bed of inert SiC pellet material, and (3) an extremely small and narrow pulse of approximately 10^{16} molecules is injected into the reactor by a high speed molecular beam valve. Therefore, gas transport in the catalyst zone of the

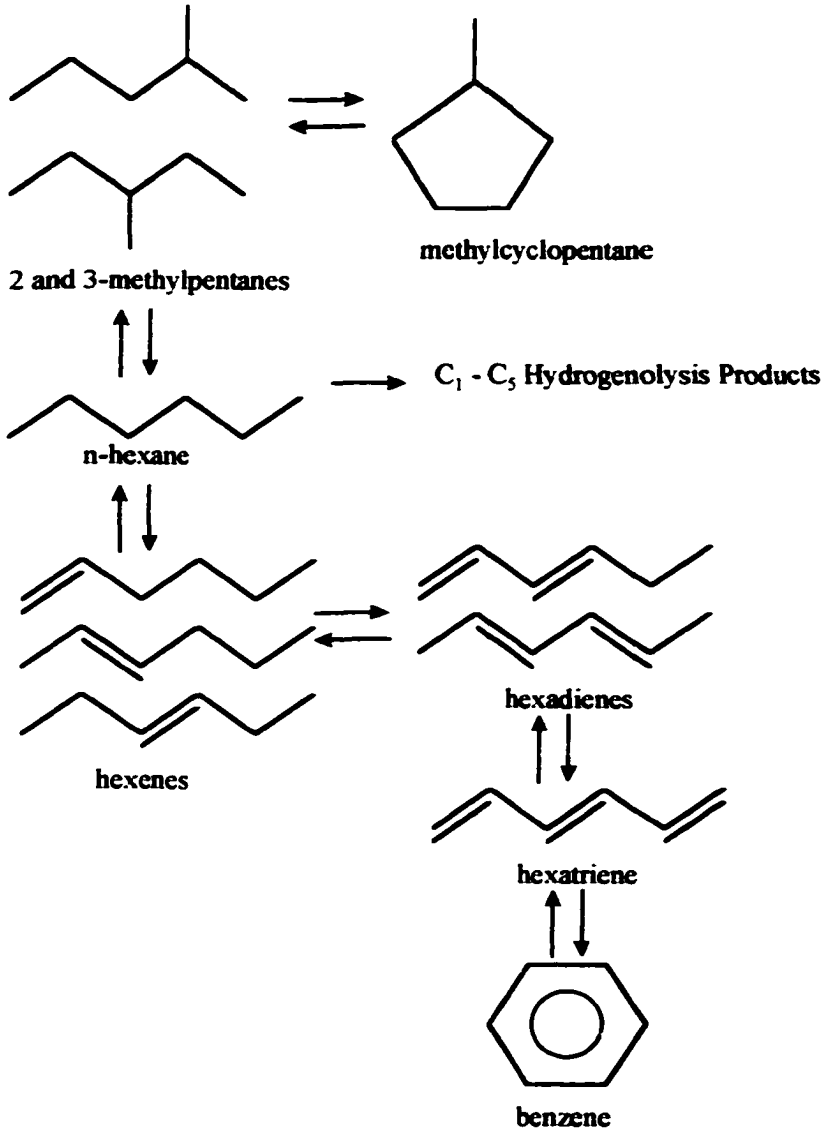

Figure 1.3: Reaction pathways for n-hexane over basic supported Pt catalysts.

microreactor is dominated by Knudsen diffusion, so that collisions between gas-phase molecules are minimized. These conditions give TAP reactors great advantages over conventional atmospheric pulse reactors, because in the latter, the frequency of gas-gas collisions is much higher, and short-lived intermediates cannot be observed by a mass spectrometer. In TAP reactors, the transient responses of product molecules are indicative of the combination of gas-phase transport, adsorption-desorption, and surface reaction, and control experiments can be performed to isolate the surface reaction contribution. For a detailed review of TAP reactors, the following reference provides a description [14].

As shown in Figure 1.3, over platinum catalyst in the absence of acid sites, the pathway from n-hexane to benzene passes through dehydrogenation intermediate hexenes, hexadienes, and hexatrienes. Normal hexane can also reversibly undergo isomerization to 2 and 3-methylpentanes, which can subsequently ring close to form methylcyclopentane. Finally, n-hexane can irreversibly undergo hydrogenolysis to form light products, including C_1-C_5. Work on Pt/KL catalysts includes understanding structural-property relationships of the catalyst, so that the conversion, selectivity, and stability of the catalyst for n-hexane aromatization can be improved. The next section outlines the problems surrounding Pt/KL catalysts and introduces the studies conducted by our group to address those issues.

1.5 INTRODUCTION

Ever since the discovery of Pt/KL in 1980 by Bernard [2], controversy has arisen as to if and why Pt/KL is unique for the aromatization of n-hexane reaction. In

the literature, roughly five independent studies have yielded five different possible explanations attesting to the uniqueness of Pt/KL for aromatization, and these explanations, which offer either geometric or electronic interpretations, are outlined briefly below:

(a) *Molecular Die (Geometric) Effects*: Tauster and Steger [15] analyzed the hydrogenolysis product distribution found during n-hexane reactions over Pt/KL catalysts. In their reports, they plotted the benzene selectivity parameter as a function of a term they coined the terminal cracking index (TCI). The TCI was defined as the molar ratio of C_5/C_4 product observed in reactions of n-hexane over Pt/KL catalysts. As a reference, they used an inert and nonmicroporous Pt/Silica catalyst. The idea was that high values of the TCI would correlate with hydrogenolysis occurring at the terminal carbon-carbon bond of n-hexane, producing C_5 and methane, while lower values would indicate a higher selectivity for internal carbon-carbon bond scission. For platinum clusters supported inside the channels of the L-zeolite, Tauster and Steger hypothesized that the n-hexane would preferentially adsorb onto the Pt cluster at a terminal carbon, which would favor ring closure to form benzene. Indeed, their results showed that Pt/KL catalysts exhibited both higher benzene selectivity and TCI's than on Pt/Silica.

(b) *Preorganization of n-hexane for ring closure*: Derouane and Vanderveken [16] published a molecular graphics study showing an n-hexane molecule and a Pt cluster inside the ellipsoid cages of the channels of the L-zeolite. They offered that the space inside the L-zeolite was similar to that of a cyclic, six carbon species. Therefore, they hypothesized that the adsorbed hexane curls around on

itself in the zeolite cage in order to maximize its van der Waals interactions. Therefore, the resulting transition state would put the free terminal carbon in close proximity with the active Pt cluster. They hypothesized that this preorganization of the n-hexane molecule favored ring closure, and was responsible for the high activity and selectivity of Pt/KL for aromatization.

(c) *Electronic Effects*: Larsen and Haller [17,18] concluded that the high activity and selectivity of Pt/KL catalysts for aromatization derived from a unique electronic structure. They conducted studies on different cation-exchanged L-zeolites, including samples back-exchanged with Mg^{+2}, Ca^{+2}, and Ba^{+2} ions. They hypothesized that larger, softer, cations like Ba^{+2}, with diffuse charge, would allow greater donation of electron density from zeolite oxygen anions to the Pt metal, whereas smaller, harder, cations like Mg^{+2}, would interfere with this transfer. As a test, the competitive hydrogenation of benzene and toluene was used. Since toluene is a better electron donor than benzene, hydrogenation of toluene was expected to be hindered with increased electron donation from the support. Indeed, Larsen and Haller found that $K_{toluene}/K_{benzene}$ increased with Lewis acidity (Mg > Ca > Ba).

(d) *Inhibition of Bimolecular Pathways*: Iglesia and Baumgartner [19,20] ascribed the uniqueness of Pt/KL catalysts with the ability of KL's microporous structure to inhibit bimolecular reactions leading to the formation of coke on the surface of the Pt clusters. After considerable reaction testing, they found that Pt/KL, Pt/Silica, and Pt/Alumina had similar activation energies, but very different turnover rates. Since confinement effects should lower activation energies,

Iglesia and Baumgartner ruled out the previous molecular die and preorganization models. Their comparison of catalysts at different times on stream suggested that a high fraction of active metal sites were still available on Pt/KL in comparison with other catalysts.

(e) *Stabilization of Small Pt Clusters*: Hong et al. [21,22] formulated a somewhat different conclusion. In their work, a number of different inert microporous and nonmicroporous supported Pt catalysts were synthesized, including Pt/KL, Pt/BaL, Pt/KBaKL, Pt/NaY, Pt/CsNaY, Pt/NaFAU, Pt/hex, Pt/SSZ-24, Pt/silica, and Pt/carbon. Although the general trend observed was that microporous materials offered superior selectivity and conversion over nonmicroporous materials, which were shown to have a higher production of olefins, the group concluded that microporosity was not required for aromatization, because high selectivity and conversion was achieved, though not as high as Pt/KL, on a Pt/carbon catalyst. They hypothesized that the exceptional reactivity for Pt/KL resulted from the ability of the ellipsoid cages making up the channels of the L-zeolite, to stabilize small clusters.

One other group concluded that Pt/KL was not unique for aromatization, and that the basicity of the support was the essential feature for aromatization over Pt clusters [23]. This was a surprising contrast to earlier reports. In one study, it was found that using Pt catalysts supported on a non-microporous basic carrier, Al-stabilized MgO, the n-hexane conversion at a given contact time, as well as the aromatization selectivity at a given conversion, were virtually identical to those obtained on a Pt/KL

catalyst under the same conditions. Consequently, this result gave strong support to theories promoting the idea that the basicity of the support was the essential feature and the main role of the support was to electronically modify the Pt particles. In our first investigation, Chapter 3, we screened the two materials under several conditions to help resolve the conflicting reports [24]. In addition, due to the low sulfur tolerance of Pt/KL catalysts [25], we investigated both Pt/KL and Pt/Mg(Al)O under sulfur poisoned conditions to determine if the latter might exhibit enhanced sulfur tolerance.

The determination was made that Pt/KL catalysts are unique for n-hexane aromatization, and that clusters inside the zeolite channels are protected from bimolecular reactions leading to coke deposition on the surface of Pt. In contrast, the nonmicroporous Pt/Mg(Al)O catalyst quickly deactivated by coking. Therefore, as described in Chapter 4, we undertook to study the role of Pt cluster morphology inside the L-channels [26] by using two preparation methods, incipient wetness impregnation (IWI) and vapor phase impregnation (VPI), both of which achieve virtually all of the Pt internal to the zeolite micropores. These methods are described in detail in Section 2.1. That is, the goal was to vary the morphology, shape, and location of the platinum, while keeping the Pt clusters inside the ellipsoid cages making up the channels of the L-zeolite, by preparing series of VPI and IWI catalysts with three different loadings of Pt. Interestingly, the two preparation methods yielded catalysts with significantly different stabilities under n-hexane flow reaction, with the IWI catalyst deactivating to about half its initial activity, while the VPI catalyst exhibited very little deactivation. In Chapter 4, we use a battery of characterization

methods to understand the subtle role of Pt cluster morphology inside the L-zeolite channels, and its impact on the activity, selectivity, and stability under n-hexane flow reaction. Characterization methods employed included transmission electron microscopy (TEM), Fourier transform infrared spectroscopy (FTIR) of adsorbed CO, extended X-ray absorption fine structure spectroscopy (EXAFS), and the methylcyclopentane ring opening pulse reaction (MCP-RO), which was used successfully in earlier studies [27,28]. These methods were correlated with results of both n-hexane pulse reaction, which studies the catalyst under clean Pt surface, and flow reaction, which examines the deactivation pattern of the catalyst.

As described in Chapter 4, the VPI catalysts were found to have a desired Pt morphology, whereby the Pt clusters were more homogeneously distributed in the channels of the L-zeolite, and small enough to reside in the lobes, allowing for molecules to easily diffuse around the cluster. In contrast, the IWI catalysts were found to have a greater fraction of Pt located in the near surface region, which was large enough to block or partially block the L-channels. Under reaction at 500°C, these more heterogeneously distributed catalysts were found to deactivate by agglomeration of these clusters, which led to blocking of the micropores. Because sulfur poisoning leads in part to growth and agglomeration of Pt clusters [25], the IWI catalysts were found to be more sensitive to sulfur poisoning than their VPI counterparts.

After developing a consistent picture that the morphology and location distribution of Pt clusters largely governed the activity, selectivity, and stability of Pt/KL catalysts, we turned our attention to the preparation of the catalyst [29].

Typically, industrial catalysts are prepared by ion exchange of Pt^{+2} salts with extrudates. Extrudates are required to relieve the pressure drop through the reactor bed. In Chapter 5, we examined the preparation parameters of Pt/KL powder and pellet catalysts prepared by ion exchange, incipient wetness impregnation, and vapor phase impregnation. For example, we compared Pt/KL catalysts prepared by standard ion exchange methods with a more novel ion exchange technique extracted from the patent literature. We also examined IWI catalysts prepared with different degrees of hydration of the L-zeolite, to determine the sensitivity to that parameter. Finally, we looked at VPI catalysts prepared using a moderate vacuum and a helium flow technique, both of which would be more conducive to commercial scale-up of this important preparation method. Detailed characterization by FTIR of adsorbed CO and hydrogen chemisorption of these catalysts is provided in Chapter 5. It is interesting to note that the standard ion exchange method largely resulted in a catalyst with a considerable fraction of Pt clusters external to the channels of the L-zeolite, and these catalysts deactivated rapidly by coke formation, in agreement with our earlier results on nonmicroporous Pt/Mg(Al)O catalysts.

In Chapter 6, we again focused on the sulfur tolerance of the catalyst, which is a very important problem, since maintaining the required low levels of sulfur to avoid deactivation in commercial operations (i.e. less than about 50 ppb) is very costly. As mentioned previously, it has been shown that in the presence of less than 1 ppm sulfur, Pt/KL catalysts deactivate in hours [25]. This problem presents a major obstacle for the commercial use of these catalysts [30]. As noted earlier, some authors have suggested that, in the presence of sulfur, Pt particle growth is

accelerated, resulting in plugging of the zeolite channels [25,31]. However, others have proposed that the K^+ cations directly participate in the aromatization process and that they, rather than Pt, are preferentially poisoned by sulfur [32].

Few reports have been published on investigations attempting to develop sulfur-tolerant Pt/KL aromatization catalysts [33], but one possible alternative could be the addition of promoters. There are a number of ways in which these promoters might operate [34]. They may act to anchor the Pt particles in the channels of the L-zeolite, preventing migration and pore blockage. They may also act as sulfur gettering sites, protecting Pt temporarily from sulfur poisoning.

Li et al. [35,36] have studied the addition of rare earth elements to Pt/KL catalysts using the co-impregnation of Pt and the rare earth with aqueous solutions, and have indicated a positive effect on aromatization performance, and quite possibly, the sulfur resistance. Chapters 4 and 5 show that by varying the preparation method of Pt/KL catalysts, one can greatly influence the location and morphology of the Pt particles inside the channels of the zeolite. It is clear that morphology variations alone have strong effects on the stability of the catalysts under both sulfur-free and sulfur-poisoned conditions. In Chapter 6, the combined effects of the preparation method and the addition of a rare earth, thulium (Tm), are investigated, with a primary focus on the vapor phase impregnation technique as a means to achieve finely distributed Pt and Tm_2O_3 clusters [37]. In that study, one preparation method, the sequential vapor phase impregnation of Tm and Pt, was found to improve the Pt dispersion. This had a positive effect on the activity, selectivity, and stability of the catalyst over the unpromoted VPI catalyst. Also, as detailed in Chapter 6, TPO

results suggest that the Tm may also act a getter for sulfur. Catalytic testing further revealed that the Tm promoted catalyst was more resistant to sulfur poisoning.

Chapter 7 examines the possibility of an electronic modification to the Pt clusters as the cations on the L-zeolite are changed from K^+ to Li^+, a harder, more polarizing cation. Ever since the discovery of Pt/KL as a hexane aromatization catalyst, researchers have incorporated different Group I and II cations in KL in order to determine if electronic modifications could result [17,18,38-41] in efforts to improve the n-hexane aromatization rate.

Besoukhanova et al. [38] concluded a positive effect on the aromatization of n-hexane rate when the size of the Group I cation was increased in the order Li < Na < K < Rb < Cs - i.e., with increasing basicity. The catalysts used in that work were 0.6% Pt/L catalysts, as used industrially. Larsen and Haller [17,18] used competitive benzene/toluene hydrogenation to study the possibility of electronic effects on differently cation-exchanged Pt/KL catalysts, as mentioned earlier.

A carefully conducted XANES study by McHugh et al. [39] of reduced samples purged in helium resulted in negative binding energy shifts for Pt loaded on Mg-exchanged KL in comparison with the Pt foil. Therefore, it was suggested that electron transfer from the zeolite lattice oxygen atoms to the Pt clusters might be important, because added electron density would more effectively screen the electron from the nucleus, thus decreasing its binding energy.

Fukunaga and Ponec [40] studied various nonmicroporous and microporous supports including L promoted with K^+ and Mg^{2+} cations. Due to enhancement in aromatization of n-hexane activity with the incorporation of the promoter, they

concluded that the effect of the cation was of an electrostatic nature, promoting the ring-closure.

Recently, Ramaker et al. [41] have advanced a new method of XANES shape resonance analysis for studying the electronic modification of Pt by changing support alkalinity. This method focuses on the changes in the Fermi level of Pt induced by changes in the Madelung interatomic potential of Pt with the zeolite lattice oxygen atom. The idea is that a smaller, more polarizing cation would decrease the alkalinity of the zeolite lattice oxygen atoms, which, in turn, would cause an increased rollover of the interatomic potential barrier between Pt and the zeolite lattice oxygen. Based on AXAFS results [41], the distance of the interatomic potential barrier between the Pt atom and the zeolite lattice atom, as well as the position of the Fermi level, change, while the electron density on Pt remains constant. Therefore, they concluded that there was no need to invoke a charge transfer explanation to explain the changes in the Fermi level of Pt. To obtain information on the changes in the Fermi level with support alkalinity, the proposed XANES method was based on the different information contained in the L_{III} and L_{II} white lines of the catalyst with and without chemisorbed hydrogen.

In Chapter 7, our aim was to test this XANES method on Pt/KL catalysts, one of which was promoted with Li^+ cation, to determine the extent to which electronic modification of Pt occurred at temperatures required for n-hexane aromatization. The catalysts were prepared by vapor phase impregnation (VPI), because their superior small particle size and uniform distribution inside the micropores made them resistant to agglomeration after high temperature reduction treatment.

In Chapter 7, results of the shape resonance XANES method were correlated with FTIR of adsorbed CO, microcalorimetry of adsorbed hydrogen and CO, hydrogen chemisorption, pulse neopentane hydrogenolysis testing, and pulse/flow n-hexane aromatization to reveal that an electronic modification of the Fermi level of Pt by changing the cation was likely. Results suggested that increasing the acidity of the support by incorporating Li^+ cation moved the position of the Fermi level of Pt away from the Pt-H antibonding state, resulting in a strengthening of the chemisorption bond. In reaction testing, this modification of Pt resulted in increased neopentane hydrogenolysis and a decrease in n-hexane aromatization performance in favor of hydrogenolysis.

Finally, Chapter 8 examines catalyst regeneration. The understanding of the regeneration process is an issue of great industrial relevance [42-44]. However, only a few papers in the open literature [45] have focused on the effect of different treatments after reaction under clean and sulfur-poisoned conditions. In Chapter 8, we investigated different regeneration procedures on three sulfur poisoned Pt/KL samples, one prepared by IWI, one by VPI, and a third one prepared by VPI containing Tm. Catalysts were characterized by EXAFS and FTIR of adsorbed CO, and tested for pulse n-hexane aromatization in the fresh state, after poisoning, after air treatment, and after air/haloalcohol regeneration.

The regeneration in air alone was found to result in sintering of Pt. However, oxychlorination treatment after the air treatment of the poisoned samples resulted in redispersion of Pt and increased aromatization activity. The addition of Tm was noted to help maintain the dispersion of Pt particles under the regeneration process.

CHAPTER II: EXPERIMENTAL METHODS

This chapter covers the common characterization techniques that were used routinely throughout this thesis. Other more specialized methods, such as XANES shape resonance spectroscopy, microcalorimetry, and various pulse mode reaction methods, are covered in the chapters in which they are specifically used.

2.1 CATALYST PREPARATION METHODS

2.1.1 Ion Exchange

Ion exchange (IE) is widely used in the preparation of industrial and laboratory catalysts. In this technique, the precursor salt (e.g., tetraammine platinum(II) nitrate) interacts with the support. The interactions are controlled by several factors, including the number of cation exchange sites, the loading solution pH, the concentration of the precursor, and the presence of competitive ions.

First, the support is suspended in an aqueous solution of desired pH (basic solution for cation exchange). Then, the aqueous loading solution containing the precursor salt is added dropwise with stirring. The slurry is stirred for a given time, filtered, and washed. The resulting product is then dried. To decompose the platinum precursor, the catalyst was ramped in air flow (100 cm^3/min per g cat) to a temperature of 350°C and held at 350°C for 2 h.

One drawback of the technique is that the cations tend to saturate the first exchange sites, so that most of the compound adsorbs near the mouth of the pore [46].

This problem is covered in Chapter 5, and further discusses a modified IE approach that achieves a more uniform Pt distribution.

2.1.2 Incipient Wetness Impregnation

In the incipient wetness impregnation (IWI) method, the support is first dehydrated by calcination under air flow. We used an air flow rate of 100 cm^3/min per gram of L-zeolite. The temperature ramp was 2 h to 400°C, and 5 h at 400°C. The sample was quickly transferred to an inert atmosphere to prevent pore fillage with ambient water, and the L-zeolite was impregnated with an aqueous solution containing tetraammine platinum(II) nitrate, whereby the amount of solution was approximately equal to the volume of the support (0.7 ml aqueous solution per g of KL), drawn into the pores by capillary action. The main advantage of the IWI method over IE is that there is little interaction of the precursor with the support. The loading solution is removed by evaporation during drying. To dry the catalyst, we covered the mortar with a watchglass, and let it stand at room temperature for 4 h, and then transferred it to a 110 °C oven, where it dried overnight. To decompose the platinum precursor, the catalyst was ramped in air flow (100 cm^3/min per g cat) to a temperature of 350°C and held at 350°C for 2 h. It is important to note that there is no washing step after impregnation, because this method involves little interaction between the precursor and the support. In fact, washing an IWI catalyst removes the precursor phase from the support [46].

2.1.3 Vapor Phase Impregnation (Chemical Vapor Deposition)

Vapor phase impregnation (VPI), or chemical vapor deposition (CVD) involves the use of a sublimable organic metal or organometallic salt, which is small enough to enter the micropores of the material [21,22,47-49]. In this case, the KL zeolite was pre-calcined for 5 h at 400°C to remove chemisorbed water. In an inert atmosphere, $Pt(AcAc)_2$ was physically well-mixed with the KL, and the solid mixture was transferred to a reactor tube, which was sealed at one end. The reactor tube was connected to a vacuum and evacuated overnight to $< 10^{-5}$ Torr using a turbomolecular pump. The catalyst was then slowly ramped to 60°C and held there for 1 h to remove traces of water, and then ramped again to 80°C and held again for 1 h to remove water. After further ramping to 100°C, the catalyst was held for 1 h to sublime the $Pt(AcAc)_2$, at which temperature the pressure increased substantially. After sublimation, the catalyst was slowly ramped to 130°C and held for 15 min to ensure that virtually all of the $Pt(AcAc)_2$ was sublimed. The reactor tube was cooled to room temperature, and the sample was removed. At this point, the sample was light yellow in color, indicating that the $Pt(AcAc)_2$ did not decompose during the procedure. During the preparation, it is important to dehydrate the L-zeolite and keep it very dry during the entire procedure. At no point during the preparation or storage of the catalyst should the L-zeolite or the Pt acetylacetonate be allowed to come into contact with moisture. To decompose the platinum precursor, the catalyst was ramped in air flow (100 cm^3/min per g cat) to a temperature of 350°C and held at 350°C for 2 h.

2.2 CATALYST TREATMENTS

2.2.1 Calcination

Calcination is carried out under air flow or oxygen to either dehydrate the molecular sieve, decompose the Pt precursor once it has been dispersed, or to remove carbonaceous impurities, which were possibly introduced during a preparation. For KL, we found by microcalorimetry that the water is removed from the zeolite at a temperature of approximately 250°C. For decomposition of a Pt precursor, which converts it to the oxide form, the temperature 350°C was used, because previous pulse methylcyclopentane ring opening studies have indicated that, above this temperature, sintering of the Pt oxide occurs [27,28].

2.2.2 Reduction

Reduction in hydrogen is carried out over the previously calcined catalyst. This procedure activates the metal for reaction, by removing the oxygen atoms in the form of water, as follows:

$$PtO_2 + 2H_2 \Rightarrow Pt^0 + 2H_2O$$

For nucleation in metal oxide reduction, high temperatures favor more rapid initial reduction of the metal oxide and a higher density of nuclei, but sintering of the particles becomes problematic. It is therefore recommended that a high hydrogen flow rate be used with a slow temperature ramp. We used a high flow rate of 100 cm^3/min per gram of catalyst and a slow temperature ramp of 2 h to 500°C and held at that temperature for 1 h, before adding feed to the reactor. This high flow rate of hydrogen lowered the partial pressure of water vapor created during the reduction

step, and increased the rate of reduction at the lower temperatures. When nucleation occurs, hydrogen dissociatively chemisorbs to the metal surface, and these mobile hydrogen atoms migrate to the metal-metal oxide interface, to cause rapid reduction of the metal. It is noted that hydrogen atoms react with the metal ion or oxide ion much more readily than the molecular form [46].

2.3 CATALYST CHARACTERIZATION METHODS

2.3.1 Hydrogen Chemisorption

Hydrogen chemisorption measurements were conducted in a static volumetric adsorption Pyrex system, equipped with a high capacity, high vacuum pumping station that provided vacuum on the order of 10^{-9} Torr. A schematic of the system is provided in Figure 2.1. The aim of conducting chemisorption experiments was to obtain information on the dispersion of Pt.

In the procedure, the catalyst was first reduced in flowing H_2, which saturated the surface of the Pt with chemisorbed hydrogen. To remove the chemisorbed hydrogen and obtain a clean Pt surface, the flow of hydrogen was switched off at the reduction temperature, the system was sealed, and the valve between the catalyst chamber and the turbo pump was opened. After 15 min at the reduction temperature, the system was allowed to cool under vacuum to room temperature. The vacuum valve was then closed to seal the system, and the dosing section was leak tested appropriately. Isotherms were constructed by first pressurizing the dosing chamber with H_2 to the desired initial pressure, P_i. Then the valve to the reactor chamber was

opened, and the pressure decreased rapidly at first by expansion of the gas and then more slowly by dissociative chemisorption of hydrogen onto the surface of the Pt

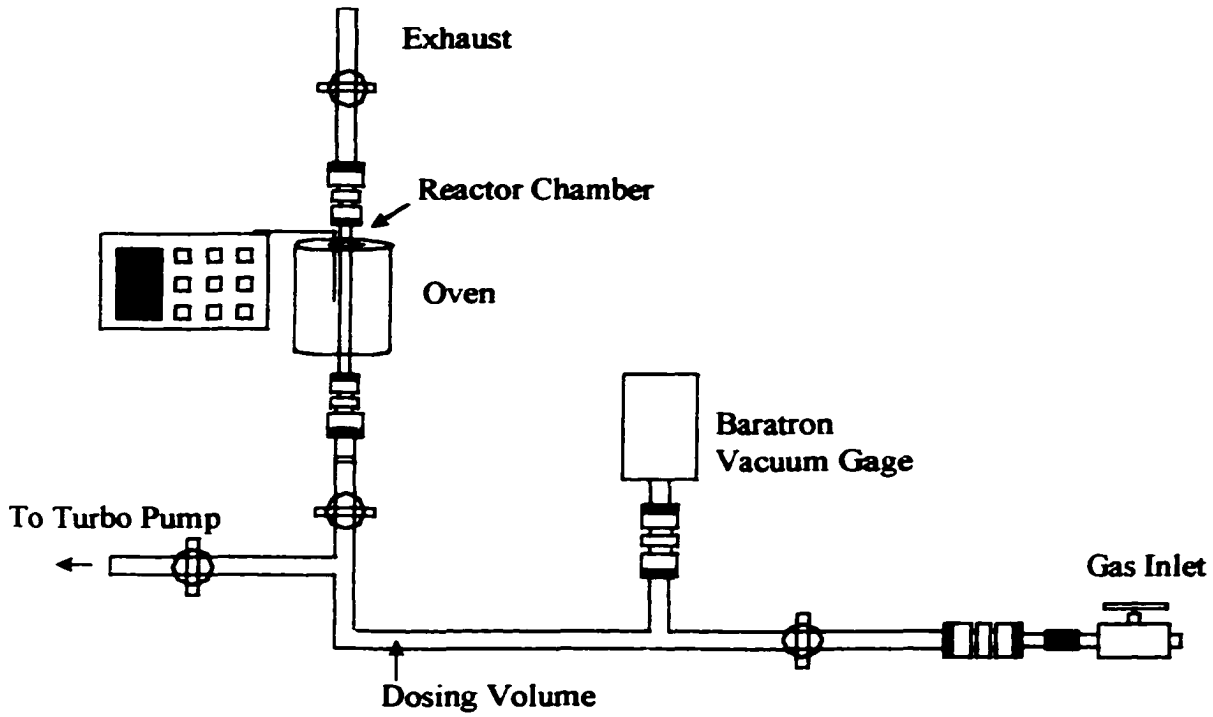

Figure 2.1: Schematic of volumetric chemisorption system.

clusters. When the equilibrium pressure was reached, it was recorded as P_f. We dosed pressures at 40 Torr, 60 Torr, 80 Torr, and 100 Torr to obtain good isotherms for Pt/KL in our system. The amount of hydrogen adsorbed after each point was measured and calculated based on the fact that the volumes of the system were known from previous expansion experiments using helium, which is inert. At some high hydrogen dosing pressure, the surface of the Pt would become saturated with hydrogen, and only expansion of the gas would occur. At those high pressures, the slope of the isotherm was extrapolated back to zero pressure and the H/Pt value was recorded. To calculate the dead volume in the reactor, expansions with helium were

carried out after each experiment, because the amount of quartz wool and catalyst would change with each experiment, changing the reactor dead volume.

To quantify the amount of reversibly adsorbed hydrogen, after obtaining the first isotherm, the sample was evacuated for 5 min at room temperature and a second isotherm was determined. The irreversible H/Pt was obtained by subtracting the two isotherms.

2.3.2 Transmission Electron Microscopy (TEM)

Transmission electron microscopy (TEM) images were obtained using a JEOL 200FX-TEM on catalysts after they were reduced in H_2 at 500°C and passivated in He/air. It is known that exposure to the TEM beam causes destruction of the zeolite structure and metal agglomeration [50]. Therefore, to avoid beam damage, we used low beam intensities and minimized the exposure times. Also, samples were cooled to liquid nitrogen temperatures using a cryogenic attachment.

2.3.3 Fourier Transform Infrared Spectroscopy of Adsorbed CO

The absorption of infrared radiation is followed by transitions between discrete vibrational levels. We recall that absorption of infrared photons occurs only if a dipole moment changes during a vibration. Since CO is a permanent dipole, FTIR of CO as an adsorbate can successfully be applied to identify adsorption sites. It also gives information about the metal-CO bond, so it is particularly useful for probing electronic and geometric effects. Adsorption of CO is typically described in terms of the Blyholder model, which is represented in Figure 2.2.

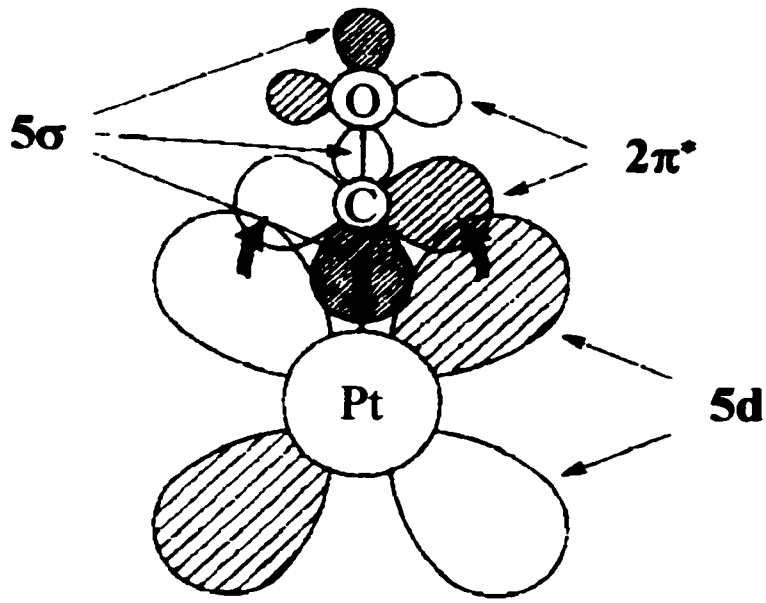

Figure 2.2: Adsorption of CO onto Pt surface according to Blyholder [51].

According to the Blyholder model, electrons are donated from CO via the 5σ molecular orbital into the metal d-bands. Simultaneously, electrons are backdonated from the metal to the empty $2\pi^*$ antibonding molecular orbitals of CO, which weakens the bond between C and O. Because of this decreased bond strength, the infrared bands are shifted to lower wavenumbers relative to the position for gas phase stretching , which is at 2143 cm^{-1}. The stretching vibration of CO is determined by the location of the adsorption site (i.e., edges, steps, kinks, faces, etc.), surface coverage due to dipole-dipole interactions (e.g., bands shift to higher wavenumbers with increasing coverage), interactions between CO and cations in the L-zeolite, extent of Pt cluster disruption and formation of Pt-carbonyl species for small Pt clusters, and amount of backdonation by the metal.

Infrared spectroscopy measurements of adsorbed CO were performed on a Bio-Rad FTS-40 spectrometer, equipped with a MCT detector. Experiments were conducted in a diffuse reflectance cell from Harrick Scientific, type HVC-DR2 with ZnSe windows that allowed us to perform in-situ thermal pretreatments. For each IR spectrum, taken at a resolution of 8 cm^{-1}, 128 scans were added. Samples were pre-reduced ex-situ under H_2 flow at the desired reduction temperature for 1 h, and then passivated. Prior to each spectrum, the catalyst was re-reduced in-situ in a flow of H_2 for 30 min at 300°C, cooled under He flow, and purged in He at room temperature for 30 min. The background was recorded at this time. Then, the catalyst was exposed to a flow of 3% CO in He for 30 min at room temperature and purged in He for 30 min, prior to obtaining the scans, to remove the contributions from gas phase and weakly adsorbed CO.

2.3.4 Extended X-ray Absorption Fine Structure Spectroscopy (EXAFS)

EXAFS is especially useful in providing structural information when long-range order is absent. Therefore, for examining the tiny Pt clusters in this thesis, it was an important tool. X-ray Absorption Near Edge Spectroscopy, which falls in the energy range of electronic transitions and multiple scattering, is described in Chapter 7, and is typically used to probe the electronic state of the atom. In XANES, we usually examine the white line intensity, with a large white line indicative of increased availability of empty states in the valence band, usually brought about by oxidation or decreased cluster size. EXAFS, on the other hand, occurs at higher photoelectron kinetic energies ($E_k = h\nu - E_b$), in the single scattering regime (Figure

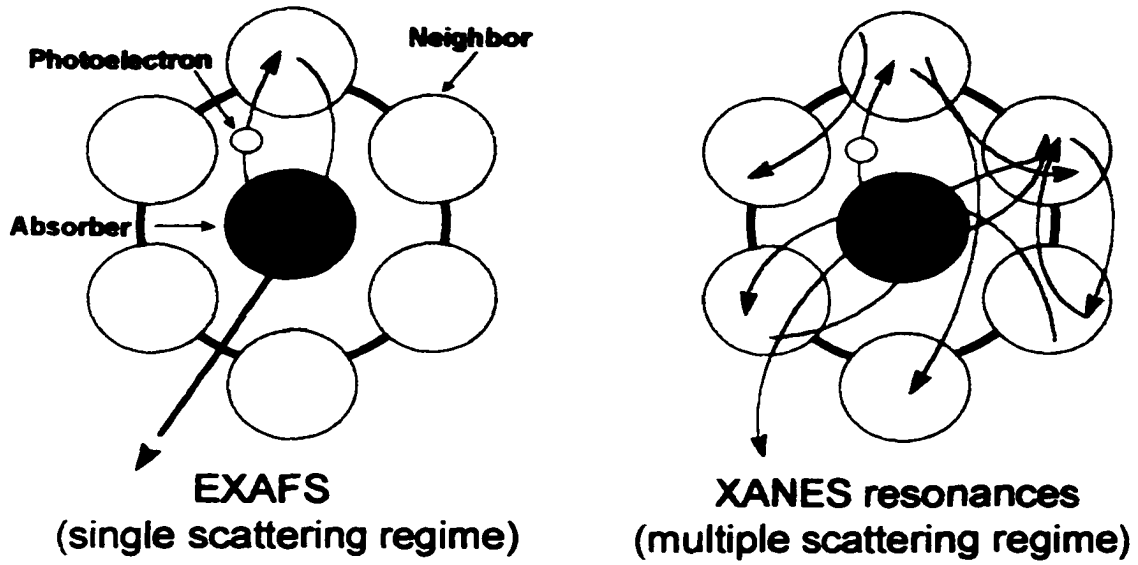

Figure 2.3: Particle picture of EXAFS and XANES.

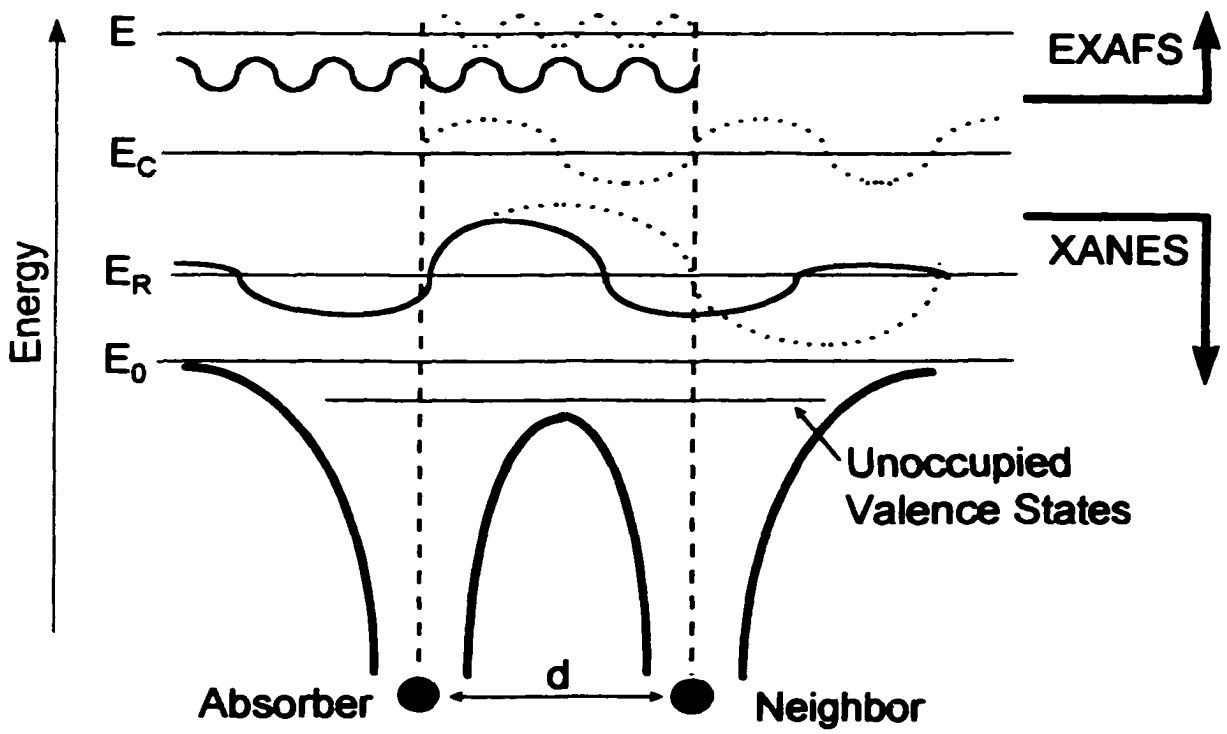

Figure 2.4: Wave picture of EXAFS and XANES.

2.3), and is used to obtain structural parameters, like interatomic distances and coordination numbers. In a typical EXAFS experiment, we scanned using a double crystal monochromator X-ray energies before and after the binding energy of a particular electron in Pt, for example. The onset of single scattering (EXAFS regime) occurs at approximately 50 eV after the absorption edge. In this range, fine structure in the shape of oscillations, are observed. Here, X-ray absorption depends on the initial state and the final state of the photoelectron, which is emitted as a wave and backscattered by its surrounding neighbors (Figure 2.4). At certain energies, where the outgoing and backscattered waves are in phase, constructive interference occurs, and the probability for X-ray absorption increases. At those points, we see an increase in X-ray absorption, and the same argument can be made for energies corresponding to destruction interference. Qualitatively, the intensity of oscillations goes up with increased coordination, the number of oscillations increases with decreased interatomic distance, and the edge jump is proportional to concentration.

Treatment of the data is not terribly difficult, but analysis of the data is and can be very time-consuming. To treat the data [52], the χ function is extracted from the spectrum by removing the parabolic background and the edge jump, which normalizes the spectrum to one atom. Next, it is customary to convert to k-space, where k is the photoelectron wave number. The photoelectron wave vector is related to the kinetic energy by $k = 2\pi/h(2m_e(h\nu - E_b)$. The EXAFS function is the sum of scattering contributions of all neighboring atoms, which surround the absorber atom in coordination shells, and is given by $\chi_k = \Sigma_j A_j(k)\sin(2kr_j+\phi_j(k))$, where A is the amplitude function, j is the coordination shell, r is the interatomic distance, and ϕ is

the total phase shift, which is equal to the phase shift of the backscatterer plus twice that of the absorber. The amplitude of each scattering contribution is given by $A_j(k)=N_j(e^{-2r_j/\lambda(k)}/kr_j^2)\ S_0^2(k)\ F_j(k)e^{-2k^2\sigma_j^2}$, where N_j is the coordination number in shell j, S_0 is the correction for relaxation effects in the emitter, F_j is the backscattering factor for atoms in shell j, λ is the inelastic mean free path of the electron, and σ^2 is the mean-squared displacement of atoms in the sample. Our first qualitative picture of the EXAFS function comes into focus when we look at the Fourier transform of $\chi(k)$, which is almost the radial distribution function, and is given by the following: $\theta_n(r)=1/(2\pi)^{1/2}\ {}_{k_{min}}\int^{k_{max}} k_n\ \chi(k)e^{2ikr}dk$, where n is an integer, depending on whether one wants to weight the transform for light (n=1) or heavy (n=3) atoms. To obtain the true radial distribution function, phase shift correction must be made, since the phase shift causes each shell to peak at the wrong distance, as well as amplitude correction, due to element specific backscattering. The corrections are derived from reference samples or theoretical calculations, giving the phase-and-amplitude corrected Fourier Transform, $\theta_n(r)=1/(2\pi)^{1/2}\ {}_{k_{min}}\int^{k_{max}} k_n\ \chi(k)[e^{-i\phi(k)}/F_j(k)]e^{2ikr}dk$.

The analysis of the EXAFS spectra were carried out using the following simple (a and b) and non-trivial (c) steps.

a. First, $\chi(k)$ was extracted from the experimental data.

b. The k-interval was selected and the k^3 weighted FT determined.

c. Individual contributions were identified and used to construct a set of parameters used to fit (i.e., using software) $\chi(k)$ and the magnitude and imaginary parts of the Fourier transform.

EXAFS data on in-situ-reduced samples were obtained at the National Synchrotron Light Source (NSLS) at Brookhaven National Laboratory, Upton, New

York using beam line X-18b equipped with a Si (111) crystal monochromator. The X-ray ring at the NSLS has an energy of 2.5 GeV and a ring current of 80-220 mA. EXAFS data were taken near the L_{III}-edge of Pt (11,564 eV). The experiments were conducted in a stainless steel sample cell, which allowed in situ treatments at temperatures ranging from 500°C to liquid nitrogen temperature. Before each measurement, the catalysts, previously reduced at 500°C, were re-reduced in situ at 300°C (heating ramp of 10°C /min) for 30 min in flowing H_2. The EXAFS spectra were recorded at liquid nitrogen temperatures under H_2 flow. Six scans were recorded for each sample. The average spectrum was obtained by adding the six scans. The pre-edge background was subtracted by using power series curves. Subsequently, the post-edge background was removed using a cubic spline routine. Spectra were normalized by dividing by the height of the absorption edge. To avoid overemphasizing the low energy region [53], the χ data were k^3-weighted. The range in k-space utilized to do the analysis was 3.5-13.5 A^{-1}. Theoretical references for Pt-Pt, and Pt-O bonds (also Pt-S, for the case of poisoned samples) were obtained by using the FEFF program from the University of Washington [54-56]. The FEFFIT fitting routine was employed to obtain the structural parameters of the Pt clusters after the various thermal treatments on the different supports. The Debye Waller factors for each bond type (σ), the edge energy difference (ΔE_o), the coordination number N, and the difference in bond distances (ΔR) with respect to the theoretical reference, were used as fitting parameters.

2.3.5 Temperature Programmed Oxidation (TPO)

Temperature Programmed Oxidation (TPO) measurements of spent catalysts were performed in a continuous flow of 5%O_2/He while the temperature was linearly increased. The reaction was conducted in a fixed bed quartz reactor and 40-50 mg of spent catalyst was supported on a bed of quartz glass wool. The catalyst was flushed in He at least for 30 min before performing the TPO. The evolution of CO_2 produced by the oxidation of the carbon species was monitored by a mass spectrometer. Quantification of the CO_2 produced was calibrated with 100 μl pulses of pure CO_2. The evolved CO_2 partial pressure was normalized by the total pressure and the maximum signal in the pulses of CO_2.

2.4 REACTION TESTING

2.4.1 Flow Mode Reaction Testing

Catalytic reaction tests were conducted at atmospheric pressure using two fixed-bed, single pass, and continuous-flow reactors in parallel. One reactor was only used for clean n-hexane runs, while the other reactor was only used for sulfur deactivation studies. To avoid contamination of the clean runs, all lines leading to each reactor were kept segregated. Each reactor consisted of a 0.5-inch stainless steel tube with an internal K-type thermocouple. The oven was controlled with a J-type thermocouple. The experiments were conducted using between 0.10 and 0.40 g of catalyst in each run. Each catalyst was sieved to give pellet sizes between 300 and 425 microns (40/50 mesh granules). The catalyst bed was supported on a bed of quartz glass wool. The reactor was operated under flowing hydrogen, and n-

hexane (Aldrich, 99+ % purity, < 50 ppb sulfur, measured) was added by infusion with a syringe pump (Sage model M365) through a T-junction prior to the reactor. In all experiments, the hydrogen/n-hexane ratio was kept at 6. Prior to reaction, the catalyst was slowly ramped in flowing hydrogen at 100 cm^3/min per gram of catalyst for 2 h to the desired reaction temperature and reduced in situ at that temperature in flowing hydrogen for 1 h. Reactions were conducted at 450 or 500°C, while the space velocity was varied to achieve different conversions and selectivities of products for study.

A purge-valve was used to send samples to a gas chromatograph/mass spectrometer (Hewlett Packard G1800A GCD System) for analysis, or alternately, to a HP6890 gas chromatograph. The gas chromatograph utilized helium as the carrier gas and sent purged products of reaction through the column (HP-PLOT/Al_2O_3"S" Deactivated) to achieve product separation. Finally, products were ionized by the mass spectrometer, incorporating an electron ionization detector (EID), or by using a flame ionization detector (FID). A temperature ramp program provided the means for adequate peak separation in the GC column. To determine the signal/abundance ratio and quantify the concentration of each component in the products, normalization curves were obtained using pure compounds. A schematic of the reactor system is provided in Figure 2.5.

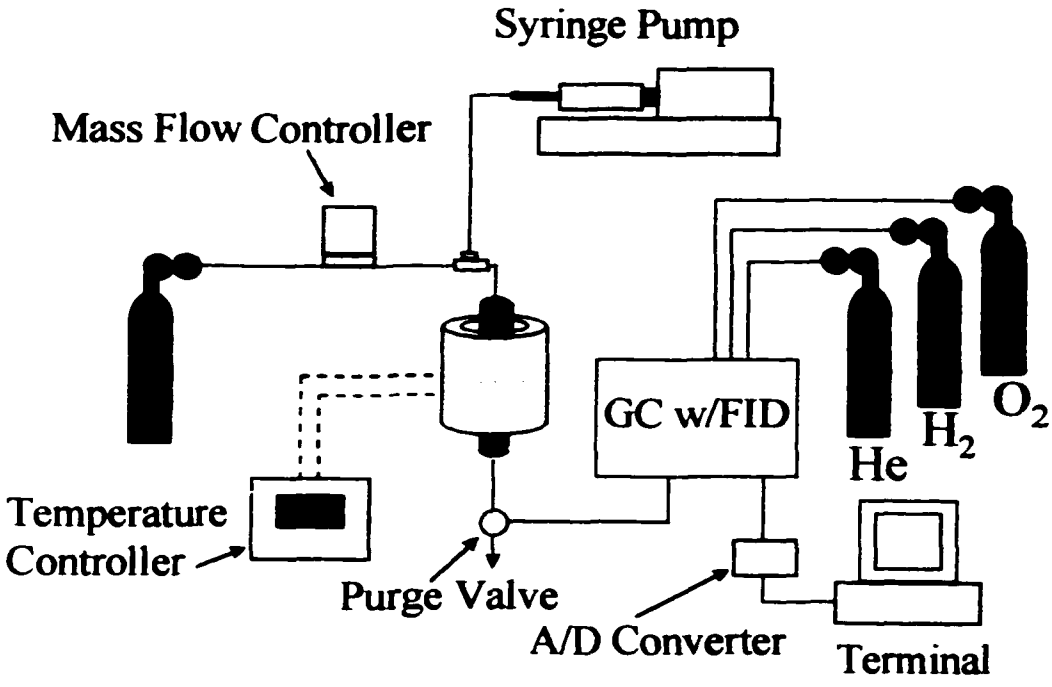

Figure 2.5: Flow-mode microreactor system.

CHAPTER III: CATALYST SCREENING – Is Pt/KL unique?

The n-hexane aromatization reaction was studied on Pt/KL, Pt/Mg(Al)O, and Pt/SiO_2 catalysts at 500°C using sulfur-free and 0.6 ppm sulfur-containing feedstocks. Examination of the product distribution as a function of conversion suggested that the formation of benzene was preceded by the formation of hexenes. In contrast with previous reports, it was found that the Pt/KL catalyst exhibited much higher aromatization activity than the Pt/Mg(Al)O catalyst. On Pt/KL, the main product was benzene, with hexenes and lighter compounds as the principal by-products. By contrast, on the Pt/Mg(Al)O, the main products were hexenes. Since hexenes were primary products and benzene was a secondary product, the exceptional aromatization activity of Pt/KL was explained in terms of its ability to convert hexenes into benzene. In the presence of sulfur, the Pt/KL exhibited a rapid loss in n-hexane conversion and benzene selectivity. Under these conditions, the sulfided Pt/KL catalyst presented a catalytic behavior typical of Pt/Mg(Al)O and Pt/SiO_2, generating larger amounts of hexenes.

The observed results were consistent with the hypothesis that the most important role of the zeolite was to inhibit bimolecular interactions leading to coke formation. The formation of coke had the net effect of selectively deactivating aromatization sites requiring a larger ensemble of atoms to constitute the active site but not affecting the dehydrogenation activity, which was less ensemble-sensitive. Therefore, those particles not protected against coking inside the channels of the zeolite rapidly became unselective. In support of this hypothesis, the

hydrogenolysis reaction, also requiring a larger ensemble of atoms, decreased in parallel with aromatization. The high sensitivity of Pt/KL to sulfur may be due to a combination of effects involving growth of metal particles outside the zeolite, which would become unselective, and partial poisoning of the particles inside the zeolite, causing a similar selective deactivation.

3.1 INTRODUCTION

The exceptionally high activity and selectivity exhibited by Pt/KL zeolite catalysts for the aromatization of n-hexane to benzene are well established [1-3,57], and have lead to the development of successful commercial processes [1,30]. However, a major shortcoming for these catalysts is their extremely high sensitivity to even minute concentrations of sulfur (e.g., parts per billion), requiring very expensive and complicated sulfur-removal operations. Therefore, for years there has been a strong impetus in finding catalysts able to effect the aromatization reactions in the presence of sulfur.

Although it is well accepted that the aromatization reaction on these catalysts is monofunctional, catalyzed only by the metal function, the fundamental reasons for both their exceptional catalytic properties and their high sulfur sensitivity are still unresolved. Possible explanations about the high aromatization activity have been considered [4], and these were reviewed in Section 1.5.

Despite the great disparity in the possible explanations offered by several authors, most of them agreed in the uniqueness of the L zeolite to promote high aromatization selectivity. However, a surprising result was reported in 1991 [23].

It was found that using Pt catalysts supported on Al-stabilized MgO, the n-hexane conversion at a given contact time, as well as the aromatization selectivity at a given conversion, were almost identical to those obtained on a Pt/KL catalyst under the same conditions. This result would certainly disfavor any explanation involving the role of the L zeolite structure as being mainly responsible for the aromatization activity, since the Mg(Al)O support is not microporous. Consequently, this result gave strong support to theories promoting the idea that the basicity of the support was the essential feature and the main role of the support was to electronically modify the Pt particles. Nevertheless, more recent results have suggested that, in fact, Pt/Mg(Al)O may not be nearly as active and selective as Pt/KL [21,58]. In this investigation, a direct comparison of the two materials is made under several conditions to help resolve the conflicting reports. In addition to the Pt/KL and Pt/Mg(Al)O catalysts, we studied a Pt/SiO_2 catalyst as a non-microporous reference material, in which minimal metal-support effects should be expected.

The second important part of our study is the sensitivity to sulfur. As mentioned above, one of the most serious drawbacks exhibited by the Pt/KL catalysts is their low sulfur tolerance. It is our interest to determine whether Pt/Mg(Al)O has the same high sensitivity to sulfur as Pt/KL, or if it is more resistant and can have potential as a practical catalyst.

3.2 EXPERIMENTAL

3.2.1 Catalyst Preparation - Pt/KL, Pt/Mg(Al)O, and Pt/SiO_2

Three support materials were used in this study. The K-LTL zeolite (series TSZ-500, BET area 292 m^2/g, SiO_2/Al_2O_3 ratio = 6) was provided by Tosoh Company. Before addition of the metal, the K-LTL zeolite was dried in an oven at 110°C for twelve hours and calcined at 400°C for 5 hours. The Al-stabilized magnesium oxide support, Mg(Al)O, was prepared by coprecipitation of aluminum nitrate and magnesium nitrate from an aqueous solution at 60-75°C, following the procedure reported in previous studies [23,59,60]. The Mg/Al ratio in the solution was kept at 5:1 and the total cation concentration was 1 M. A potassium hydroxide-potassium carbonate solution was prepared to keep a molar ratio of $CO_3^{2-}/Al = 0.5$ while potassium hydroxide solution was required to keep the pH stable at 9. The filtrate was washed with ultrapure water and dried first at room temperature for 10 h, and then placed in an oven at 110°C for 24 h. The dried sample was calcined at 600°C in air for twelve hours (BET area 150 m^2/g, average pore radius 100 Å). The material was characterized during several stages in the synthesis process using XRD and it was confirmed that, at every stage, the structure was the same as those reported in previous work [27]. The SiO_2 support employed in this study was a silica gel (Davison Grade 923) provided by W. R. Grace.

The incorporation of the platinum was realized by two methods – IWI and VPI, using the procedures outlined in Sections 2.3.2 and 2.3.3. The characteristics of the four catalysts investigated are summarized in Table 3.1.

Table 3.1: Catalyst Characteristics

Catalyst	BET Surface Area (m^2/gram)	Pore Radius (Angstroms)	Preparation Method	Amount of Pt (wt. %)
Pt/KL (IWI)	292	7.1 (min.), 13 (max.)	IWI	1
Pt/KL (VPI)	292	7.1 (min.), 13 (max.)	VPI	1
Pt/Mg(Al)O	100	Ave. 100	IWI	1
Pt/Silica	470	Ave. 25	IWI	1

3.2.2 Catalyst Characterization – BET Surface Area, TEM, and EXAFS

The surface areas and pore size distributions of the supports were determined using an adsorption unit ASAP 2010 from Micromeritics. Transmission electron microscopy (TEM) images were obtained according to Section 2.3.2 on all fresh catalysts, as well as those that were exposed to reaction conditions using sulfur-free feed, and feed containing 0.6 ppm sulfur.

Fresh and spent samples were characterized by EXAFS spectroscopy at the National Synchrotron Light Source (NSLS) at Brookhaven National Laboratory according to Section 2.3.4.

3.2.3 Reaction Testing – Clean and Sulfur-poisoned Feeds

Catalytic reaction tests were conducted according to Section 2.4.1. The reactor conditions during catalytic activity tests were as follows: temperature of 500°C, a weight hourly space velocity (WHSV) of 5 h^{-1}, and atmospheric pressure. For the sulfur poisoning studies, thiophene was premixed into the feed at a concentration of 0.6 ppb.

3.3 RESULTS

3.3.1 Catalytic Activity Measurements Using Sulfur-free nC_6

Several activity tests were conducted under sulfur-free conditions. The yields of the different products obtained at 500°C after 1.5 h on-stream over the three catalysts are summarized in Table 3.2.

Table 3.2. Yields of different products obtained at 500°C after 1.5 hours on stream at WHSV of 5 hr^{-1}

Product	Pt/K L (IWI)	Pt/K L (VPI)	Pt/Mg(Al)O	Pt/SiO_2	Equilibrium Hexenes
Benzene	45.69%	48.68%	4.59%	13.82%	-
Methane	4.65%	3.12%	0.40%	4.03%	-
Ethane	3.16%	1.92%	0.30%	2.41%	-
Propane	2.09%	1.45%	0.32%	2.07%	-
Total Hexenes:	1.19%	0.69%	8.35%	5.47%	12.6 - 26.1%
Trans-3-Hexene	0.21%	0.12%	1.50%	1.03%	2.1 - 4.26%
Trans-2-Hexene	0.50%	0.29%	3.25%	2.32%	6.6 - 13.64%
1-Hexene + Cis-3-Hexene	0.23%	0.13%	1.77%	1.00%	2.0 - 4.2%
Cis-2-Hexene	0.25%	0.15%	1.84%	1.12%	1.9 - 4.04%
2,4 Hexadiene	0.10%	0.02%	0.54%	0.15%	-
Methylcyclopentane	0.44%	0.22%	0.75%	2.22%	-
2-Methylpentane	0.42%	0.28%	0.39%	1.08%	-
Methylcyclopentenes	0.31%	0.11%	1.20%	2.06%	-
Cyclopentene	0.23%	0.15%	0.42%	0.75%	-
3-Methylpentane	0.12%	0.12%	0.14%	0.38%	-
1,3 Methylcyclopentadiene	0.09%	0.06%	0.67%	0.73%	-
1,2 Dimethyl, cis-cyclopropane	0.07%	0.05%	0.11%	0.20%	-

The differences between the product distribution obtained on Pt/KL and those on the non-zeolitic materials are clearly remarkable. For Pt/KL, the main product was benzene, with hexenes and lighter compounds as the principal by-products. By contrast, on Pt/Mg(Al)O, the main products were hexenes. For comparison, the equilibrium yields of hexenes are included in Table 3.3. They vary

with benzene yield due to a change in H_2 partial pressure, but they are always higher than the observed yields. Since it is well known that the benzene selectivity is a strong function of the overall conversion, we have made a similar comparison at the same total conversion (28%) for the three catalysts. This comparison is illustrated in Table 3.3, which does not include the C_1-C_5 products.

Table 3.3. Yields of different products (C_1-C_5 products are not included) obtained at the same overall conversion (28%) at 500°C, H_2/n-hexane feed ratio = 6.0

Product	Pt/K L	Pt/Mg(Al)O	Pt/SiO2
Benzene	20.14%	4.00%	8.67%
Total Hexenes	3.28%	10.48%	5.20%
Trans-3-Hexene	0.43%	1.81%	0.91%
Trans-2-Hexene	1.34%	4.28%	2.11%
1-Hexene*	0.77%	2.00%	1.06%
Cis-3-Hexene	0.74%	2.39%	1.13%
Cyclopentene	0.80%	0.69%	0.71%
Methylcyclopentenes	0.75%	2.33%	1.37%
1,3 Methylcyclopentadiene	0.67%	2.07%	0.53%
Methylcyclopentane	0.51%	0.89%	0.77%
1,2 Dimethyl, cis-cyclopropane	0.21%	0.17%	0.18%
3-Methylpentane	0.06%	0.13%	0.13%
2-Methylpentane	0.03%	0.14%	0.35%

Once again, Pt/KL exhibited a much higher benzene selectivity than Pt/Mg(Al)O and Pt/SiO_2. In addition to the products listed in Tables 3.2 and 3.3, a small fraction of condensation products (C_6+) were obtained with the Pt/SiO_2 and the Pt/Mg(Al)O catalysts. These products were not observed when the Pt/KL catalyst was employed. The superior performance of Pt/KL in comparison with the other two catalysts is further demonstrated in Fig. 3.1, which shows the overall initial benzene yield (extrapolated to zero time) as a function of the space time.

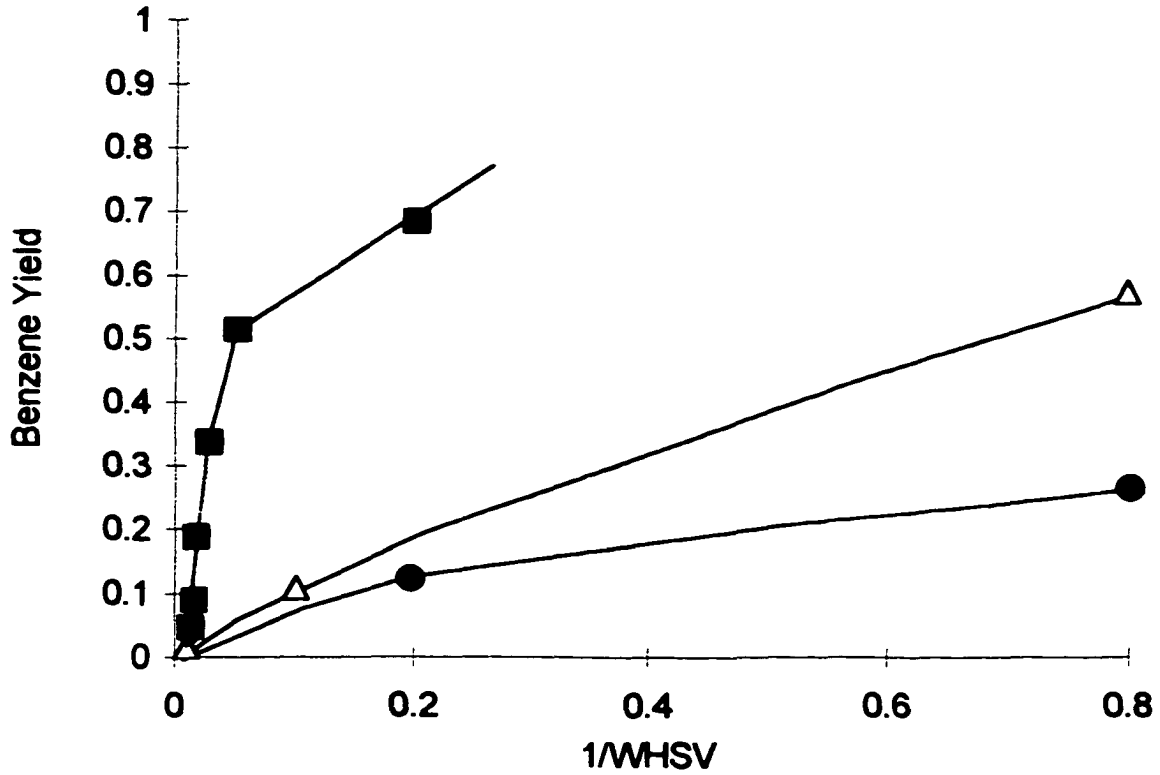

Figure 3.1. Benzene yield as a function of reciprocal weight-hour space velocity for the three catalysts investigate: Pt/KL (squares), Pt/SiO_2 (triangles), and Pt/Mg(Al)O (circles)

The Pt/KL zeolite displayed the highest activity, while the Pt/Mg(Al)O was even less active than Pt/SiO_2.

In the catalytic activity tests, it was observed that, even in the absence of sulfur, all catalysts presented moderate activity decay. To analyze the effect of catalyst deactivation on product distribution, the benzene and hexenes yields were measured as a function of time on stream at several space velocities. Figures 3.2 and 3.3 make a comparison of the evolution of these yields on the Pt/KL and Pt/Mg(Al)O catalysts, respectively.

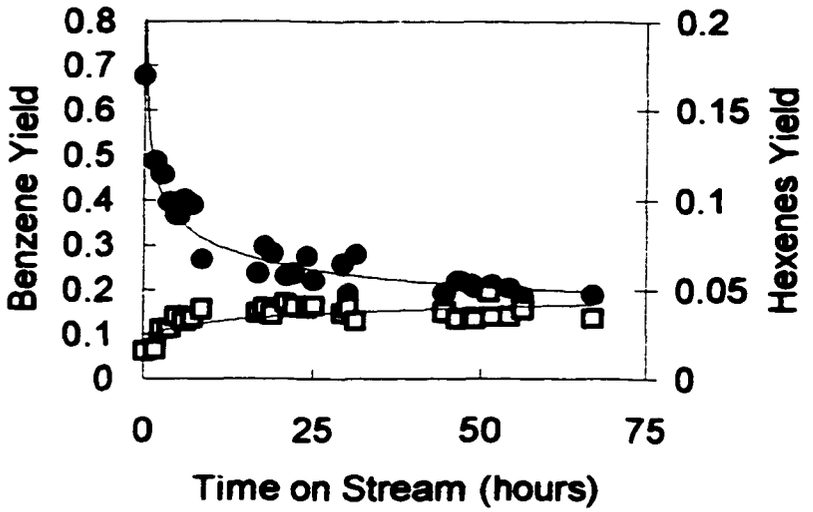

Figure 3.2. Yield of benzene (full circles) and hexene (open squares) as a function of time on stream (WHSV; 5 h^{-1}) on Pt/KL. Note the scale change for hexenes.

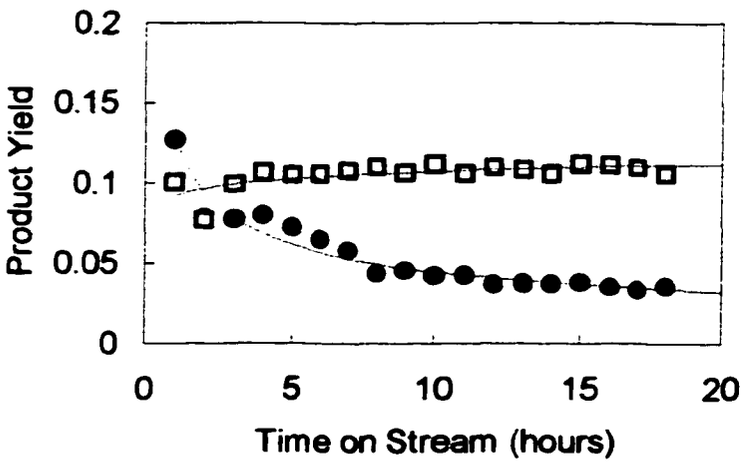

Figure 3.3. Yield of benzene (full circles) and hexene (open squares) as a function of time on stream (WHSV; 5 h^{-1}) on Pt/Mg(Al)O

A clear trend is observed. While the benzene yield decreased as a function of time, the hexene yield increased. This trend is less pronounced on the Pt/Mg(Al)O

catalysts, on which the benzene yield is much lower at all times. For example, while on Pt/Mg(Al)O, the benzene yield dropped to less than 3% after 20 h on stream, on Pt/KL, it remained above 20% even after 70 h.

We have observed that when benzene and hexene selectivity data are plotted versus conversion, they all seem to lie on the same curves, regardless whether the conversion had been varied by letting the catalyst deactivate (time on stream) or by changing the space velocity. Figures 3.4 and 3.5 illustrate the selectivity curves for Pt/KL and Pt/Mg(Al)O, respectively.

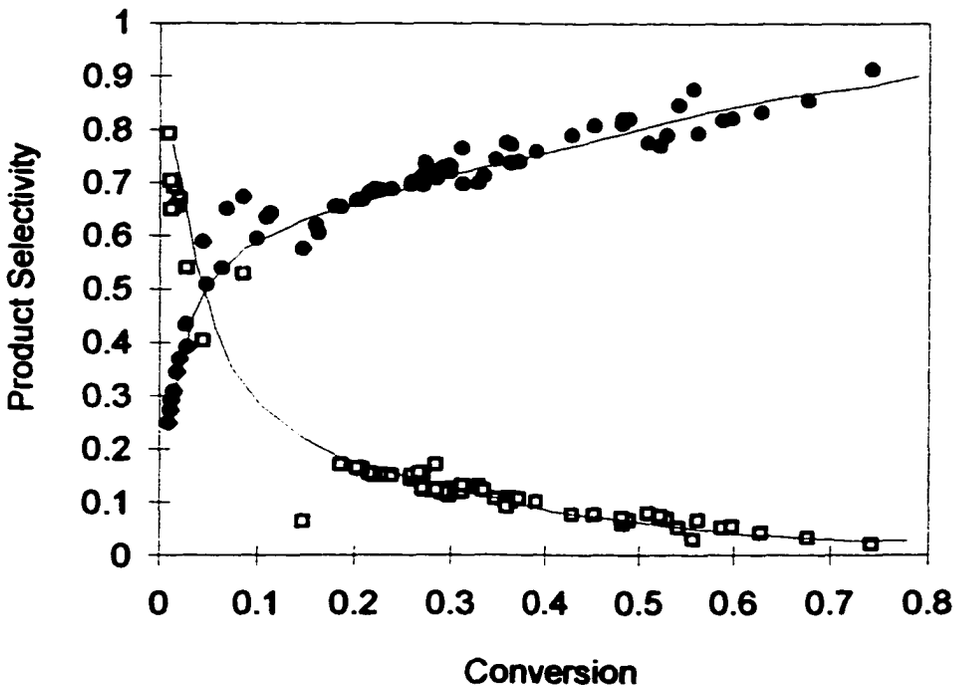

Figure 3.4. Benzene (full circles) and hexene (open squares) selectivities as a function of conversion on Pt/KL. Conversion was varied by catalyst deactivation and by changing space velocity.

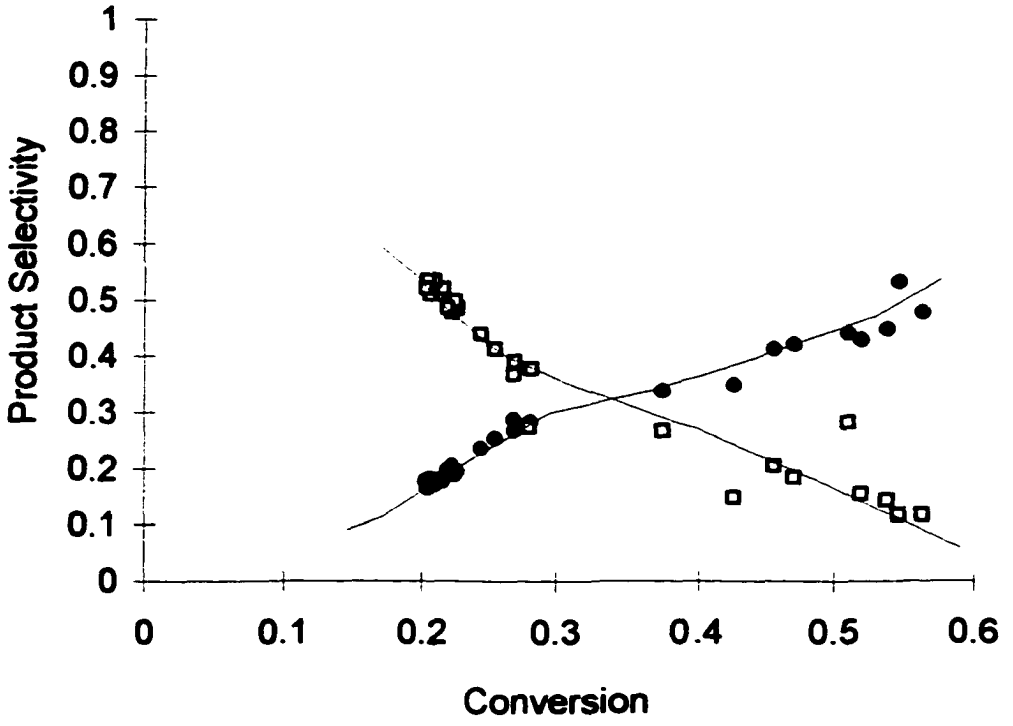

Figure 3.5. Benzene (full circles) and hexene (open squares) selectivities as a function of conversion on Pt/Mg(Al)O. Conversion was varied by catalyst deactivation and by changing space velocity.

For both catalysts, the hexene selectivity is higher at low conversions while benzene dominates at high conversions. The important difference between the two catalysts is that on Pt/KL the selectivity to benzene begins to dominate at much lower conversions than on Pt/Mg(Al)O. From the mechanistic point of view, it is important to note that on both catalysts, benzene appears as a secondary product while hexene is an intermediate that eventually can be converted into benzene. This conversion is more clearly visualized in Fig. 3.6, which shows the variation of hexene yield versus benzene yield.

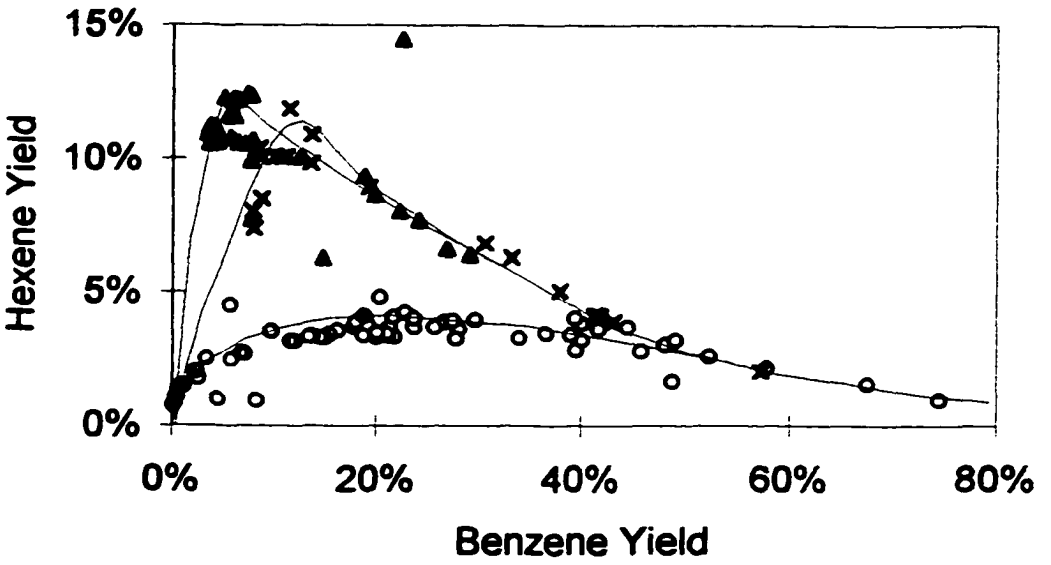

Figure 3.6. Correlation between hexene yield and benzene yield for Pt/KL (open circles), Pt/Mg(Al)O (full triangles), and Pt/SiO_2 (crosses). The data were taken at various space velocities and various times on stream.

It is clearly seen that, at low conversions, both benzene and hexene yields are low and initially increase together, but as the benzene yield increases, the hexene yield goes through a maximum and then decreases. The behavior of Pt/KL is clearly different from that of the non-microporous catalysts. It is evident that Pt/KL is much more efficient in converting hexene into benzene than the other catalysts. At the high conversion end, both catalysts show high selectivity to benzene, although the activity for Pt/Mg(Al)O is significantly lower.

We have made no attempts in this work to optimize the preparation and performance of the IWI Pt/KL catalyst. For example, the addition of KCl, CF_3Cl, or back-exchange of ion-exchanged catalysts have been found to increase the benzene selectivity [18,61,62]. Also, eliminating the traces of sulfur in the feed [63], could result in an important increase in activity and selectivity. Those changes

would only enhance the great differences between Pt/KL and Pt/Mg(Al)O in favor of the Pt/KL.

For example, the hydrogenolysis activity of the Pt/KL prepared by IWI is higher than that of Pt/Mg(Al)O. However, this higher hydrogenolysis activity is not an intrinsic property of Pt/KL. The IWI procedure, as demonstrated by TEM, leaves a heterogeneous sample, with some larger clusters outside the channels of the zeolite. In order to achieve a more uniform distribution of small particles located inside the channels of the zeolite, a vapor phase impregnation technique by sublimation of $Pt(AcAc)_2$ was also carried out. In this case, the hydrogenolysis products were reduced as compared with the IWI catalyst, while aromatization activity was higher for all time onstream (Fig. 3.15). The methane yield on the VPI catalyst dropped from 3.1% at TOS = 1.5 h (Table 3.2) to 1.7% at TOS = 70 h.

3.3.2 Catalytic Activity Measurements Using Sulfur-containing nC_6

To compare the effect of sulfur poisoning on the different catalysts, activity tests were conducted in the presence of controlled amounts of thiophene that resulted in a sulfur concentration of 0.6 ppm. Figure 3.7 shows the evolution of activity on the Pt/KL as a function of time on stream for sulfur-free and sulfur-containing feeds.

As previously reported [25], a strong deactivation is seen for the run with 0.6 ppm sulfur. The deactivation was evident not only in the overall conversion but also in the benzene selectivity. By contrast, as shown in Fig. 3.8, the Pt/Mg(Al)O exhibited a much lower sensitivity to the presence of sulfur.

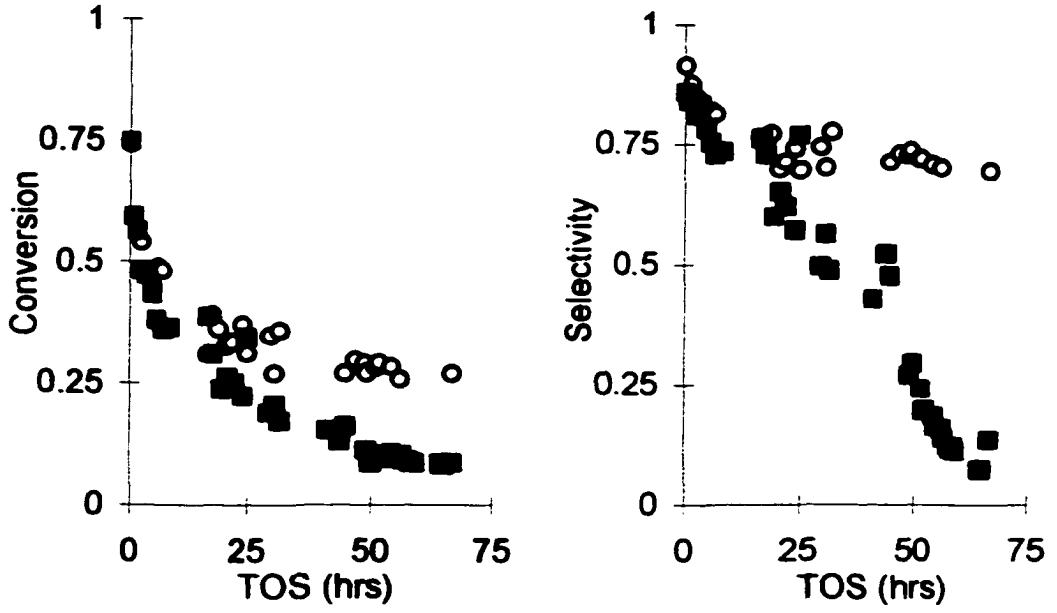

Figure 3.7. Deactivation of the Pt/KL catalyst as a function of time on-stream at 500°C, using sulfur free (open symbols) and 0.6 ppm sulfur-containing (full symbols) feeds. a) overall conversion; b) benzene selectivity.

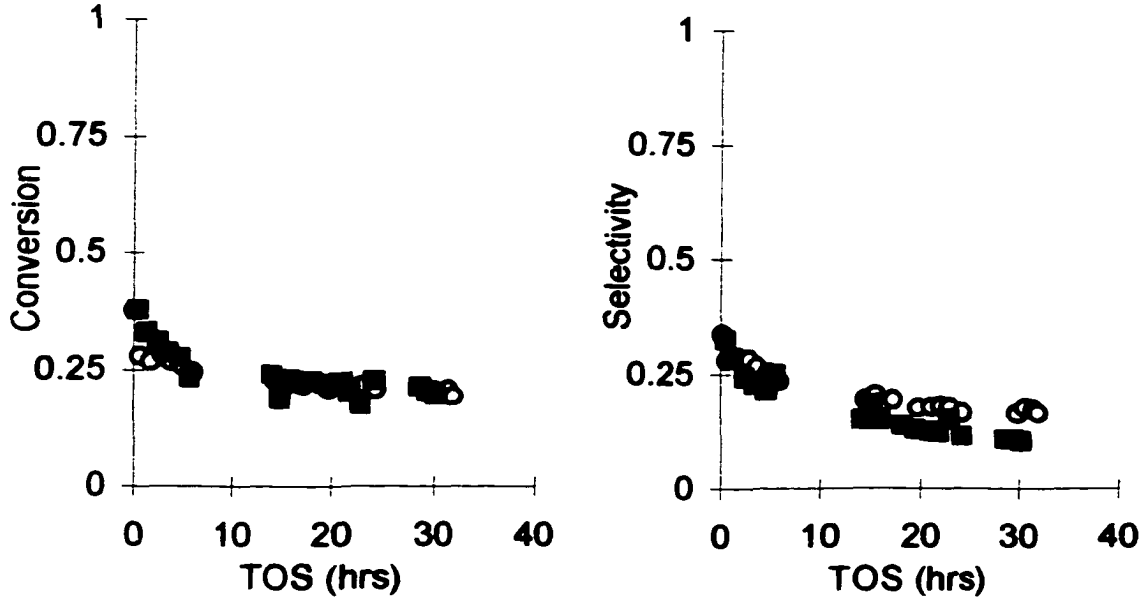

Figure 3.8. Deactivation of the Pt/Mg(Al)O catalyst as a function of time on-stream at 500°C, using sulfur free (open symbols) and 0.6 ppm sulfur-containing (full symbols) feeds. a) overall conversion; b) benzene selectivity.

In fact, both conversion and benzene selectivity were already low in the absence of added sulfur and the acceleration in deactivation by the addition of sulfur was only apparent in the benzene selectivity.

The most remarkable feature of the deactivation by sulfur is the increase in hexene selectivity. As shown in Table 3.4, the increase in hexene selectivity upon sulfur poisoning also occurs on Pt/Mg(Al)O and Pt/SiO_2 catalysts.

Table 3.4. Effect of sulfur -poisoning on product selectivity distribution after 30 hrs on-stream at 500°C, H_2/n-hexane feed ratio = 6.0

Product	Pt/KL		Pt/Mg(Al)O		Pt/SiO_2	
	nil S	0.6ppm S	nil S	0.6 ppm S	nil S	0.6 ppm S
Benzene	74.97%	57.69%	17.57%	10.18%	36.79%	23.57%
Total Hexenes:	10.51%	25.14%	50.86%	57.46%	16.30%	23.11%
Trans-3-Hexene	1.54%	4.34%	8.42%	10.14%	2.96%	4.42%
Trans-2-Hexene	4.28%	10.47%	20.69%	23.30%	6.77%	9.57%
1-Hexene*	2.36%	4.68%	9.87%	10.46%	3.05%	4.17%
Cis-3-Hexene	2.33%	5.66%	11.89%	13.56%	3.52%	4.94%
1,3 Methylcyclopentadiene	2.22%	2.06%	6.69%	4.82%	1.43%	1.66%
Methylcyclopentenes	2.58%	4.48%	6.36%	7.65%	4.89%	6.31%
Methylcyclopentane	1.60%	4.58%	2.86%	3.51%	5.24%	9.24%
Cyclopentene	2.71%	0.99%	1.45%	0.73%	1.72%	1.22%
1,2 Dimethyl, cis-cyclopropane	0.72%	0.28%	0.43%	0.20%	0.42%	0.31%
3-Methylpentane	0.22%	0.82%	0.28%	0.34%	0.52%	1.27%
2-Methylpentane	0.14%	0.74%	0.18%	0.23%	1.58%	3.68%

However, the relative increases in hexene selectivity on these non-microporous catalysts are less pronounced than on Pt/KL.

When the benzene and hexene selectivities are plotted as a function of overall conversion (Fig. 3.9), the pattern observed for the poisoned Pt/KL becomes significantly different from that for the clean Pt/KL (Fig. 3.4).

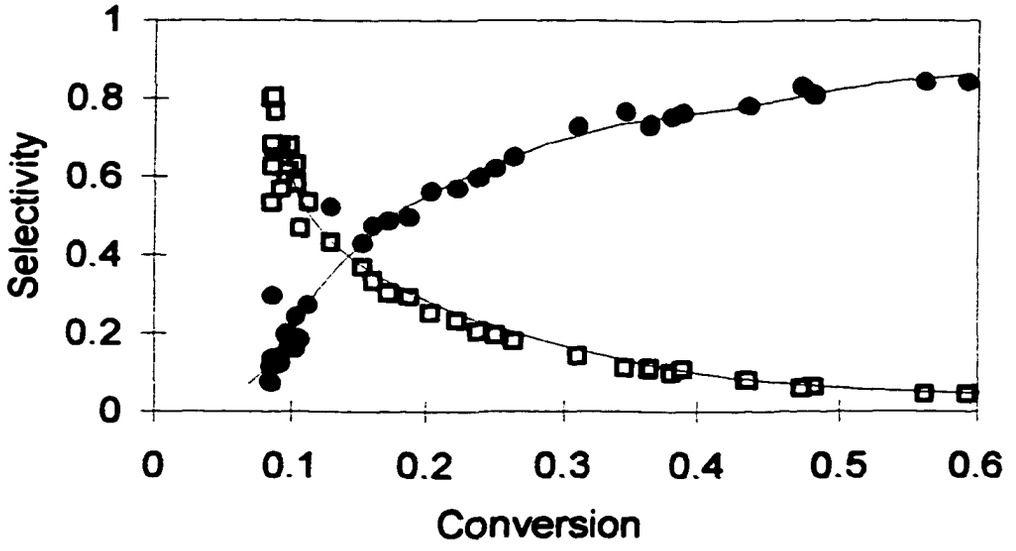

Figure 3.9. Benzene (full circles) and hexene (open squares) selectivities as a function of conversion on Pt/KL in the presence of 0.6 ppm of sulfur.

In fact, it begins to look like that of the non-microporous Pt/Mg(Al)O shown in Fig. 3.5. For instance, while the selectivity curves intersect at about 4-5 % on the sulfur-free Pt/KL, they intersect at 35 % on the Pt/Mg(Al)O catalyst. Under sulfur-containing feeds, the intersection of the curves for the Pt/KL catalyst shifts to higher conversions, i.e., about 16 %.

The change in behavior of the Pt/KL catalyst under sulfur-containing feeds is also illustrated in Fig. 3.10, which shows the variation of hexene yield as a function of benzene yield.

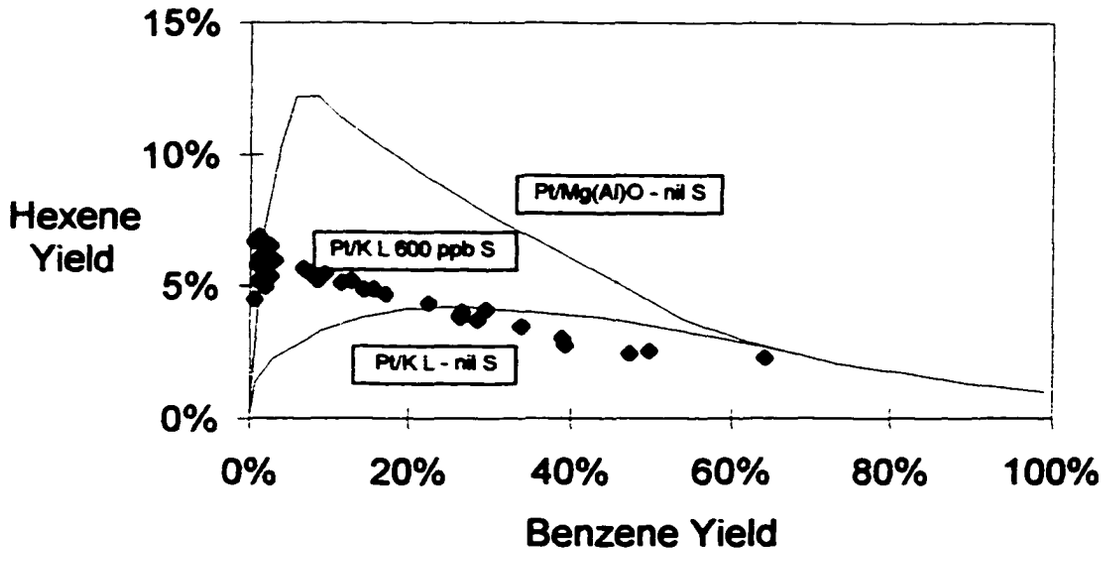

Figure 3.10. Correlation between hexene yield and benzene yield for sulfur-poisoned Pt/KL. The arrow indicates the sequence in which the data were obtained as a function of time on stream over a period of 67 h. The feed contained 600 ppb sulfur (full symbols). The two curves represent the data obtained on the sulfur-free runs reported in Fig. 3.6 for Pt/KL and Pt/Mg(Al)O, respectively.

The figure includes the curves corresponding to data on sulfur-free Pt/KL and Pt/Mg(Al)O. It can be observed that, as the catalysts poisons, the hexene yield starts increasing until it reaches the curve corresponding to Pt/Mg(Al)O. From this trend, it could be said that the catalytic behavior of a poisoned Pt/KL catalyst looks similar to that of Pt/Mg(Al)O.

It is instructive to compare the variation of hexene yield over the Pt/KL catalyst under sulfur-free and sulfur-containing feed conditions. This comparison is made in Fig. 3.11 that shows the evolution of hexene yield with time on stream for the two runs.

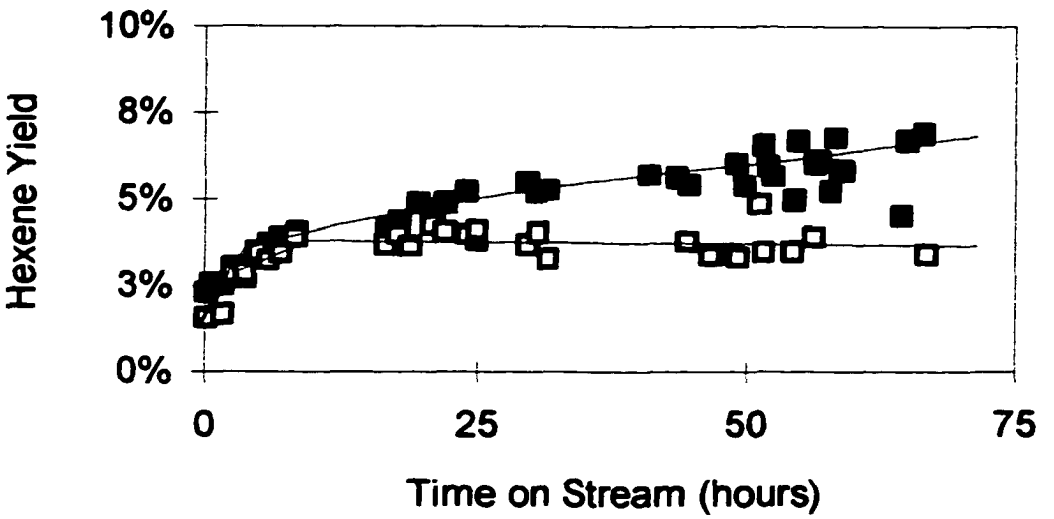

Figure 3.11. Variation of hexene yield as a function of time on stream over the Pt/KL catalyst with a) sulfur-free feed (open symbols) and b) 0.6 ppm sulfur-containing feed (full symbols). WHSV= 5 h^{-1}, T = 500°C.

It is observed that the rate of production of hexenes, not just the selectivity, increases as a result of the catalyst deactivation process. There is an important difference between the two runs. While in the sulfur-free case, the hexene yield increased during the first few hours on stream and then stabilized at about 3.5 %, in the 0.6 ppm S run the hexene yield continued to increase for a much longer time and after 70 h had reached about 7.5 % yield. As opposed to the trend exhibited by the production of hexenes, the production of methane paralleled that of benzene; that is, it decreased as a function of time on stream. It is interesting to see in Fig. 3.12 that the declines in benzene and methane production followed the same trend for both the sulfur-free and sulfur-containing runs.

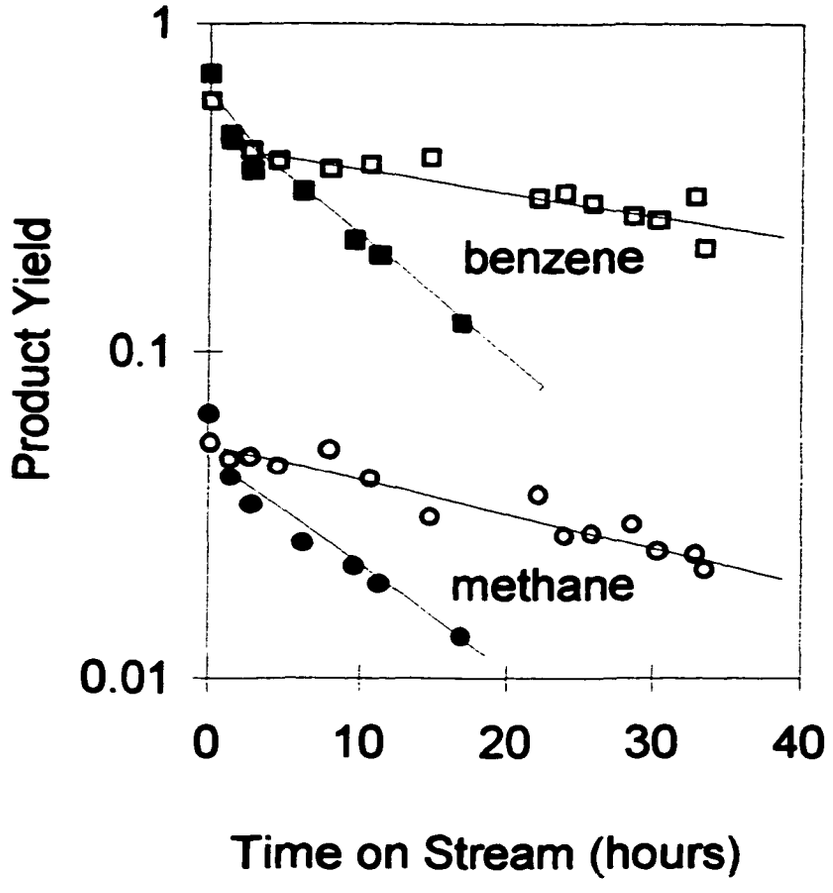

Figure 3.12. Variation of benzene (squares) and methane (circles) yields as a function of time on stream over the Pt/KL catalyst with a) sulfur-free feed (open symbols) and b) 5 ppm sulfur-containing feed (full symbols). WHSV= 5 h^{-1}, T = 500 °C

3.3.3 Physical Characterization of the Spent Catalysts

The Pt catalysts on the three different supports were characterized by electron microscopy and X-ray absorption spectroscopy, as fresh samples and after reaction with sulfur-free or sulfur-containing feeds. It has been shown that an incipient wetness impregnation procedure similar to that used in this paper results in a large fraction of the Pt particles located inside the channels of the zeolite [64].

Figure 3.13 shows TEM micrographs and, as expected, most of the Pt particles

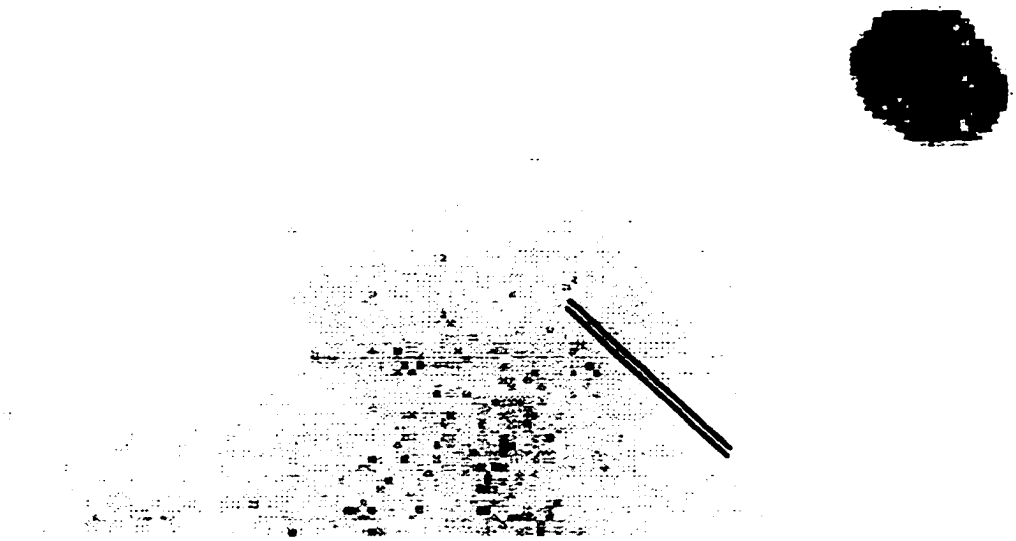

Figure 3.13: TEM micrographs of Pt/KL catalyst after 70 h on-stream at 500°C: (above) sulfur-free conditions, (below) feed containing 0.6 ppm sulfur. The channels provide an internal standards. Unfortunately, some loss in resolution occurred with scanning.

in the freshly reduced sample were too small to be observed at 2×10^5 magnification, and they are probably located inside the channels of the zeolite. However, some larger particles were also observed. After 70 hours of run with the clean n-hexane feed, most of the particles were still small with a small fraction of particles in the range of 15-20 nm. When the catalyst was exposed for 70 h to 0.6 ppm S, particle growth was evident, although a large fraction of small particles was still observed.

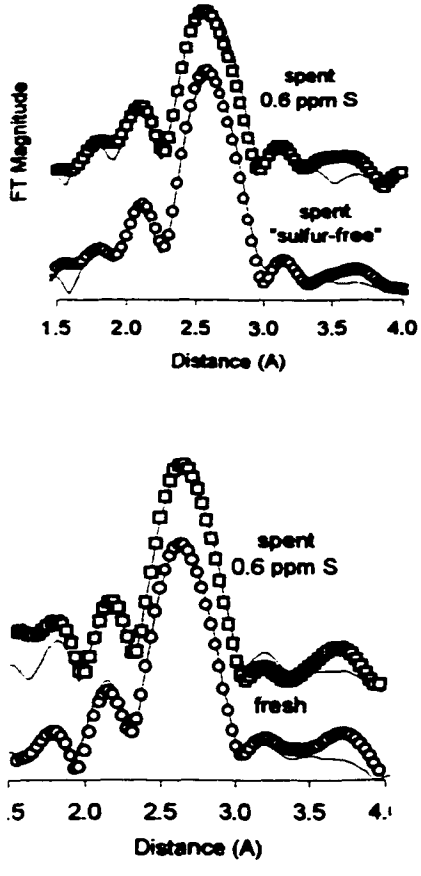

Figure 3.14. Fourier transform (magnitudes) (k^3, $\Delta k = 3.5\text{-}15$ A^{-1}) of the EXAFS data obtained at liq. N_2 temperature on "in-situ" reduced samples of: a) Pt/KL catalyst: sample spent under sulfur-free conditions (circles) and sample spent under 0.6 ppm sulfur (squares) and b) Pt/Mg(Al)O catalyst: freshly reduced sample (circles) and sample spent under 0.6 ppm sulfur (squares).

Platinum particle growth in the presence of sulfur is consistent with results reported by McVicker et al. [25]. However, the corresponding EXAFS analysis on the same set of Pt/KL catalysts did not show a significant increase in Pt-Pt coordination number, which would parallel the particle size increases observed by TEM. As shown in Fig. 3.14, the Fourier Transforms of the sample run for 70 h under sulfur-free feed and that run under 0.6 ppm sulfur were very similar. Structural parameters were obtained by curve fitting analysis, using theoretical amplitude and phase functions for Pt-Pt, Pt-S, and Pt-O contributions obtained with the FEFF program. The results of the fit in the R-space are summarized in Table 3.5.

Table 3.5. Structural parameters obtained from the fitting of EXAFS data using Pt-Pt and Pt-S theoretical references developed with FEFF.

CATALYST	N		R (nm)			σ	
	Pt-Pt	Pt-S	Pt-Pt	Pt-S	ΔE_o	Pt-Pt	Pt-S
Spent Pt/KL Sulfur-free run	4.3	0.2	0.282	0.230	2.7	0.0033	-
Spent Pt/KL 0.6 ppm S run	3.8	1.0	0.271	0.228	1.9	0.0036	0.0066
Fresh Pt/Mg(Al)O	8.7	0	0.275	-	7.8	0.0035	-
Spent Pt/Mg(Al)O 0.6 ppm S run	8.8	0.6	0.274	0.229	8.8	0.0035	0.0035

The Pt-Pt coordination numbers for both spent catalysts were about 4, and close to the value of 3.7 reported before for a fresh Pt/KL catalyst [65]. The catalyst spent in sulfur-containing feed exhibited a Pt-S coordination close to 1. The appearance of Pt-S coordination is in agreement with the results reported by Vaarkamp et al. [31] and implies that sulfur may be, at least partially, poisoning the Pt particles. No

contribution of Pt-O bonds were predicted by the model calculations. When only Pt-Pt, or Pt-Pt and Pt-O contributions were used in the fit, the quality of the fitting was much lower than when Pt-S was included. It is interesting to note that a very small contribution of Pt-S was obtained in the fit of the sample spent with the sulfur-free sample. This is not unreasonable considering that small traces of sulfur can be present in the feed and accumulate on the Pt surface over the 70 hour-run. They may be responsible for part of the deactivation observed in the "sulfur-free" runs.

TEM analysis (not shown) of the Pt/Mg(Al)O catalyst demonstrated that the platinum particles were significantly larger on the Mg(Al)O support than on KL. The fresh sample showed a large fraction of the particles with sizes of about 4 nm and a smaller fraction of larger particles ranging between 15 and 20 nm. No appreciable changes in size were detected after the run with clean n-hexane feed and only a slight growth after the run with the sulfur-containing feed. The EXAFS data are in good agreement with these observations (see Fig. 3.15). As shown in Table 3.6, the coordination number obtained for the sample exposed to sulfur-containing feed for 70 h was about the same as that of the fresh sample. Finally, the silica-supported catalyst exhibited particles smaller than 4 nm.

3.4 DISCUSSION

One of the first important conclusions of these results is that, in contrast with previous reports [23], Pt/Mg(Al)O is significantly less active and selective than the Pt/KL zeolite. This conclusion has crucial consequences, since it corroborates the exceptional ability of the Pt/KL catalyst and will eliminate the

erroneous concept that only the basicity of the support was responsible for the high activity and selectivity of Pt/KL.

Our analysis of product distribution on the various catalysts investigated shows that the amount of hexenes produced in the n-hexane reaction is a good indication of the quality of the Pt/KL catalyst. That is, a well prepared Pt/KL catalyst should exhibit a very low selectivity to hexenes even at moderate overall conversions. By contrast, a poorly prepared catalyst or a sulfur-poisoned catalyst results in a high selectivity to hexenes, and this selectivity only decreases at very high conversions. From this analysis, we could infer that the comparative work of Pt/KL and Pt/Mg(Al)O catalysts [23] resulted in very similar catalytic properties because the Pt/KL sample employed in those early studies was not optimized. In that case, it was found that at an overall conversion near 40%, the hexene selectivity was the same for both catalysts. By contrast, our data indicate that on a well-prepared Pt/KL catalyst, the selectivity to hexenes is much lower than on Pt/Mg(Al)O. For example, at an overall conversion of 40%, the benzene/hexene yield ratios obtained in the present work are 7.3 and 1.8 for Pt/KL and Pt/Mg(Al)O, respectively. A similar comparison made from the data of reference [23] results in ratios of 2.7 and 2.5, respectively. Both results are close to the ratio of about 1.9, observed on our Pt/SiO_2 catalyst at the same overall conversion.

A similar conclusion can be drawn from the comparison of the activity level made in Table 3.6. The benzene yields reported on the early work for both Pt/KL and Pt/Mg(Al)O are about the same as those found in this work for Pt/Mg(Al)O. However, the yield reported on the present work over Pt/KL is significantly greater.

Table 3.6. Comparison of catalytic activity of Pt/KL and Pt/Mg(Al)O H_2/n-hexane feed ratio = 6.0

CONTACT TIME (sec)	TEMPERATURE (°C)	CATALYST	BENZENE YIELD	REFERENCE
3.35	500	Pt/KL	70 %	this work
		Pt/Mg(Al)O	12 %	this work
3.50	477	Pt/KL	17 %	[14]
		Pt/Mg(Al)O	15 %	[14]
0.7	500	Pt/KL	53 %	this work
		Pt/Mg(Al)O	4 %	this work
1	477	Pt/KL	5 %	[14]
		Pt/Mg(Al)O	4 %	[14]

Even though it was early recognized that the n-hexane aromatization on Pt/KL would involve dehydrogenated intermediates [16], only a few papers have paid attention to the role of hexenes [4]. It must be noted that, as shown in Table 3.2, the hexane-hexenes equilibrium is not established. In all cases, the conversions to hexenes were much lower than the equilibrium conversions. However, the concentration of hexenes in the gas phase greatly changes from catalyst to catalyst. In fact, an analysis of the evolution of hexenes may provide important information about the state of the catalyst. For example, in agreement with the data from Manninger et al. [66,67], our results indicate that hexenes are primary products, while benzene is essentially a secondary product. As these authors pointed out, hexenes as well as dienes and trienes are precursors for benzene on Pt [68,69]. A comparison of the observed trends on the different catalysts clearly shows that Pt is much more efficient in converting hexenes to benzene when supported on KL than

when supported on SiO_2 or Mg(Al)O, but this ability is greatly reduced in the presence of sulfur. In previous work, conducted at conversions higher than 5%, benzene seemed to be a primary product [57]. Our results show that, on Pt/KL, the conversion of hexene into benzene can only be noticed at very low conversions, i.e., < 4%. Therefore, in a well prepared Pt/KL, benzene may appear as a primary product while, in fact, it is secondary.

The trends presented in this work indicate that Pt on all supports undergo the n-hexane dehydrogenation very easily. The exceptional aromatization activity of Pt/KL must then be explained in terms of its ability to convert hexene into benzene. To explain this one may refer to the interpretation of Iglesia et al. [19,20] who ascribed the high aromatization selectivity of this catalyst to its ability to resist coke formation. These authors have proposed that the high aromatization selectivity is intrinsic of clean Pt, and the role of the KL zeolite was to inhibit bimolecular interactions that lead to coke formation. In support of this interpretation, calorimetric studies conducted by Sharma et al. [70] indicated that Pt/K(Ba)L exhibited similar heats of adsorption as those over Pt on an inert support such as SiO_2. However, after the n-hexane aromatization reaction, the carbon deposition on Pt/K(Ba)L resulted in a much lower suppression of adsorption sites than on Pt/SiO_2. These results clearly demonstrated the ability of Pt/KL to resist deactivation by coke.

Based on this interpretation and the trends in product distribution discussed above one would conclude that, on Pt/SiO_2 or Pt/Mg(Al)O, the formation of coke would rapidly inhibit the Pt ability for converting hexenes to benzene. This coke,

however, would have a much lower effect on the dehydrogenation activity, causing the observed increase in hexene selectivity on these catalysts. This can be easily explained in terms of required ensemble size. It is well known that the addition of inert metals to clean platinum surfaces results in strong modification of the product distribution in the conversion of n-hexane. For example, when Au-Pt surface alloys were made on Pt (111) single crystals, large decreases in n-hexane aromatization and hydrogenolysis rates were observed [71]. These results demonstrate that the n-hexane aromatization reaction on Pt requires a relatively large ensemble of atoms. By contrast, the alkane dehydrogenation reaction is known to require a small number of metal atoms, perhaps as little as one [72], which would explain the resistance of the dehydrogenation function to deactivation. On the other hand, on KL the Pt particles would remain clean and conserve their aromatization capacity, consuming most of the hexene that is produced as a primary product.

In a recent TAP reactor investigation, Lafyatis et al. [13] have calculated turnover frequencies and selectivities for benzene formation on Pt/KL and Pt/Mg(Al)O. In that investigation they have found similar TOF and benzene/hexene ratios for both catalysts. However, since nonmicroporous catalysts lose their aromatization activity more quickly than microporous Pt/KL under reaction conditions due to coke formation, the TAP results conducted by sending small hydrocarbon pulses on a clean catalyst do not reflect the ability of the catalyst under reaction conditions. TAP reactors operate under conditions of Knudsen diffusion such that gas-phase collisions are minimized. Therefore, the effects of coking, which occur under reaction conditions, are deliberately suppressed.

The deactivation by sulfur requires further discussion. It has been proposed by McVicker et al. [25] and by Vaarkamp et al. [31] that, in the presence of sulfur, Pt particle growth is accelerated. Our TEM observations agree with those results but the EXAFS data did not show any metal particle growth. It is possible that the particle growth observed by TEM only reflects a growth of those particles located outside the zeolite channels, while the majority of the particles remain inside the channels and maintain a small size, even after 70 h in sulfur-containing atmosphere. The next important issue that needs to be discussed is the cause for the observed shift in benzene and hexene selectivities in the presence of sulfur. As mentioned in the previous section, the sulfided catalyst begins to behave as Pt/Mg(Al)O and Pt/SiO_2. One possible explanation is the migration of the metal particles from the interior of the zeolite channels to the outer surface [25,31]. That being the case, the metal particles in the outer surface would not be protected from coking and thus would lose their ability to aromatize the hexene. On the other hand, it is also possible that those particles remaining inside the channels may get partially poisoned by sulfur, even in minute concentrations, breaking up ensembles and losing their ability to aromatize [19]. The parallel trends observed in Fig. 3.12 for the drops in the production of benzene and methane are in line with these concepts. They indicate that both aromatization and hydrogenolysis require a relatively large ensemble of atoms to constitute the active site.

If one analyzes the trend shown in Fig. 3.11 for the hexene yield as a function of time on stream, one can see that, in the first run, the effect of coke alone results in a relatively rapid increase in hexene production followed by a long

stability. This can be interpreted by a rapid coking of the Pt particles outside the zeolite. These coked particles would remain active only for hexene production while those inside continue making hexenes, which are rapidly converted to benzene.

In the second run, the combined effect of coke and sulfur would result in:

a) an initial increase in hexene yield due to the coking of those particles outside the zeolite, and
b) a longer-term increase in hexene production that could be due to two possible phenomena (i.e., slow migration of Pt particles which subsequently get coked or slow sulfur poisoning inside the channels of the zeolite).

In both cases, the effect would be the same, a slow increase in hexene production and a decrease in benzene production. In a recent paper, Paal et al. [73] have shown that while clean Pt blacks are active for n-hexane aromatization, they completely lose their aromatization activity after sulfidation treatments. After that treatment, only hexenes were observed as products. A similar behavior was observed on carbonized Pt blacks. These results fully agree with the proposal that both, increased coke deposition on Pt outside the zeolite and sulfur poisoning are responsible for the deactivation of Pt/KL. The lower sensitivity to sulfur exhibited by the Pt/Mg(Al)O is also consistent with the proposed explanation. On this catalyst, the Pt particles do not have the protection of the microporous structure existing in the Pt/KL catalysts and, therefore, are rapidly poisoned by coke, even in the absence of sulfur. The addition of sulfur only causes a small additional deactivation. Regarding the potential of Pt/Mg(Al)O as a practical catalyst, its lower sensitivity to sulfur may not be enough to compensate for the low activity and selectivity that the catalyst has with or without sulfur.

A different interpretation has been recently offered by Fukunaga and Ponec [32]. They have proposed that the presence of K^+ inside the channels of the zeolite is responsible for the enhanced aromatization activity. This hypothesis has been supported by an increased aromatization observed when K^+ was added as a promoter to a Pt/SiO_2 catalyst and it was followed by the conclusion that the effect of sulfur was not to poison the Pt, but rather to poison the K^+, and making it lose its promoting effect. The fact that not only the benzene production, but also the methane formation rate, are greatly affected by the presence of sulfur (Fig. 3.12) would contradict this hypothesis, unless K^+ is also a promoter for hydrogenolysis. In fact, Zaera and Somorjai [74], have found that the hydrogenolysis selectivity on Pt(111) increases by addition of K^+, although the hydrogenolysis rate decreases, as could be expected in a reaction that requires a large ensemble.

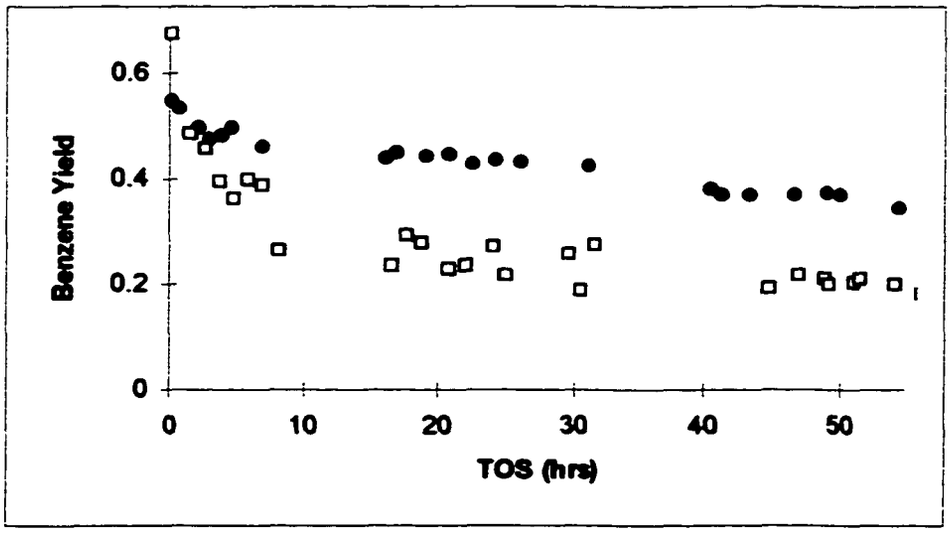

Figure 3.15. Comparison of Pt/KL catalyst prepared by IWI (Open Squares) and VPI (Full Circles).

3.5 CONCLUSIONS

In summary, this chapter has demonstrated that Pt/KL has a much higher activity and selectivity than Pt/Mg(Al)O or Pt/SiO_2 catalysts. It can be concluded that the basicity of the support alone cannot explain the high performance of Pt/KL catalysts for aromatization. The presence of hexenes, products that are generated in the reaction as precursors for benzene, is an indication of the loss of aromatization activity. This loss may be brought about by the presence of a significant fraction of the metal particles outside the zeolite channels or by the partial poisoning of the metal surface. In most cases, these two phenomena are interconnected since the Pt particles outside the channels of the zeolite are more susceptible to coke formation and are rapidly deactivated. In the presence of sulfur, some accelerated particle growth is observed. However, the pronounced deactivation may also be due to the deposition of small amounts of sulfur on the Pt particles outside and inside the zeolite, which effectively block and deactivate the large ensembles required for aromatization and hydrogenolysis. As a result, the selectivity to hexenes increases as the catalyst deactivates.

The IWI technique used is not the optimal preparation method for Pt/KL catalysts, because the resulting catalyst is heterogeneous and some large clusters remain outside the pores of the zeolite. These larger clusters are more active for hydrogenolysis than are those found on Pt/Mg(Al)O. Better Pt/KL catalysts can be prepared by vapor phase impregnation methods, resulting in more homogeneous distributions of small Pt clusters inside the channels of the zeolite. These catalysts

result in decreased hydrogenolysis activity and remarkably higher aromatization activity.

SPECIAL ACKNOWLEDGEMENTS

This work is the result of a collaborative effort of the OU Heterogeneous Catalysis Group. I would like to thank our postdoctoral researchers Dr. Cristina L. Padro (INCAPE) and Dr. Haiyang Liu for their help in the preparation of catalysts, especially the Pt/Mg(Al)O. Also, I would like to acknowledge Dr. Padro again for her work with EXAFS analysis, Greg Strout (OU S.R. Noble Electron Microscopy Laboratory) for his assistance with the TEM experiments, and Dr. Walter E. Alvarez (INTEMA) for helpful discussions. I would also like to thank the Oklahoma Center for the Advancement of Science and Technology (OCAST) for funding and NSF for my GRT traineeship, and Phillips Petroleum for a scholarship. Finally, I would like to thank personnel at Brookhaven National Laboratory, especially Syed Khalid, for help with EXAFS experiments.

CHAPTER IV: THE ROLE OF THE MORPHOLOGY OF Pt CLUSTERS

Two series of Pt/KL catalysts with varying metal loading were synthesized by the methods of incipient wetness impregnation (IWI) and vapor phase impregnation (VPI) to compare the effects of the different morphologies that result when the metal loading and, in particular, the preparation method are varied. Catalysts were characterized by a variety of techniques. For both preparation techniques, TEM and FTIR of adsorbed CO results indicated that the majority of particles are located inside the channels of the L-zeolite. In agreement with recent studies, the DRIFTS results displayed the formation of Pt carbonyls giving evidence of the existence of very small particles. EXAFS and TEM showed that the VPI catalysts resulted in smaller particles than the catalysts prepared by the IWI method. In addition, EXAFS demonstrated for this series a higher degree of interaction with the L-zeolite framework oxygen atoms. Pulse testing of the methylcyclopentane (MCP) ring opening showed that the very small clusters produced by the VPI preparation did not result in collimation of the MCP molecule, implying that the reactants and products could easily diffuse over the cluster. This is in contrast with the particles produced by the IWI method, which clearly displayed a collimation effect. The characteristic morphology produced by the VPI method was found to improve the performance of the catalyst under clean and sulfur poisoned conditions, enhancing the catalyst's resistance to the formation of coke and decreasing the particle agglomeration rate.

4.1. INTRODUCTION

The relationships between the structure and properties of the Pt/KL zeolite catalysts have attracted the attention of researchers for almost two decades. Although their exceptionally high activity and selectivity for the aromatization of n-hexane to benzene are nowadays well established [1-3, 30,57] the fundamental reason for these unique properties is not completely understood [4, 75], and are outlined in Section 1.5.

Despite the different interpretations found in the literature about the fundamental reason for the high activity and selectivity, most authors agree that an effective Pt/KL catalyst should have as much Pt as possible inside the channels of the zeolites [24,50]. However, even when most of the particles reside in the zeolite, different particle sizes and shapes could result. Obviously, if the Pt particles are located inside the zeolite, they must be smaller than the channel dimensions (i.e., lobe-shaped cages : 1.1 nm in diameter, 0.6 nm in length, apertures of 0.71 nm. [9]). However, it is not known what morphology they may adopt and what fraction of the channel may be blocking. The information obtained from EXAFS varies significantly with different preparation and pretreatments. For example, several studies have reported average coordination numbers of about 4 [65,76]. The correspondence between coordination number and number of atoms in the particle strongly depends on the assumed morphology of the metallic particle. For spherical morphology in an FCC metal, a coordination number of 4 would correspond to 5 atoms. However, this number may represent as many as 12 atoms if the morphology is that of a (111) disk [77]. Other studies on Pt/KL catalysts have

reported coordination numbers between 5 and 6, which in spherical morphology would correspond to 15-20 atoms [21]. One might wonder whether these differences could significantly affect the catalytic behavior. In other words, the question that remains unanswered is whether there is a particle morphology effect, even when most of the particles are inside the zeolite.

To address this question, we investigated two series of Pt/KL catalysts, with varying Pt loading, prepared by two different methods. Our goal was to have the majority of the Pt particles inside the zeolite, while varying their location distribution and morphology. Therefore, we kept the metal loading at or below 2.5 wt % and used two different preparation methods. The first method was the standard incipient wetness impregnation (IWI), which is the preparation preferred in most studies on Pt/KL catalysts [64]. The second method was the vapor phase impregnation (VPI), as discussed in Section 2.2.3.

We anticipated that these two families of catalysts would only exhibit small variations in microstructure. Therefore, in order to properly characterize these variations, we used a combination of techniques, including EXAFS, DRIFTS, TEM, hydrogen chemisorption, and probe reactions. We attempted to obtain a detailed description of the microstructure of these catalyst series and analyze the consequences of the subtle differences observed on catalytic behavior (aromatization activity, selectivity, and deactivation).

4.2 EXPERIMENTAL

4.2.1 Catalyst Preparation

The K-LTL zeolite (series TSZ-500, BET area 292 m^2/g, SiO_2/Al_2O_3 ratio = 6) was provided by Tosoh Company. Before addition of the metal, the K-LTL zeolite was dried in an oven at 110°C for twelve hours and calcined at 400°C for 5 h. The incorporation of the platinum was realized by two different methods - IWI and VPI, as described in Chapter 2.

The 1% Pt/SiO_2 catalyst used as a reference material was prepared by incipient wetness impregnation on a silica gel support (from W. R. Grace, grade 923, surface area 450 m^2/gr), using an aqueous solution of $H_2PtCl_6.xH_2O$ from Aldrich and a liquid/solid ratio of 0.63 cm^3/g. The sample was first dried overnight at room temperature and then during 8 h at 110°C. Finally, it was calcined in flow of air at 350°C for 2 h and reduced at 500°C for 2 h under flow of H_2.

The Pt loadings present in each sample were measured by inductively coupled argon plasma (ICP) analysis after complete dissolution of the samples in aqua regia/HF solution at Galbraith Laboratories. In all cases, the measured loading was practically the same as the corresponding nominal loading. In the paper, the catalysts are identified according to the method of preparation and nominal Pt loading, e.g., IWI-1 representing the sample prepared by incipient wetness impregnation with 1 wt % Pt.

4.2.2 Catalyst Characterization

Hydrogen chemisorption measurements, transmission electron microscopy (TEM) imaging, and infrared spectroscopy of adsorbed CO, were obtained according to procedures outlined in Chapter 2. EXAFS measurements on in-situ-reduced samples were taken at the National Synchrotron Light Source (NSLS) at Brookhaven National Laboratory and analyzed according to Section 2.3.4. Before each measurement, the catalysts, previously reduced ex-situ at 500°C, were re-reduced in situ at 300°C (heating ramp of 10°C /min) for 30 min in flowing H_2.

4.2.3 Catalytic Activity

The methylcyclopentane ring opening (MCP-RO) was employed as a test reaction in a pulse microreactor. In each run, 0.025 g of sample was placed in a Pyrex reactor, reduced in-situ at 500°C, and cooled to the reaction temperature, which varied from 260 to 350°C. At each reaction temperature, three consecutive 100 μl-pulses, containing 6.46×10^{-7} moles of MCP were sent over the catalyst. The products were analyzed in a Hewlett Packard 5890 chromatograph, equipped with a flame ionization detector (FID) and a packed column 30% DC200 – Chromosorb 60/80 P AW from Alltech.

In all runs, the main products detected were 2MP, 3MP, and hexane, with only small amounts of C_1-C_5 products and benzene. On the same system, the n-hexane aromatization reaction was also studied in the pulse-mode operating at 450°C and 500°C, using in this case 100 μl-pulses containing around 6.57×10^{-7} moles of n-hexane. As in the previous case, the carrier gas was hydrogen.

At the same time, steady-state reaction tests were conducted on continuous-flow reactors, according to Section 2.4.1. In all experiments, the hydrogen/n-hexane ratio was kept at 6. Prior to reaction, the catalyst was slowly ramped in flowing hydrogen at 100 cm^3/(min.g cat.) for two hours to a temperature of 500°C and reduced in situ at 500°C in flowing hydrogen at 100 cm^3/(min.g cat.) for one hour. All reactions were conducted at 500°C at a WHSV of 10 h^{-1}, so that the deactivation could be examined after relatively short periods of time on stream.

4.3 RESULTS

4.3.1 Catalyst Characterization

4.3.1.1 XANES/EXAFS

X-ray absorption spectroscopy continues to be one of the most powerful techniques available to characterize a series of samples like the ones we investigated, which only exhibited very subtle differences. The XANES spectra for the two catalyst series at the Pt L_{III}-edge, together with that of a Pt foil, are shown in Fig. 4.1. No significant shifts were found in the absolute edge positions, so all edges were zeroed to the inflection point. It is clear that the structures of Pt L_{III}-edges were very similar for all the Pt/KL catalysts, regardless of Pt loading or preparation method. The spectra were displaced in the figure for the sake of clarity, because when plotted together, they almost fell on top of each other.

Moreover, only little differences were detected in XANES between the catalysts and the Pt foil. A slight broadening of the Pt white line, typical of highly

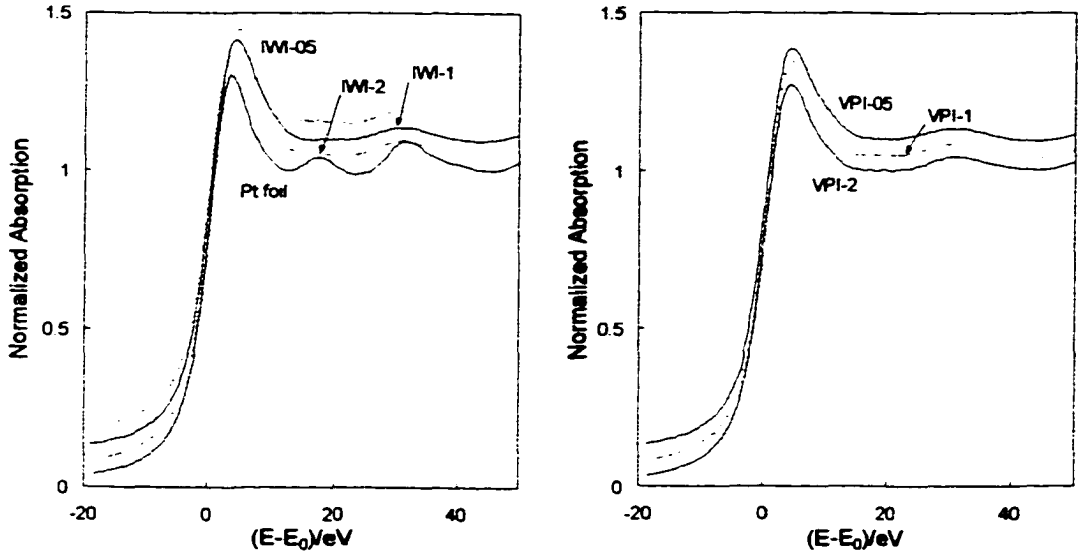

Figure 4.1. XANES spectra of Pt L_{III}-edge. (a) Pt foil and IWI series, (b) VPI series obtained at liquid nitrogen temperature.

dispersed supported metallic particles in the presence of H_2 [78], was observed for all the Pt/KL catalysts in comparison to the foil. Thus, analysis of the XANES spectra suggested that the electronic state of the Pt clusters was not significantly different from one series to the other.

In order to obtain further insight into the structure of the Pt clusters, a detailed EXAFS analysis of both catalyst series was conducted. The magnitudes of the Fourier transforms (FT) of the k^3-weighted EXAFS spectra, filtered from 3.5 to 13.5 $Å^{-1}$ are shown in Fig. 4.2.

From the inspection of this figure, it is clear that the morphology of the metallic particles may indeed vary for the two series. While the FT of the catalysts with 2 wt% Pt (IWI-2, VPI-2) look very similar and are typical of metallic Pt, they

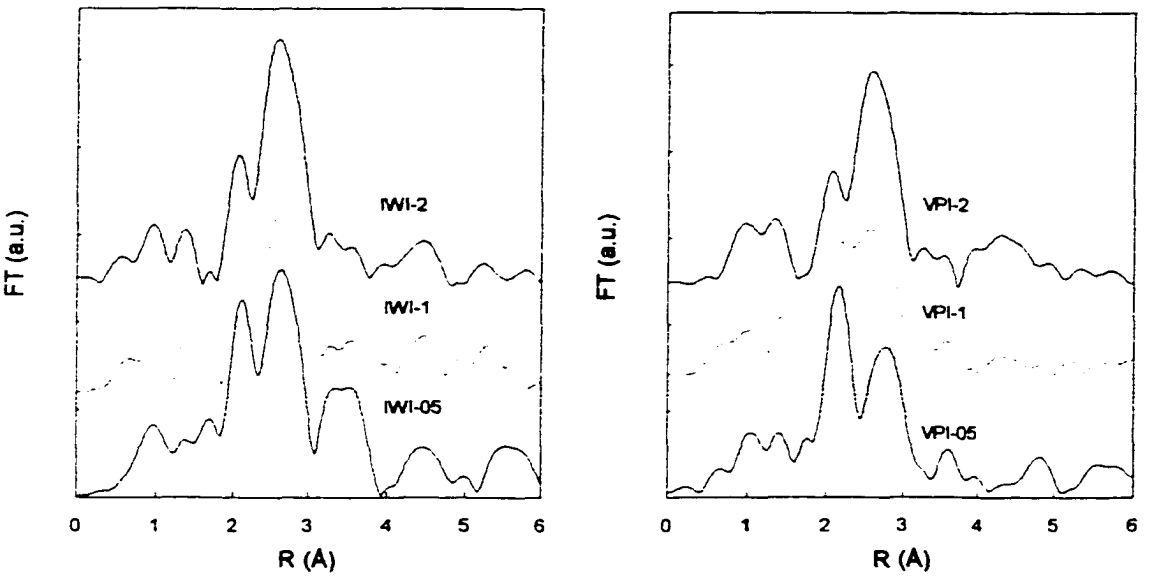

Figure 4.2. Fourier Transforms corresponding to the k^3-weighted Pt L_{III}-edge EXAFS spectra obtained at liquid nitrogen temperature on in-situ reduced Pt/KL catalysts. (a) IWI series, (b) VPI series.

significantly change as the Pt loading decreases. In fact, the FT of IWI-2 and VPI-2 exhibit a main peak at approximately 2.60 Å and a satellite peak at around 2.05 Å, which is normally observed for bulk Pt when the FT has not been corrected for the amplitude and phase shift of Pt [79]. As the metal loading decreased in the series, the relative intensity of the satellite peak increased significantly. As shown in the figure, for the VPI-05 catalyst, the intensity of this satellite peak was even higher than that of the main peak. An increase in the relative intensity of the satellite peak seems to reflect that the environment of Pt was not only constituted solely by Pt atoms. This trend would indicate that the structure of the Pt clusters was strongly modified as the Pt loading decreased. This modification is particularly strong for the lowest loadings and for the series prepared by vapor phase impregnation.

The structural parameters from the EXAFS data were determined by a fitting procedure. An inverse Fourier transform was applied over a restricted range of r, 1.3-3.7 Å, isolating the EXAFS contribution of the first coordination sphere of platinum. According to the Nyquist Theorem [80] and the EXAFS specific modifications described by Stern [81], the maximum number of parameters that could be used to describe the EXAFS function was given by the following equation:

$$n_{max} = 2\Delta k \Delta r/\pi + 2$$

Therefore, the use of the seven parameters to fit our data was statistically justified, since for the k and r ranges employed in this work, the Nyquist criterion would allow up to 17 parameters. The filtered data were fitted using the FEFFIT program [82]. In a first approach, the data were fitted with one Pt-Pt shell, using theoretical standards generated by the FEFF software [54-56]. Although the fits obtained with only one coordination could be considered satisfactory for the catalysts with 2% of Pt (IWI-2 and VPI-2), poor fits were obtained for the other samples with lower metal loading. Therefore, new fittings including a second Pt-O shell were performed. Theoretical amplitudes and phase shifts corresponding to the Pt-O distances were derived with FEFF, assuming Pt-O bonds at 2.56 Å. These "long Pt-O distances" were previously reported by Koningsberger et al. [31,83] for Pt particles inside the channels of the KL zeolite, corresponding to distances between Pt and the zeolite lattice oxygen atoms. The addition of Pt-O distances in the first coordination sphere of Pt greatly enhanced the quality of all fits. However, for the samples with the lowest metal loadings the fits were less satisfactory, indicating that the structure of the smallest Pt particles may be even

more complex. The structural parameters resulting from the fits with two shells, Pt-Pt and Pt-O distances, are summarized in Table 4.1.

Table 4.1. Structural parameters determined from EXAFS analysis.

Catalyst	ΔE_0 (eV)	Pt-Pt distance			Pt-O distance		
		N	R (Å)	σ^2 (Å^2)	N	R (Å)	σ^2 (Å^2)
IWI-2	5.2	4.5	2.73	0.0058	0.3	2.60	0.0041
IWI-1	3.8	3.9	2.73	0.0058	0.4	2.57	0.0060
IWI-05	-0.9	3.9	2.71	0.0049	0.6	2.56	0.0060
VPI-2	6.0	4.0	2.73	0.0058	0.4	2.59	0.0033
VPI-1	3.6	3.0	2.72	0.0058	0.6	2.58	0.0043
VPI-05	1.7	2.6	2.72	0.0048	0.8	2.56	0.0055

A slight contraction of the Pt-Pt distances compared to that of bulk Pt is observed for all samples. Such a distance contraction had already been reported for highly dispersed systems [50]. As previously proposed, the "long Pt-O distances" gave evidence for the interaction between zero-valent Pt atoms and the support, probably having the presence of H_2 in the interfacial layer between the Pt particles and the support [84].

The evolution of the calculated Pt-Pt and Pt-O coordination numbers as a function of the metal loading is represented in Fig. 4.3 for the two preparation series. Clear trends are observed, indicating an increase in Pt-Pt coordination and a decrease in Pt-O coordination as the metal loading increases. Two different morphologies have been suggested in the literature for metal clusters inside the channels of the zeolite with coordination numbers as low as those reported here [77,85]:

i) Small spherical clusters consisting of 6 to 10 Pt atoms, with a Pt-Pt coordination number between 4 to 5 and a low metal-support coordination, i.e., low Pt-O coordination.

ii) Pt spread on the support, forming small Pt "rafts". In this morphology the Pt-Pt coordination significantly decreases and the Pt-O coordination increases.

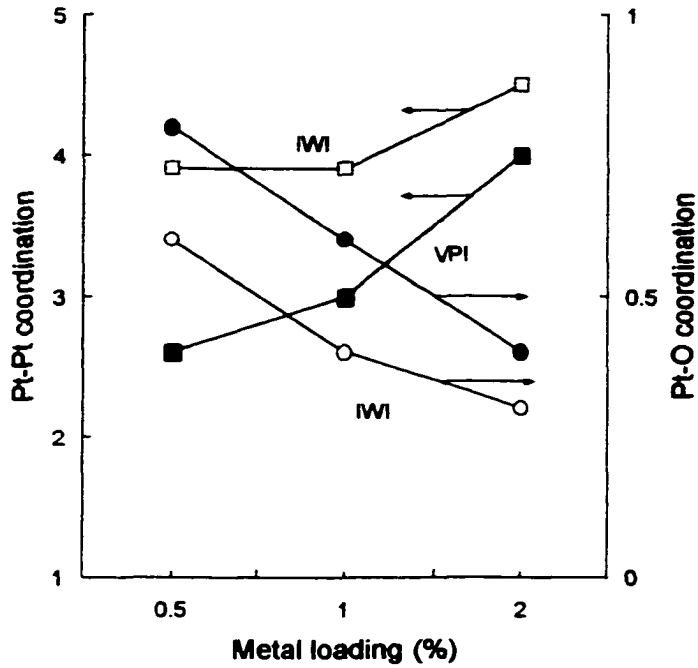

Figure 4.3. Evolution of the Pt-Pt and Pt-O coordination numbers obtained from the EXAFS analysis as a function of the metal loading for IWI and VPI series.

From the above EXAFS results, it seems that, for a fixed metal loading, the VPI method leads to a higher population of Pt clusters small enough so all their atoms are in close proximity to the zeolite walls. This is reflected by decreased Pt-Pt coordination and increased Pt-O coordination for the VPI series compared to the IWI series. Within each series, the fraction of atoms interacting with the walls increases with decreasing metal loading.

In agreement with the EXAFS data that reflect a very high metal dispersion for all the catalysts in the series, hydrogen uptakes measured by volumetric chemisorption resulted in high H/Pt values, ranging from 1.2 to 1.8. In previous studies, it was shown that calcination of Pt/KL catalysts at temperatures above 400°C resulted in particle growth and channel blocking that lead to large decreases in chemisorption capacity [18]. Those large chemisorption losses were obtained when the catalysts were calcined at high temperatures prior to the reduction treatment. Here, we have compared the effect of re-calcining the IWI-1 and VPI-1 samples at 500°C after the initial low-temperature calcination and reduction. It was observed that, while the catalyst prepared by incipient wetness impregnation exhibited a large loss in chemisorption capacity after re-calcination (about 30%), the one prepared by vapor phase impregnation had a very modest loss (15 %). We will identify these re-calcined catalysts as RC-IWI-1 and RC-VPI-1, respectively.

4.3.1.2 Transmission Electron Microscopy

The TEM observations agreed very well with the EXAFS and hydrogen chemisorption data, which indicated a very high degree of metal dispersion. Only on the 2% Pt samples, Pt particles outside the zeolite were detected. Images of the IWI-05 and VPI-05 catalysts are shown in Fig. 4.4. The zeolite channels are very clearly seen, some of them containing very small particles. The sample prepared by IWI exhibited some particles that appeared to partially fill the diameter of the channels. However, they were not present in the VPI sample, in accordance with the EXAFS data, which indicated a significantly higher ratio of (Pt-Pt)-to-(Pt-O) coordination for

the IWI-05 catalyst than for the VPI-05. If the particles are very small and perhaps raft-like in the VPI-05, one may not expect to see them by TEM.

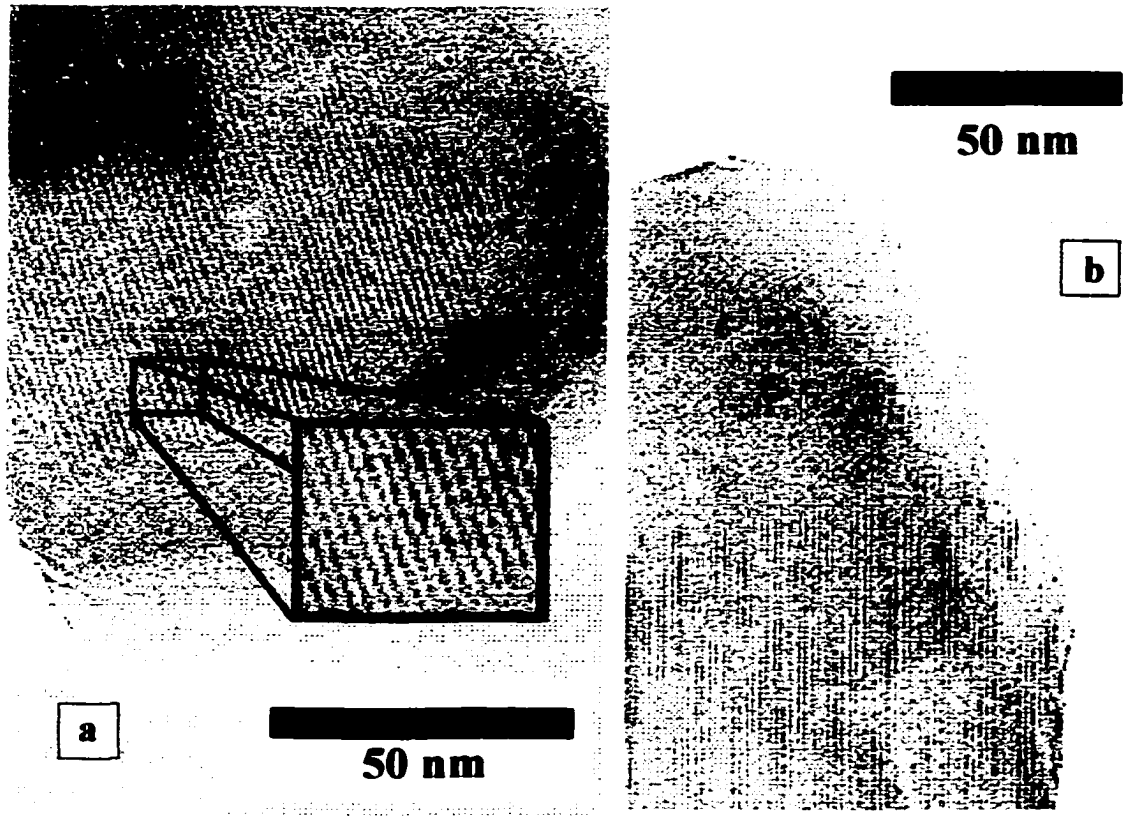

Figure 4.4. TEM micrographs of Pt/KL catalysts calcined at 350°C and reduced at 500°C. (a) IWI-05, (b) VPI-05.

4.3.1.3 DRIFTS of adsorbed CO

FTIR of adsorbed CO has been widely employed to characterize Pt/KL catalysts. Typically, the IR spectrum obtained with Pt/KL catalysts is much more complex than that normally observed on Pt/SiO_2. In most FTIR studies of CO adsorption on Pt/KL a series of bands between 2080 and 1950 cm^{-1} has been observed. The different bands have often been ascribed to various degrees of metal-zeolite interaction [86]. Our results were similar to those typically observed before.

For example, the DRIFTS spectra of CO adsorbed at room temperature over the IWI series are shown in Fig. 4.5.

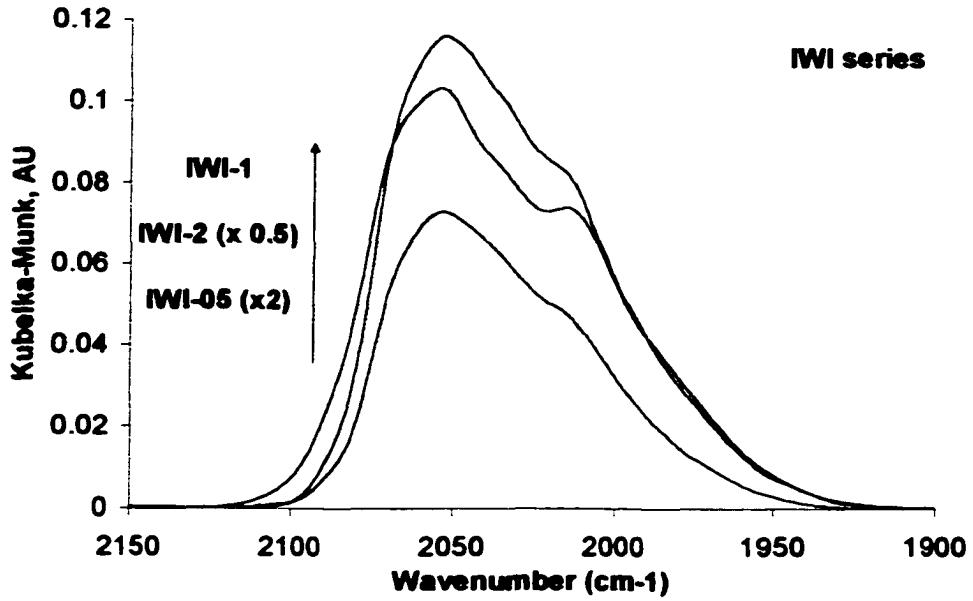

Figure 4.5. DRIFTS spectra of CO adsorbed on Pt/KL IWI series. The reduced catalysts were exposed to a flow of 3% CO in He for 30 min at room temperature and purged in He for 30 min.

As the loading of Pt increased in the series the intensity of the bands increased, but there were no significant differences in the position or relative intensities. The VPI series (not shown) exhibited an equivalent trend, without significant changes in band positions. Therefore, although the EXAFS data indicated a varying degree of metal-zeolite interaction, and possibly, varying particle morphologies, the DRIFTS data did not give evidence for such variations.

On the other hand, the evolution of the IR bands as a function of time after introduction of CO presented interesting features that may explain why the final spectra look all alike, despite changes in Pt morphology. Such evolution of the bands as a function of exposure time is illustrated in Fig. 4.6 for the VPI-1 catalyst.

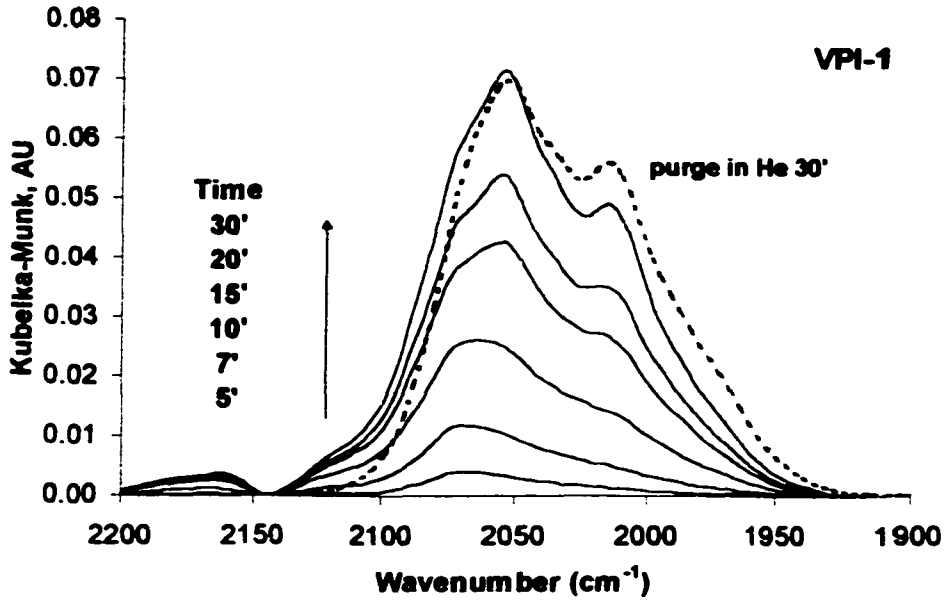

Figure 4.6. Evolution of DRIFTS spectra of CO adsorbed on VPI-1 as a function of exposure time. The reduced catalyst was exposed to a flow of 3%CO in He at room temperature and purged in He for 30 min (dotted line).

It can be seen that during the first few minutes a band developed, centered at about 2068 cm^{-1}. Only after 10 min, new bands started emerging at about 2057 and 2014 cm^{-1}. As discussed below, it seems that, during the exposure to CO, modifications of the sample occurred that were responsible for the appearance of the lower frequency bands. When the gas phase CO was removed by purging with He, the typical double bands corresponding to gas-phase CO quickly disappeared, and the band at 1970 cm^{-1} became more apparent.

Although DRIFTS did not show important differences for the freshly reduced catalysts, it did exhibit significant changes after poisoning with sulfur. Figs. 4.7 a and 7b compared the IR spectra of adsorbed CO after exposing the IWI-1 and VPI-1 catalysts to reaction conditions for 10 h with feeds containing 1 ppm and 10 ppm

sulfur. Interesting differences were observed. While the spectra for the IWI-1 catalyst showed a significant decrease in the region of the 2014 and 1970 cm^{-1} bands, the spectra for the VPI-1 only showed a modest change in this region. Below we will discuss this lower sensitivity to sulfur when we discuss the higher stability of the VPI

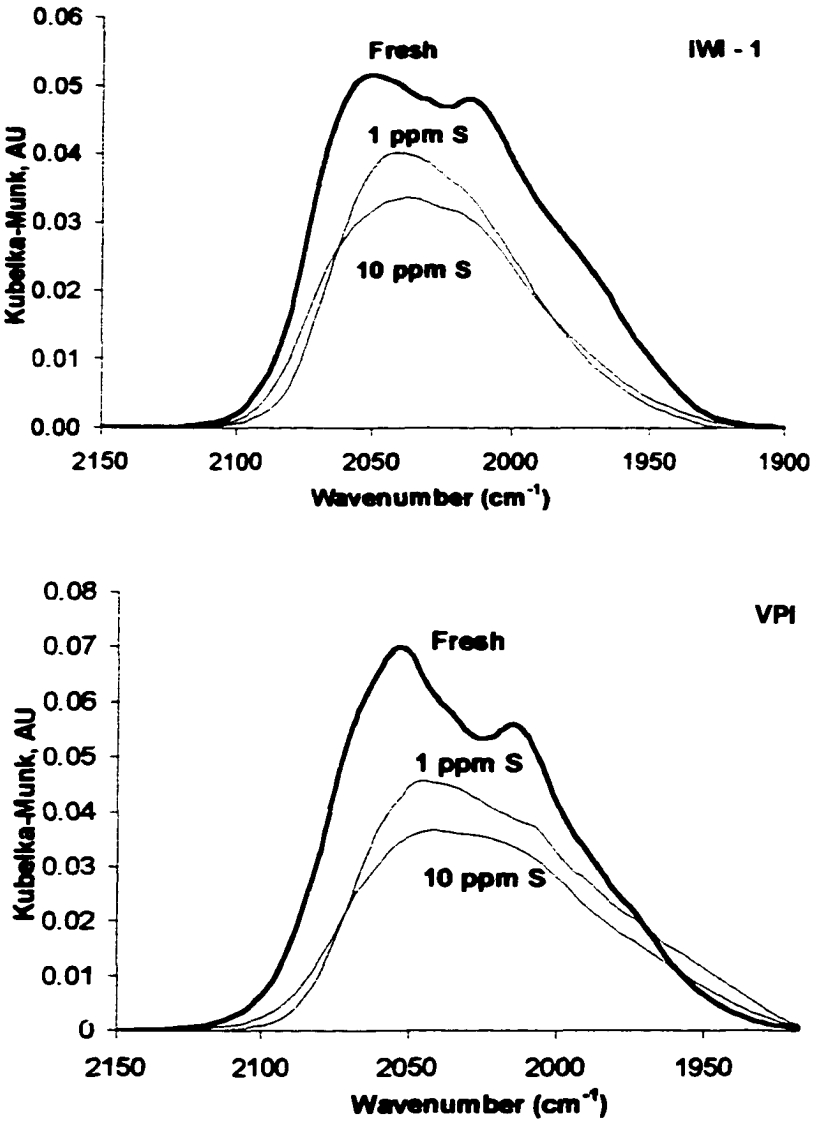

Figure 4.7. DRIFTS spectra of CO adsorbed on Pt/KL. The reduced catalysts were exposed to a flow of 3%CO in He for 30 min at room temperature and purged in He for 30 min. (a) IWI-1 fresh and poisoned catalysts. (b) VPI-1 fresh and poisoned catalysts.

series under sulfur.

Another set of samples that displayed meaningful variations in the DRIFTS spectra were the RC-IWI-1 and RC-VPI-1. As mentioned above, the re-calcination treatment caused a much less pronounced loss in hydrogen chemisorption on the catalyst prepared by VPI than on the one prepared by IWI. This difference correlated well with the IR spectra. As shown in Fig. 4.8 for the RC-IWI-1, the high temperature treatment caused the appearance of a clear shoulder at about 2084 cm^{-1} that we attributed to Pt particles which migrated to the outer surface of the zeolite during the high-temperature calcination. This assignment is in agreement with the very low 3MP/2MP ratio observed for these catalysts in the MCP-RO reaction. By contrast, the RC-VPI-1 sample did not show this band and was therefore more resistant to high temperature treatments. Similar resistance of catalysts prepared by VPI to oxidation/reduction thermal treatments has been previously proposed [49].

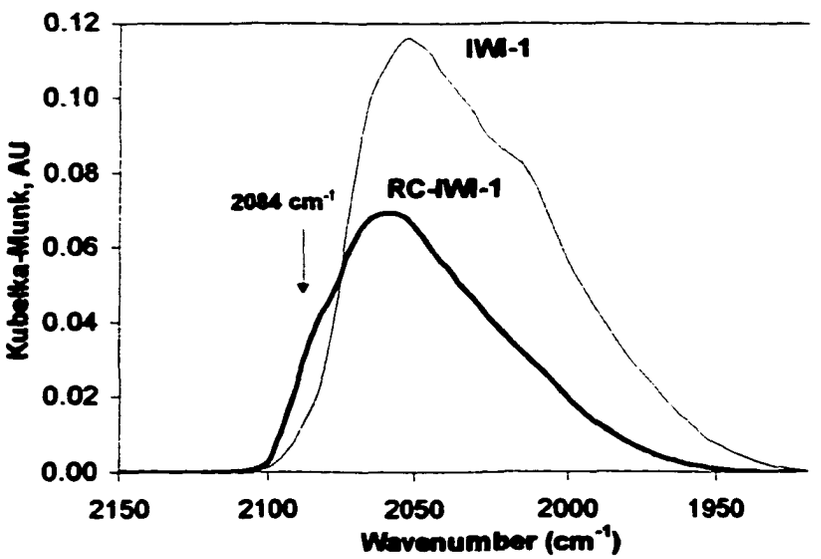

Figure 4.8. DRIFTS spectra of CO adsorbed on IWI-1 fresh and re-calcined at 500°C (RC-IWI-1). The reduced catalysts were exposed to a flow of 3%CO in He for 30 min at room temperature and purged in He for 30 min.

The study of the time evolution of the absorption bands on the RC-IWI-1 catalyst provided further insight on the nature of the species present during this experiment. As shown in Fig. 4.9, the features that immediately appeared were a band at 2084 cm^{-1} and another at 2068 cm^{-1}. During the CO exposure, the former did not shift while the latter shifted slightly. As opposed to the dramatic modification exhibited by the standard IWI-1 catalyst, the one re-calcined at 500°C, RC-IWI-1, did not show the appearance of any new absorption bands.

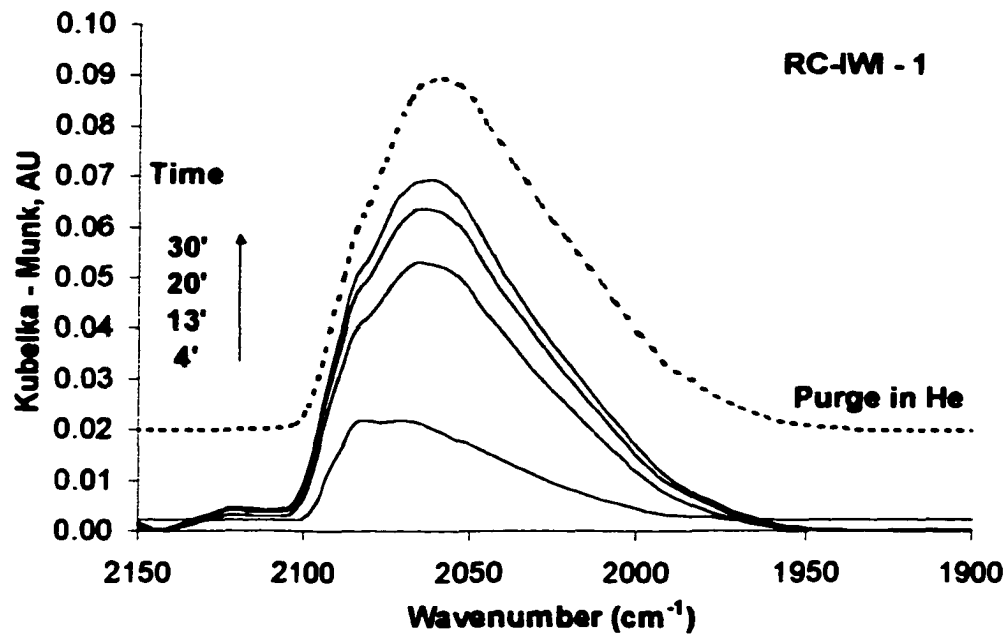

Figure 4.9. Evolution of DRIFTS spectra of CO adsorbed on RC-IWI-1 as a function of exposure time. The reduced catalyst was exposed to a flow of 3%CO in He at room temperature and purged in He for 30 min (dotted line).

4.3.2 Catalytic Activity Measurements

4.3.2.1 Methylcyclopentane Ring Opening in a Pulse Mode Reactor

The use of MCP ring opening to determine the existence of collimating effects was first recognized by Sachtler et al. [87-89] for the case of Pt on Y zeolite. The ring opening of MCP can occur on three different C-C bond positions, two in α

(yielding n-hexane), two in β (yielding 2MP), and one in γ (yielding 3MP). Therefore, the statistical distribution is n-Hex:2MP:3MP = 40:40:20. Due to the microgeometry of the system, it is expected that an incoming MCP molecule inside the pores of the zeolite will be preferentially oriented with its longer axis parallel to the direction of the pores. As a result, when a molecule encounters a metal particle inside the pores, opening in the γ position should be favored in comparison to opening in the two β positions. If that is the case, the resulting 3MP/2MP product ratio should be higher than the statistical value of 0.5. In previous work on Pt/KL catalysts prepared by IWI, earlier work has indeed found 3MP/2MP higher than on supports without microporosity. It was also observed that this ratio decreased when the Pt/KL catalyst had a large fraction of Pt particles outside the channels of the zeolite [27,28].

In this contribution, we have used this test reaction again to compare the two catalyst series. As illustrated in Fig. 4.10, the first difference exhibited by the two series was with respect to their hydrogenolysis activity. The IWI catalysts showed a significantly higher activity than the VPI catalysts for this reaction. As a result, different temperatures were needed in order to work at comparable conversions. We have chosen to represent the catalytic activity in terms of the temperature needed to reach 10% MCP conversion, because this way of presenting the data does not require extrapolations in temperature. In any case, a similar activity trend could be obtained if the conversion data were extrapolated to the same temperature. As illustrated in the figure, it was observed that the activity of the IWI-05 sample was comparable to that of the VPI series. By contrast, the higher-content IWI catalysts showed activities comparable to that of the Pt/SiO_2 catalyst.

As mentioned above, our main motivation to study the MCP ring opening on the two Pt/KL series was to analyze the 3MP/2MP product ratio, and compare it to

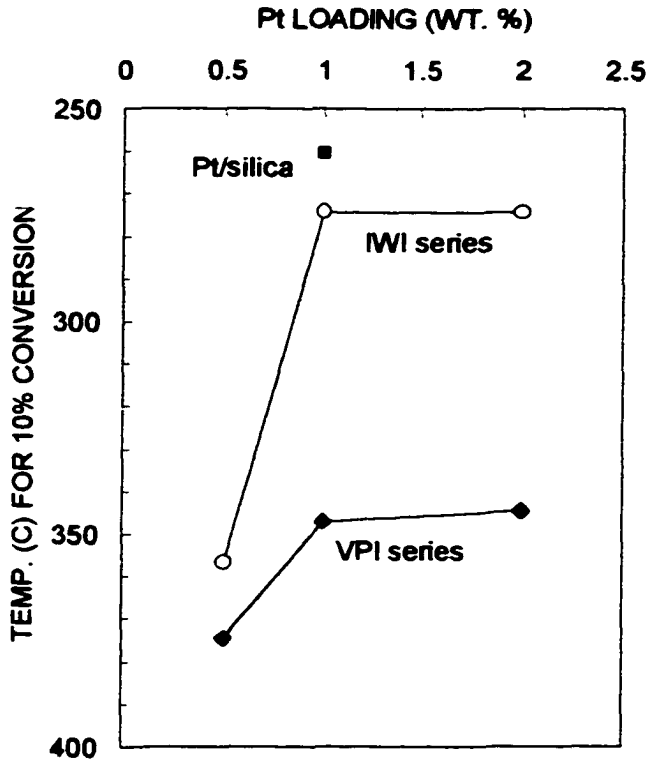

Figure 4.10. Hydrogenolysis activity expressed in terms of the temperature needed to reach 10% MCP-RO conversion as a function of the metal loading.

the 0.5 statistical value. It was observed that this ratio strongly depended on the catalyst, but varied little with temperature or conversion. Fig. 4.11 shows a comparison of the 3MP/2MP ratios obtained on the two series at the same overall conversion (10 %). A clear trend was observed. The higher loading IWI-1 and IWI-2 catalysts exhibited significantly higher 3MP/2MP ratios than the low loading IWI catalyst and the VPI series, as well as the silica-supported catalyst. The interpretation

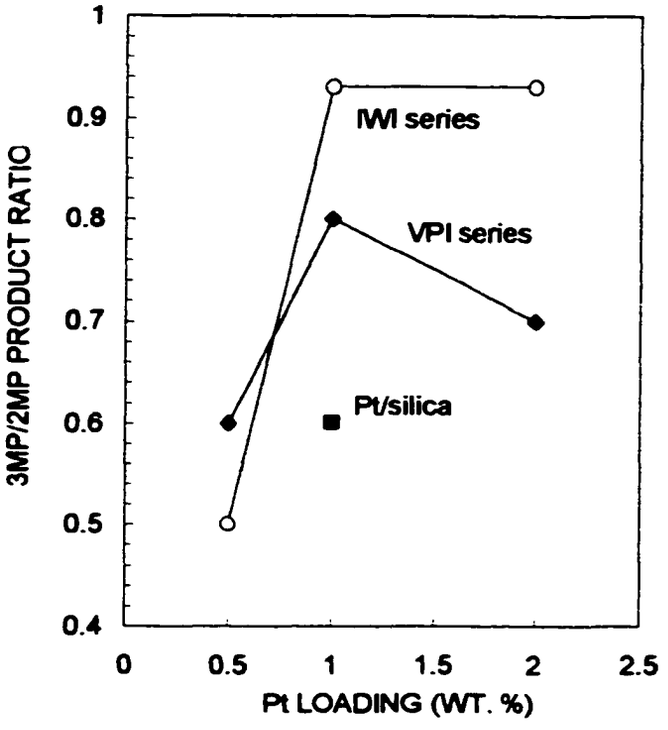

Figure 4.11. MCP ring opening selectivity obtained at the same overall conversion (10 %). 3MP/2MP ratio as a function of the metal loading.

that one can give to these results is that only the higher-loading Pt/KL catalysts presented a clear collimation effect. This effect was absent on the Pt/SiO_2 catalyst, which was reasonable, but it was also absent on the low loading IWI catalyst and the VPI series. This result was important and is further discussed below.

The MCP-RO reaction was also conducted on the RC-IWI-1 catalyst. As mentioned above, this sample, which was re-calcined at high temperature and reduced after the first calcination/reduction treatment, exhibited an absorption band at 2080 cm^{-1}, not observed on the standard IWI-1 sample. In this case, the MCP-RO activity was much lower than on the standard catalysts and the 3MP/2MP ratio was only 0.3. In previous work, we have indicated that this low 3MP/2MP ratio was typical of Pt

present in the form of large, well ordered particles [90]. These results indicated that the high temperature re-calcination treatment caused the agglomeration of particles outside the channels of the zeolite.

4.3.2.2 n-Hexane Aromatization in a Pulse Mode Reactor

The yields of benzene and hydrogenolysis products obtained in the pulse reactor are depicted in Figs. 4.12 a and 4.12 b as a function of Pt loading.

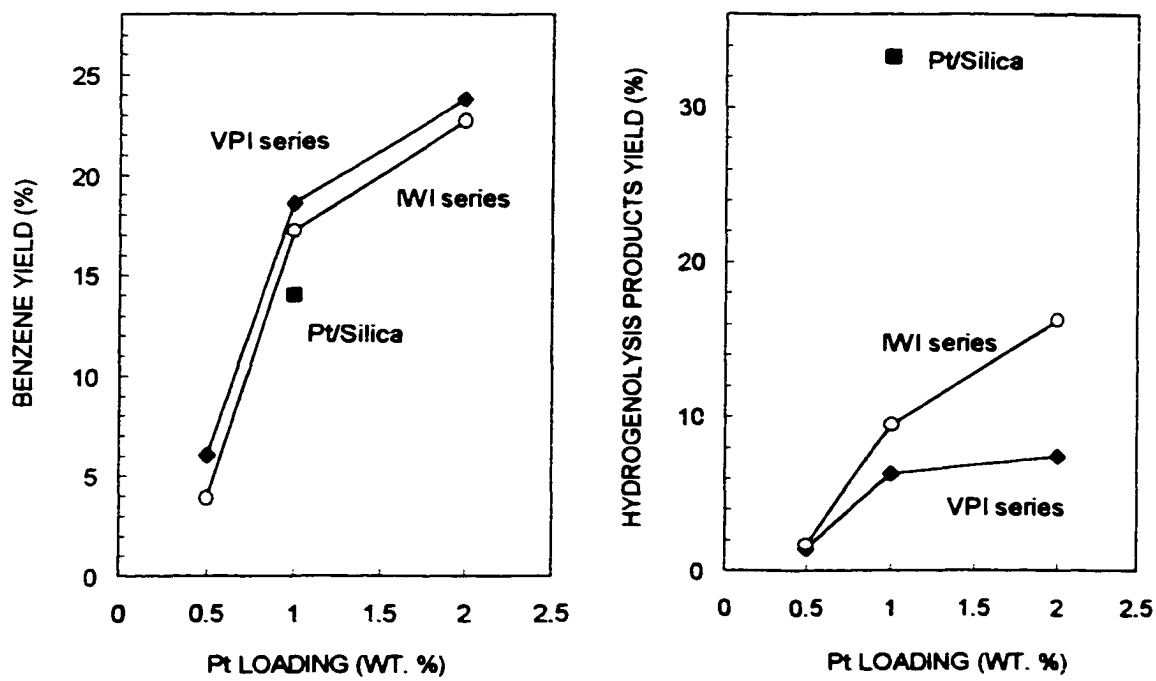

Figure 4.12. n-hexane aromatization (pulse mode) at 450°C for Pt/KL and Pt/SiO_2 catalysts. (a) Benzene yield as a function of Pt loading, (b) Hydrogenolysis yield as a function of Pt loading.

One must note here that, in the pulse mode, a small amount of n-hexane is passed over the catalyst under pure hydrogen. Therefore, particularly at the lower temperatures, the results represented the behavior of a clean catalyst. It is interesting to note that the observed benzene yields were only a function of the metal loading and

varied very little from one series to the other. Also, in agreement with earlier reports, in the absence of deactivation by coke, Pt supported on silica exhibited a benzene yield similar to that of the Pt/KL catalysts. When the pulse measurements were conducted at 500°C and the overall conversion increased, the silica-supported catalyst exhibited a lower benzene yield, which may be due to some degree of deactivation already present under these conditions. Although at 450°C, the benzene yields obtained in the pulse reactor showed little differences among the series, the undesired side reaction hydrogenolysis did exhibit significant differences among VPI, IWI, and silica-supported catalysts. The hydrogenolysis activity was highest for the 1% Pt/SiO_2 and lowest for the VPI series. Within each series, it increased with Pt loading.

As described in previous work, in addition to the hydrogenolysis (C_1-C_5) products, the main by-products observed during our flow reaction experiments were hexenes. Those experiments were conducted at 500°C and using a H_2:hydrocarbon ratio of 6:1. By contrast, in the pulse experiments conducted at lower temperatures and in excess hydrogen, which was used as a carrier, the main by-products were MCP, 2MP, and 3MP.

4.3.2.3 n-Hexane Aromatization in a Flow Mode Reactor

The two catalyst series exhibited significant differences in their deactivation patterns, both in the absence and in the presence of sulfur. Fig. 4.13a shows the variation of benzene yield as a function of time on stream over the IWI-1, VPI-1, and

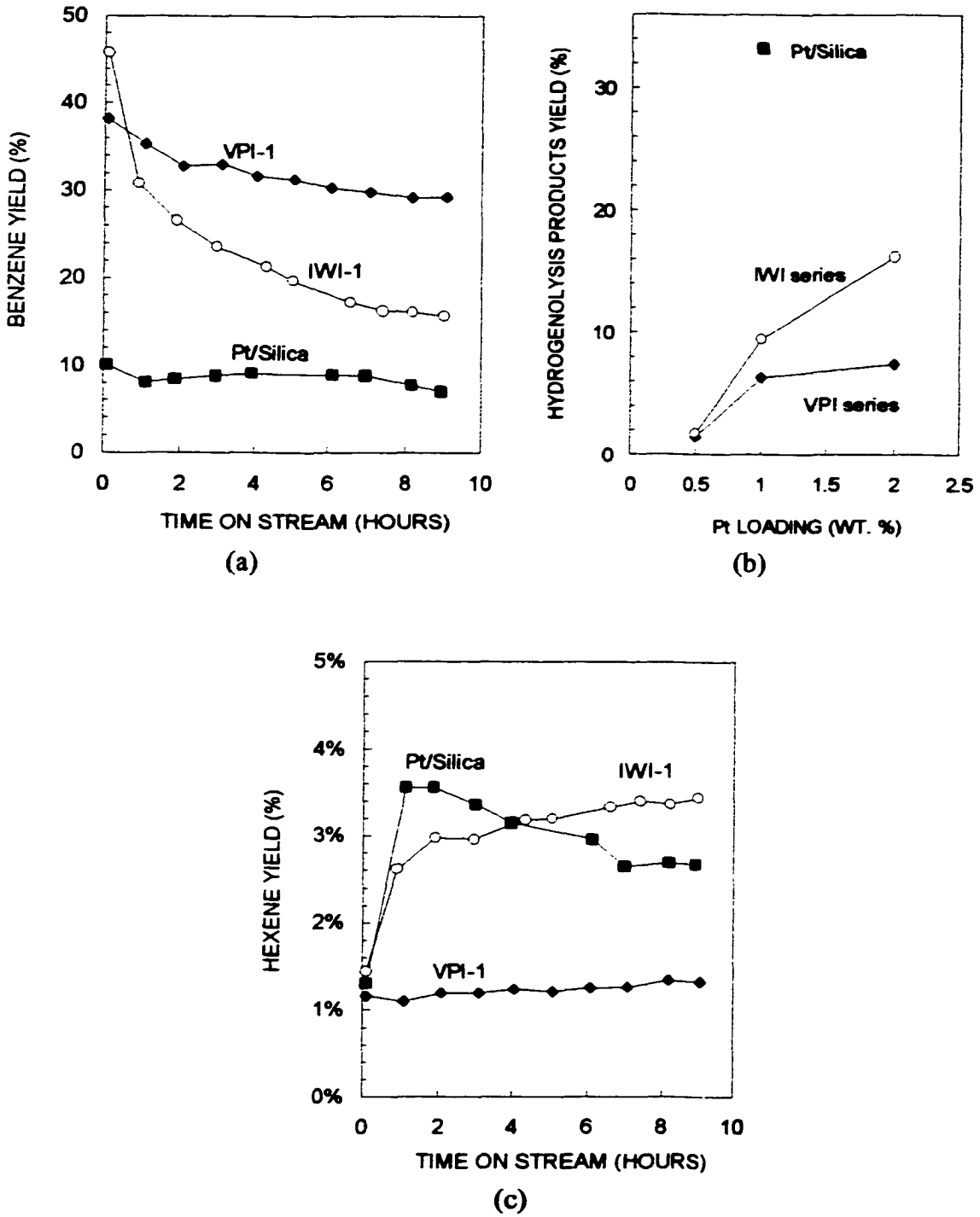

Figure 4.13. n-hexane aromatization (flow mode) at 500°C for Pt/KL and Pt/SiO_2 catalysts (WHSV: $10h^{-1}$). (a) Benzene yield as a function of time on stream, (b) Methane yield as a function of time on stream, (c) Hexene yield as a function of time on stream.

Pt/SiO_2 catalysts. It is clear that, in the flow experiments, the silica-supported catalyst deactivated so rapidly that, by the time the first experimental point was measured, it had already deactivated. It is interesting to compare these results with those of the pulse experiments. In that case, the benzene yield obtained on the Pt/SiO_2 catalyst was very similar to that obtained on the Pt/KL catalysts. In the flow-mode however its activity was much lower. Perhaps, the most important result to draw from this experiment is the dramatic difference in deactivation pattern exhibited by the two 1% loaded Pt/KL catalysts. In parallel with the lower hydrogenolysis activity presented in the pulse experiments, the catalyst prepared by VPI exhibited a much higher stability.

The differences exhibited in the benzene yields over the three catalysts correlated with similarly important differences in the generation of methane and hexenes. The evolution of methane and hexenes with time on stream are illustrated in Figs. 4.13(b) and 4.13(c). On the Pt/SiO_2 catalyst, the methane produced by hydrogenolysis was initially very high, which agreed well with the pulse experiments. However, it rapidly dropped in the flow mode as the catalyst deactivated. Simultaneously, the production of hexenes on this catalyst was considerable. On the Pt/KL catalysts, the more selective VPI-1 exhibited a very low production of either methane or hexenes.

In general, catalysts prepared by VPI resulted in higher aromatization selectivities, lower formation of hexenes, lower hydrogenolysis, and lower rates of deactivation. An accepted way to compare the performance of Pt/KL catalysts is using benzene selectivity vs. conversion plots. Fig. 4.14 summarizes the performance

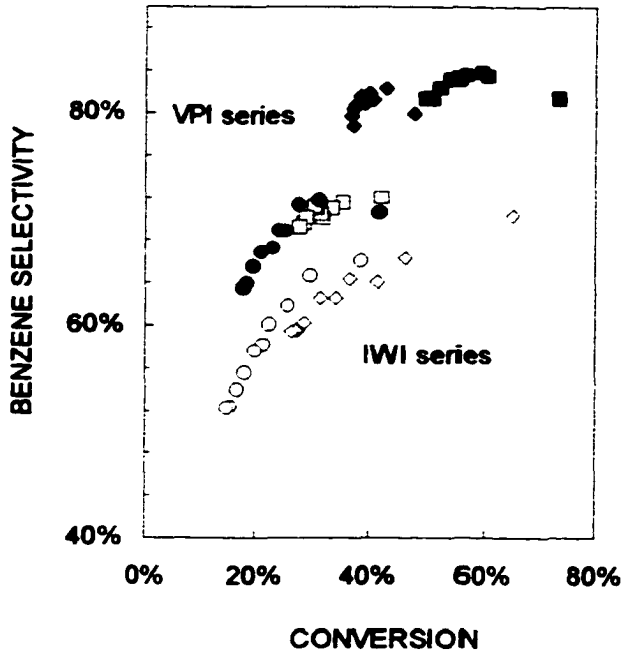

Figure 4.14. n-hexane aromatization (flow mode) at 500°C for IWI and VPI series (WHSV: $10h^{-1}$). Benzene selectivity as a function of the conversion. IWI series (open symbols) and VPI series (full symbols). Pt loading: 0.5% (circles), 1% (diamonds), 2.5% (squares).

of the catalysts in the two series. It is clear that the VPI series exhibited a better catalytic behavior than the IWI series and among the best ever reported in the literature (for a comparison see ref. [50]).

Finally, as illustrated in Fig. 4.15 a, the VPI catalysts displayed significantly higher aromatization activity in the presence of 1 ppm sulfur. When the sulfur content was increased to 10 ppm, both catalysts rapidly deactivated. It is interesting to note that although after 9 h under 10 ppm sulfur the aromatization activity was almost completely lost, the dehydrogenation activity was still relatively high. As shown in Fig. 4.15 b, the yield of hexenes was higher for the IWI-1, but after 9 h under 10 ppm S, the VPI-1 catalyst reached about the same yield of hexenes. This

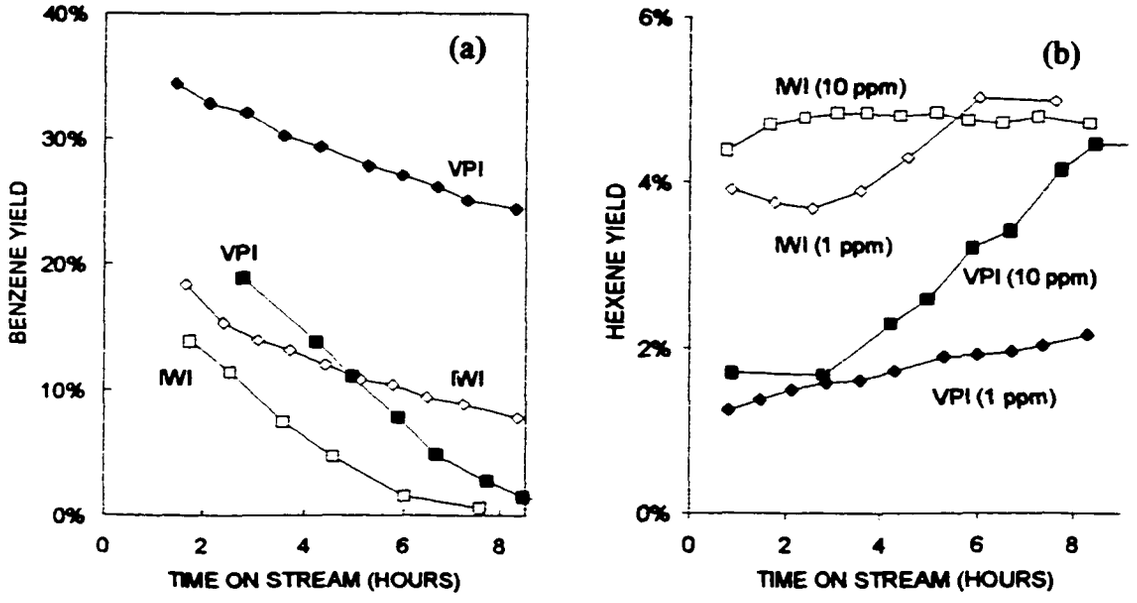

Figure 4.15. n-hexane aromatization (flow mode) in the presence of 1 ppm (diamonds) and 10 ppm (squares) sulfur at 500°C for IWI-1 (open symbols) and VPI-1 (full symbols) catalysts (WHSV: $10h^{-1}$). (a) Benzene yield as a function of time on stream, (b) Hexene yield as a function of time on stream.

result correlated well with the residual CO adsorption capacity of the two poisoned catalysts as shown in DRIFTS spectra depicted in Fig. 4.7 a and 4.7 b.

4.4 Discussion

As stated above, the aim of this work was to compare catalysts with most of the Pt particles in the interior of the zeolite, but with different morphology, and to try to relate these differences to the catalytic properties. Therefore, we will analyze first what we have learned from our detailed characterization and then the implications on the performance of the catalysts.

4.4.1 Catalyst Morphology

The EXAFS analysis has demonstrated that the VPI method resulted in a larger fraction of Pt clusters constituted by only a few atoms, and as a result they were in very close interaction with the zeolite walls. The MCP-RO results were combined with the EXAFS and DRIFTS data to draw an interesting picture. As mentioned above, only the higher-loading IWI catalysts presented high 3MP/2MP ratios. This ratio was lower, as expected, for the Pt/SiO_2 catalyst, which had no microporosity that would lead to collimation of MCP. However, this ratio was also low for the low-loading IWI and VPI catalysts. This low ratio was certainly not due to the massive presence of Pt particles outside the channels of the zeolite. DRIFTS data did not show for these catalysts larger absorption bands in the characteristic region around 2070 cm^{-1}. The fact that the ratio for the VPI catalysts is lower than that for the IWI-1 and IWI-2 is an indication that, for the IWI catalysts, the Pt particles may be large enough to partially block the path of the incoming MCP molecule, forcing the C-C scission to occur at the γ position. By contrast, on those catalysts with very small Pt particles, having a very small Pt-Pt coordination and relatively large Pt-O coordination, the collimation effect did not result in preferential cleavage in the γ position since the path of the MCP molecule was not impeded. These two different morphologies and their effect on MCP-RO are illustrated in the schematic representation shown in Fig. 4.16. The case of the VPI-2 catalyst deserves some further discussion. This catalyst exhibited almost the same Pt-Pt and Pt-O coordinations as the IWI-1, but yet the VPI-2 catalyst showed no collimation while

the IWI-1 did. To explain this apparent discrepancy one needs to realize that EXAFS provides average coordination numbers.

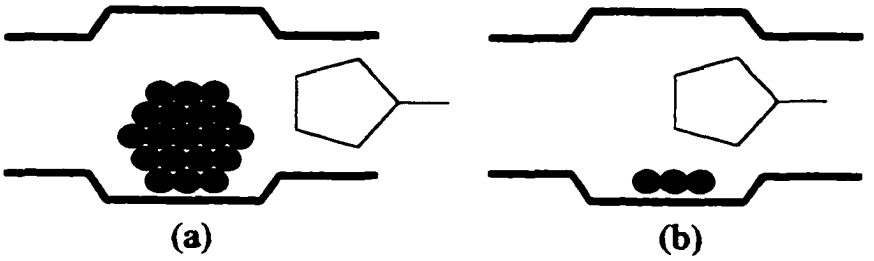

Figure 4.16. Schematic representation of Pt particles inside the pores of the KL zeolite. In case (a) the Pt particle partially blocks the path of the MCP molecule; in case (b) the flat Pt particle does not block the path of the MCP molecule.

The analysis of the IR data may also help in elucidating the state of Pt particles in the two catalyst series. Here, however, one needs to be careful since the interpretation of the FTIR data is not straightforward. Besoukhanova et al. [38] were the first to identify the appearance of several distinct bands in the region 2070-1950 cm^{-1}. Many authors [90] have subsequently observed this series of bands, but the origin of these bands is still unclear.

The analysis of the IR bands could be divided into two regions, above and below 2050 cm^{-1}. Those above 2050 cm^{-1} are thought to be due to CO adsorbed on Pt particles located outside the zeolite and in the near-surface region [91,92]. According to the positions of the higher frequency region observed on the two series of catalysts investigated in this work (see Fig. 4.5), we can conclude that only a small fraction of particles reside outside. The main band at 2060-2068 cm^{-1} may be

associated with particles near the surface of the zeolite rather than outside the channels. In fact, only when the IWI catalyst was calcined at high temperature did a shoulder arise at 2078 cm^{-1} (see Fig. 4.8). That position was clearly associated with large Pt particles outside the channels of the zeolite and coincided with the position observed on Pt/SiO_2.

The region below 2050 cm^{-1} is more complicated to explain. It has been proposed that the bands appearing in the 2030-1950 cm^{-1} range corresponded to CO adsorbed on Pt particles inside the channels, with an electronic structure strongly perturbed by the zeolite [91]. Lane et al. [93] have paid particular attention to the bands appearing around 1970 cm^{-1}. They pointed out that the exact position of this band depended on the basicity of the cation exchanged into the zeolite and showed that a band at about the same position could be generated on a Pt/SiO_2 catalyst when it was impregnated with K^+. Therefore, they interpreted this band as a result of an electrostatic attraction between the linearly bonded CO with the alkali cations. They found no correlation between the appearance of this band and the aromatization activity.

The time evolution of the bands that we have observed (see Fig. 4.5) is difficult to rationalize in terms of simple adsorption of CO. That is, unless there is a strong mass transfer limitation it is unreasonable that the bands at 2060-2068 cm^{-1} develop very quickly, but those at lower frequencies take more than 10 min. An idea recently advanced by Stakheev et al. [92] that may well explain our results, is that CO itself modifies the structure of the Pt clusters inside the KL zeolite. Consequently, CO adsorption does not probe the metal particles in their original structure, but rather

generates new molecular arrangements that are stabilized inside the zeolite. These authors have proposed that during CO adsorption, Pt carbonyls can be formed. They observed that the intensity of the bands greatly increased when the CO pressure was increased from 1 to 500 mbar, although in normal adsorption of CO, it was expected to reach a saturation coverage at relatively low pressures. Based on this assumption, they matched the observed IR frequencies with known Pt carbonyls and indicated that although Pt carbonyls containing only CO ligands were very unstable, substitution with other ligands could greatly increase their stability. Therefore, they proposed that the zeolite could act as a ligand and affect the stabilization of these species. In support of this idea, EXAFS data of Mojet and Koningsberger [94] have shown that the 5-6 atom metallic particles present in the KL zeolite before the admission of CO, completely disrupted and Pt carbonyls formed in the presence of CO. At the same time, the XANES spectrum exhibited a profound change indicating significant changes in the electronic structure of Pt. Menacherry and Haller [95] have also observed drastic changes in the FTIR spectrum upon heating under low pressures of CO. They reported that, when the equilibration temperature under 1000 ppm CO was increased from room temperature to 200°C, a band at 1940 cm^{-1} greatly increased. It is possible that in that case, Pt carbonyls did not form under low CO pressures but they did form when the temperature was increased.

In light of these ideas, an interesting comparison could be made from Figs. 4.6 and 4.9, which depict the time evolution of the DRIFTS spectra under CO exposure. It was seen that while the catalyst that was pre-calcined at low temperature exhibited marked band shifts, the one pre-calcined at high temperature simply showed a

monotonic increase in band intensity as a function of time. This difference would indicate that on the catalyst calcined at 500°C, (RC-IWI-1) the formation of Pt carbonyls occurred to a much lesser degree than on the other catalyst. Stakheev et al. [92] have pointed out that the formation of Pt carbonyls can only occur when the Pt clusters are very small. They indicated that the metal-metal bond strength is much lower than that of the bulk metal only for particles with less than 15-20 atoms. Therefore, one may not expect the Pt particles outside the zeolite in the RC-IWI-1 sample (i.e., band at 2080 cm^{-1}) to be converted to Pt carbonyls.

Similarly, the different changes observed in the DRIFTS spectra of the VPI and IWI samples after exposure to sulfur may be rationalized in terms of formation of carbonyls. Upon exposure to sulfur (see Fig. 4.7) the lower frequency bands (i.e., below 2000 cm^{-1}) did not decrease as markedly on the VPI catalyst as on the IWI catalyst. One may conclude that Pt carbonyls could still be formed on the poisoned VPI catalyst, but not on the poisoned IWI catalyst. This difference may help to understand the mechanism of sulfur poisoning. If the sulfur poisoning was due to an agglomeration of Pt particles inside the channels of the zeolite, as suggested by McVicker et al. [25], it is possible that this agglomeration results in a particle size that exceeds the maximum (i.e. 15-20 atoms) beyond which the carbonyl formation is no longer favorable. If that is the case, the VPI catalysts, which have a high concentration of small particles in close contact with the zeolite, could be more resistant to particle growth. Consequently, at least during the 9 h of the run under sulfur, they would not reach the size preventing the formation of carbonyls during exposure to CO. An alternative is that the sulfur poisoning occurred on the potassium

cations, as suggested by Ponec [32]. If that were the case, then the lack of carbonyl formation with IR bands below 2000 cm^{-1} on the poisoned IWI catalysts could be attributed to a possible stabilization requirement of those carbonyls by the potassium cations. However, this would not explain why the VPI catalyst exposed to the same sulfur treatment could still form those carbonyls. Therefore, it appears that the sulfur has a stronger influence on the Pt clusters on the IWI sample than on those of the VPI sample.

4.4.2 Catalytic Properties

The pulse experiments allowed us to compare the aromatization activity of the different catalysts in the absence of significant deactivation. Based on the benzene yields shown in Fig. 4.12 a, and in agreement with Iglesia et al. [19,20], one may conclude that Pt on silica is intrinsically as active as Pt/KL. However, it is important to realize that n-hexane aromatization is an ensemble-sensitive reaction [96] and based on that requirement alone we would not expect a high catalytic activity on particles that are composed of a few atoms. In fact, hydrogenolysis, which is known to be ensemble-sensitive occurs at a much lower rate on the Pt/KL catalysts than on the Pt/SiO_2 catalyst. Therefore, the idea that the environment provided by the KL zeolite increases the C_6-ring closure is not discredited by our pulse experiments. On the other hand, the pulse experiments clearly show that the hydrogenolysis activity correlates with the propensity of the catalyst to deactivate in the flow mode. A catalyst such as Pt/SiO_2 or a poorly prepared Pt/KL catalyst with a large fraction of Pt

outside the channels of the zeolite should exhibit a high hydrogenolysis activity and a rapid deactivation in the flow reaction.

In agreement with the conclusions drawn from the IR data, the reaction data has shown that the VPI catalysts not only are more active and selective than the IWI catalysts. They are also more resistant to deactivation by calcination at high temperatures, by coke, and by sulfur. It has been observed that in the absence of sulfur, the VPI-1 catalyst display a very low deactivation rate. In fact, the same catalyst has been run for 70 h and kept a benzene yield of 40% at a WHSV of 5 h^{-1}, as described in the previous chapter. If the VPI preparation resulted in extremely small Pt particles in close contact with the zeolite walls, they could tolerate more coke deposits and greater particle growth before plugging the pores and subsequent deactivation. By contrast, if the catalyst prepared by IWI resulted in Pt clusters that partially filled the channels (see Fig. 4.16), then small amounts of coke or minor particle growth could cause a much greater deactivation, as verified experimentally.

4.5 Conclusions

The distribution of Pt clusters and their resulting characteristic morphology largely varied with loading and method of preparation. Over a wide range of catalysts studied, we observed three different types of particles that profoundly affected activity, selectivity, stability, and results of catalyst characterization. The different particles, as described elsewhere in the literature, included large particles formed outside of the channels, small particles located inside the channels, but large

enough to block or partially block them, and clusters that were small enough to reside in the lobes of the L-zeolite channels.

TEM and EXAFS revealed the existence of Pt clusters having very small size located inside the L-zeolite channels for both IWI and VPI preparation methods. In addition, these results were confirmed by FTIR of adsorbed CO, which gave evidence that the particles were small enough to allow the formation of Pt carbonyls. Furthermore, the increase in coordination of Pt with the oxygen of the L-zeolite framework and the decrease in Pt-Pt coordination observed for the VPI series relative to the IWI series clearly indicated that the particles produced were smaller and of different characteristic morphology. In line with this finding, lower collimation effects were observed for VPI catalysts with respect to IWI catalysts during pulse testing of MCP-RO. This lower collimation strongly suggested that the clusters produced by VPI were small enough to allow for the diffusion of reactants and products around the cluster during the aromatization of n-hexane reaction.

The characteristic location distribution and morphology of the particles produced from the different preparation procedures had important consequences on the conversion, selectivity, and stability of catalysts under reaction conditions. Under continuous flow conditions, VPI catalysts displayed higher aromatization activity and selectivity, lower hydrogenolysis activity, lower hexenes and a significantly lower deactivation rate.

This work demonstrated that the characteristic morphology produced by the VPI method substantially improved the performance of the catalyst under clean and sulfur poisoned conditions. The VPI method lead to the formation of very small

particles in close interaction with the zeolite walls. Consequently, the catalysts displayed less coke formation, higher activity under sulfur poisoned conditions, and greater resistance to particle agglomeration during calcination treatment at high temperature.

SPECIAL ACKNOWLEDGMENTS

This work is the result of a collaborative effort of the OU Heterogeneous Catalysis Group. I would like to thank our postdoctoral researchers Dr. Adriana Pisanu and Dr. Walter E. Alvarez for their contributions with the FTIR work and pulse experiments. Also, I would like to especially acknowledge Firoz Ghadiali for his contributions, which included construction of the pulse reaction system and carrying out the pulse measurements. I would like to acknowledge Greg Strout at the OUSR Noble Electron Microscopy Laboratory for help with TEM measurements, and Dr. Armando Borgna (INCAPE) for his EXAFS analysis work. Dr. Borgna was funded by Fundacion Antorchas and the Fulbright Commission. I would also like to thank the Oklahoma Center for the Advancement of Science and Technology (OCAST) for funding and NSF for my GRT traineeship, as well as Phillips Petroleum for a scholarship. Finally, I would like to thank personnel at Brookhaven National Laboratory, especially Syed Khalid, for help with EXAFS experiments.

CHAPTER V: PREPARATION – Achieving desired Pt Cluster Morphology

Pt/KL powder and pelletized catalysts were synthesized by different methods including ion exchange (IE), incipient wetness impregnation (IWI), and vapor phase impregnation (VPI) methods. A detailed characterization was conducted on the various samples in order to determine the distributions of Pt particle morphology and location resulting from each preparation, as well as the relationships between these distributions and the catalytic performance. The catalysts were pretreated at two different reduction temperatures – 400°C and 500°C - to investigate the sensitivity of each catalyst to thermal treatment. All catalysts showed high dispersion, with H/Pt ratios greater than unity. However, FTIR of adsorbed CO showed that more important than dispersion, it was the distribution of Pt cluster morphology and location, which influenced the resulting catalytic stability. Standard IE catalysts were found to have a high fraction of Pt particles external to the L-zeolite and were the most sensitive to thermal treatment, displaying Pt migration out of the L-zeolite. These catalysts deactivated rapidly by coke formation. The addition of excess K^+ ions in the exchange solution and a longer aging period, as suggested in the patent literature, improved the Pt dispersion.

IWI and VPI catalysts showed a majority of Pt clusters inside the L-zeolite channels. However, after high temperature reduction treatment, the IWI catalysts displayed particle growth inside the channels, in contrast with the VPI. The IWI catalysts were found to deactivate to about half their initial activity, while the VPI

maintained the highest activity and stability. Different VPI methods including a moderate vacuum and a helium flow technique were examined and they showed similar Pt cluster distributions and catalytic performance to the catalysts synthesized using high vacuum. Preparation directly on the pellet for the methods investigated in this work (standard IE, IWI, and VPI) resulted in large fractions of Pt clusters external to the pores and likely on the binder. Thus, rapid deactivation by coke formation was evident. These results indicate that pelletized catalysts prepared by any of these techniques would require preparation on the powder prior to pellet extrusion.

5.1 INTRODUCTION

Over the past 20 years, researchers have used different methods to prepare Pt/KL catalysts for the aromatization of n-hexane reaction. These typically involved ion exchange (IE), incipient wetness impregnation (IWI) and more recently, vapor phase impregnation (VPI) methods, as described in Chapter 2. These procedures resulted in catalysts with differences in the distributions of Pt particle morphology and location. The first consideration is the residual acidity that may remain on the zeolite after each preparation. Therefore, for the IE catalysts, a back-exchange procedure is deemed necessary in order to exchange out Bronsted sites arising from reduction of Pt^{2+} exchanged in the zeolite, as described by Ostgard et al. [64]. In contrast, less residual acidity is generated for IWI catalysts during the reduction step, because there is little exchange with the L-zeolite during preparation. Coimpregnation of KCl during the IWI step to reduce Bronsted acidity displayed an

increased selectivity to benzene. Finally, the VPI method avoids the exchange of K^+ with Bronsted sites altogether [48,49].

The second important aspect to consider is the morphology and location of the Pt clusters in the zeolite. The preparation method is critical to the distribution of the Pt clusters and directly influences the stability of the catalyst under aromatization conditions, as discussed in Chapter 4 for IWI and VPI catalysts. Briefly, the morphology of the Pt clusters inside the channels also had a strong influence on the deactivation rate. Large clusters located inside the L-zeolite channels were more sensitive to agglomeration, resulting in blockage of the channels and entombment of Pt particles. On the other hand, small clusters located in the lobes of the channels were less sensitive to Pt growth. In a previous study in the literature, results of MCP ring opening for small Pt clusters indicated that the standard IE procedure resulted in a considerable fraction of Pt external to the channels of the L-zeolite [64]. A TPR investigation of catalysts calcined at 400°C [64] demonstrated that IE catalysts displayed a greater fraction of platinum in the form of Pt^{+2} ions coordinated to the zeolite walls, while IWI catalysts predominantly showed Pt^{+4} species in the form of PtO_2 clusters located inside the channels. From MCP-RO testing, less Pt was found on the exterior surface of the L-zeolite for the IWI catalysts than in the case of the IE [64]. However, although most of the Pt resides inside the L-channels after IWI preparation, a fraction of particles inside the pores were found to be large enough to cause pore blockage, as discussed in detail in Chapter 4.

In this chapter, we have conducted a systematic comparison of the different preparation methods, analyzing the distribution of Pt clusters resulting from each

method, and its direct influence on the stability of Pt/KL catalysts. Three methods were compared – standard ion exchange, incipient wetness impregnation, and vapor phase impregnation. FTIR of adsorbed CO and hydrogen chemisorption were employed as characterization techniques. Results from this characterization were correlated with the deactivation patterns of the catalysts under the n-hexane flow reaction. As we have demonstrated before, the catalysts prepared by the VPI method show the highest activity, selectivity, and stability for n-hexane aromatization. However, the VPI method previously studied involved the use of high vacuum, which is not convenient for commercial applications. Therefore, in this chapter, we investigated slight modifications to the method to make it more suitable for industrial practice. Finally, we examine effect of the degree of zeolite hydration during preparation of IWI catalysts, and consider the effects on catalyst stability.

5.2. EXPERIMENTAL

5.2.1 Catalyst Preparation

The K-LTL zeolite powder (series TSZ-500, BET area 292 m^2/g, SiO_2/Al_2O_3 ratio = 6) was provided by Tosoh Company. Pellets were extruded using 10% K-Sil binder and 1.5% stearic acid. Prior to incorporation of Pt metal, the zeolite powder or pre-formed pellet was dried in an oven at 110°C for 12 h and calcined at 400°C for 5 h. Incorporation of platinum metal into the zeolite was performed using the three following methods:

5.2.1.1 Standard Ion Exchange (SIE) Method

In the standard ion exchange method, as reviewed in Section 2.1.1, tetraammine platinum (II) nitrate salt (Alfa Aesar) was used as the precursor. For the 0.5% Pt/KL catalyst, the precursor was added dropwise over an 8 h period to the 200 ml agitated suspension of L-zeolite. The slurry was further stirred for 24 h, filtered using a Buchner funnel, and dried at room temperature. The catalyst powder was further dried in an oven at 110°C for 12 h and calcined at 350°C for 2 h under flow of air. The calcined sample was reduced at 400°C or 500°C under flow of hydrogen. This catalyst was designated as *SIE-PWD-NBE* for "not back exchanged". In order to remove residual acidity generated during the reduction step, a portion of the catalyst was back-exchanged using an aqueous solution of 0.01 M KNO_3 added dropwise over 8 h. The catalyst was then filtered again, dried, and re-calcined. This catalyst was designated as *SIE-PWD-BE* for "back exchanged". In the case of the preparation on the KL pellets, the same procedure was used, except that the pellets were suspended in a Teflon basket to prevent attrition. This catalyst was designated *SIE-PEL-NBE.*

5.2.1.2 Modified Ion Exchange (MIE) Method

An Exxon process patent [97] claims that contacting the L-zeolite with an aqueous loading solution containing soluble Pt salt as well as additional K^+ cations assures that acid sites are not formed on the catalyst during the drying step. More specifically, the amount of K^+ cation initially present in combination with the platinum salt in the loading solution is such that after loading, the initial amount of the K^+ plus the amount of K^+ cation added to the solution by ion-exchange of the

platinum salt with the L-zeolite is present in the loading solution in a concentration equal to the concentration of K^+ metal salt added to the solution by ion-exchange between the platinum salt and the L-zeolite at incipient wetness. Our preparation following the guidelines of Poeppelmeier et al. [97] is provided below for clarity. We employed tetraammine platinum (II) chloride as the source salt, and additional K^+ was added to the loading solution from KCl source. Furthermore, a critical aging step is also described whereby excess liquid is removed from the carrier and the solids are allowed to be aged for a time at the prescribed temperature. The patent claims that this aging step allows the platinum to migrate and uniformly distribute throughout the L-zeolite. Afterwards, the catalyst is dried and calcined, prior to the reduction step. For 10 g KL, 0.17 g of $Pt(NH_3)_4Cl_2$ was required. Since each mole of Pt^{2+} cation displaces 2 moles of K^+ from the L-zeolite support during ion exchange, an additional 1.03×10^{-3} moles of K^+ was included in the loading solution. The volume of solution required to reach incipient wetness for 10 g of KL was 6.9 ml. The total volume of loading solution was 17 ml, so the required amount of K^+ to be added to the initial loading solution was calculated to be $1.5\text{x}10^{-3}$ moles. This corresponded to 0.112 g of KCl. After circulating the solids for 75 min, the wet solids were collected and aged at 50°C for 72 h. in a closed vessel. The solids were then dried and calcined at 110°C for 16 h., further calcined at 200 °C for 2 h., and again calcined further at 350°C for 3 h. according to the recipe. This catalyst was designated *MIE-PWD*.

5.2.1.3 Incipient Wetness Impregnation (IWI) Method

The standard sample, prepared according to Chapter 2, was designated *IWI-PWD*. However, to analyze the effect of introducing excess water during the procedure, three additional catalysts were synthesized. In the first case (*IWI-PWD-EXP*), after calcination, the L-zeolite was exposed to ambient conditions for 12 h, so water from the ambient humidity penetrated in the pores. In this case, the pores were still filled to incipient wetness by using only the required liquid to solid ratio measured separately, which in this case was lower (i.e., 0.49 cm^3/g). In the second case (*IWI-PWD-XS*), after calcination, the L-zeolite was again exposed to ambient conditions for 12 h, but now the original 0.69 cm^3/g ratio was used. Therefore, the pores were overfilled beyond incipient wetness. Finally, in the third case (*IWI-PWD-NCL*), the L-zeolite was dried at 110°C, but not calcined. The same 0.69 cm^3/g was employed during impregnation, resulting in overfilling of the pores. In each modification, the resulting catalysts were dried and calcined in the usual way.

For the case of impregnation on the KL pellets, the extrudates were dip impregnated by lowering the perforated Teflon basket containing dehydrated L-zeolite into solution and removing quickly. This sample was named *IMP-PEL*. The resulting Pt loading was in this case only 0.57 wt %.

5.2.1.4 Vapor Phase Impregnation (VPI) Methods

The third method employed was VPI, as described in Chapter 2. The standard vapor phase preparation method was designated *VPI-PWD-HV* for high vacuum preparation.

However, to examine more convenient methods for preparing VPI catalysts on a large scale, we examined two additional preparation methods. The first one (*VPI-PWD-MP*) was prepared using a mechanical pump to achieve a moderate vacuum ($\sim 10^{-3}$ Torr). The second one (*VPI-PWD-HEF*) was done performing the sublimation at atmospheric pressure under a low flow rate of He (< 10 cm^3/min). For the case of the pellets (*VPI-PEL-HEF*), the low helium flow method was used.

Table 5.1. Summary of Catalysts and Loadings

Catalyst Description	**Catalyst Designation**	**Pt Loading**
Standard Ion exchange (SIE) with no back exchange	*SIE-PWD-NBE*	0.50%
Standard IE with back exchange of potassium	*SIE-PWD-BE*	0.50%
Modified Ion Exchange (MIE)	*MIE-PWD*	0.50%
Incipient wetness impregnation (IWI)	*IWI-PWD*	1%
IWI with prior exposure of L-zeolite to ambient conditions	*IWI-PWD-EXP*	1%
IWI with prior exposure of L-zeolite to ambient and overfilling	*IWI-PWD-XS*	1%
IWI without calcination of L-zeolite resulting in overfilling	*IWI-PWD-NCL*	1%
Vapor Phase Impregnation (VPI) using high vacuum	*VPI-PWD-HV*	1%
VPI using moderate vacuum (mechanical pump)	*VPI-PWD-MP*	1%
VPI using low helium flow	*VPI-PWD-HEF*	0.89%
Standard IE of L-pellets using basket	*SIE-PEL-NBE*	0.51%
Dip impregnation of L-pellets using basket	*IMP-PEL*	0.57%
VPI of L-pellets using low helium flow	*VPI-PEL-HEF*	0.65%

The Pt loadings were determined by ICP analysis after complete dissolution of the samples in aqua regia/HF solution at Galbraith Laboratories. A summary of the catalysts, nomenclature, and measured loading, is presented in Table 5.1.

5.2.2 Catalyst Characterization

Hydrogen chemisorption and infrared spectroscopy of adsorbed CO measurements were conducted according to procedures detailed in Section 2.3.

5.2.3 Catalytic Activity Testing

Steady-state n-hexane reaction testing was conducted in a continuous-flow reactor, according to Section 2.4.1. In all experiments, the hydrogen/n-hexane ratio was kept at 6. Prior to reaction, the catalyst was slowly ramped in flowing hydrogen at 100 cm^3/g catalyst for 2 h to a temperature of 450°C (except where otherwise noted). Reaction testing was conducted at a WHSV of 10 h^{-1} at atmospheric pressure and a temperature of 450°C, unless otherwise noted.

Products were detected using a flame ionization detector (FID). A nonlinear 1.5 h temperature ramp from 40°C to 200°C provided the means for adequate peak separation in the GC column.

5.3 RESULTS

5.3.1 Catalyst Characterization

5.3.1.1 Hydrogen Chemisorption

The H/Pt results obtained on the powder samples after reduction at either 400°C or 500°C are reported in Table 5.2. As in previous reports [22,39], very high H/Pt values were obtained. A significant difference was obtained between the total and the irreversible adsorption values, showing that in all cases, contributions from weakly adsorbed hydrogen were significant. Nonetheless, high irreversible H/Pt

Table 5.2. Results of Hydrogen Chemisorption for Powder Catalysts.

Catalyst	H/Pt Red 400 °C (Total)	H/Pt Red 400 °C Irreversible	H/Pt Red 500°C (Total)	H/Pt Red 500 °C Irreversible	Difference Between R500 and R400
SIE-PWD-NBE	1.8	1.3	1.5	1.0	0.3
IWI-PWD	1.9	1.6	1.5	1.2	0.3
IWI-PWD-EXP	1.8	-	1.5	-	0.3
IWI-PWD-XS	1.8	-	1.4	-	0.4
IWI-PWD-NCL	1.5	-	0.9	-	0.6
VPI-PWD-HV	2.0	1.7	1.7	1.4	0.3
VPI-PWD-MP	2.0	-	1.7	-	0.3
VPI-PWD-HEF	2.0	-	1.7	-	0.3

values above 1.0 were observed in all cases, indicating very high metal dispersion in all the samples, particularly in the VPI catalysts. By increasing the reduction temperature from 400°C to 500°C, clear drops in H/Pt values were observed for all samples. Interestingly, in general, for the IE, IWI, and VPI powder catalysts, the losses were approximately the same for each case. However, the IWI catalysts prepared with excess water (*IWI-PWD-XS* and *IWI-PWD-NCL*) displayed a higher sensitivity to reduction temperature. Finally, no differences were detected among the H/Pt values for all the different vapor phase preparation methods tested, indicating that the three VPI methods were similarly effective in dispersing Pt.

5.3.1.2 Infrared Spectroscopy

It was shown in Chapter 4 that FTIR of adsorbed CO is an important tool to probe the state of Pt clusters in Pt/KL. It was concluded that CO adsorption does not

probe the small metal particles in their original structure, but rather generates by disruption over time new molecular arrangements that are stabilized inside the zeolite.

In review, Stakheev et al. [92] have tabulated the reproducibility of the position of these bands from several authors, and suggested that several different molecular species were formed with distinct stoichiometric ratios of Pt_x and CO_y. They proposed that during CO adsorption, Pt carbonyls can be formed and stabilized by the zeolite, which could act as a ligand. It was also shown that saturation of CO was reached at 1 mbar P_{CO} after approximately 30 minutes. However, after increasing P_{CO} to 500 mbar, the intensity of the bands increased by a factor of 5, giving clear evidence of Pt-carbonyl formation. The important point to notice is that the formation of Pt carbonyls can only occur when the Pt clusters are very small, due to the lower metal-metal bond strength for particles with less than 15-20 atoms compared with that of the bulk metal. Therefore, one may not expect the Pt particles outside the zeolite to be converted to Pt carbonyls. Even though disruption of the small Pt clusters occurs, FTIR of adsorbed CO is still a useful technique for making general conclusions about the location (i.e., inside the L-zeolite or external) and distribution of the Pt clusters prior to disruption. For our purposes, the results are strongly consistent with the idea that the distribution of low wavenumber bands reflects the distribution of the morphology of Pt clusters located inside the channels of the L-zeolite.

In contrast, the bands at and above 2075 cm^{-1} indicate the Pt external to the pores. Bands present between 2050 cm^{-1} and 2075 cm^{-1} are likely caused by the Pt clusters in the near surface region of the L-channels. In support of this assignment,

Stakheev et al. [92] showed loss of Pt carbonyl bands and an increase in bands at these wavenumbers after several adsorption and desorption cycles, in which the temperature was increased to 400°C. Furthermore, in Chapter 4, we observed an increase in these bands after agglomeration of the Pt clusters in an IWI catalyst after conducting oxidation-reduction cycles. In agreement with these observations, TEM results have indicated the high tendency of small clusters of Pt to disrupt and agglomerate if small amounts of CO are present in the hydrogen during the reduction step, resulting in activity loss [98].

We first probed our best Pt/KL SIE, IWI and VPI powder catalysts at two reduction temperatures, 400°C and 500°C. The results are depicted in Figures 1a and b. As reported in our previous study found in Chapter 4, we noted again that the FTIR spectra changed as a function of CO exposure time, in agreement with the idea of Pt cluster disruption followed by stabilization inside the zeolite. In order to make comparisons about the morphology of the Pt in the KL catalysts, for every sample, we stopped CO exposure after exactly 30 min, and flushed in helium to remove gas phase CO.

For *IWI-PWD* and *VPI-PWD-HV* catalysts, Fig. 5.1a and b show that the positions of the bands resulting from the adsorption of CO were similar, extending from 2065 cm^{-1} to 1930 cm^{-1}. These bands are associated with Pt inside the channels of the L-zeolite [92]. As demonstrated by the low wavenumber bands (2010 cm^{-1}-1930 cm^{-1}) in Fig. 5.1a and b, the VPI catalyst displayed higher capability than the IWI and SIE catalysts for disrupting Pt clusters after reduction at both 400°C and 500°C. No large differences were observed for IWI and VPI

catalysts after reduction at 400°C. However, after reduction at 500°C, the IWI catalyst showed a larger decrease in bands associated with Pt-carbonyls and a more pronounced shoulder at 2065 cm^{-1}, resulting in a shift to higher wavenumbers. In contrast with the IWI and VPI catalysts, the *SIE-PWD-NBE* catalyst did not show the bands related to the presence of small clusters/carbonyls. Also, this IE catalyst displayed bands which extended to frequencies higher than 2075 cm^{-1}, indicating the presence of external Pt particles. The effect of reducing the catalyst at higher temperatures was severe. We observed a large decrease in intensity of the 2010, 2034, and 2053 cm^{-1} bands, with a strong growth in intensity of the 2080 cm^{-1} and higher frequency bands.

We examined the effect of the back exchange procedure on the standard ion exchange powder catalyst. As Figure 5.2 a indicates, no major differences in the band positions were noted for the back-exchanged catalyst *SIE-PWD-BE*, reduced at 400°C and 500°C. After reduction at 400°C, in comparison with the *SIE-PWD-NBE* catalyst, however, there was a greater fraction of high wavenumber bands between 2075 cm^{-1} and 2080 cm^{-1} after back exchange than before the procedure. In contrast, after reduction at 500°C, no large differences were observed before or after the back exchange.

Figure 5.2 b shows a DRIFTS comparison of the standard IE with the modified IE catalyst prepared by the method of Poeppelmeier et al. [97]. The modified IE catalyst displayed a greater fraction of low wavenumber bands than the standard IE catalyst after reduction at 500°C, and showed virtually no bands

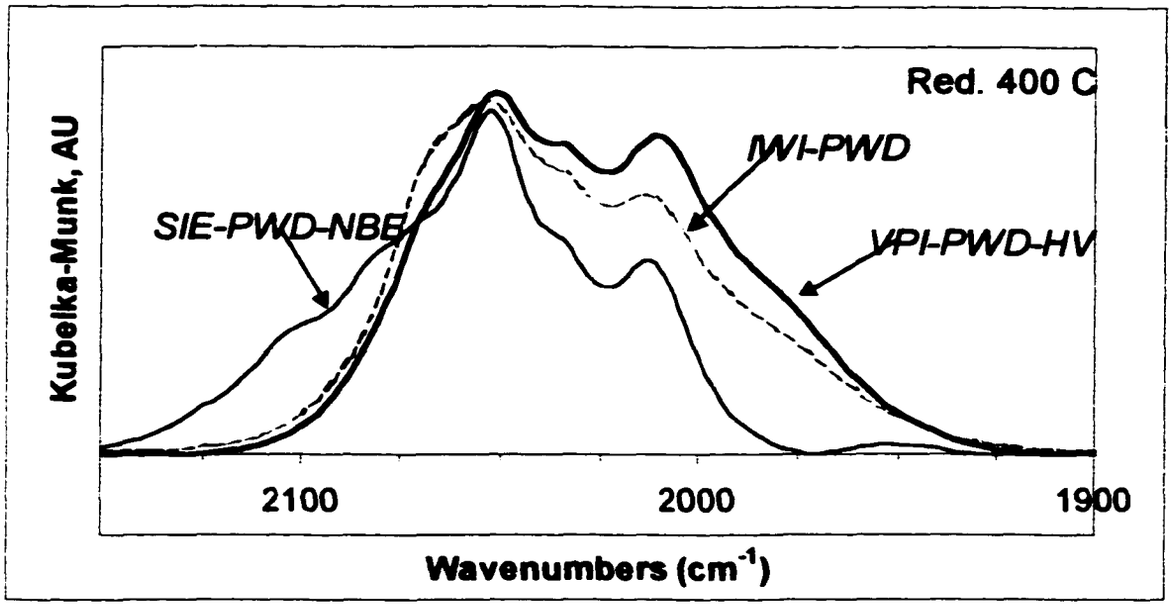

Figure 5.1(a): DRIFTS spectra of CO adsorbed on powder catalysts prepared by standard ion exchange without back-exchange (*SIE-PWD-NBE*), incipient wetness impregnation (*IWI-PWD*), and vapor phase impregnation high vacuum (*VPI-PWD-HV*) after reduction at 400°C.

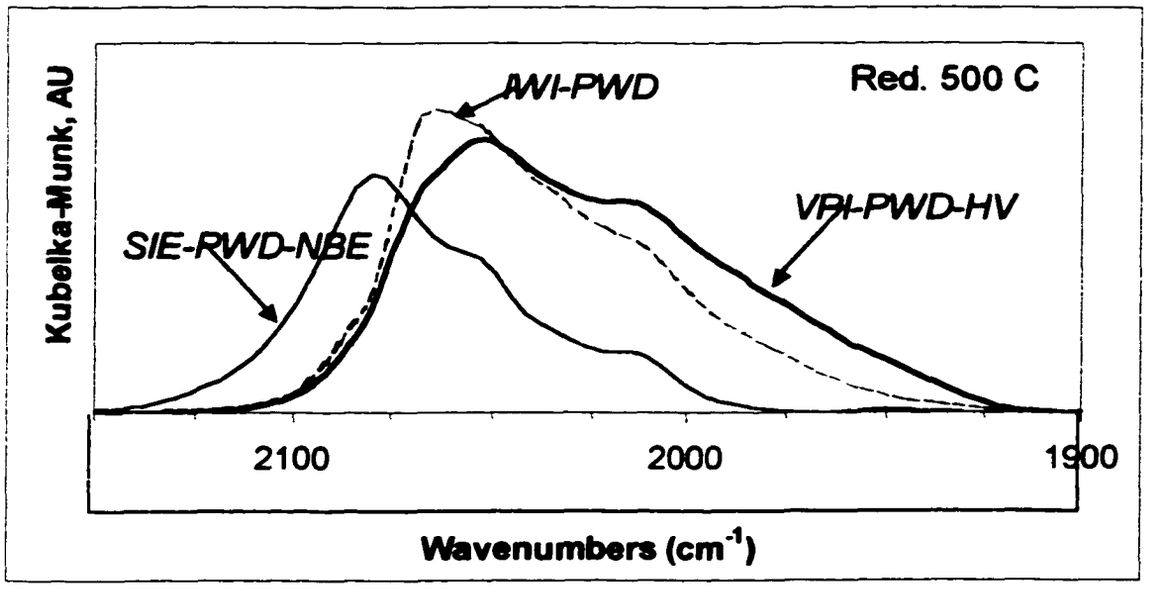

Figure 5.1(b): DRIFTS spectra of CO adsorbed on powder catalysts prepared by standard ion exchange without back-exchange (*SIE-PWD-NBE*), incipient wetness impregnation (*IWI-PWD*), and vapor phase impregnation high vacuum (*VPI-PWD-HV*) after reduction at 500°C.

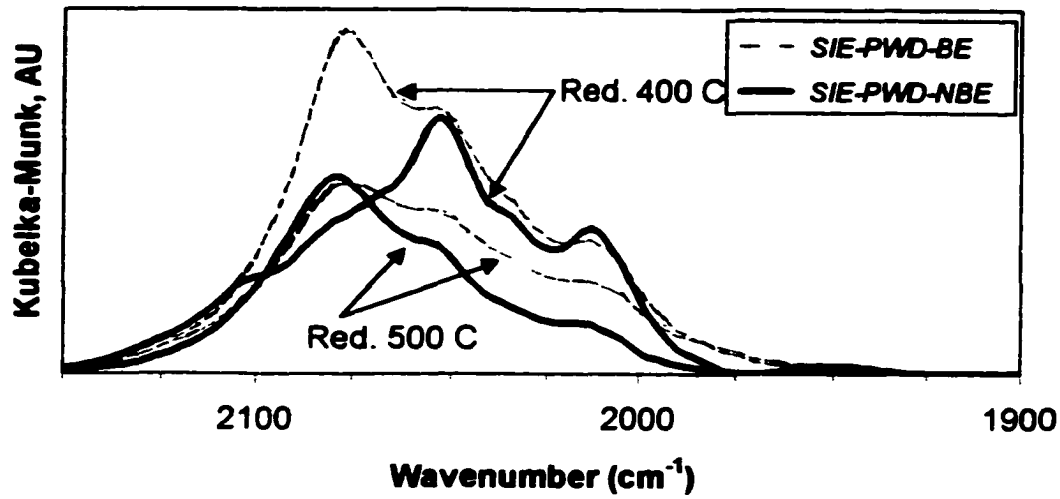

Figure 5.2(a): DRIFTS spectra of CO adsorbed on standard ion exchanged powder catalysts with and without back-exchange (*SIE-PWD-BE* and *SIE-PWD-NBE*, respectively) after reduction at 400°C and 500°C.

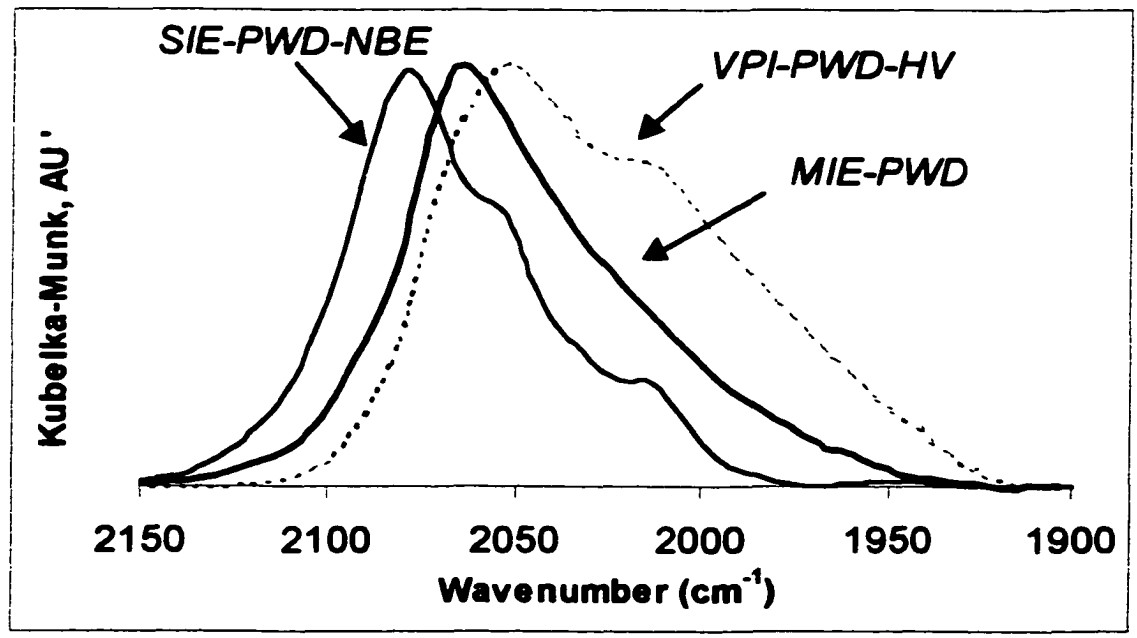

Figure 5.2(b): DRIFTS spectra of CO adsorbed on ion exchanged catalysts prepared by the standard ion exchange method without back exchange (*SIE-PWD-NBE*) and by using the modified ion exchange method (*MIE-PWD*) of Poeppelmeier et al. [97] after reduction at 500°C.

associated with external Pt, in contrast with the standard IE catalyst. It is clear that the aging step during preparation aided in dispersing the salt throughout the channels. However, the VPI catalyst still presented a marked improvement over either of the two IE preparations, as indicated by the greater fraction of low wavenumber Pt-carbonyl bands.

We also investigated the role of excess water during the IWI preparation procedure. No major shifts in peak positions were observed for the catalysts prepared with excess water. Attention was also focused on preparation procedure that may lead to a large-scale implementation of the VPI method. We investigated the use of the mechanical pump (*VPI-PWD-MP*) and the helium flow (*VPI-PWD-HEF*) preparations for the powder catalysts.

Figure 5.3 shows the results after reduction at 500°C for the two catalysts in comparison with the high vacuum procedure. All VPI catalysts displayed a large

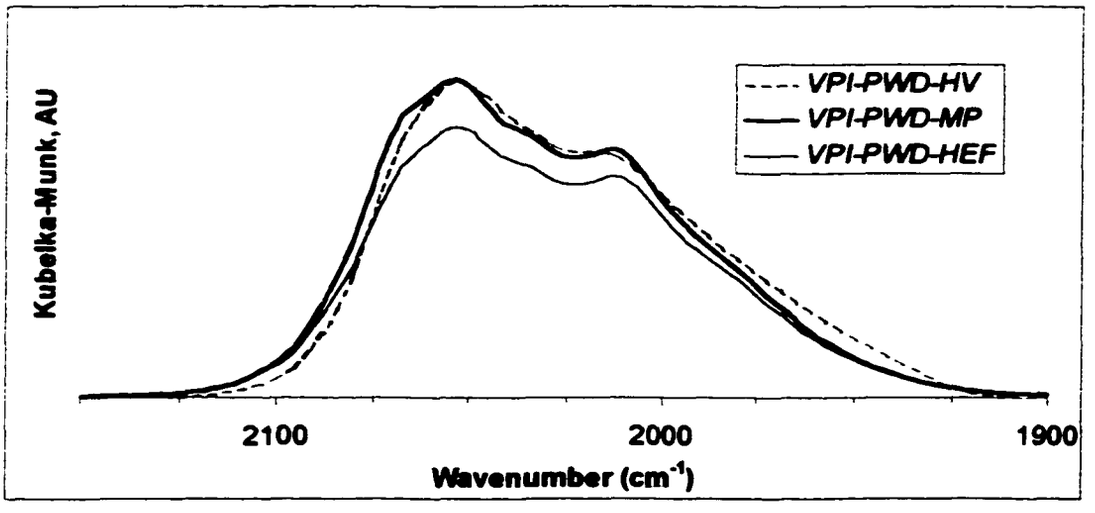

Figure 5.3: DRIFTS spectra of CO adsorbed on the catalysts prepared by vapor phase impregnation under high vacuum, 10^{-5} Torr (*VPI-PWD-HV*), moderate vacuum, 10^{-3} Torr (*VPI-PWD-MP*), and under flow of He (*VPI-PWD-HEF*) after reduction at 500°C.

fraction of bands between 2010 cm^{-1} - 1930 cm^{-1} associated with stabilized Pt-carbonyls. In addition, clear bands at 2033 cm^{-1}, 2053 cm^{-1}, and 2064 cm^{-1} were also observed. The shoulder at 2064 cm^{-1} was more pronounced for the *VPI-PWD-MP* preparation, with a contribution from a band present at 2069 cm^{-1}. Finally, we utilized FTIR of adsorbed CO to characterize three different preparation methods conducting the incorporation of the Pt directly on the pre-formed pellets. The results were very different in comparison with the powder catalysts. Unfortunately, and as expected, all the pellet catalysts showed a substantial contribution of high wavenumber bands. All of them displayed a shoulder or peak at 2080 cm^{-1} or higher. As an example, we can compare catalysts prepared by VPI and the standard IE method in the pellet form *SIE-PEL-NBE*. In Figure 5.4, the *VPI-PEL-HEF* displayed a small fraction of bands associated with the formation of Pt-carbonyls,

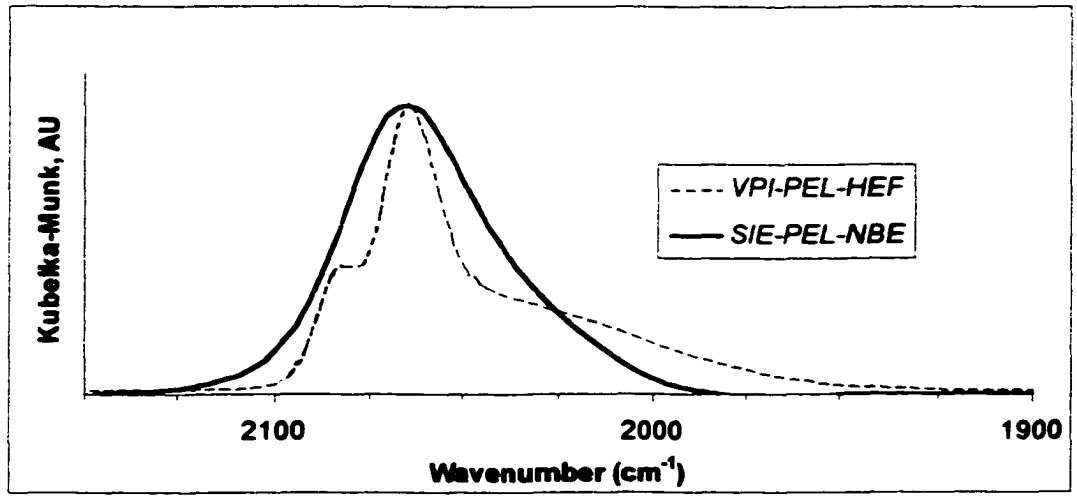

Figure 5.4: DRIFTS spectra of CO adsorbed on palletized vapor phase impregnation helium flow *VPI-PEL-HEF* and standard ion exchange without back exchange *SIE-PEL-NBE* catalysts after reduction at 500°C.

while the SIE pellet catalyst did not show any. Both presented peaks at 2065 cm^{-1} and between 2080 cm^{-1} and 2084 cm^{-1}, reflecting a large number of particles outside the channels of the zeolite. Note that the modified ion exchange method [97] was not carried out on extrudates in this work, and would likely result in a much improved IE pellet catalyst, in light of the results in Figure 5.2b for powder catalysts.

5.3.2 Catalytic Testing of n-Hexane Aromatization in a Flow Reactor

5.3.2.1 Powder Catalysts

The three catalyst preparation methods displayed significant differences in their deactivation patterns for the aromatization of n-hexane reaction at 450°C. Figure 5.5 shows the benzene yield for the *SIE-PWD-NBE*, *IWI-PWD*, and *VPI-PWD-HV* catalysts at 10 min, 1.5 h, and 9 h on stream. The *SIE-PWD-NBE* showed a low aromatization activity and low stability. Similarly, as in previous testing, the IWI showed a significant drop in initial activity, not as pronounced as the IE, but significantly worse than the VPI catalyst. As expected, the differences correlated well with important differences in the production of methane and hexenes. That is, the VPI resulted in higher aromatization selectivities, lower production of hexene intermediates, lower hydrogenolysis activity, and a lower deactivation rate.

A comparison of the *VPI-PWD-HV* and *IWI-PWD* catalysts was also conducted at 500°C, a temperature that is commonly reported in the literature for catalytic testing of Pt/KL. Results of catalytic testing, shown in Figure 5.6,

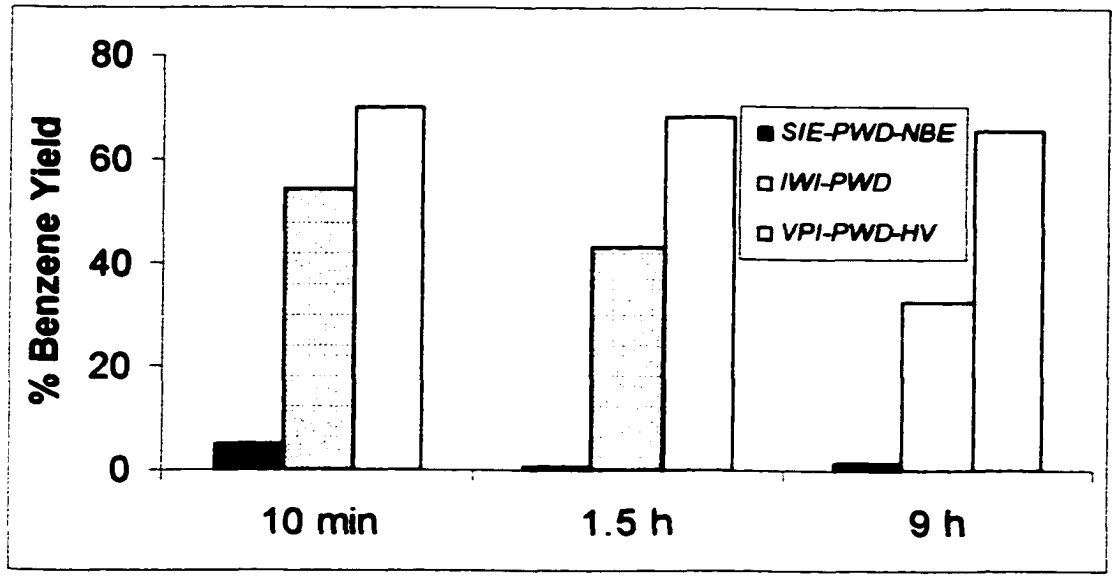

Figure 5.5: Benzene yield versus time onstream obtained under flow conditions (T: 450°C, WHSV: 10 h^{-1}, P: 1 atm) on powder catalysts prepared by the standard ion exchange method without back exchange (*SIE-PWD-NBE*), incipient wetness impregnation (*IWI-PWD*), and vapor phase impregnation high vacuum (*VPI-PWD-HV*).

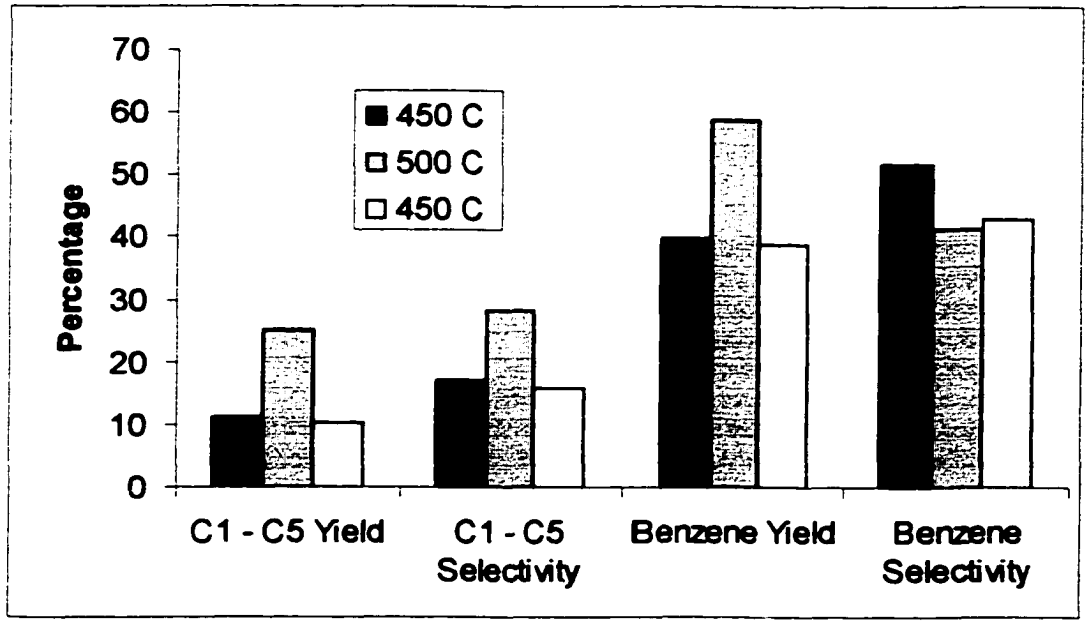

Figure 5.6: Yield and selectivities of hydrogenolysis ($C_1 - C_5$) and benzene for a Pt(1%)/IWI catalyst tested for n-hexane aromatization at 450°C, followed by ramping and testing at 500°C, and then reducing the temperature back to 450°C and testing one final time.

indicated much higher hydrogenolysis at 500°C in comparison with the results obtained at 450°C. To determine whether the loss in aromatization selectivity at 500°C was due to an irreversible Pt particle growth or simply to kinetic reasons, we conducted the following experiment. First, we tested the VPI catalyst at 450°C, increased the temperature and tested at 500°C, and then reduced the temperature to 450°C to take the final measurement. The result was that increasing the temperature led to an increase in hydrogenolysis. After reducing the temperature back to 450°C, the hydrogenolysis pathway was as low as before. Results are reported in Figure 5.6. For a well-prepared catalyst, 450°C appears as an appropriate choice for aromatization, yielding satisfactory activity and selectivity. Higher temperatures may yield higher conversion, but they are detrimental for selectivity and particularly stability. However, a word of caution is important since this conclusion was drawn from data obtained at near-atmospheric pressure and it may not hold valid under the high pressures employed in the industrial process.

In order to test the effect of excess water on the preparation of IWI catalysts, comparisons were made for the *IWI-PWD*, *IWI-PWD-EXP*, *IWI-PWD-XS*, and *IWI-PWD-NCL* catalysts. Reaction results for the four catalysts are displayed in Figure 5.7. The *IWI-PWD-EXP* catalyst, which contained water in the pores before impregnation, but was then impregnated just to incipient wetness, did not show any marked difference with the *IWI-PWD* catalyst. However, the *IWI-PWD-XS* and *IWI-PWD-NCL* catalysts, which were filled beyond incipient wetness, clearly displayed lower activity and a more significant deactivation than catalysts filled to incipient wetness. These results correlated well with hydrogen chemisorption data,

which showed lower H/Pt values for the catalysts prepared with excess water. Therefore, excess water during IWI preparation results in a distribution of Pt with greater sensitivity to particle growth during the reduction step.

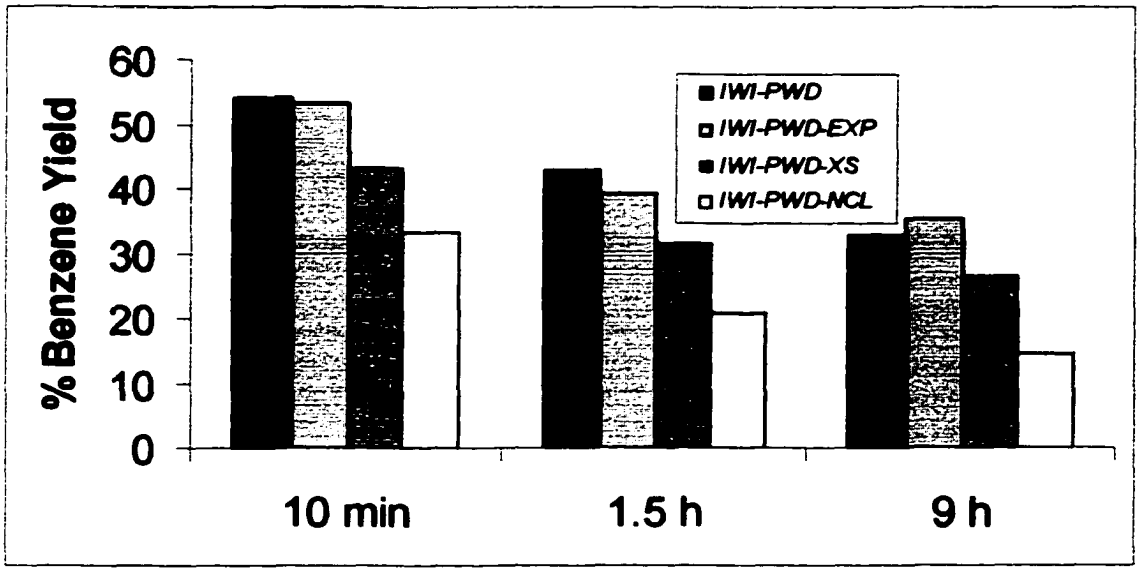

Figure 5.7: Benzene yield versus time onstream under n-hexane aromatization flow conditions (T: 450°C, WHSV: 10 h^{-1}, P: 1 atm) for IWI powder catalysts prepared by calcining and keeping the L-zeolite very dehydrated before salt solution addition *(IWI-PWD)*, exposing calcined L-zeolite to ambient conditions before salt solution addition *(IWI-PWD-EXP)*, exposing calcined L-zeolite to ambient conditions and overfilling during salt solution addition *(IWI-PWD-XS)*, and without calcination of the L-zeolite prior to salt solution addition *(IWI-PWD-NCL)*.

Testing was further conducted on the different VPI preparation methods. Comparisons are shown in Figure 5.8 for the *VPI-PWD-MP*, *VPI-PWD-HEF*, and *VPI-PWD-HV* catalysts. In line with hydrogen chemisorption and FTIR of adsorbed CO results, no notable differences were detected between the *VPI-PWD-HV* and *VPI-PWD-MP* catalysts. The *VPI-PWD-HEF* catalyst exhibited a somewhat lower yield but most of this difference was due to a lower metal loading.

In this preparation, the Pt precursor was physically mixed to obtain a loading of 1% Pt, but the final loading was determined to be 0.89%, evidencing some loss of metal during the sublimation under flow.

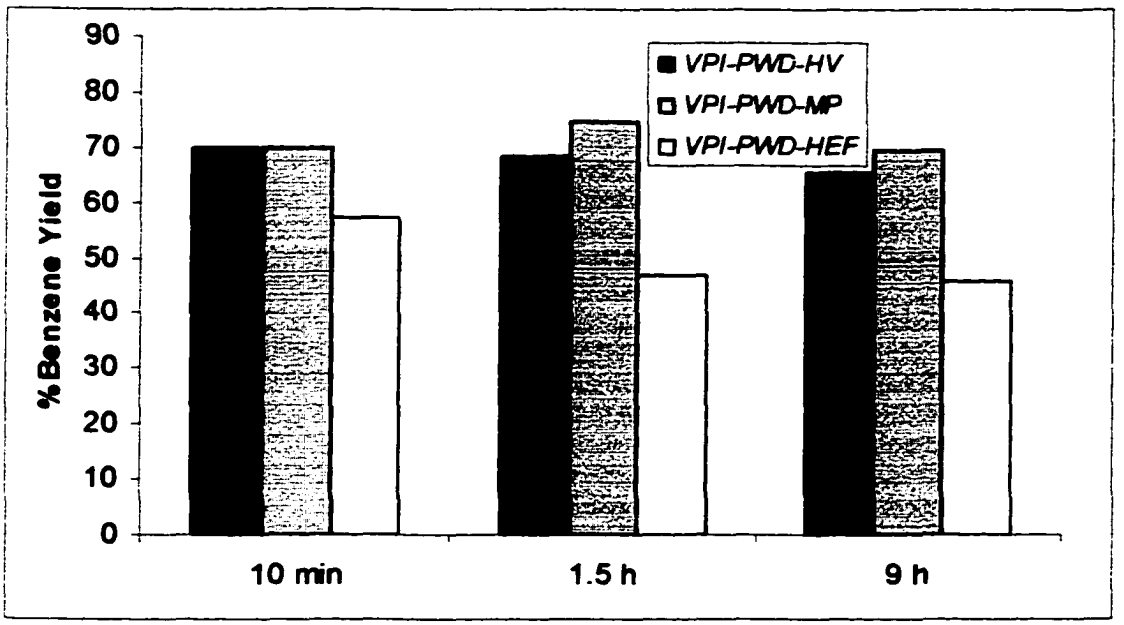

Figure 5.8: Benzene yield versus time onstream under n-hexane aromatization flow conditions (T: 450°C, WHSV: 10 h^{-1}, P: 1 atm).for VPI powder catalysts prepared by using high vacuum (*VPI-PWD-HV*), a mechanical pump vacuum (*VPI-PWD-MP*), and under helium flow (*VPI-PWD-HEF*).

5.3.2.2 Pellet Catalysts

Results for the pellet catalysts are reported in Figure 5.9. Although the impregnation catalysts, and especially the vapor phase impregnation catalysts, showed good catalytic performance for the powder preparation, these attributes were not reproduced when the incorporation of the metal was done on the pellet. It is possible that even if the initial activity may have been relatively high, the deactivation of these catalysts is so rapid that by the time the first data point was obtained they had virtually deactivated. A similar behavior was reported in our

previous work for nonmicroporous Pt/SiO_2 and Pt/Mg(Al)O catalysts, which exhibited comparable aromatization activities in the pulse-mode operation, but quickly deactivated under flow, as shown in Chapters 3 and 4.

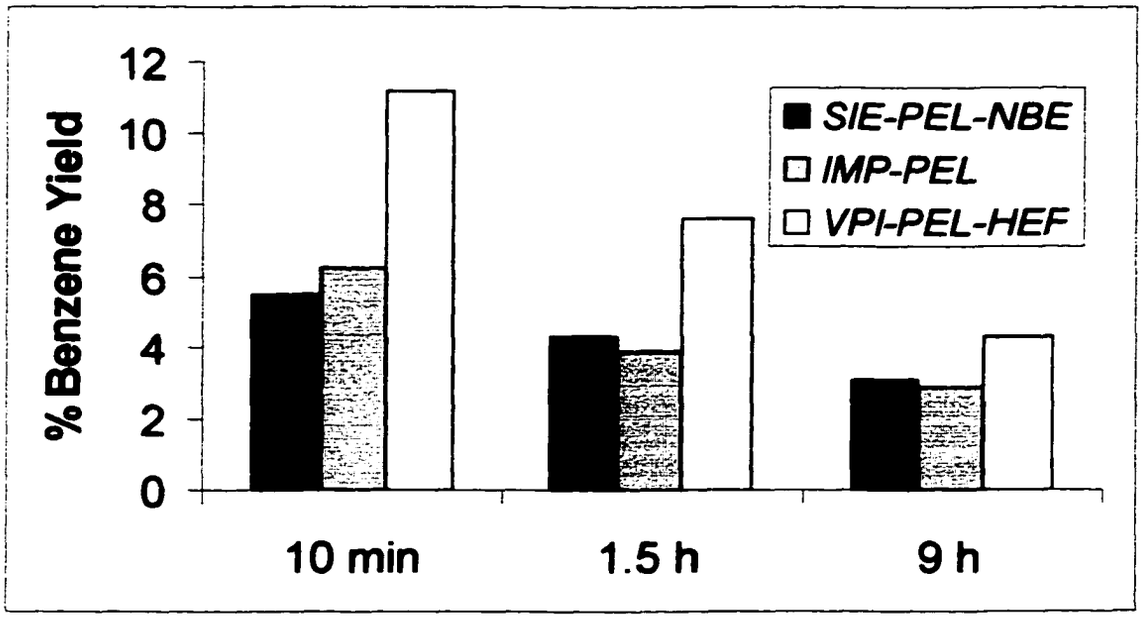

Figure 5.9: Benzene yield versus time onstream under n-hexane aromatization flow conditions (T: 450°C, WHSV: 10 h^{-1}, P: 1 atm) for palletized catalysts prepared by the standard ion exchange method (*SIE-PEL-NBE)*, dip impregnation (*IMP-PEL)*, and vapor phase impregnation using helium flow (*VPI-PEL-HEF)*.

5.4 DISCUSSION

The purpose of this work was to study how different preparation procedures affected the resulting distribution of Pt cluster morphology and location, and to correlate these changes with the resulting catalytic performance and stability of Pt/KL powder and pellet catalysts for the aromatization of n-hexane. We can first analyze the results of the characterization methods and interpret the wide range in activity and stability displayed by the catalysts when we systematically varied the

method of incorporation of Pt. We will then discuss the implications of these results in the production of effective industrial Pt/KL catalysts.

Hydrogen chemisorption results demonstrate that with all preparation techniques employed, the Pt clusters were very highly dispersed. However, important changes in the overall stability of the various samples were observed under the flow reaction. Therefore, dispersion measurements alone are not good indicators of a well-prepared catalyst. Therefore, we attempted to determine the morphology and location distributions of the catalysts to find out if this distribution can be correlated with catalytic performance and stability. As mentioned, FTIR of adsorbed CO is a tool that probes the location (i.e., inside the L-zeolite or external) and distribution of the Pt clusters loaded to KL [92]. As discussed previously, a broad distribution of bands (2080 cm^{-1} – 1930 cm^{-1}) for linearly bonded CO has been observed for Pt/KL catalysts. As discussed in the previous section, this distribution can be divided into three important regions: (1) bands below 2050 cm^{-1} are assigned to Pt-CO species arising from the disruption of small Pt clusters inside the L-zeolite channels; (2) bands between 2050 and 2075 cm^{-1} are associated with larger Pt clusters in the near-surface region of the L-zeolite; and (3) bands at around 2080 cm^{-1} are in general assigned to larger Pt particles on the external surface of the L-zeolite.

The assignments are not only useful for probing the state of Pt clusters at a specific temperature (e.g., a temperature required for a specific reaction), but they also give dynamic information about the resistance of Pt clusters to agglomeration when the reduction temperature is increased. This resistance is related not only to

the cluster morphology, but also to the location (internal or external as well as distance from the pore mouth) of the cluster and its proximity relative to neighboring clusters. This information is particularly useful for screening different preparations of Pt/KL catalysts.

From Figures 5.1 a and b, it is evident that after reduction at 400°C, a large fraction of Pt clusters in the standard IE catalyst (*SIE-PWD-NBE*) are either outside the L-zeolite channels or close to the pore mouth. Only a small fraction of Pt-carbonyls was observed at 2033 cm^{-1} and 2010 cm^{-1}, while lower wavenumber bands were absent almost entirely. However, after reduction at 500°C, the spectrum was drastically shifted to even higher wavenumbers, and the peak at 2080 cm^{-1} dominated the spectrum. These results suggested that with the standard ion exchange procedure, the Pt particles end up close to the mouth of the pores. The sensitivity to high temperature treatment suggested that the Pt particles were in close proximity to one another, resulting in agglomeration. The near-surface species also migrated after the high temperature treatment to the external surface of the L-zeolite. Figure 5.2a shows that the back–exchange procedure, which was normally effective in removing unwanted acidity, offered no real improvement in Pt cluster morphology. Similarly, the IE pellet catalyst prepared by the standard ion exchange method (Figure 5.4) displayed poor characteristics. Figure 5.2b showed, however, that the modified IE catalyst displayed a greater fraction of low wavenumber bands after reduction at 500°C than the standard IE catalyst, and showed virtually no bands associated with external Pt, in contrast with the standard IE catalyst. It is clear that the aging step during preparation aided in dispersing the

salt throughout the channels. It is likely that these characteristics are carried over to extrudates.

The IWI procedure offered a marked improvement over the standard IE method. Figures 5.1 a and b illustrate that except for a small fraction as indicated by a slight shoulder at 2075 cm^{-1}, virtually all of the Pt is located inside the channels of the L-zeolite. After reduction at 400°C, little differences were observed in the spectra in comparison with the VPI catalyst. However, increasing the reduction temperature to 500°C demonstrated that the IWI catalyst was more susceptible to agglomeration than the VPI. This was indicated by the growth in bands between 2050 cm^{-1} and 2075 cm^{-1} and the loss of the bands associated with Pt-carbonyls. In our previous study in Chapter 4, we showed by EXAFS, MCP-RO, and TEM that a fraction of particles large enough to block the channels existed for IWI catalysts after reduction at 500°C. While the IWI procedure incorporated small clusters into the L-zeolite, it appears that after preparation, a fraction of the clusters were in close proximity to one another. After high temperature treatment, this fraction of small particles, located near the mouth of the pore, agglomerated to fill and partially block the channels.

Further improvement in catalyst preparation was achieved with the VPI procedure. Fig 5.1a shows that after reduction at 400°C, not only most of the Pt in this catalyst was located inside the channels of the L-zeolite, but this sample also showed the highest intensity of bands in the range of Pt-carbonyls. Besides, as shown in Fig 5.1b, after reduction at 500°C, the bands did not display a shift to higher wavenumbers as the other catalysts did. Again, these results were consistent

with our previous VPI results (Chapter 4) from EXAFS, which displayed lower Pt-Pt coordination and higher Pt coordination to zeolite lattice oxygen atoms in comparison with IWI catalysts.

Therefore, we conclude that the VPI preparation procedure resulted in small Pt clusters that were more evenly distributed throughout the L-zeolite channels than those produced from the IWI and IE methods. The results of FTIR after reduction treatment at 500°C suggested that the VPI procedure did not selectively deposit a greater fraction of Pt clusters at the near-surface region, in contrast with the IWI and standard IE catalysts. The Pt clusters in this region were located further apart for the VPI catalyst, resulting in a catalyst that was more resistant to agglomeration at high temperature. Note that the modified IE powder (*MIE-PWD*) catalyst showed a considerable improvement in Pt cluster morphology over the standard method. However, the fraction of Pt carbonyl bands in the low wavenumber region were considerable lower than the VPI powder catalysts, indicating the VPI is a marked improvement over even the modified IE method for preparation on the powder.

The use of a moderate vacuum (e.g., mechanical pump) or a low helium flow to prepare the VPI powder catalyst resulted in a catalyst with a similar distribution to the catalyst prepared using high vacuum (Figure 5.3). However, as shown in Figure 5.4, preparation on the pellet resulted in a considerable fraction of Pt external to the L-zeolite and likely on the binder. The fraction of bands associated with Pt-carbonyls was much lower than on the VPI powder catalysts. The implication of these results is very important. Using the VPI preparation

method directly on L-zeolite pellets does not lead to a catalyst with improved catalytic properties. However, if a method existed to prepare pellets extruded directly from the VPI powder catalyst without affecting the Pt clusters, the result would likely be a major development.

5.4.1 Catalytic Performance and Stability

Fig. 5.5 shows that under n-hexane flow reaction at 450°C and WHSV = 10 h^{-1}, the standard IE catalyst rapidly deactivated. In fact, by the time the first point was taken at 10 min, the catalyst had already virtually deactivated. In conjunction with FTIR results, which demonstrate a considerable fraction of external Pt and large clusters at the pore mouth, and considering the dark appearance of the catalyst after reaction, it is clear that the catalyst deactivated by coke formation. This result is in agreement with the interpretation by Iglesia and Baumgartner [19,20]; they proposed that external Pt is susceptible to bimolecular reaction pathways which lead to the formation of coke.

In contrast to the standard IE catalyst, Figure 5.5 shows that the deactivation of the IWI catalyst was a slower process. The catalyst approaches steady state after approximately 9 h on stream. Results from FTIR show that Pt is mostly located inside the channels of the L-zeolite. Therefore, the mechanism of deactivation is not simply coking of external Pt. The high temperature reduction treatment in the FTIR study demonstrated that the Pt clusters from the IWI procedure have a fraction prone to agglomeration in the near-surface region of the channels. This

agglomeration accounts for the slow deactivation of the catalyst to a benzene yield which is approximately half that of the VPI catalyst after 9 h on stream.

Further evidence for this mode of deactivation, reported elsewhere in the literature [99], is provided by examining the IWI catalysts prepared with excess water. In the FTIR results (not shown), the band positions were the same as the standard IWI catalyst. However, results of hydrogen chemisorption (Table 5.2) demonstrated that these catalysts were more sensitive to Pt particle growth after high temperature reduction, and especially in the case of the catalyst prepared without dehydrating the L-zeolite support. This indicated a fraction of the Pt deposited selectively near the pore mouth, resulting in smaller distances between Pt clusters after the calcination and reduction steps.

FTIR results for the dip impregnation pellet catalyst were not shown for clarity. However, the presence of a large fraction of bands at 2080 cm^{-1} and only a small contribution from the Pt-carbonyl range indicated a significant fraction of external Pt. Therefore, the Pt likely deposited in large part on the binder. Reaction testing (Figure 5.9) was in agreement with those findings. The catalyst deactivated rapidly by the formation of coke.

As demonstrated in Figures 5.5 and 5.8, the VPI catalysts displayed the highest activity and selectivity and the lowest deactivation rates. FTIR results showed that in addition to the Pt being located inside the L-channels, the Pt clusters were also more resistant to high temperature reduction. Therefore, under reaction, the catalysts showed little or no evidence for deactivation from agglomeration of Pt. The VPI catalysts prepared by moderate vacuum (*VPI-PWD-MP*) performed as well

as the high vacuum catalyst (*VPI-PWD-HV*). However, the helium flow VPI catalyst (*VPI-PWD-HEF*) showed slightly lower activity. This difference can be explained by the fact that a fraction of the Pt precursor was lost during the sublimation procedure (Table 5.1). The helium flow procedure resulted in a lower loading of Pt than the vacuum preparation techniques. It is important to note that the L-zeolite must be kept moisture free during the VPI preparation. We have observed previously that introducing traces of water into the L-zeolite by exposure to ambient conditions prior to sublimation of the Pt acetylacetonate resulted in a catalyst that deactivated under n-hexane aromatization.

The VPI pellet catalyst, which displayed a considerable fraction of near-surface and external Pt from FTIR, deactivated almost completely during 9 h under flow reaction. This demonstrated further that the VPI procedure was ineffective when directly conducted on extrudates. However, preparation of the pellet directly from extruding the VPI powder catalyst may lead to a good catalyst for commercial scale-up.

5.5. CONCLUSIONS

The method of preparation and the choice of either powder or pellet for the support strongly influence the resulting Pt cluster morphology and location distribution. All powder catalysts – IE, IWI, and VPI - were found to exhibit high H/Pt ratios, all of which were greater than unity. However, FTIR of adsorbed CO showed that, more important than dispersion, it is the distribution of Pt cluster

morphology and location that influences the activity and stability of the catalyst for the n-hexane aromatization reaction.

For catalysts reduced at 400°C, FTIR showed that the IE catalyst prepared by the standard method had a large fraction of Pt external to the L-zeolite. In contrast, the IWI and VPI catalysts displayed virtually all of the Pt inside the L-zeolite channels. After reduction at 500°C, the catalysts displayed differences in sensitivity to the treatment. Our standard IE catalysts showed growth in bands at high wavenumbers indicative of Pt migration out of the L-zeolite channels. These catalysts rapidly deactivation by coke formation. An ion exchange catalyst with improved Pt cluster morphology was also prepared using a modified ion exchange procedure found in the patent literature. In that case, an aging step allows the salt to distribute inside the channels of the L-zeolite, as revealed by DRIFTS of adsorbed CO. IWI catalysts also displayed growth in bands assigned to Pt clusters inside the channels, but near the surface. The IWI catalysts were found to slowly lose activity, reaching a steady state activity approximately half that of the initial activity. VPI catalysts maintained low wavenumber bands after high temperature reduction, indicating that the small Pt clusters were more evenly distributed, and not localized near the pore mouth. These catalysts showed the highest activity and selectivity, with long-term stability. The IWI and IE catalysts were also less reproducible than the VPI preparation.

Reaction testing and characterization demonstrated that the VPI catalyst could be scaled-up using either a moderate vacuum or a helium flow preparation method. These catalysts displayed very little differences from the high vacuum

preparation method when probed with FTIR of adsorbed CO. No differences in activity or stability were observed between the catalyst prepared by moderate or high vacuum. The catalyst prepared by the helium flow VPI method showed no differences in band positions, but 10% of the Pt was lost during the preparation procedure. Preparation directly on the pellets resulted in a large fraction of Pt external to the pores and likely on the binder for the methods studied in this work – standard IE, IWI, and VPI. However, in light of the results of DRIFTS of adsorbed CO for the powder catalyst, it is likely that the modified IE method could result in a pelletized catalyst with better characteristics than the one prepared by the standard IE method. Finally, preparation of the pellet directly from extruding the VPI powder catalyst may lead to a good catalyst for commercial use.

SPECIAL ACKNOWLEDGMENTS

I am grateful for the help of Dr. Walter Alvarez for helping me with the preparation of this work, as well as for teaching me how to conduct the FTIR experiments. I would also like to acknowledge NSF for my GRT traineeship, that supported this work, as well as Phillips Petroleum for a scholarship.

CHAPTER VI: LANTHANIDE PROMOTERS – Improving sulfur tolerance, reactivity

Tm containing Pt/KL catalysts were prepared by a variety of techniques, including incipient wetness impregnation (IWI), ion exchange (IE), and vapor phase impregnation (VPI) methods. The Pt morphology resulting by the addition of Tm and Pt sequentially using the VPI method was found to yield the greatest enhancement to the aromatization performance of the Pt/KL catalysts studied.

The presence of Tm in the sequential VPI Pt/Tm/KL catalyst resulted reproducibly in a catalyst with higher Pt dispersion than an unpromoted VPI catalyst, as determined by EXAFS analysis and DRIFTS of adsorbed CO. VPI catalysts themselves have been demonstrated to give more finely dispersed Pt clusters than either conventional IWI or IE methods. From TPO of poisoned catalysts, Tm was also found to act as a getter for sulfur, so it delays the poisoning of Pt under sulfur-containing feeds, as further evidenced by reaction studies. In addition, the initial activity of the Tm-promoted VPI catalysts was found to be higher than that of the unpromoted Pt/KL VPI catalysts, suggesting that Tm may directly modify Pt or even participate in accelerating the aromatization reaction.

The amount and method of incorporation of Tm was found to be critical to the morphology of the Pt clusters and, subsequently, on catalyst performance under sulfur free and sulfur-poisoned reaction conditions. While the sequential vapor phase impregnation method with a small amount of Tm (0.15%) yielded a catalyst with improved catalytic properties, some of the other methods such as coimpregnation of Pt and Tm were found to hinder the dispersion of Pt. This may cause the blocking of

the L-zeolite channels, as demonstrated by DRIFTS of adsorbed CO, and a higher deactivation rate under reaction.

6.1 INTRODUCTION

Pt/KL catalysts are highly active and selective for the aromatization of hexane, but they display a very high sensitivity to even small concentrations of sulfur in the feed, as reviewed in Section 1.5.

Few reports have been published on investigations attempting to develop sulfur-tolerant Pt/KL aromatization catalysts [100]. One possible approach to increase sulfur tolerance could be the addition of promoters. There are a number of ways in which these promoters could operate [101]. They may act as anchoring sites for Pt particles, thus preventing their growth. They may also act as sulfur getters, thus protecting Pt, albeit temporarily, from sulfur poisoning. Alternatively, they might modify the chemical properties of Pt, making it less susceptible to poisoning. For example, the support acidity has in some cases been associated with increased sulfur tolerance [102, 103]. The rationale for this tolerance is that, on acidic supports, the metal particles are electron deficient, and this electron deficiency would result in weaker metal-sulfur bonds. In support of this idea, the sulfur coverage has been found to decrease with increasing support acidity [104].

Few authors have studied the addition of rare earth elements as promoters [35,36,105,106]. Li et al. [35,36] have indicated that the addition of rare earth elements may have a positive effect on the aromatization activity and the sulfur resistance of Pt/KL catalysts. In those studies, the preparation method employed was

the co-impregnation of Pt and the rare earth with aqueous solutions. In Chapter 4 and 5, we pointed out that by varying the preparation method of Pt/KL catalysts, one can greatly influence the location and morphology of the Pt particles inside the channels of the zeolite. These morphology variations have strong effects on the stability of the catalysts under both sulfur-free and sulfur-containing feeds. Chapter 4 and 5 reveal that the characteristic morphology produced by the VPI method was found to improve the performance of the catalyst under clean and sulfur poisoned conditions, enhancing the catalyst's resistance to the formation of coke and decreasing the particle agglomeration rate. A detailed TEM study has recently been published by Treacy [99] demonstrating the impact of platinum morphology of Pt/KL on pore blockage by agglomeration and coke production. The best Pt/KL catalysts were found to have the platinum inside the channels in a very well dispersed state. In this contribution, we have investigated the combined effects of the preparation method and the addition of a rare earth (Tm), with a primary focus on the vapor phase impregnation technique as a means to achieve finely distributed Pt clusters.

6.2 EXPERIMENTAL

6.2.1 Catalyst Preparation

The K-LTL zeolite (series TSZ-500, BET area 292 m^2/g, SiO_2/Al_2O_3 ratio = 6) was provided by Tosoh Company. Before addition of precursor salts, the K-LTL zeolite was dried in an oven at 110°C for 12 h and calcined by ramping the zeolite for 2 h in flow of UHP air to 400°C and holding at 400°C in air flow for 5 h. Platinum was loaded by two methods, incipient wetness impregnation (IWI) and vapor phase

impregnation (VPI), as discussed in Section 2.1. For the thulium-promoted catalyst, Tm and Pt were either loaded sequentially or simultaneously. Table 6.1 summarizes the various catalysts investigated in this work. The preparation parameters investigated were the Tm loading, the method, and the order of incorporating the components. For all preparation methods, the KL-zeolite was first calcined by ramping the zeolite for 2 h in flow of UHP air to 400°C and holding at 400°C in air flow for 5 h.

Table 6.1. Characteristics of the catalysts investigated.

Samples	Preparation Method	wt % Tm	wt % Pt
IWI	Incipient wetness impregnation	0	1.0
VPI	Vapor phase impregnation	0	1.0
Tm-s-VPI	Sequential vapor phase impregnation	0.15	1.0
Tm-S-VPI	Sequential vapor phase impregnation	1.50	1.0
Tm-co-VPI	Co-impregnation, vapor phase	0.15	1.0
Tm-s-IWI	Sequential incipient wetness impregnation	0.15	1.0
Tm-rs-IWI	Sequential incipient wetness impregnation (reverse sequence)	0.15	1.0
Tm-co-IWI	Co-impregnation, incipient wetness	0.15	1.0
Tm-IE	Tm added by ion exchange, Pt by IWI	0.15	1.0

Seven Tm-containing catalysts were prepared by different methods. Four samples were prepared by impregnation with aqueous solutions of thulium nitrate and tetraammineplatinum (II) nitrate. One of them was prepared by co-impregnation (Tm-co-IWI), one was prepared by sequential impregnation (Tm-s-IWI) where Tm was added prior to Pt addition, and one was prepared in the reverse sequence (Tm-rs-IWI). For sequential impregnation, intermediate drying and calcination steps were conducted before the second precursor was impregnated. The amount of Tm varied, as shown in Table 6.1. A fourth sample (Tm-IE) was prepared by ion exchanging the Tm and impregnating the Pt salt.

Two samples of different Tm loading were prepared by the VPI method. In this case, the Tm was first incorporated by sublimation of thulium 2,4-pentanedionate (Alfa, Stock #13164); following the same protocol as described earlier. In the final step, Pt was added by the VPI method. These samples are identified as Tm-s-VPI (0.15% wt. Tm) and Tm-S-VPI (1.5 wt. % Tm). Finally, a seventh sample (Tm-co-VPI) was prepared by co-impregnation by the vapor phase method, where the two precursors were sublimed simultaneously.

6.2.2 Catalytic Activity Testing

In the pulse mode, the n-hexane reaction was studied using a pyrex reactor and 0.025 g of sample in each run. The catalysts were reduced in situ at 500°C The reaction was carried out at 450°C and 500°C using 100 μl pulses containing around 6.57×10^{-7} moles of n-hexane. The carrier gas (35 cm^3/min) used was hydrogen. The products were analyzed in a Hewlett Packard 5890 gas chromatograph, equipped with

a FID detector and a packed column, 30% DC200-Chromosorb 60/80P AW from Alltech.

In the flow mode, reaction tests were conducted according to Section 2.4.1 at WHSV = 10 h^{-1}, employing 0.40 g of catalyst in each run. In all experiments, the hydrogen/n-hexane ratio was kept at 6. Prior to reaction, the catalyst was slowly ramped in flowing hydrogen at 100 cm^3/min for 2 h to a temperature of 500°C and reduced in situ at these conditions. All reactions were conducted at 500°C. For sulfur poisoning studies, thiophene was mixed into the n-hexane feed prior to reaction.

6.2.3 Catalyst Characterization

EXAFS data on in-situ-reduced samples were obtained at the National Synchrotron Light Source (NSLS) at Brookhaven National Laboratory according to Section 2.3.4. Before each measurement, the catalysts, previously reduced ex-situ at 500°C, were re-reduced in situ at 500°C (heating ramp of 10°C /min) for 30 min in flowing H_2.

Infrared spectroscopy (DRIFTS) of adsorbed CO was conducted on samples according to Section 2.3.3, while temperature programmed oxidation (TPO) of the spent catalysts was performed using methods outlined in Section 2.3.5.

6.3 RESULTS AND DISCUSSION

6.3.1 Catalytic Activity Measurements

6.3.1.1 n-Hexane Aromatization in a Pulse Reactor

In a pulse reactor, a small amount of n-hexane is passed over the catalyst under pure hydrogen carrier. Therefore, particularly at the lower temperatures, the

pulse results represent the behavior of a bare catalyst, free of pre-adsorbed hydrocarbons or coke deposits. In this case, the pulse reactor was used to compare the hexane conversions obtained over fresh samples and on samples that had been exposed for 9 h in the flow reactor to a feed containing 1 ppm sulfur. As described in Chapter 3 and 4, in addition to the hydrogenolysis (C_1-C_5) products, the main by-products observed during our flow reaction experiments were hexenes. Those experiments were conducted at 500°C and using a H_2:hydrocarbon ratio of 6:1. By contrast, in the pulse experiments conducted in excess hydrogen, which was used as a carrier, the main by-products were MCP, 2MP, and 3MP. Table 6.2 summarizes the overall conversions and selectivities towards aromatization, isomerization, and hydrogenolysis products at 400°C and 500°C.

In agreement with our previous findings from Chapter 4, we see that at 400°C, the fresh catalysts did not show great differences in activity or selectivity in the pulse reactor. At the moderate conversions obtained at this temperature, the selectivity towards isomerization products was significant. However, at 500°C, the conversion for the three catalysts was 100%. At this high conversion, the isomerization products are further converted to either benzene or hydrogenolysis products. The interconversion of the C6 products has been previously observed by other authors [57], who incorporated the concept of *ultimate selectivity* to differentiate between the conversion to compounds that at high enough conversions may lead to benzene, and the irreversible hydrogenolysis to C_1-C_5 products. Under these conditions, a

Table 6.2. n-hexane conversion in the pulse reactor. Carrier gas H_2, flow rate 35 cm^3/min. Catalyst amount 0.025 g. TOF (s^{-1}) is the number of benzene molecules turned over per Pt atom per second.

Fresh catalysts	*T(K)*	*X (%)*	$S_{Aro}^{\bullet}$	$S_{Iso}^{\bullet\bullet}$	$S_{Hydr}^{\bullet\bullet\bullet}$	*TOF* (s^{-1})
IWI	673	38	32	54	14	0.92
VPI	673	46	33	52	15	1.15
Tm-s-VPI	673	32	35	50	15	0.85
IWI	773	100	70	0	30	5.29
VPI	773	100	73	0	26	5.51
Tm-s-VPI	773	100	79	0	20	5.96
2 ppm S - poisoned catalysts	*T(K)*	*X (%)*	$S_{Aro}^{\bullet}$	$S_{Iso}^{\bullet\bullet}$	$S_{Hydr}^{\bullet\bullet\bullet}$	*TOF* (s^{-1})
IWI	773	10	44	43	13	0.33
VPI	773	90	69	8	23	4.69
Tm-s-VPI	773	80	68	14	18	4.11

$^{\bullet}$ Selectivity to Aromatization (mole %)

$^{\bullet\bullet}$ Selectivity to Isomerization (mole %)

$^{\bullet\bullet\bullet}$ Selectivity to Hydrogenolysis (mole %)

moderate improvement in benzene selectivity at 500°C is observed on the VPI and Tm-s-VPI catalysts compared to IWI. This difference is even more pronounced on the poisoned catalysts. As seen in the table, at 500°C the conversion was only 10% on the IWI catalyst, while stayed very high for the other two.

6.3.1.2 n-Hexane Aromatization in a Flow Reactor

The aromatization of n-hexane was conducted in the flow reactor at 500°C, keeping a H_2/n-hexane feed ratio of 6 and a space velocity of 10 h^{-1} over the three catalysts IWI, VPI, and Tm-s-VPI. During the first 9 h on stream, the feed contained no sulfur. After that initial period, 2 ppm of sulfur was incorporated in the feed. As reported in previous chapters, the catalyst prepared by the VPI method was more active and selective than that prepared by IWI. An interesting increase in activity by the presence of Tm was also observed. An activity enhancement was also reported by Li et al. [35]. As the time on stream increased, the advantages of the VPI and Tm-VPI catalysts over the IWI catalyst became even more pronounced. Similarly, the VPI, and particularly the Tm-s-VPI exhibited significantly higher tolerance to sulfur poisoning. Remarkably, the greatest differences were on benzene selectivity more than on overall conversion. This difference is illustrated in Figs. 6.1 a and 6.1 b, which show the variation of the conversion and benzene selectivity with time on stream first in sulfur-free conditions, and subsequently in the presence of 2 ppm S, for each of the three catalysts.

As mentioned above, the main products obtained under the conditions of our flow reaction studies were benzene, hexenes, and hydrogenolysis products ($< C_5$).

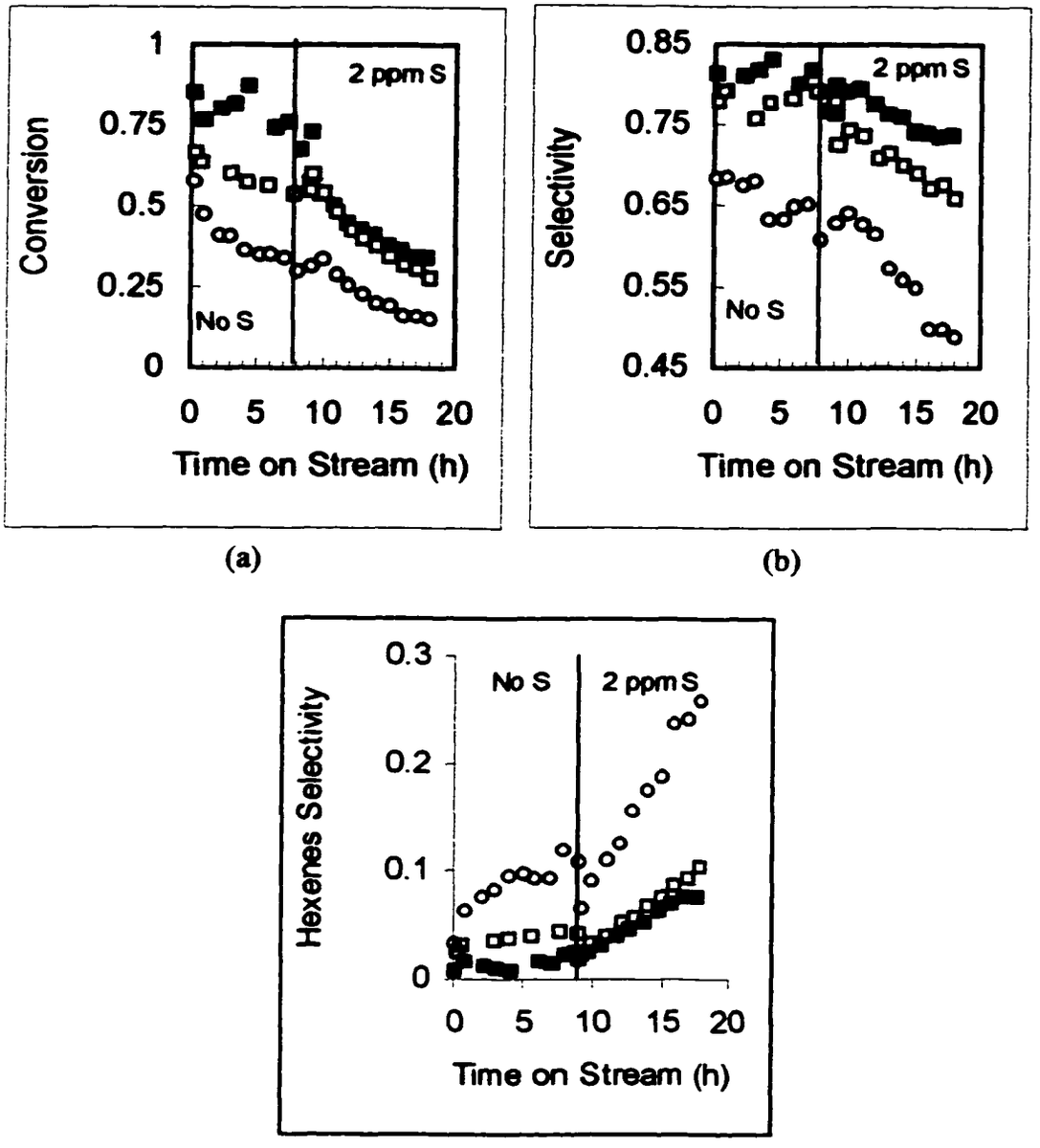

Figure 6.1. The variation of the (a) conversion, (b) benzene selectivity, and (c) hexenes selectivity with time on stream first in sulfur-free conditions, and then in the presence of 2 ppm S, for the IWI (open circles); the VPI (open squares); and Tm-s-VPI (filled squares), respectively, at 500°C (WHSV: 10 h^{-1}).

Isomerization products, which were more abundant in the pulse reactor, were in this case, only present in minor concentrations. The hydrogenolysis products were always low for all the catalysts. For example, the highest methane yield barely exceeded 1%.

As previously observed in Chapters 3 and 4, the evolution of methane yield followed a parallel deactivation pattern to that of aromatization. By contrast, the production of hexenes by dehydrogenation increased with time on stream and this increase was more pronounced when the catalyst deactivated by sulfur poisoning. This behavior is illustrated in Fig. 6.1c. In good agreement with our previous studies in Chapters 3 and 4, it was observed that the catalysts that exhibited the highest aromatization activity produced the lowest amount of hexenes. The VPI sample and particularly the Tm-s-VPI sample produced very little hexenes. Only after deactivation by sulfur suppressed the aromatization activity did the hexene yield become significant.

In the presence of 2 ppm S, the thulium-promoted VPI catalyst showed superior aromatization activity in comparison with the unpromoted VPI and IWI catalysts. However, 10 ppm S was enough to cause all three catalysts to completely lose their ability for aromatization. While the IWI catalyst deactivated completely in 6 hours, the Tm-s-VPI and VPI deactivated completely in 8 hours. The activity and selectivity for aromatization during poisoning followed the trend Tm-s-VPI > VPI > IWI. It is also interesting to note that the Tm-s-VPI catalyst still retained a high degree of dehydrogenation activity after the aromatization activity was completely lost.

When the Tm-promoted catalysts prepared by different methods were compared, the ones prepared by sequential VPI exhibited the best performance. Both the Tm-s-VPI and Tm-S-VPI were much more active, selective, and sulfur tolerant than the others. Fig. 6.2 illustrates the behavior of the Tm-s-VPI compared to that of the Tm-co-VPI and Tm-s-IWI, showing that the addition of Tm alone does not

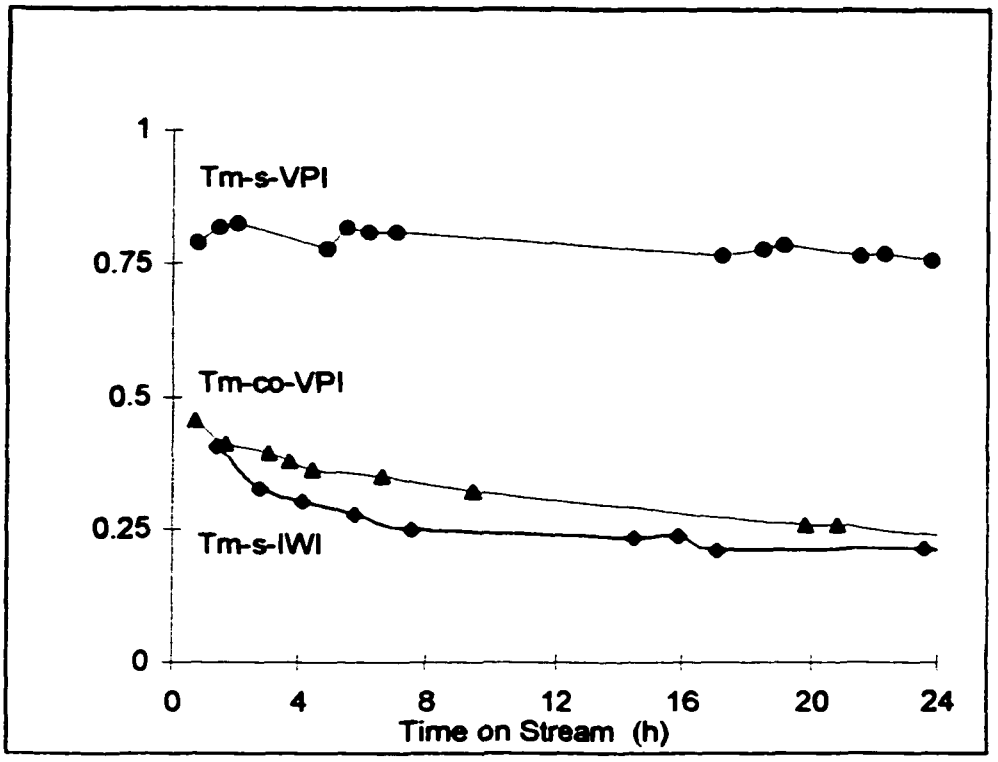

Figure 6.2. Yield of benzene as a function of time onstream (T=500°C, WHSV: 5 h^{-1}) for Tm-s-VPI, Tm-co-VPI, and Tm-s-IWI catalysts.

guarantee a good performance. Similarly, Fig. 6.3a makes a comparison of the selectivity vs. conversion patterns for the preferred Tm-s-VPI preparation with the ones prepared by the other methods. Plotting selectivity versus conversion is a basis generally accepted as a way to compare Pt/KL catalysts. Figure 6.3b compares our selectivity versus conversion results with some of those found in the literature [21,50]. Both the VPI and Tm-s-VPI catalysts display very high selectivity as a function of conversion, and are among the best reported in the literature.

Table 6.3 provides a comparison of our results from reaction testing with some results found in the literature. Most authors used different reaction conditions, loadings, and methods of preparation. In comparing our TOF data with those of Fang

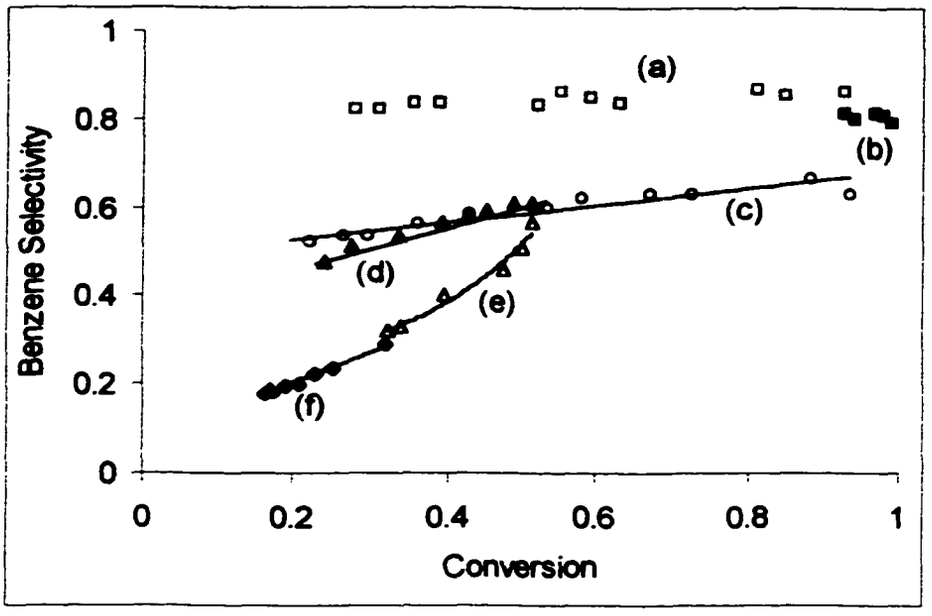

(A)

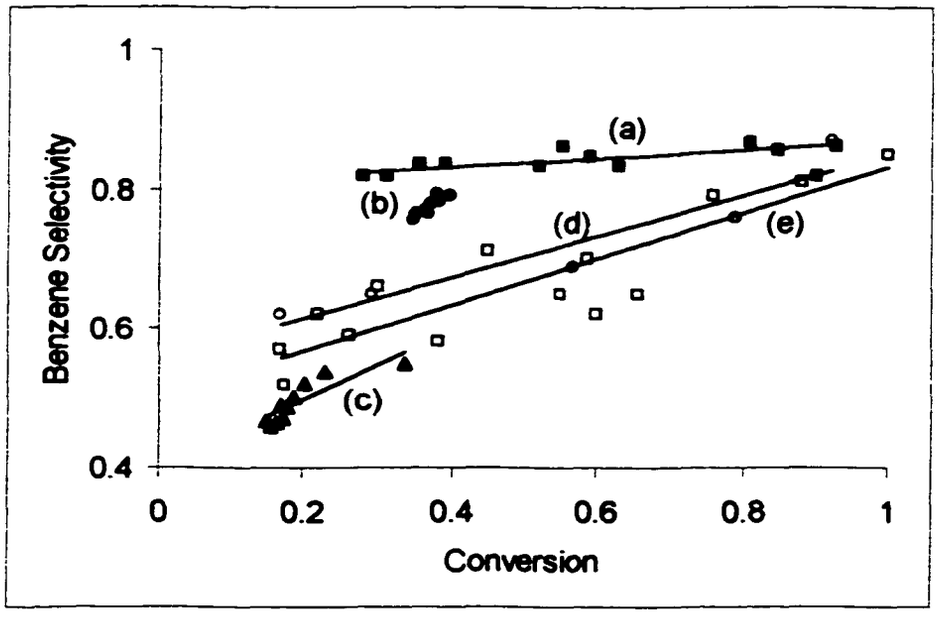

(B)

Figure 6.3. (A) Comparison of the selectivity vs. conversion patterns for the preferred (a) Tm-s-VPI preparation with the ones prepared by (b) Tm-S-VPI, (c) Tm-s-IWI, (d) Tm-rs-IWI, (e) Tm-IE, and (f) Tm-co-IWI. (B) Comparison of the selectivity vs. conversion patterns for our (a) Tm-s-VPI, (b) VPI, and (c) IWI catalysts with those found in the literature including (d) Jentoft et al. and (e) Mielczarski et al.

Table 6.3. Comparison of flow-mode reaction testing. Turnover frequency (TOF) in molecules of benzene turned over per Pt atom per second.

Author	% Pt	% Tm	T (°C)	P (atm)	Method	H_2/HC	% Bz Yield	% Bz Selec.	TOS (h)	TOF (s^{-1}) at T (°C)
Besouk. et al.	0.6	0	460	1	IE	6	40	80	1	0.36
McVicker et al.	0.6	0	510	8.1	IE Pell	6	67	75	20	0.46
Fang et al.	0.8	0	500	1	IWI	-	35	-	4	0.09
Fang et al.	0.8	0	500	1	IWI	-	30	-	10	0.08
Fang et al.	0.8	0.20	500	1	Co-IWI	-	80	-	4	0.20
Fang et al.	0.8	0.20	500	1	Co-IWI	-	80	-	10	0.20
This Work	1.0	0	500	1	IWI	6	24	65	4	0.15
This Work	1.0	0	500	1	IWI	6	18	61	10	0.12
This Work	1.0	0	500	1	VPI	6	55	78	4	0.34
This Work	1.0	0	500	1	VPI	6	45	75	10	0.28
This Work	1.0	0.15	500	1	Tm-s-VPI	6	62	82	4	0.39
This Work	1.0	0.15	500	1	Tm-s-VPI	6	60	80	10	0.38

et al. [35], we chose two points of comparison - 4 h and 10 h on stream. The catalysts prepared by IWI are relatively in agreement. However, our Tm-s-VPI catalyst presents a significant improvement in preparation to the coimpregnation method used by Fang et al. [35].

6.3.2 Catalyst Characterization

6.3.2.1 EXAFS Analysis

A detailed EXAFS analysis of several reduced catalysts was conducted under H_2 flow, before and after 30 h reactions under 1 ppm of sulfur (WHSV: 10 h^{-1}). The structural parameters were determined by the fitting procedure outlined in Section 4.3.1, applying an inverse Fourier transform over the r range 1.5-3.6 Å to isolate the EXAFS contribution of the first coordination sphere of platinum. The filtered data were fitted using the FEFFIT program [82]. The data were fitted using theoretical standards

generated by the FEFF package, as previously discussed. Although the fits obtained with only one Pt-Pt coordination could be considered satisfactory for the IWI catalyst, poor fits were obtained for the other samples with higher metal dispersion, as indicated by the r-factor values in Table 6.4. Therefore, more complex models were also studied. New fittings were conducted which included an interaction between the Pt and the L-zeolite oxygen atoms (Pt-O bond) for Pt particles inside the channels of the L-zeolite, as previously discussed in Section 4.3.1. Theoretical amplitudes and phase shifts corresponding to the Pt-O distances were derived with FEFF, assuming Pt-O bonds at 2.56 Å. It has been suggested that these Pt-O interactions are affected by the presence of H_2 in the interfacial layer between the Pt particles and the zeolite walls [84]. A second model was also investigated. Because the structure of the smallest Pt particles may be more complex, we incorporated a second type of Pt-Pt bond, corresponding to shorter Pt-Pt bonds existing in the smallest particles. It is conceivable that the samples with very high dispersions may contain a fraction of very small Pt particles, with Pt-Pt distances slightly different from those of larger particles. We reported such a distance contraction in Chapter 4. Therefore, a third model was investigated combining both the Pt-O contributions and the second Pt-Pt distance. As shown in Table 6.4, the addition of Pt-O distances in the first coordination sphere enhanced the quality of the fits. However, for the samples with the highest dispersion and those containing Tm, the fit was only marginally improved. For example, for the VPI fresh catalyst, the r-factor was only reduced from 0.034 to 0.033, while for the Tm-s-VPI fresh catalyst, the r-factor was reduced from 0.17 to 0.13. However, after we incorporated a second Pt-Pt distance, the r-factor was markedly improved.

Table 6.4: Changes in fit quality with addition of contributions.

VPI

Fitting	E_0	σ^2	N_{Pt-Pt}	N_{Pt-O}	R (Å)	r-factor
1 Pt-Pt distance	1.8	0.0080	6.7	--	2.71	0.034
1 Pt-Pt distance +	0.05	0.0054	3.7	--	2.69	0.033
Pt-O distance		0.0015	--	1.7	3.0	
2 Pt-Pt distances						
2 Pt-Pt distances +	8.6	0.0025	2.1	--	2.81	0.014
Pt-O distance		0.0025	2.7	--	2.69	
		0.0020	--	0.6	2.67	

Tm-s-VPI

Fitting	E_0	σ^2	N_{Pt-Pt}	N_{Pt-O}	R (Å)	r-factor
1 Pt-Pt distance	0.04	0.0097	6.35	--	2.69	0.17
1 Pt-Pt distance +	12.5	0.0077	2.6	--	2.74	0.13
Pt-O distance		0.00001	--	1.5	2.68	
2 Pt-Pt distances						
2 Pt-Pt distances +	-5.1	0.0012	2.2		2.74	0.028
Pt-O distance		0.0012	2.1		2.61	
		0.0021		1.1	2.39	

Table 6.5: Structural parameters determined from EXAFS analysis.

Fitting	E_0	σ^2	N_{Pt-R}	N_{Pt-O}	R (Å)	r-factor
IWI fresh	6.7	0.0056	7.6	–	2.74	0.012
		0.0060	–	0.25	2.73	
IWI	9.1	0.0056	8.2	–	2.75	0.008
1 ppm Sulfur		0.0030	–	0.35	2.71	
(30 h)						
VPI fresh	8.6	0.0025	2.1	–	2.81	0.014
		0.0025	2.7	–	2.69	
		0.0020	–	0.6	2.67	
VPI	5.4	0.0020	3.1	–	2.77	0.026
1 ppm Sulfur		0.0020	2.6	–	2.67	
(30 h)		0.0045	–	0.5	2.67	
Tm-s-VPI fresh	-5.1	0.0012	2.2		2.74	0.028
		0.0012	2.1		2.61	
		0.0021		1.1	2.39	
Tm-s-VPI	9.1	0.0035	1.9	–	2.80	0.0034
1 ppm Sulfur		0.0035	2.8	–	2.69	
(30 h)		0.0036	–	0.95	2.67	

For the VPI fresh catalyst, the r-factor dropped by a factor of 2, while for the Tm-s-VPI fresh catalyst, the r-factor dropped by a factor of 5. The structural parameters resulting from the fits of the fresh and poisoned catalysts with two Pt-Pt distances and one Pt-O distance are summarized in Table 6.5. The Fourier transforms of the EXAFS data for the freshly reduced Tm-s-VPI, VPI, and IWI catalysts, together with the 30 h sulfur poisoned catalysts, are shown in Figs. 6.4 a, b, and c, respectively. Note the change in scale for each spectra.

In agreement with our previous studies, the resulting parameters indicate that the VPI method leads to a metal dispersion higher than the IWI and, consequently, to a higher population of Pt clusters in close proximity to the zeolite walls. This trend was manifested by lower Pt-Pt and higher Pt-O coordination numbers in the VPI samples compared to the IWI samples. The Tm-s-VPI catalyst exhibited even lower Pt-Pt and higher Pt-O coordination numbers, suggesting that the addition of Tm results in a better dispersion of Pt, in agreement with an earlier study [35]. Also the coordination distances are somewhat lower for this catalyst than for the other Pt/KL catalysts. It is clear that the preparation of the catalyst is critical to the resulting morphology and distribution of Pt clusters. This can result in variations between different batches, as noted by comparison with our previous work [18]. In our experience, the IWI is more sensitive to the preparation than the VPI method. Finally, it is important to point out that, regardless of the model used in the EXAFS analysis, the presence of Tm in the Tm-s-VPI catalyst was found to increase the dispersion of the Pt. By comparing the 30 h 1 ppm sulfur poisoned runs, growth is

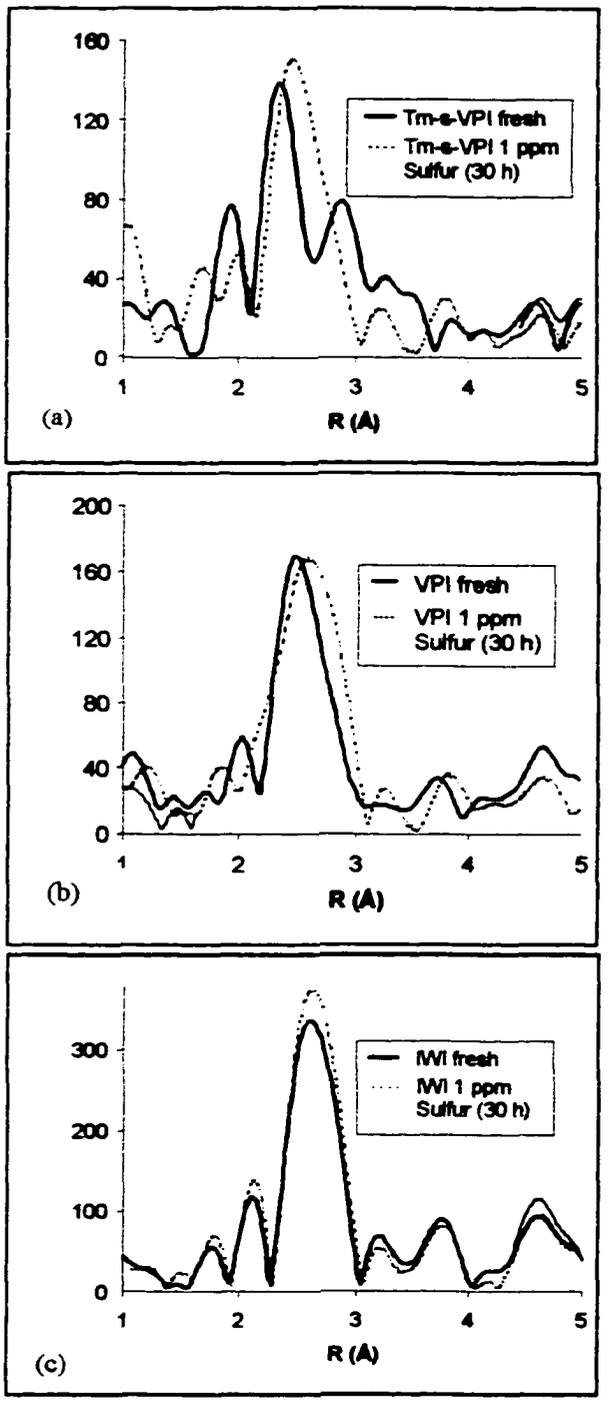

Figure 6.4. Fourier transforms of k^3-weighted EXAFS spectra obtained at liq. N_2 temp on *in-situ* reduced fresh and 30 h 1 ppm sulfur poisoned (a) Tm-s-VPI, (b) VPI, and (c) IWI catalysts.

apparent for all of the catalysts. However, the resulting particle size after poisoning by the vapor phase impregnated catalysts is much smaller than the poisoned IWI catalyst. The smallest particle size was retained by the Tm-s-VPI catalyst after poisoning. Previous modeling and TEM studies [25,99] have shown that after particle growth reaches a point where two or more channel blockages by Pt occur, a large portion of Pt clusters become entrapped and the catalyst deactivates. Since the IWI catalyst has a fraction of large particles inside the channels of the zeolite, slight growth is enough to cause substantial pore blockage under 1 ppm 30 h sulfur poisoning. The VPI catalysts, however, and especially Tm-s-VPI, still retain high enough dispersion that channel blockage, and therefore, deactivation, is marginal, as evidenced under reaction testing.

One of the possible explanations given in the literature for the increased activity and sulfur tolerance exhibited by the Tm-promoted catalysts is an electronic modification of Pt due to an electron transfer from Tm. To test such a hypothesis, we have analyzed the shape and position of the near edge structure in the X-ray absorption spectra of the VPI and Tm-S-VPI catalysts, reduced in situ and cooled in hydrogen flow. Fig. 6.5 shows that the shape and position of the two edges are identical, indicating that the presence of Tm does not result in any significant electronic perturbation of Pt.

6.3.2.2 DRIFTS of adsorbed CO

Fig. 6.6 shows the DRIFTS spectra of CO adsorbed on the IWI and Tm-s-VPI catalysts. Important differences are observed. First, in line with a higher metal dispersion, the absorption bands are more intense on Tm-s-VPI than on IWI. Second,

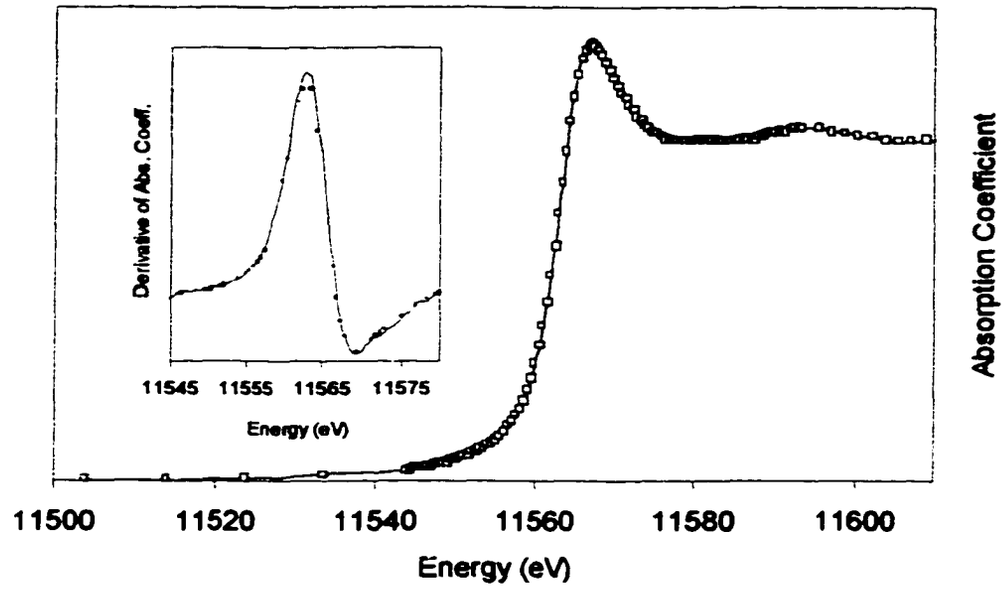

Figure 6.5. XANES spectra and derivative of absorption coefficient of Pt L_{III}-edge for VPI (solid line) and Tm-s-VPI (open squares) catalysts.

the greatest difference in intensity is observed preferentially for the low frequency bands, i.e. below 2050 cm^{-1}.

Lane et al. [93] considered several hypotheses regarding the species responsible for the low frequency bands. They reported three bands resulting from adsorption of CO - the typical linear band at 2060 cm^{-1},the bridged band at 1790 cm^{-1}, and an additional low wavenumber band at 1960 cm^{-1}. They speculated that the support structure influences the location of the platinum and adsorbed CO relative to the potassium cations. From these three bands, they postulated that by the position of the potassium and platinum in Pt/KL catalysts, two environments existed for linear bound CO - one oriented through the pore window and a second oriented to a potassium cation near the wall. In support of this idea, the additional band was also apparent on a platinum supported potassium cation-promoted silica catalyst.

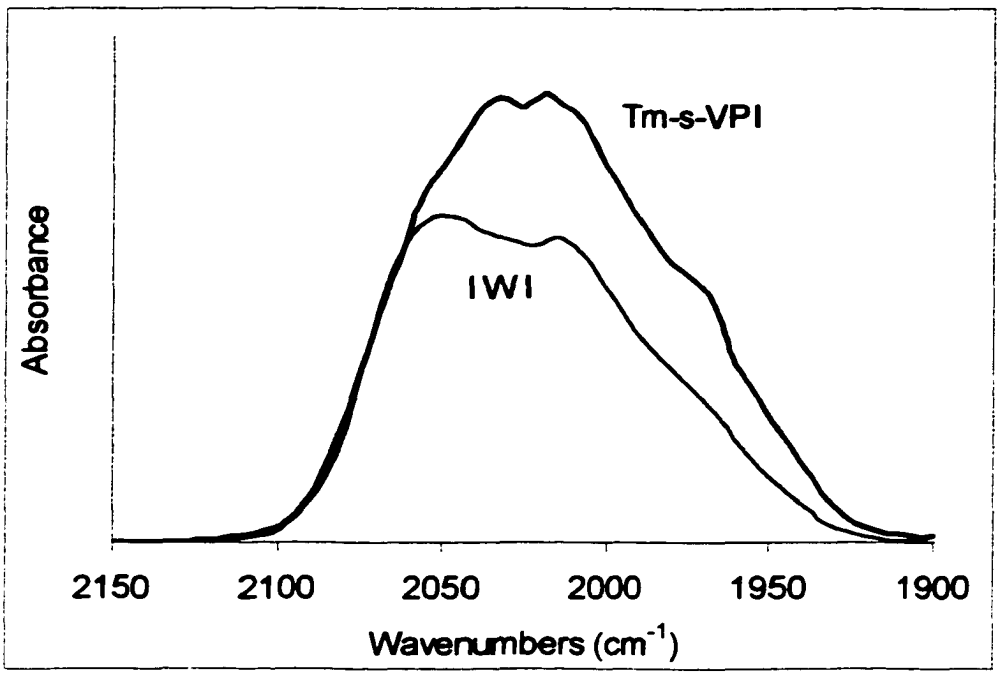

Figure 6.6. DRIFTS spectra of CO adsorbed on IWI and Tm-s-VPI catalysts. The reduced catalysts were exposed to a flow of 3% CO in He for 30 min at room temperature and purged in He for 30 min.

In Chapters 4 and 5, we employed DRIFTS of adsorbed CO to compare the morphology of Pt particles inside the KL zeolite, prepared by different methods. In that case, our results agreed very well with a somewhat different hypothesis, that CO itself modifies the structure of the small Pt clusters inside the KL zeolite [92]. This is discussed in detail in Section 4.3. We found that even though disruption of the small Pt clusters occurs, FTIR of adsorbed CO is still a useful technique for making general conclusions about the location (i.e., inside the L-zeolite or external) and distribution of the Pt clusters prior to disruption.

Although the hypotheses differ regarding the nature of the structures responsible for the low wavenumber bands (2050 cm^{-1} - 1930 cm^{-1}), all are in general

agreement that they reflect the small Pt clusters inside the channels of the L-zeolite. In contrast, the bands at and above 2075 cm^{-1} indicate the Pt external to the pores. Bands present between 2050 cm^{-1} and 2075 cm^{-1} are likely caused by the Pt clusters in the near surface region of the L-channels. Supported with other techniques like EXAFS and in correlation with catalytic performance and stability, this technique can be used to characterize the distribution of Pt clusters and their location.

Based on this hypothesis, we can explain the observed differences in the DRIFTS spectra in terms of a higher dispersion of the Tm-s-VPI catalyst, which favors the formation of Pt carbonyls. As demonstrated by the XANES experiments, no significant differences in the electronic state of Pt are observed by the addition of Tm. Therefore, the appearance of low-frequency bands cannot be ascribed to electronic effects, but rather to a direct interaction of the Pt carbonyls with the cations in the zeolite. The increase in the intensity of the bands in this region is simply a reflection of a greater extent of carbonyl formation/stabilization on the Tm-promoted catalysts, which accordingly would have a higher population of ultra-small particles inside the zeolite than the IWI catalyst. In our previous work in Chapter 4, we observed that catalysts treated under a reduction / oxidation / reduction cycle exhibited formation of Pt carbonyls to a much lower extent than freshly reduced catalyst.

DRIFTS has also been used to characterize the catalysts after exposure to reaction in the presence of sulfur. Fig. 6.7 compares the spectra of adsorbed CO on the three catalysts IWI, VPI, and Tm-s-VPI after being exposed to 9 h reaction at

500°C under 1 ppm S. A clear difference is observed for the Tm-promoted catalyst in comparison with the unpromoted ones. The integrated area for the Tm-s-VPI catalyst

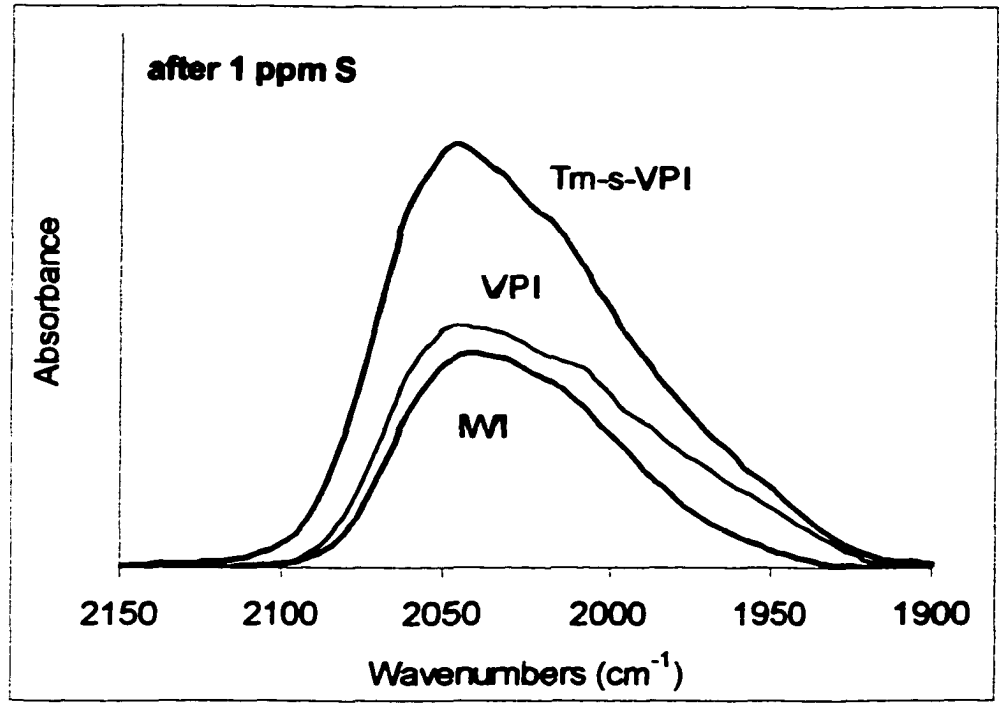

Figure 6.7. DRIFTS spectra of CO adsorbed on IWI, VPI, and Tm-s-VPI catalysts after the catalysts were exposed to 9 h reaction at 500°C, under 1 ppm sulfur (WHSV: 10 h^{-1}). The reduced catalysts were exposed to a flow of 3% CO in He for 30 min at room temperature and purged in He for 30 min.

exposed to 1 ppm S is almost the same as that for the fresh catalyst, indicating that the poisoning of Pt has been minimal. By contrast, a significant reduction in absorbance was observed for the VPI, and even more for the IWI catalyst. The most important effect of sulfur on the Tm-s-VPI catalyst is a decrease in the 1970 cm^{-1} band. As discussed before, this band can be ascribed to carbonyls stabilized by the zeolite cations. Since this band is most intense on the Tm-s-VPI, it is possible that some of the cations that stabilize the carbonyls responsible for this band may be Tm. The

disappearance of this band could indicate that Tm gets poisoned by sulfur, losing the ability to stabilize the carbonyls, but keeping the Pt surface free. When the addition of sulfur exceeds the trapping capacity of Tm, Pt starts being poisoned. This is illustrated in Fig. 6.8, which shows the spectra of the three samples after exposure to reaction under 10 ppm S. In this case, there is no difference in the DRIFT spectra for the three catalysts.

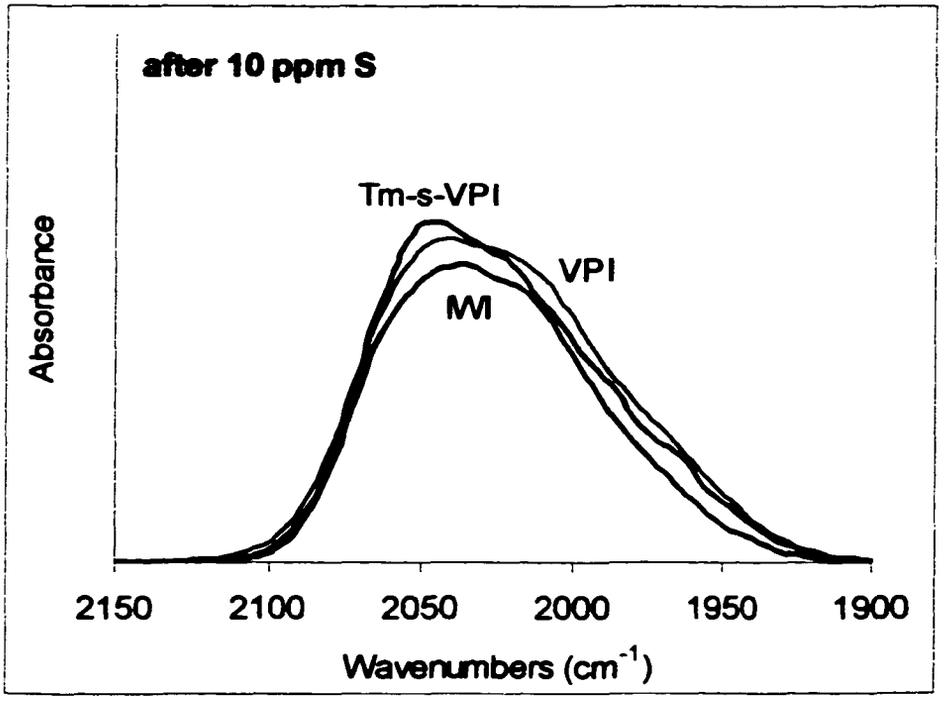

Figure 6.8. DRIFTS spectra of CO adsorbed on IWI, VPI, and Tm-s-VPI catalysts after the catalysts were exposed to 9 h reaction at 500°C, under 10 ppm sulfur (WHSV: 10 h^{-1}). The reduced catalysts were exposed to a flow of 3% CO in He for 30 min at room temperature and purged in He for 30 min.

As noted earlier, the addition of Tm alone does not guarantee an enhancement in catalyst performance. When the Tm-promoted catalysts prepared by different methods were compared, the ones prepared by sequential VPI exhibited the best performance. Fig. 6.9 shows the spectra of adsorbed CO on two Tm catalysts, the

Tm-s-VPI and the Tm-co-VPI. A clear difference is observed. The Tm-co-VPI catalyst, which exhibited much poorer activity and selectivity than the Tm-s-VPI

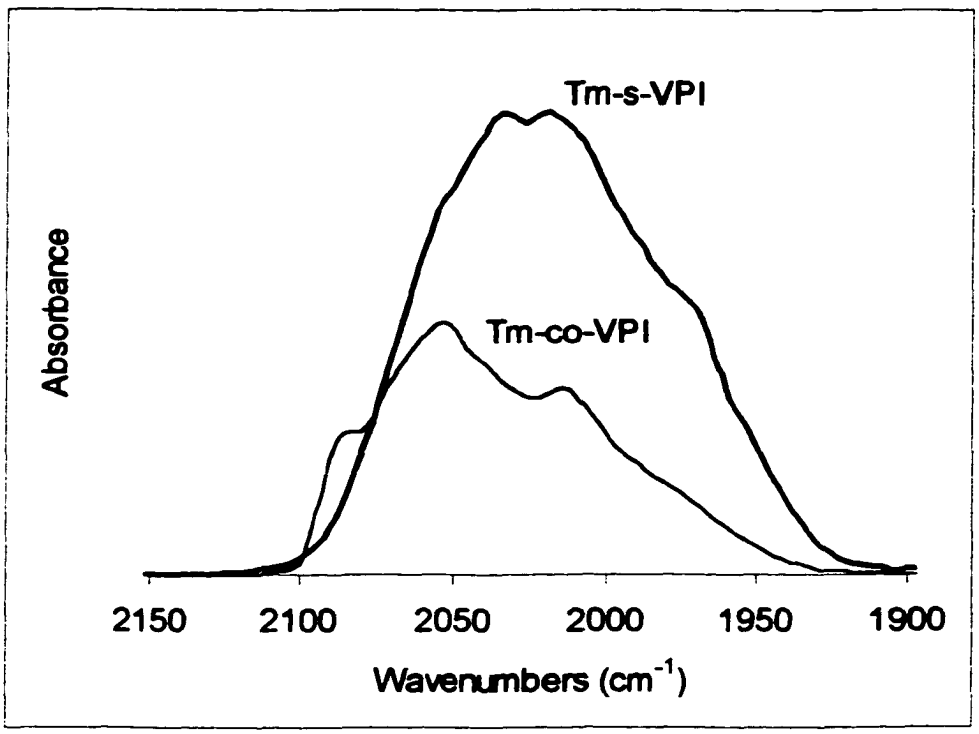

Figure 6.9. DRIFTS spectra of CO adsorbed on Tm-s-VPI and Tm-co-VPI fresh catalysts. The reduced catalysts (T=500°C) were exposed to a flow of 3% CO in He for 30 min at room temperature and purged in He for 30 min.

catalyst, displays a more pronounced shoulder in the region around 2080 cm^{-1}, indicative of linear CO on larger Pt particles. This suggests that the sublimation of both metals simultaneously in the vapor phase leads to blocking of the channels, resulting in a poor dispersion. On the other hand, the Tm-s-VPI catalyst, as described earlier, has a greater fraction of bands at lower wavenumbers where Pt carbonyls form, indicative of very small well-dispersed Pt.

6.3.2.3 Temperature Programmed Oxidation (TPO) of coke deposits

To characterize the amount and nature of the coke deposited on the different catalysts during runs with and without sulfur, we have conducted TPO measurements on spent samples. Table 6.6 summarizes the amount of C deposited on each catalyst after 9 h on stream with a sulfur-free feed and 1 ppm S. Two trends are immediately apparent: a) the IWI catalysts formed considerably more coke than the two VPI catalysts, and b) the presence of sulfur in the feed did not have a pronounced effect on the amount of carbon deposited.

Table 6.6. Amount of carbon deposited under n-hexane aromatization reaction, as determined by TPO.

Catalyst	% C after 9 h run, S-free	% C after 9 h run, 1 ppm S
IWI	2.7	2.7
VPI	1.1	1.1
Tm-VPI	1.2	1.1

That the IWI catalysts form more coke is not surprising. In our previous findings from Chapters 3-5, the Pt clusters formed by the IWI procedure were less well-dispersed than those produced by the VPI catalyst. TEM has shown that, though in a very small fraction, some larger Pt clusters outside the channels of the L-zeolite were detected for catalysts prepared by IWI. Iglesia and Baumgartner [19,20] have shown that under the n-hexane aromatization reaction, the Pt that is well-dispersed inside the channels of the L-zeolite is protected from bimolecular collisions which lead to coke formation, while those outside, quickly become coked. Furthermore, microcalorimetric studies performed by Sharma et al. [70] clearly demonstrated the uniqueness of Pt/KL to resist deactivation by coke. After n-hexane aromatization,

coking on Pt/Silica, which has no protection from microporous channels, was found to suppress adsorption sites much greater than a Pt/K(Ba)L catalyst. On the other hand, the amount of coke formed is not affected by the presence of sulfur in the feed because the deactivation of the catalyst by coke deposition occurs during the first several hours on-stream, as noted in previous studies [24,50]. The poisoning by sulfur takes a much longer period of time to be observed.

The analysis of the TPO profiles also provides some interesting information that will allow us to further understand the role of Tm. When comparing the profiles of the IWI catalyst used under sulfur-free and 1 ppm S, a clear difference emerges. Fig. 6.10 shows that the TPO of the catalyst that was not exposed to sulfur exhibits a

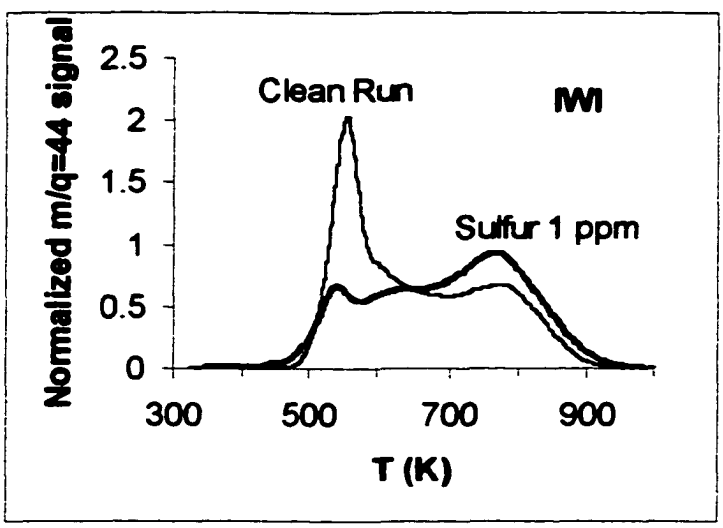

Figure 6.10. TPO profiles for the IWI catalyst after a sulfur-free run and a run with 1 ppm sulfur present in the feed.

prominent carbon oxidation peak at the lower temperature region, which is drastically reduced on the TPO of the sulfur-poisoned sample. We ascribe this low temperature

peak to Pt catalyzed oxidation. However, on the poisoned catalyst, the oxidation shifted to higher temperatures, while the overall area under the profile remained exactly the same. Similar changes were observed on the Tm-VPI and VPI catalysts.

In all cases, the samples that were not exposed to sulfur presented the low temperature peak, but this peak was greatly reduced on the sulfur-poisoned samples. Since the amount of carbon was almost unchanged, it seems that the presence of sulfur on the poisoned platinum clusters inhibited Pt catalyzed oxidation of carbon during the TPO, thus shifting it to higher temperatures, rather than modifying the nature of the coke deposits. Based on this premise, the presence of the sharp, low-temperature TPO peak could be taken as a fingerprint for sulfur-free Pt.

To investigate whether Tm may act as a sulfur-getter, we prepared reactors which contained three consecutive beds. In the first case, the front and back beds each contained 0.2 g of the VPI catalyst. They were separated by a middle bed, containing 0.4 g. 1.5 % Tm/KL. The results obtained in this arrangement were compared to those obtained in a similar reactor in which the middle bed only contained 0.4 g. of bare SiO_2. This comparison is illustrated in the TPO profiles of the coke deposits shown in Figs. 6.11 and 12, obtained after 9 h on stream with a feed containing 2 ppm S. A clear difference is immediately obvious. For the set that had the Tm/KL bed in the middle, the TPO of the bottom bed shows a prominent peak at low temperatures, indicating that the Pt has not been poisoned. However, for the set which had the bare SiO_2 bed in the middle, the TPO of both bottom and top samples were almost the same, clearly showing that both were almost equally poisoned. These experiments demonstrate that one of the effects of Tm is to capture

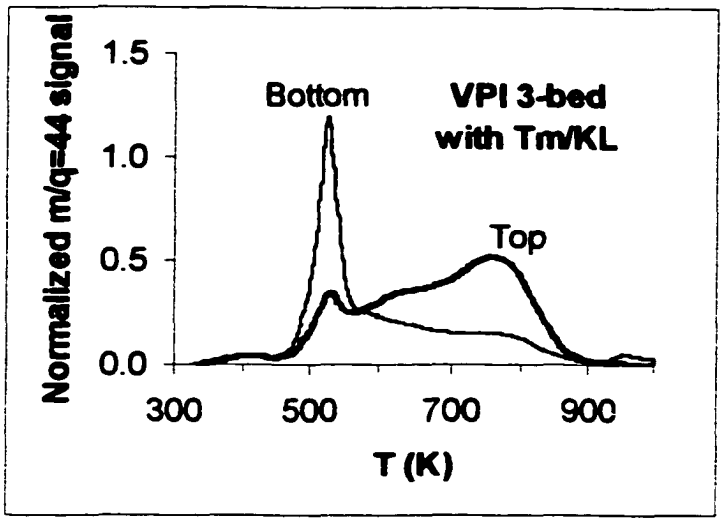

Figure 6.11. Three consecutive beds in series, two VPI beds separated by a bed of Tm(1.5%)/KL in the middle. TPO profiles for the top and bottom VPI beds are shown after 9 h on stream (T: 500°C, WHSV: 10 h^{-1}) with a feed containing 2 ppm S.

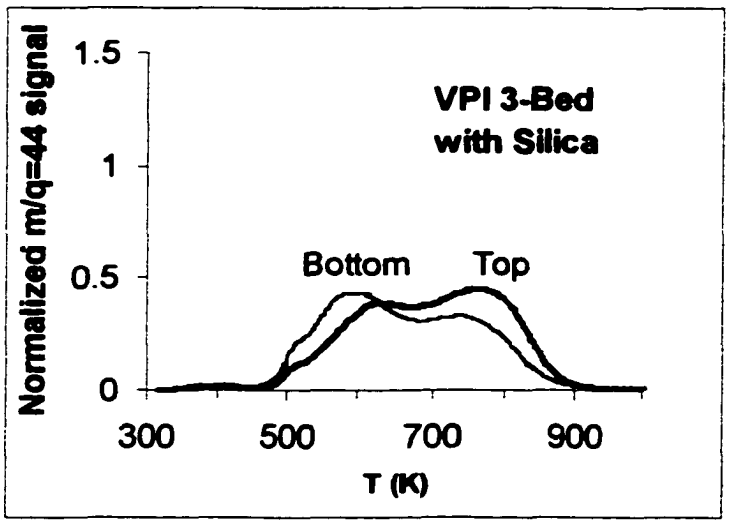

Figure 6.12. Three consecutive beds in series, two VPI beds separated by a bed of silica in the middle. TPO profiles for the top and bottom VPI beds are shown after 9 h on stream (T: 500°C, WHSV: 10 h^{-1}) with a feed containing 2 ppm S.

sulfur, therefore guarding the Pt particles from poisoning.

6.4 CONCLUSIONS

When prepared correctly, the addition of Tm has important consequences on the aromatization performance of Pt/KL catalysts.

a) The presence of Tm results in a catalyst with higher Pt dispersion. As demonstrated before, a higher dispersion by itself results in a much better catalyst, even without the addition of any promoter.

b) Tm acts as a sulfur getter, so it delays the poisoning of Pt.

c) The initial activity of the Tm-promoted catalysts is higher than that of unpromoted Pt/KL, even those prepared by VPI. This higher activity would suggest that Tm may directly modify Pt or may even participate in accelerating the aromatization reaction. However, further investigation is necessary to elucidate an electronic modification.

However, the amount and method of incorporation of Tm is critical to the catalyst performance. While the sequential vapor phase impregnation method with a small amount of Tm (0.15%) yielded a catalyst with improved catalytic properties, other methods such as coimpregnation of Pt and Tm hindered the dispersion of Pt, causing blocking of the L-zeolite channels and a higher deactivation rate under reaction.

SPECIAL ACKNOWLEDGEMENTS

This work is the result of a long-term collaborative effort of several members of the OU Heterogeneous Catalysis Group. I would like to acknowledge Dr. Cristina Padro for initial help with catalyst preparation, Drs. Adriana Pisanu and Walter E. Alvarez for help with FTIR and TPO measurements, and Dr. Armando Borgna for EXAFS analysis. Dr. Borgna was funded by Fundacion Antorchas and the Fulbright Commission. Furthermore, I would especially like to thank Firoz Ghadiali for his work in the construction and utilization of the pulse microreactor system. I am grateful for funding for this project, which was provided by the Oklahoma Center for the Advancement of Science and Technology (OCAST) and NSF for my GRT traineeship. We also acknowledge personnel at Brookhaven National Lab, especially Syed Khalid, for help with EXAFS experiments. Finally, we are especially indebted to Phillips Petroleum for their support.

CHAPTER VII: PROMOTERS & ELECTRONIC EFFECTS – Modifying the Fermi level of Platinum

7.1 INTRODUCTION

For the past 20 years, researchers have incorporated different cations in KL in order to determine if electronic modifications could result [17,35-41,105-107] in efforts to improve the n-hexane aromatization rate and increase the sulfur tolerance property of the catalyst [35-37,105,108]. These studies are described in detail in Section 1.5.

A carefully conducted XANES study of reduced samples purged in helium resulted in negative binding energy shifts for Pt loaded on Mg-exchanged KL in comparison with the Pt foil [39]. This was a surprising result, because small Pt particles typically exhibit higher binding energies due to less final state relaxation in comparison with bulk Pt. Therefore, it was suggested that electron transfer from the zeolite lattice oxygen atoms to the Pt clusters might be important, because added electron density would more effectively screen the electron from the nucleus, thus decreasing its binding energy.

Recently, Ramaker et al. [41] have advanced a new method of XANES analysis for studying the electronic modification of Pt by changing support alkalinity. This method focuses on the changes in the Fermi level of Pt by induced by changes in the Madelung interatomic potential of Pt with the zeolite lattice oxygen atom. A smaller, more polarizing cation will increase the acidity of the zeolite lattice oxygen atoms, resulting in less negative charge, which causes an increase in rollover of the interatomic potential. Based on AXAFS results [109], the distance of the interatomic

potential barrier between the Pt atom and the zeolite lattice atom, as well as the position of the Fermi level change, while the electron density on Pt remains constant, as shown in Figure 7.1. Therefore, they concluded that there was no need to invoke a charge transfer explanation to explain the changes in the Fermi level of Pt. To obtain information on the changes in the Fermi level with support alkalinity, the proposed XANES method is based on the different information contained in the L_{III} and L_{II} white lines of the catalyst with and without hydrogen.

In this study, our aim is to test this method on Pt/KL catalysts, one of which is promoted with Li^+ cation, to determine the extent to which electronic modification of Pt occurs at temperatures required for n-hexane aromatization. In previous chapters, method of preparation has been found to directly affect the morphology of Pt/KL catalysts. In these studies, Pt/KL catalysts prepared by vapor phase impregnation (VPI) were found to offer the smallest, most uniformly dispersed, Pt clusters inside the channels of the L-zeolite. In contrast, catalysts prepared by IWI and IE resulted in catalysts with larger particles and greater fractions outside the channels of the L-zeolite. Therefore, VPI catalysts are particularly suitable for X-ray spectroscopic studies, because their superior small particle size and uniform distribution inside the micropores makes them resistant to agglomeration after high temperature reduction treatment. We recall that the white line intensity is higher for smaller clusters, due to the increased empty available states in the valence band. Therefore, especially after high temperature reduction treatment, catalysts with a heterogeneous Pt cluster distribution (e.g., catalysts prepared by IWI or IE) will display complications in the

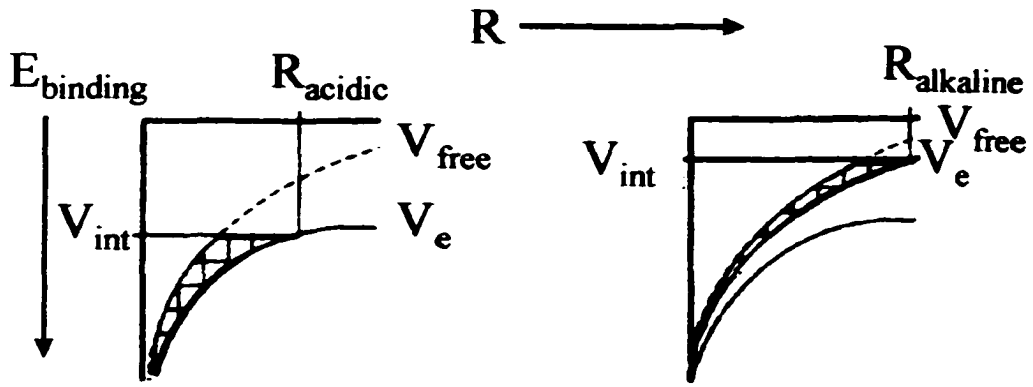

Figure 7.1: Change in rollover of interatomic potential for (left) more acidic support and (right) more alkaline support.

XANES spectrum due to particle size effects alone, while the VPI catalysts are less sensitive to this problem.

7.2 EXPERIMENTAL

7.2.1 Catalyst Preparation

The K-LTL zeolite powder (series TSZ-500, BET area 292 m^2/g, SiO_2/Al_2O_3 ratio = 6) was provided by Tosoh Company. 10 grams of the KL was exchanged with lithium cation by stirring in a 200 cm^3 aqueous solution of $Li(NO)_3$. The weight percent of lithium was determined by atomic absorption to be 0.31%. A separate batch of 10 grams of KL was also used without exchange of lithium. For each batch, prior to incorporation of Pt metal, the zeolite powder was dried in an oven at 110°C for 12 h and calcined at 400°C for 5 h. Calcination was performed under flow of air (100 cm^3/g zeolite per min), employing a temperature ramp of 3°C /min.

The platinum was incorporated into the KL to a weight loading of 0.75% by the VPI procedure, as described in Section 4.1. The Pt loadings were measured by ICP analysis after complete dissolution of the samples in aqua regia/HF solution at Galbraith Laboratories, Inc. Both catalysts had a measured Pt loading of approximately 0.75%.

7.2.2 Catalyst Characterization

7.2.2.1 Hydrogen Chemisorption, EXAFS, Infrared of Adsorbed CO

Hydrogen chemisorption and EXAFS measurements were conducted on the catalysts according to Section 2.3. EXAFS samples were reduced under hydrogen flow at 300°C for 1 h and cooled down to liquid nitrogen temperature under hydrogen flow. After measurement of the spectra under hydrogen, the samples were purged and heated under helium at 300°C for 1 h and spectra were taken at liquid nitrogen temperature under helium flow. The same procedure above was repeated for the samples at a temperature of 450°C.

Infrared spectroscopy of adsorbed CO was performed according to Section 2.3.3. Samples were pre-reduced ex-situ under H_2 flow at either 300°C or 450°C for 1 hour.

7.2.2.2 XANES Analysis

A new shape resonance XANES analysis method proposed by Ramaker et al. [41,110,111] was used. Briefly, the Pt L_{II} and L_{III} white lines provide information about the unoccupied density of states (DOS) near the Fermi level (E_F). The white

lines differ significantly, because while one transition is allowed for L_{II} (from the $2p_{1/2}$ core level to the $5d_{3/2}$ valence level), two transitions are allowed for L_{III} (from $2p_{3/2}$ to both the $5d_{5/2}$ and $5d_{3/2}$ valence levels). Relative to bulk Pt, band narrowing occurs for small clusters due to localization of electrons. Therefore, for small Pt clusters, the $5d_{3/2}$ is believed to be filled. Then, empty states in the valence band are deemed only to occur for L_{III}, accounting for the much higher XANES intensity observed. The proposed method is based on the different information contained in the L_{III} and L_{II} white lines of the catalyst with and without hydrogen.

The L_{II} edge spectrum of the Pt catalyst under helium was used as a reference, because it contains EXAFS contributions, but no valence band contributions ($5d_{3/2}$ level assumed filled). The L_{III} edge spectrum of the Pt catalyst under helium contains not only the reference information (EXAFS contributions), but also the empty states in the valence band (ΔVB). The L_{II} edge spectrum of the catalysts under hydrogen contains, in addition to the reference information, the Pt-H scattering and changes in Pt-Pt and Pt-O scattering (ΔXAFS). The L_{III} edge spectrum of the catalysts under hydrogen contains the reference information and ΔXAFS (changes in the Pt-H, Pt-Pt, and Pt-O scattering) as well as the ΔVB and the anti-bonding state (AS). As will be discussed, the AS gives electronic information about the nature of the Pt.
Through the subtraction of different edges, the anti-bonding resonance state (AS) can be isolated. However, the edges must be aligned. The L_{II} edge positions of the samples under helium and hydrogen were taken to be 0.6 of the step height after normalization. The L_{II} and L_{III} edges for the same sample have the same EXAFS oscillations. Therefore, the L_{III} edges were aligned to the L_{II} edges by matching up

the EXAFS oscillations (region > 50 eV passed the edge). The anti-bonding state was then isolated by the difference ΔL_{III-II} (Pt/H_2) - ΔL_{III-II} (Pt/He), where ΔL_{III-II} (Pt/H_2) = ΔL_{III} (Pt/H_2) - ΔL_{II} (Pt/H_2) = $\Delta VB + AS$ and ΔL_{III-II} (Pt/He) = L_{III} (Pt/He) – L_{II} (Pt/He) = ΔVB. The above procedure was conducted on Pt(0.75%)/KL and Pt(0.75%)/Li/KL samples after reduction at both 300°C and 450°C. See Figure 4.2.

7.2.2.3 Microcalorimetry of Adsorbed Hydrogen and CO in a Flow System

Microcalorimetry was conducted by first reducing the catalyst by ramping in hydrogen to 300°C for 1 h, holding at 300°C for 1 h, and then purging under helium. Next, the sample was cooled to room temperature under helium flow, prior to pulsing in 2.1 E –7 moles of hydrogen or CO at atmospheric pressure and ambient temperature. Heats were recorded by using a Setaram DSC111 microcalorimeter. Residual hydrogen or CO was recorded using a TCD detector. For the 0.75% Pt loaded KL and Li/KL catalysts, 30.5 mg of catalysts were used, while for the 1% Pt/SiO_2 reference, 22.4 mg of catalyst were used. Heat of adsorption was calculated by integrating the areas of the heat per time curves and dividing by the number of moles of hydrogen adsorbed (i.e., moles detected by a pulse using a blank reactor minus the moles of detected with catalyst present).

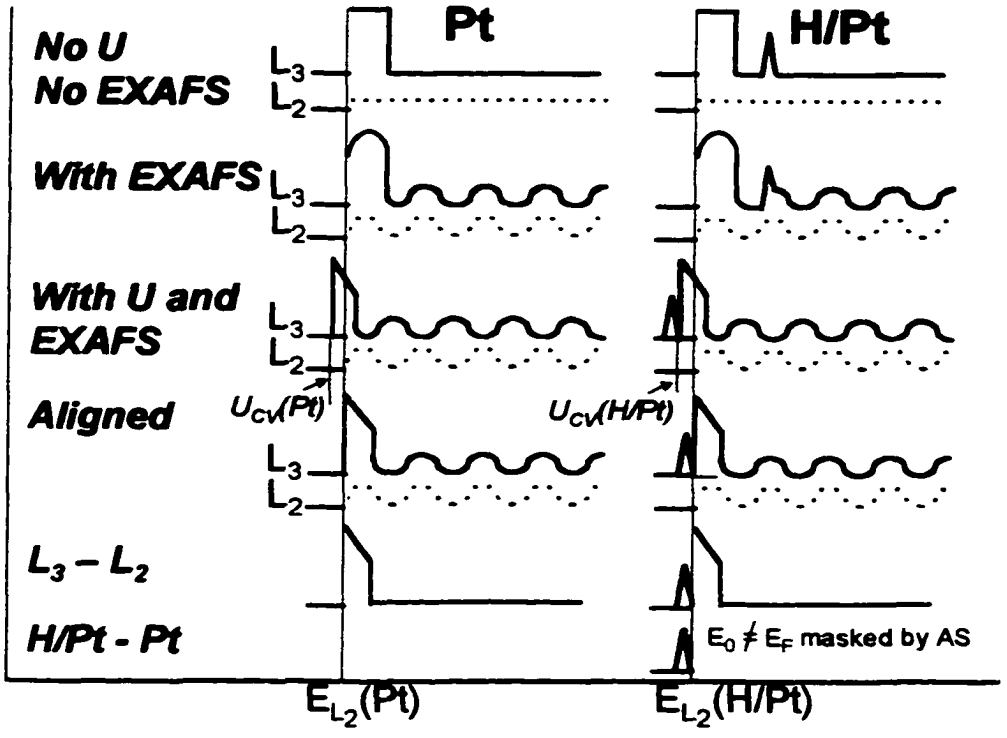

Figure 7.2: (above) Picture of alignment and difference procedure of Ramaker et al. [41]. On left, we consider spectra in absence of H_2, and on right we include the chemisorbed hydrogen: (a) white line includes both empty valence band (ΔVB) and antibonding state (AS) contribution from chemisorption of hydrogen; (b) EXAFS oscillations are included; (c) effects of core-hole interaction are provided, and ΔVB and AS are pulled down, since they are highly localized states; (d) After alignment using procedure of Ramaker; (e) difference $L_3 - L_2$ is taken to isolate ΔVB and AS; (f) difference H/Pt – Pt is taken to isolate AS. (below) Schematic of the procedure.

	L_3	L_2	$L_3 - L_2$
H/Pt	REF + ΔXAFS + ΔVB + AS	REF + ΔXAFS	ΔVB + AS
Pt	REF + ΔVB	REF	ΔVB
		H/Pt - Pt	AS

7.2.3 Catalytic Activity

7.2.3.1 Neopentane hydrogenolysis in a Pulse Reactor

Neopentane hydrogenolysis was also employed as a test reaction in the pulse mode. In each run, 25 mg of sample was placed in a Pyrex reactor and reduced/run in situ at different temperatures starting at 300°C and increasing to 380°C and 450°C. For each temperature, three consecutive 2 μL pulses containing 4.66×10^{-8} moles of neopentane were sent over the catalyst, and then to the GC equipped with packed column (Alltech 30% DC200-Chromosorb 60/80 P AW) and FID. The contact time was varied.

7.2.3.2 n-Hexane Aromatization in a Pulse Reactor

n-Hexane aromatization was used as a test reaction in a pulse microreactor. In each run, 25 mg of sample was placed in a Pyrex reactor and reduced/run in situ at three successive temperatures 400°C, 450°C, and 500°C. Hydrogen was saturated with n-hexane at 18°C by passing through a sparger and condenser apparatus, running chilled water. At each reaction temperature, three consecutive 20 μL pulses containing 6.74×10^{-8} moles of n-hexane were sent over the catalyst, and then passed to the HP6890 GC equipped with a packed column (Alltech 30% DC200-Chromosorb 60/80 P AW) and FID. The contact time was varied.

7.2.3.3 n-Hexane Aromatization in a Flow Reactor

Steady-state n-hexane aromatization reaction testing was conducted in a continuous-flow reactor according to Section 2.4.1. The experiments were conducted

using 0.40 g of catalyst in each run. Prior to reaction, the catalyst was slowly ramped in flowing hydrogen at 100 cm^3/g per min catalyst for two hours to a temperature of 450°C and reduced for 1 h. The reaction was conducted at a WHSV of 10 h^{-1}. Finally, products were detected using a flame ionization detector (FID). A nonlinear 90 min temperature ramp from 40°C to 200°C provided the means for adequate peak separation in the GC column.

7.3 RESULTS

7.3.1 Catalyst Characterization

7.3.1.1 Hydrogen Chemisorption

In order to obtain insight into how the reduction temperature affected the dispersion of Pt clusters for the Pt/KL and Pt/Li/KL catalysts, chemisorption was conducted at two different reduction temperatures: 300°C and 450°C. H/Pt results are shown in Table 7.1. In agreement with previous results, high irreversible H/Pt values, above 1.0 were observed, indicating very high dispersion. By increasing the reduction temperature from 300°C to 450°C, particle growth was observed for both samples. Interestingly, in general, the losses were the same for each case. These results indicate that similar average particle sizes were present for both catalysts at the two reduction temperatures studied.

7.3.1.2 EXAFS

The radial distribution function (RDF) of the Pt/KL and Pt/Li/KL catalysts under hydrogen and helium are shown in Figure 7.3. The RDF revealed that both

Table 7.1. Results of Hydrogen Chemisorption for Pt/KL and Pt/Li/KL.

Catalyst	H/Pt			
	Red 573K (Total)	Red 573K (Irreversible)	Red 723K (Total)	Red 573K (Irreversible)
Pt/KL	2.0	1.7	1.8	1.4
Pt/Li/KL	2.0	1.7	1.8	1.4

catalysts present similar average structures. The results of the EXAFS analysis are presented in Figure 7.4 and Table 7.2. Comparison of the experimental and calculated EXAFS functions showed that the quality of the fit obtained was good (Figure 7.4 a and b). The Pt-Pt coordination numbers of the reduced Pt/KL and Pt/Li/KL catalysts were 4.2 and 3.4, respectively. These results indicate that both catalysts have small metal particle size. The Pt-Pt distance of 2.7 Å is in agreement with previous results from Chapter 4. However, the Pt-O distances (2.4 Å) corresponding to Pt atoms coordinated to the zeolite lattice oxygen atoms were slightly shorter than previously observed [26,76]. After purging under He, the Pt-Pt and Pt-O coordination number and distance did not change. Approximately the same result was observed by Ramaker et al. [41] on Pt/KL catalysts with different K/Al ratios. They observed a small contraction of Pt-Pt and Pt-O distances after He treatment. Reifsnyder et al. [112] performed EXAFS measurements on a 1% by wt. Pt/SiO_2 catalyst under hydrogen and under vacuum. Their results revealed that evacuation did not affect the Pt-Pt and Pt-O coordination number but led to a contraction of the Pt-O distance.

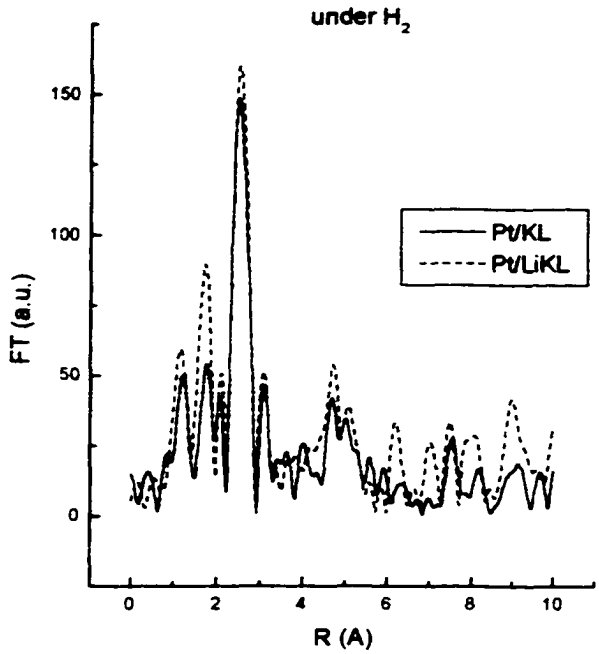

Figure 7.3: Radial distribution function of the Pt/KL (solid line) and Pt/Li/KL (dashed line) under hydrogen after reduction at 300°C and cooling to liquid nitrogen temperature.

Table 7.2. Fitting parameters for catalysts under hydrogen and under He.

Catalyst	ΔE_0 (eV)	Pt-Pt distance			Pt-O distance			r-factor
		N	R(A)	σ^2 (Å^2)	N	R(A)	σ^2 (Å^2)	
Pt/KL[a]	-3.0	4.2	2.70	0.0068	0.9	2.39	0.0030	0.0167
Pt/LiKL[a]	-1.7	3.4	2.70	0.0058	0.6	2.38	0.0030	0.0080
Pt/KL[b]	1.5	3.0	2.71	0.0055	0.7	2.41	0.0002	0.0151
Pt/LiKL[b]	-2.2	3.6	2.69	0.0057	1.0	2.36	0.0037	0.0056

[a] under hydrogen
[b] under helium

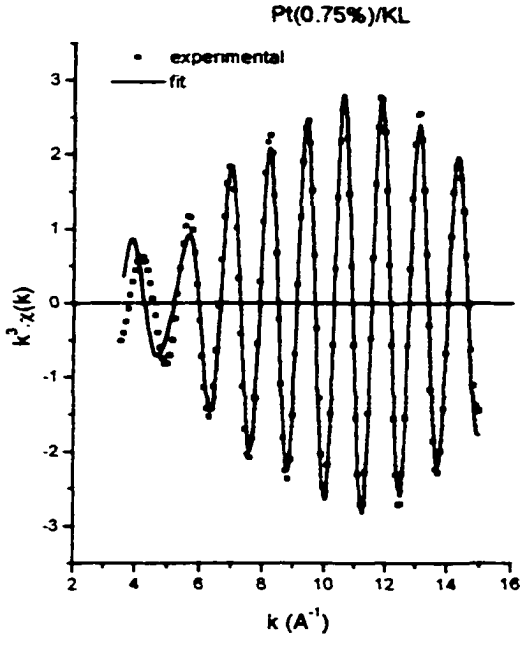

Figure 7.4. Experimental EXAFS χ–function (solid line) and theoretical fit (dotted line) for (a) Pt/KL and (b) Pt/Li/KL catalysts after reduction at 300°C and cooling to liquid nitrogen temperature.

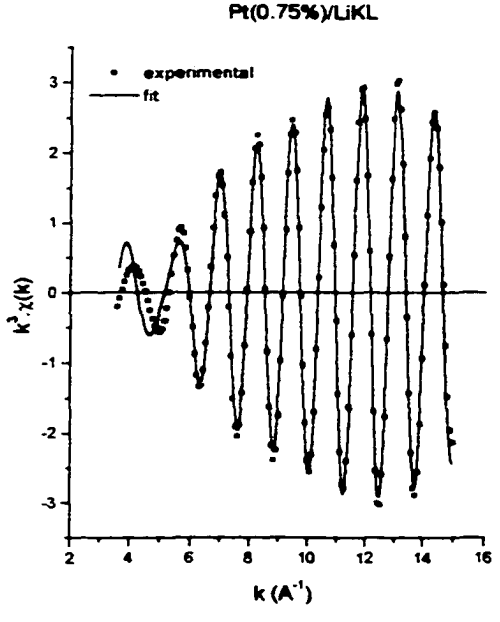

7.3.1.3 XANES

Figure 7.5 a and b show the normalized and aligned spectra of the Pt/KL and Pt/Li/KL catalysts under hydrogen and helium reduced at 300°C. For Pt/KL, hydrogen adsorption broadened the L_{III} and L_{II} edges and increased the intensity of the L_{II} white line. These results are in agreement with the literature [41,112-115]. The L_{III} edges were also shifted to lower energies relative to the L_{II} edge as previously observed [41].

The difference spectra obtained by subtracting the L_{II} from the L_{III} XANES spectra of the Pt catalysts with or without hydrogen are presented in Figures 7.6 a and b for the two reduction temperatures, respectively. The difference between the curves under hydrogen and under helium correspond to the anti-bonding state (AS) of each catalyst, as shown in Figures 7.7 and 7.8. Differences were observed in the shape of the Fano resonance curves of the AS in direct correlation to the effect of the support acidity/alkalinity on the Pt metal clusters. This is in agreement with the literature for catalysts prepared with different degrees of H-exchange with the KL support [41].

The AS is not a permanently bound state, but temporary bound state for electrons before they are ejected to the continuum. The AS also includes multiple scattering contributions. Whenever a localized state is degenerate with a continuum state, the probability of a transition to this state results in the Fano shape resonance. The shape resonance curves were fitted to the Fano resonance equation [41]:

$$\chi(E) = A/k\,[(1 - q\varepsilon)/(1 + \varepsilon^2)]\,\sin\varphi$$

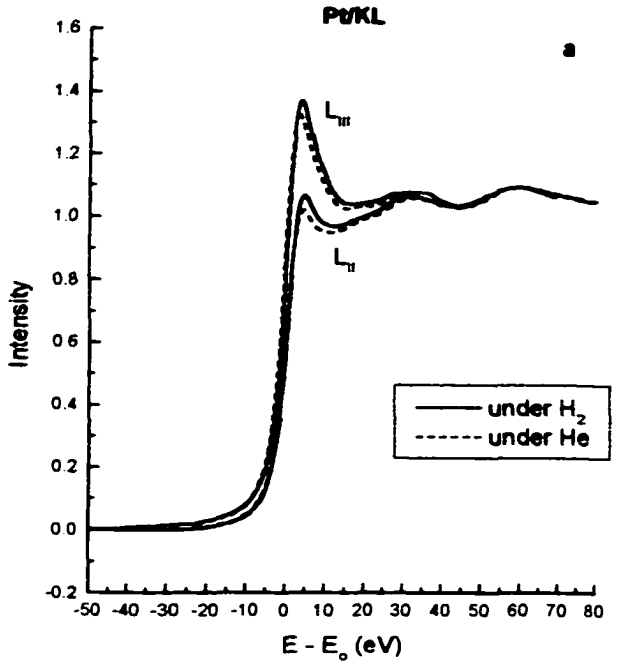

Figure 7.5: Normalized and aligned L_{II} and L_{III} edge spectra of the (a) Pt/KL and (b) Pt/Li/KL catalysts under hydrogen (solid line) and helium (dashed line) after reduction at 300°C and cooling to liquid nitrogen temperature. Spectra taken in helium were first heated to 300°C under He to remove the chemisorbed hydrogen and cooled back to down to scan.

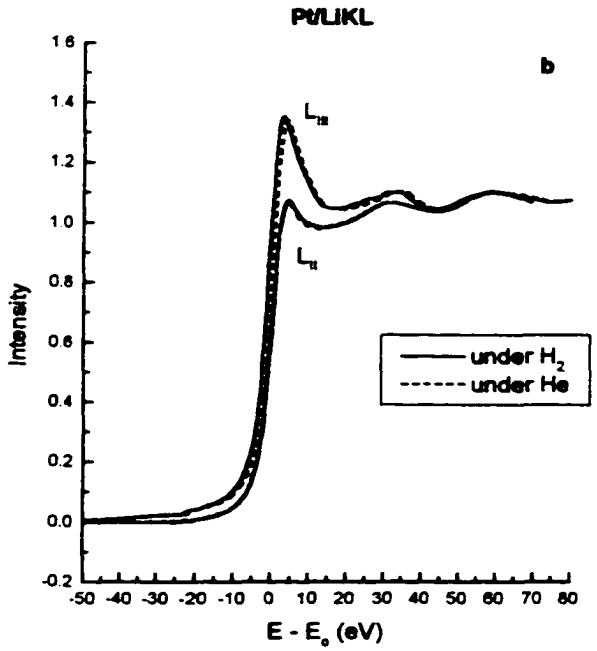

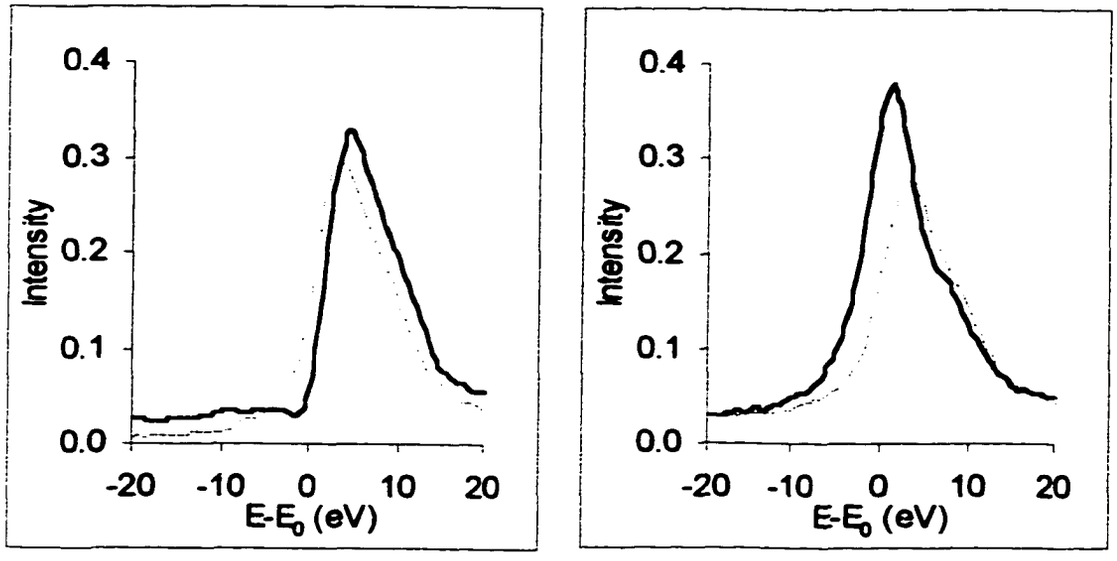

(a)

Figure 7.6: XANES difference spectra of $L_{III} - L_{II}$ under hydrogen (solid line) and under helium (dotted line) for Pt/KL (left) and Pt/Li/KL (right) catalysts after reduction at (a) 300°C and (b) 450°C and cooling to liquid nitrogen temperatures. Spectra taken in helium were first heated to 300°C under He to remove the chemisorbed hydrogen and cooled back to down to scan.

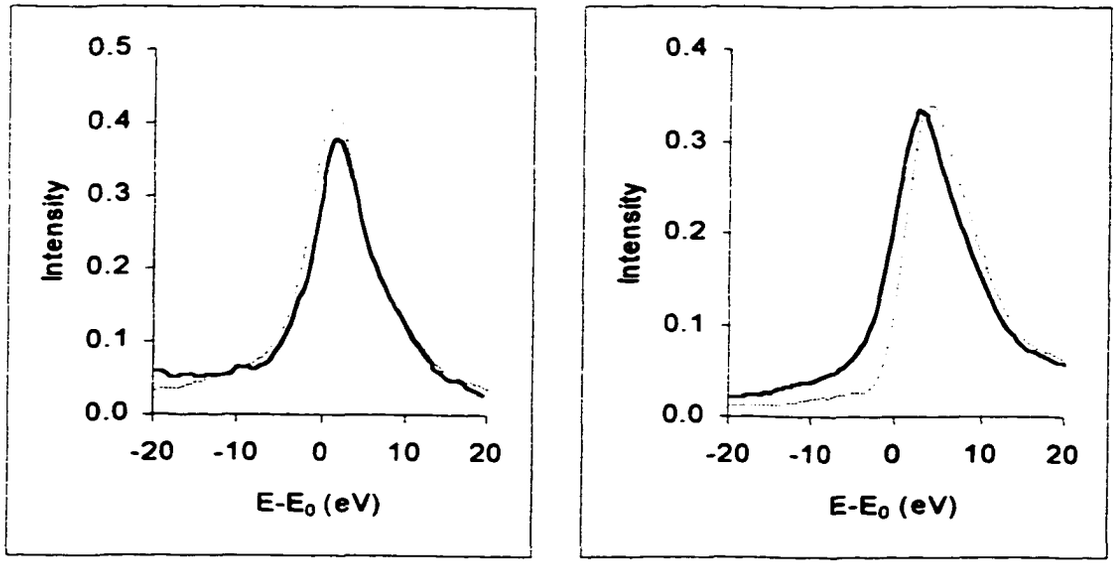

(b)

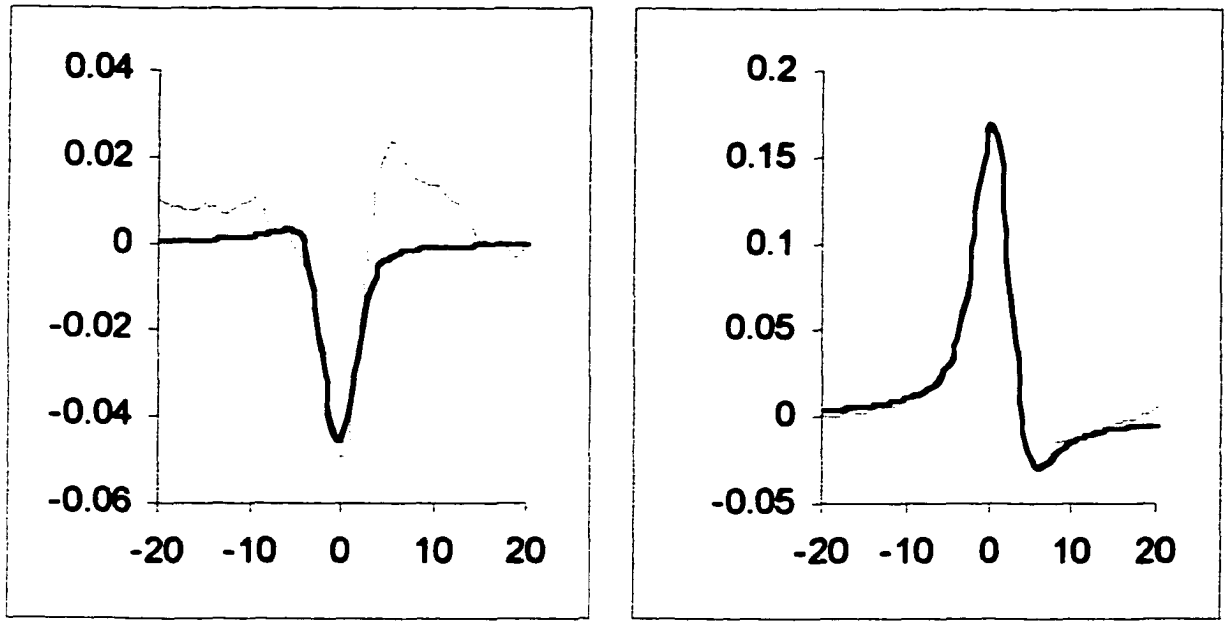

Figure 7.7. Antibonding state (AS) curves corresponding to $[(L_{III} - L_{II})_{Hyd} - (L_{III} - L_{II})_{He}]$ for Pt/KL (left) and Pt/Li/KL (right) catalysts after reduction at 300°C.

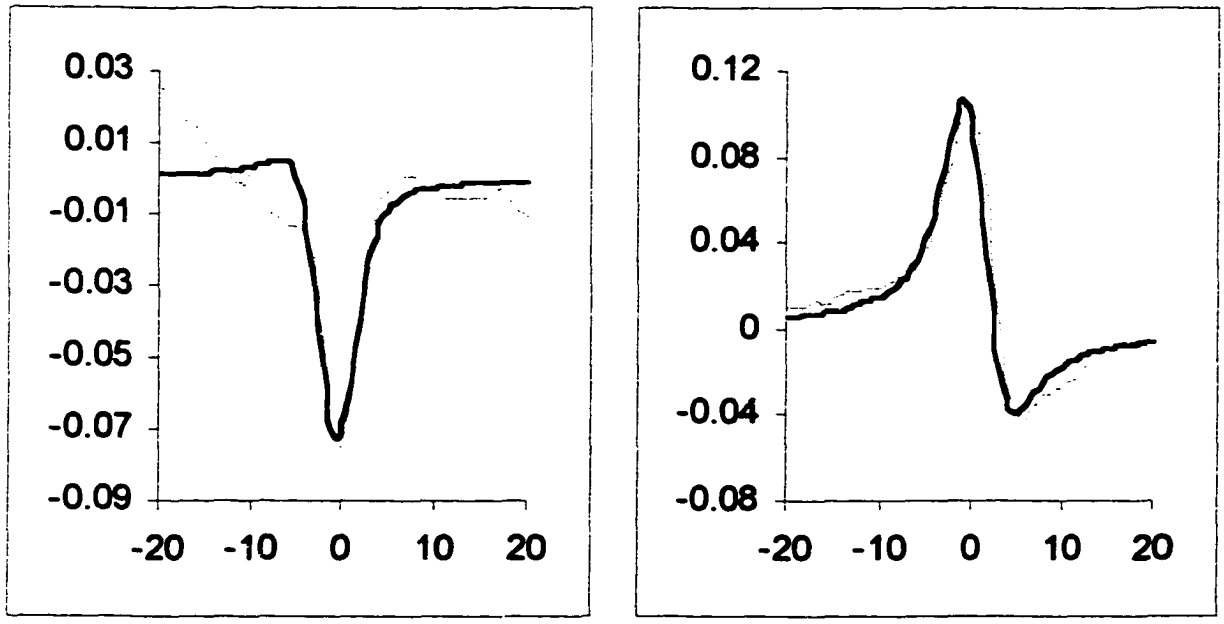

Figure 7.8. Antibonding state (AS) curves corresponding to $[(L_{III} - L_{II})_{Hyd} - (L_{III} - L_{II})_{He}]$ for Pt/KL (left) and Pt/Li/KL (right) catalysts after reduction at 450°C.

$$\varepsilon = 2(E - E_{res})/\Gamma, \text{ where } E = E - E_0$$

$$q = \cot \varphi$$

$$\varphi = a + E_{RES}b$$

In the equations, ε represents the normalized energy scale relative to E_{RES}. The background phase parameter φ controls the shape of the resonance through the parameter q and attenuates it by the sin function. Parameters used to perform a nonlinear least squares fitting to the curves included A, E_{RES}, and the resonance width Γ for each spectrum. Because the background phase parameter is a linear function of the resonance energy E_{RES}, the parameters a and b were also included, but fit across all spectra, for a total of 14 parameters, as shown in Table 7.3.

Table 7.3: Fitting Parameters for the Fano resonance.

Catalyst	T (K)	A	E_{RES} (eV)	Γ (eV)	φ	a	b
Pt/Li/KL	573	0.11	1.99	1.95	0.46	-0.25	0.38
Pt/Li/KL	723	0.56	1.20	3.85	0.16		
Pt/KL	573	0.06	-0.99	0.18	-0.67		
Pt/KL	723	0.11	-1.62	1.53	-0.91		

7.3.1.4 Infrared Spectroscopy

The FTIR spectra of adsorbed CO on Pt/KL and Pt/Li/KL VPI catalysts reduced at 300°C and 450°C are shown in Figure 7.9. All spectra exhibited several bands as observed in previous chapters, and in the literature [38,91-93,116]. Regardless of the reduction temperature, the FTIR spectra of CO adsorbed on Pt/KL presented three bands at 2050, 2034 and 2007 cm^{-1} and a shoulder around 1979 cm^{-1} (Figure 7.9 a). The increase of the reduction temperature led to a decrease mainly of

the bands at low wavenumbers and the development of a more pronounced shoulder at 2067 cm^{-1}.

In contrast to Pt/KL, the FTIR spectra of the CO adsorbed on Pt/Li/KL exhibited neither the sharp band at 2034 cm^{-1} nor the shoulder around 1979 cm^{-1} (Figure 7.9 b). On the other hand, a pronounced shoulder is identified at 2066 cm^{-1} even after reduction at low temperature. After reduction at 450°C, it is also noted a decrease in the bands at low wavenumbers and an increase of the shoulder at 2067 cm^{-1}. It is important to stress that the presence of bands below 1900 cm^{-1} corresponding to bridged-bonded CO was not observed for either VPI catalyst.

7.3.1.5. Microcalorimetry of Adsorbed Hydrogen and CO

Results of microcalorimetry are shown in Figures 7.10 a and b. The heats of adsorption for adsorbed hydrogen and CO for Pt/Li/KL were significantly higher than for the Pt/KL catalyst, as depicted in Figure 7.10 a and b. Interestingly, the heat of adsorption for adsorption of hydrogen onto platinum supported on silica as a reference was intermediate of the two catalysts.

7.3.2 Catalytic Activity

7.3.2.1 Neopentane hydrogenolysis in a Pulse Reactor

Because of the inability to form a stable carbocation, neopentane hydrogenolysis is often used as a probe reaction to test the metal-catalyzed function. Table 7.4 shows the conversion and product selectivities for this pulse reaction for the Pt/KL and Pt/Li/KL catalysts. While no activity was reported for either catalyst

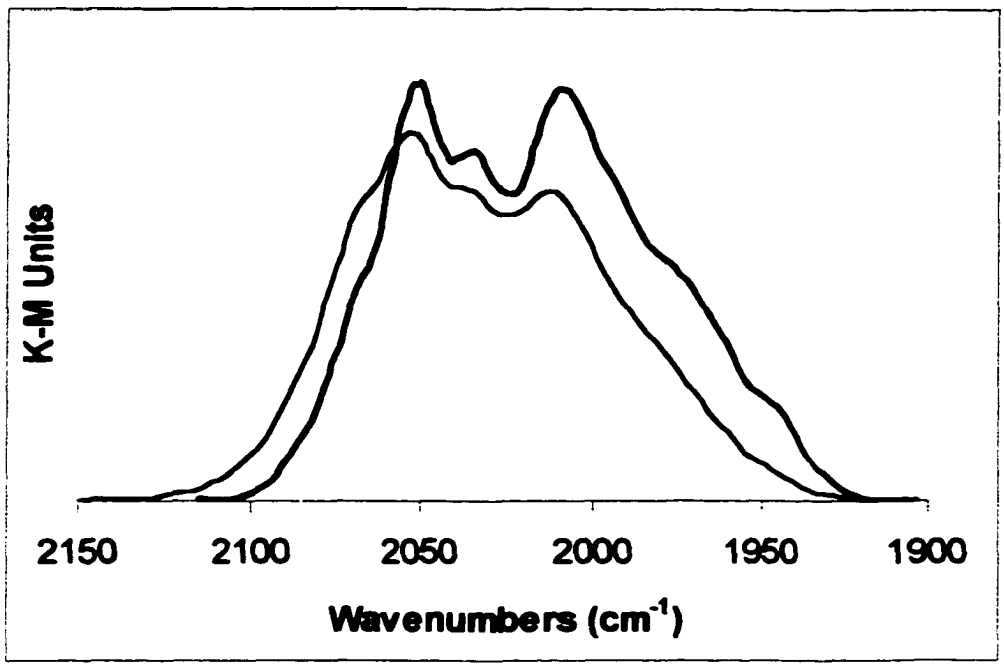

(a)

Figure 7.9. DRIFTS spectra of adsorbed CO for (a) Pt/KL and (b) Pt/Li/KL catalysts after reduction at 300°C (bold) and 450°C (light). Adsorption of CO was conducted at room temperature using 3% CO in helium for 30 min. Gas phase CO was purged in helium for 30 min prior to scanning.

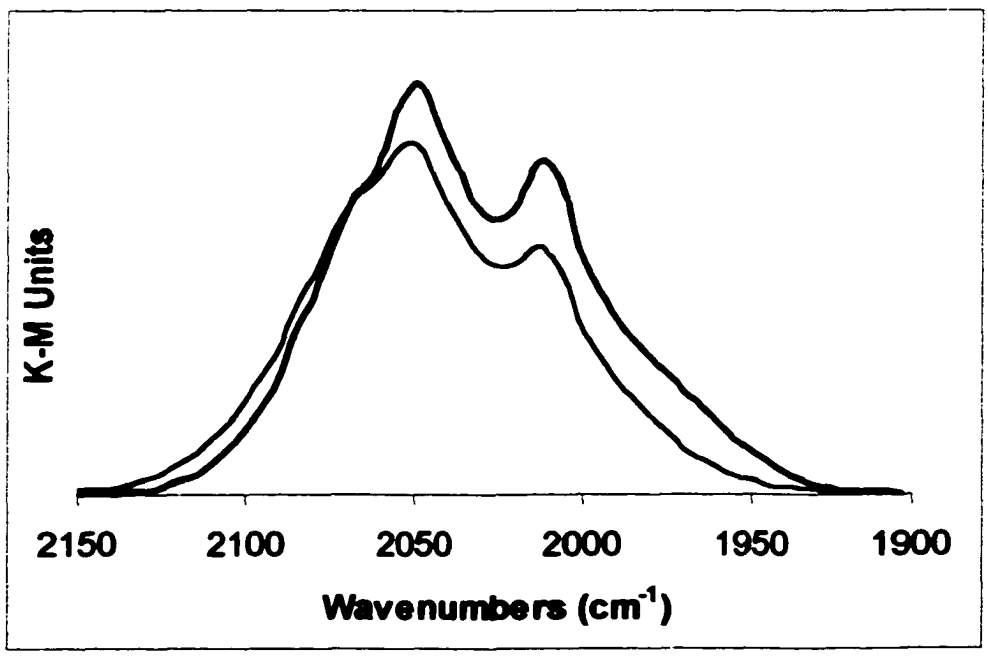

(b)

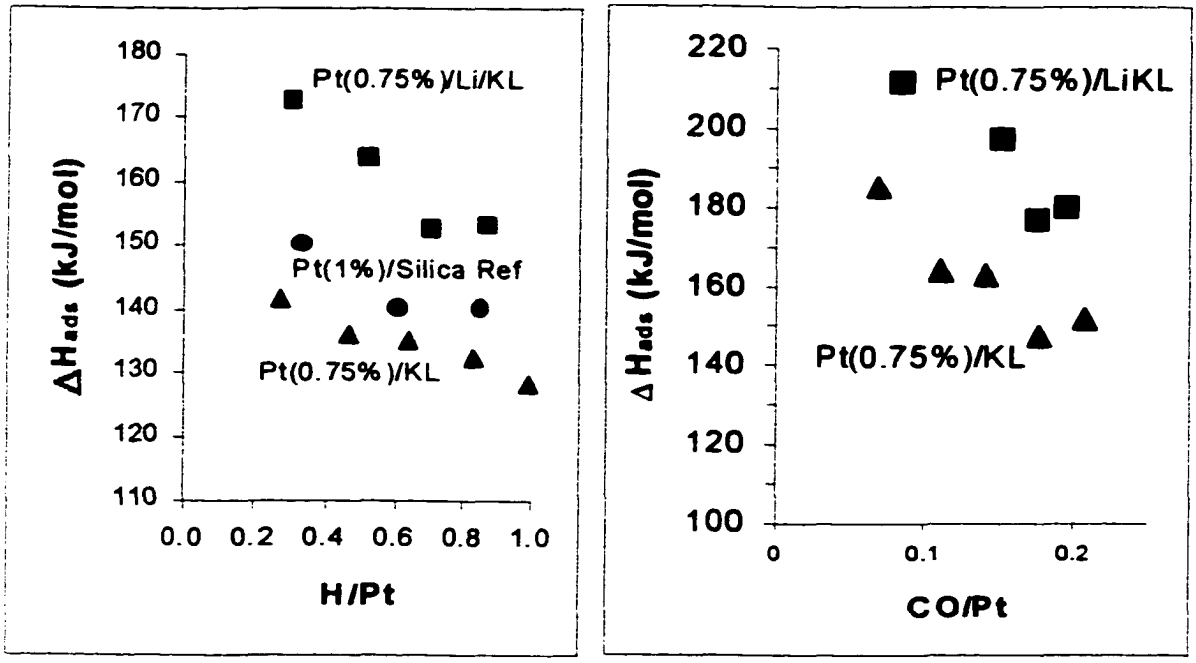

(a) (b)

Figure 7.10. Microcalorimetry measurements of adsorbed hydrogen (left) and CO (right) observed in a flow system for Pt/Li/KL (squares), Pt/KL (triangles), and Pt/Silica (circles) reference catalysts after reduction in hydrogen at 300°C, purging in helium, and adsorption of pulses of hydrogen or CO.

at 300°C, the Pt/Li/KL showed high activity and selectivity for hydrogenolysis at 380°C. Interestingly, the Pt/KL catalyst still displayed no activity at 380°C. At 450°C, the Pt/KL catalyst showed lower activity than the Pt/Li/KL catalyst at much lower temperature. The selectivity for hydrogenolysis was also very high for this case.

Table 7.4. Conversion and product selectivities for neopentane pulse reaction in a microreactor.

Catalyst	T (K)	Conversion (%)	TOF_{Hydro} (s^{-1})	TOF_{iso} (s^{-1})	Hydrogenolysis Selectivity (%)	Isomerization Selectivity (%)
Pt/Li/KL	573	BDL[a]	–	–	-	-
Pt/Li/KL	653	44	0.030	0.001	97	3
Pt/KL	573	BDL[a]	–	–	-	-
Pt/KL	653	BDL[a]	–	–	-	-
Pt/KL	723	28	0.018	0.002	92	8

[a] below detection limits

7.3.2.2 n-Hexane Aromatization in a Pulse Reactor

The yields, turnover frequencies, and selectivities of methane and benzene are depicted in Table 7.5. In the pulse mode, a small amount of n-hexane is passed over the catalyst under pure hydrogen. Therefore, the results represent the behavior of a clean catalyst. A striking difference is immediately apparent for both catalysts. For the Pt/Li/KL catalyst, hydrogenolysis is more favorable while aromatization is favored on the Pt/KL catalyst. Activation energies were determined for C_1 hydrogenolysis and aromatization for both catalysts by plotting the Arrhenius relationship – the natural log of the ratio of the TOF values versus the inverse of the temperatures and linearly interpolating to obtain E_a/R. The activation energy for aromatization on Pt/KL (17.2 kcal/mol) was much lower than that for Pt/Li/KL (30.0 kcal/mol), while the hydrogenolysis activation energies exhibited the opposite trend. For Pt/KL, the activation energy was 22.7 kcal/mol and for Pt/Li/KL, the value was 18.9 kcal/mol.

Table 7.5. Methane (C1) and Benzene (Bz) Yields, Turnover Frequencies, and Selectivities in pulse microreactor.

Catalyst	T (K)	Contact Time (s)	C1 Yield (%)	C1 TOF (s^{-1})	C1 Selec (%)	Bz Yield (%)	Bz TOF (s^{-1})	Bz Selec (%)
Pt/KL	673	0.068	8	0.08	12	17	0.30	27
Pt/Li/KL	673	0.068	39	0.40	40	3	0.03	3
Pt/KL	723	0.068	17	0.18	17	58	0.60	58
Pt/Li/KL	723	0.068	63	0.65	63	4	0.05	4
Pt/KL	723	0.034	14	0.29	15	41	0.85	46
Pt/Li/KL	723	0.034	48	0.99	48	10	0.20	10
Pt/KL	723	0.019	7	0.27	12	22	0.82	37
Pt/Li/KL	723	0.019	41	1.54	43	11	0.41	11
Pt/KL	773	0.019	19	0.72	20	50	1.86	51
Pt/Li/KL	773	0.019	56	2.12	56	14	0.53	14

7.3.2.3 n-Hexane Aromatization in a Flow Reactor

The Pt/KL catalyst exhibited a higher activity than the Pt/Li/KL catalyst (Figure 7.11). As observed in previous chapters, the Pt/KL VPI catalyst showed only a small drop in activity. However, the Pt/Li/KL VPI catalyst displayed a rapid deactivation. The Pt/KL catalyst showed a high benzene yield and a low methane and hexene production. On the other hand, the addition of lithium strongly decreased the aromatization selectivity while the hexenes and C_1-C_3 hydrocarbons were the main products. These are shown in Figure 7.12. As in past deactivation studies, the hydrogenolysis and aromatization yields decreased with time on stream.

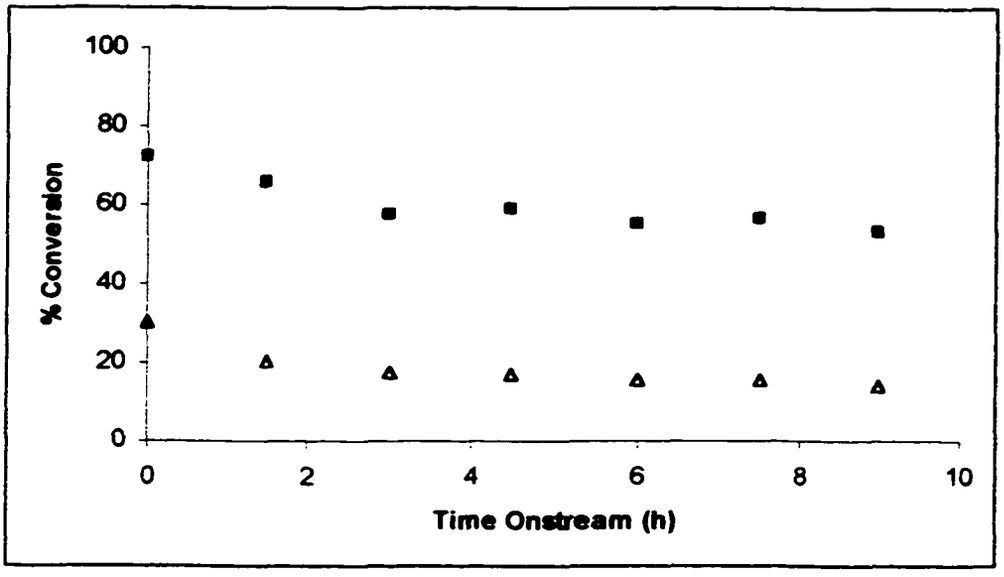

Figure 7.11: Conversion of n-hexane in a flow reactor system at WHSV=10 h^{-1} at 450°C for Pt/KL (squares) and Pt/Li/LK (triangles) catalysts.

7.4 DISCUSSION

7.4.1 Characterization

7.4.1.1 EXAFS and XANES

Hydrogen chemisorption changes the Pt $L_{II, III}$ white line intensity and shape significantly [41,112-114]. The increase in white line intensity has been ascribed to the creation of new empty d states due to bonding of hydrogen on the Pt surface [117]. Hammer and Norskov [118] performed ab initio calculations of the hydrogen adsorption on the (111) surface of different metals. Their results suggested that the interaction between the metal d bands and the adsorbate bands induce a filled bonding state and an antibonding state above the metal d levels. In particular, for Ni and Pt the antibonding state is a few electronvolts above the Fermi level. Boyanov et al. [119]

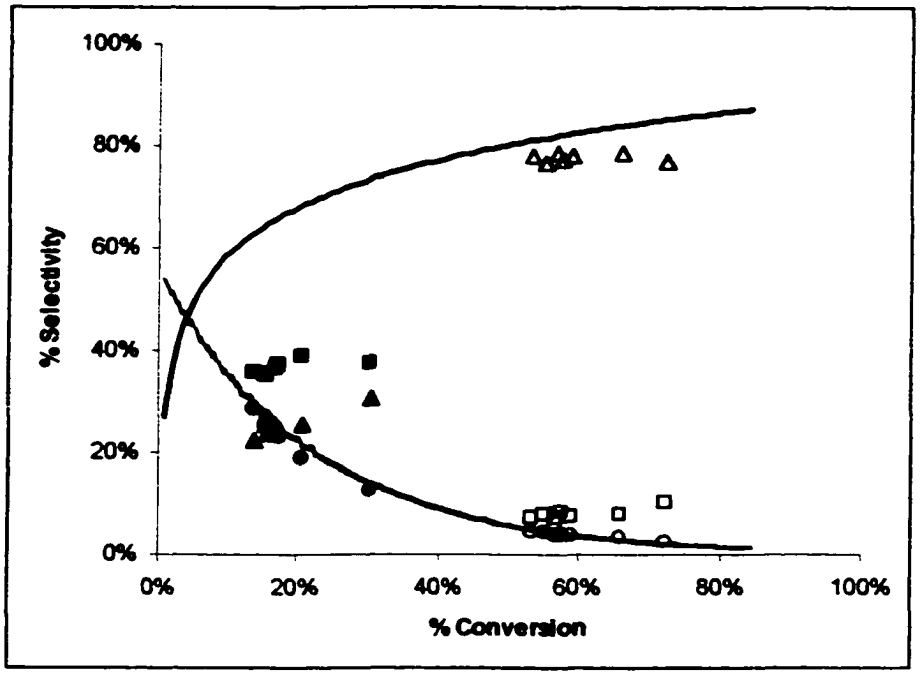

Figure 7.12. Selectivity of products for Pt/KL (open shapes) and Pt/Li/KL (filled shapes) including benzene (triangles), hexenes (circles), and methane (squares) obtained in a flow reactor system at WHSV = 10 h^{-1} at 450°C.

proposed the creation of unoccupied anti-bonding levels above the Fermi level of the supported platinum catalysts by taking the difference spectra of the catalyst and Pt foil. However, this procedure is only valid for the systems with the electronic structure close to that of the reference sample. The difference between a Pt foil and a Pt supported catalyst can also reflect a difference in scattering features (Pt-Pt coordination number and distance). In order to avoid this problem, Pt L_{II} and L_{III} XANES difference spectra in the presence and in the absence of hydrogen have been used [112-114].

Samant and Boudart [115] carried out XANES analysis on Pt supported in Y zeolite before and after hydrogen adsorption. The presence of hydrogen led to the

appearance of a peak at 9 eV on the difference spectra. They suggested that hydrogen adsorption led to the creation of unoccupied anti-bonding states above the Fermi level of Pt. However, the difference spectra for the Pt/Y catalysts with different acidities were similar. Then, no correlation between the electronic structure and the support acidity was established. It is important to stress that the coordination numbers of the catalysts were between 7.0 – 8.8, which were much higher than the ones of our work and of the work of Ramaker et al. [41]. Then, the lack of any correlation could be due to the large particle size of the catalysts.

Asakura et al. [113] performed Pt L_{III} and L_{II} XANES analyses of Pt catalysts with different dispersions on SiO_2, Al_2O_3 and MgO supports. The difference spectra of L_{III} edge of Pt supported catalysts with and without hydrogen showed a negative peak around 1 eV and a broad positive peak at 8.0 eV. The intensity of the last peak was correlated with the H/Pt ratio. They suggested that this peak should be related to the creation of a resonance state associated with the localized Pt-H interaction.

Reifsnyder et al. [112] also observed a positive peak at 9 eV in both L_{II} and L_{III} difference spectra of the Pt/SiO_2 catalyst under hydrogen and vacuum. This peak was attributed to electronic transition from Pt 2p to H 1s – Pt 5d anti-bonding level. Furthermore, the L_{III} difference spectrum showed a sharp negative peak near the edge indicating a decrease on the number of unoccupied d states near E_F. The absence of this peak at the L_{II} edge suggested that the majority of the unoccupied Pt d states were $d_{5/2}$.

However, hydrogen chemisorption on supported metal particles can also induce geometric effects on XANES spectra. Soldatov et al. [120] verified that hydrogen

atoms have an important scattering amplitude in the XANES energy range. Mojet [121] also confirmed the presence of hydrogen scattering near the white line (between 0–20 eV above the edge) on the Pt/KL catalysts.

Recently, Ramaker et al. [41] proposed a new analysis method in order to separate the electronic effects from the geometric ones by subtracting L_{II} and L_{III} white lines of the Pt/KL catalysts with and without adsorbed hydrogen. Theoretical Pt-H EXAFS functions showed that the peak around 8 eV in the difference spectra of Pt L_{III} white line under hydrogen and vacuum correspond to Pt-H scattering. The peak around 2 eV in this curve was attributed to the AS state. The AS was isolated by the subtraction of the difference curves: ΔL_{III-II}(Pt-H) – ΔL_{III-II}(Pt). The shape of the AS curve changed drastically with the support alkalinity. The peak around 0 eV is positive on the catalyst with higher support acidity whereas this peak became negative increasing the alkalinity of the zeolite. According to Ramaker et al. [41], the AS has the shape of a Fano resonance [122]. Then, the AS curve of the Pt/KL catalysts were fitted with the Fano profile. From these results, they concluded that the increase of support acidity shifts the Fermi level away from the Pt-H antibonding state, as shown in Figure 7.13.

We used the method of Ramaker et al. [41] to study the effect of the addition of a group I metal cation on the electronic structure of Pt clusters supported on KL zeolites. The shapes and the intensities of the AS curves were very different for Pt/KL and Pt/Li/KL. The first notable difference between the two catalysts is that the sign of E_{RES} changes to negative for the case of the more alkaline Pt/KL catalyst. That is, the peak in the AS curves (Figures 7.7 and 7.8) at 0 eV changes

sign from positive for the more acidic Pt/Li/KL catalyst to negative for the basic Pt/KL catalyst. Because E_{RES} represents the energy between the Fermi level of Pt and the antibonding state, this indicates that the position of the Fermi level of Pt is shifted further away from the AS (i.e., to lower energy) for the more acidic Pt/Li/KL catalyst. This shift away from the AS indicates that there is less electron population in the AS, resulting in increased chemisorption bond strength for H adsorbed on the Pt/Li/KL catalyst relative to the Pt/KL catalyst.

Also, as the resonance energy E_{RES} decreases, there is more degeneracy introduced between the empty valence band states and the antibonding state. Consequently, the transition becomes more rapid, and therefore the width Γ becomes more uncertain, and increases. However, when E_{RES} drops below the Fermi level (due to the strong core-hole interaction for the Pt/KL catalyst, a final state effect), the electron cannot escape, because there are no available states, and therefore the transition is improbable, and the width decreases. It is clear that much noise was present in the spectrum for the Pt/KL catalyst reduced at 300°C.

It is interesting to consider whether or not charge-transfer from the support to the Pt cluster could explain the differences in the Fermi level. That is, one might consider that the more alkaline Pt/KL catalyst would have more donation of electron density from the L-zeolite basic lattice oxygens to the Pt cluster, resulting in an increase of the Fermi level, and a decrease in the unoccupied available states in the valence band ΔVB. However, examination of ΔVB from XANES analysis (Figure 7.6 a and b, dotted lines) clearly shows that this is not the case. In fact, the number of

available states for Pt/KL is higher than that of Pt/Li/KL for both of the temperatures studied.

Figure 7.13: Qualitative molecular orbital diagram showing changes as a function of support alkalinity [111].

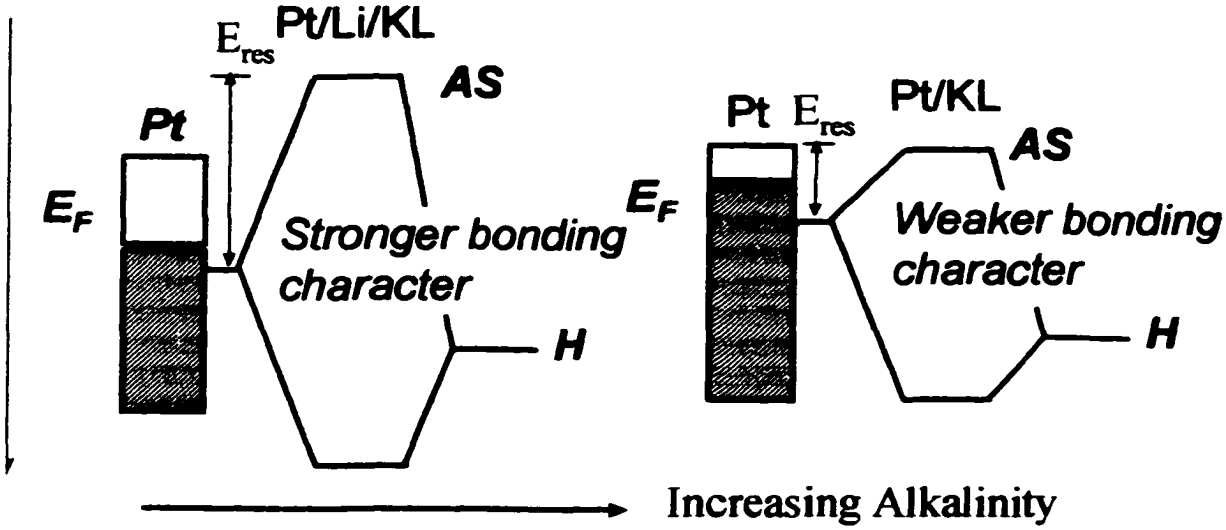

7.4.1.2 Infrared Spectroscopy

FTIR of adsorbed CO on Pt/zeolite catalysts has been used as an important tool to probe both electronic and particle morphology effects, as discussed in previous chapters. Pt/KL catalysts display complex bands, which typically extend from 2080 to 1750 cm^{-1}. Basically, the IR bands can be divided into two regions. The absorption bands between 2080 and 1900 cm^{-1} have been attributed to linearly adsorbed CO, whereas the bands between 1900 and 1750 cm^{-1} are due to bridged-coordinated CO. The first region displays several bands and their origin is still controversial.

The bands above 2050 cm^{-1} have been assigned to CO adsorbed on Pt particles located outside the channels of the zeolite and in the near-surface region, as

discussed in previous chapters. The bands below 2050 cm^{-1} have received different explanations. The bands appearing in the range 1970 – 1920 cm^{-1} were attributed to CO linearly adsorbed on small Pt particles with a higher electron density due to charge transfer from the support [38]. The frequency shifted to lower wavenumber as the basicity increased. Recently, it was seen that the back-exchange of Pt/KL and Pt/KY catalysts with K^+ led to a shift of the CO absorption bands to lower frequencies [116]. Menacherry and Haller [116] attributed this shift to an increase in the electron density of the metal particles. On the other hand, Lane et al. [93] suggested that this band at 1970 cm^{-1} results from an electrostatic interaction between the linearly adsorbed CO with the alkali cations. The same explanation was proposed by Mojet et al. [107].

Recently, Stakheev et al. [91,92] observed the presence of bands at 2068, 2031 and 2008 cm^{-1} on the IR spectrum of CO adsorbed on Pt/KL. These authors proposed the formation of neutral Pt carbonyls during CO adsorption on very small Pt particles. In previous chapters, we also observed the formation of Pt carbonyls on different Pt/KL catalysts prepared by vapor phase and incipient wetness impregnation. In Chapters 4 and 5, we used these carbonyls as a tool in conjunction with catalytic testing. Pt/KL VPI catalysts were found to retain a greater fraction of low wavenumber bands after high temperature reduction than catalysts prepared by IWI or IE, indicating smaller, more well dispersed clusters inside the channels of the zeolite. These same VPI catalysts showed much lower deactivation rates for n-hexanes aromatization. Mojet et al. [107] demonstrated a contraction of the Pt-Pt distance and a decrease of the Pt-Pt coordination number after exposure to CO. These

results indicated that the smaller Pt particles reconstructed under CO and Pt-CO aggregates formed.

The integrated intensity ratio of linear to bridged (L/B) adsorbed species has also been used to probe electronic changes on the metal [107,116,123]. The increase of the electron density of the metal was suggested to lead to a decrease of the L/B ratio. For Pt/KL catalysts, this ratio decreased with increasing support alkalinity, indicating that the electronic properties of the Pt particles are affected by the support. Menacherry and Haller [116] also observed a decrease of the L/B ratio on Pt/KL and Pt/KY catalysts back-exchanged. These results were attributed to an electron enrichment of the Pt particles.

In this work, the evolution of the bands during CO exposure indicates that Pt carbonyls were formed on both catalysts reduced at 300°C or 450°C in agreement with results from Chapters 4 - 6. The increase of the reduction temperature led to an agglomeration of the particle size as evidenced by the presence of a more pronounced shoulder around 2067 cm^{-1}. This result agrees well with the hydrogen chemisorption results (Table 7.1). However, the increase of the particle size was similar on both catalysts. Furthermore, the increase of the alkalinity did not produce a shift in the band positions as usually observed in the literature [107]. In fact, both catalysts presented the same band positions at both reduction temperatures. The only exception is the presence of a shoulder around 1979 cm^{-1} on the Pt/KL catalyst. Since both catalyst presented the same particle size, this new band could not be attributed to differences in particle size. Stakheev et al. [92] proposed that the oxygen atoms of the framework of the zeolite could act as a ligand and stabilize the Pt carbonyls. In our

Pt/KL catalyst, the shoulder appearing around 1979 cm^{-1}, not present for the Pt/Li/KL catalyst, could correspond to new Pt carbonyl species stabilized by the support alkalinity. In fact, XANES analysis revealed that the increase of the alkalinity moved the Fermi level closer to the Pt-H antibonding state. According to Mojet et al. [109], this corresponds to a weaker Pt-H bond and a decrease in the ionization potential of the Pt d orbitals due to the interactions between the support and the metal particle.

7.4.1.3 Microcalorimetry of Adsorbed Hydrogen and CO

In agreement with the results of XANES shape resonance results, which showed increased bonding character for the more acidic Pt/Li/KL catalyst, the heats of adsorption for adsorbed hydrogen and CO were also significantly higher than for the Pt/KL catalyst, as depicted in Figure 7.10 a and b. This increased chemisorption bond strength has direct implications for reaction. That is, we expect that a stronger chemisorption bond of an adsorbed hydrocarbon would lead to weakening of the internal carbon-carbon bond, therefore decreasing the activation energy required to rupture the bond and promote the rate of hydrogenolysis, at the expense of aromatization.

7.4.2 Catalytic Testing

7.4.2.1 Neopentane Hydrogenolysis

A comparison of the two catalysts in Table 7.4 shows that the hydrogenolysis activity was much higher for the Pt/Li/KL than the Pt/KL. At 380°C, the TOF of the Pt/Li/KL catalysts was 0.03 s^{-1}, while the activity for the Pt/KL catalyst was below

detection. At a higher temperature of 450°C, the TOF of the Pt/KL catalyst was 0.018 s^{-1}, still below the TOF of the Pt/Li/KL catalyst at the lower temperature of 380°C. The same trend was observed for Pt/KL catalysts with different support alkalinities [109]. In that case, the catalyst with higher acidity (K/Al of 0.63) had a neopentane TOF of 0.18 s^{-1}, while the catalyst with higher alkalinity (K/Al of 1.25) had a much lower TOF of $4.9 \cdot 10^{-5}$ at the same temperature of 325°C. According to Mojet et al. [109], the changes in the neopentane reaction rates are due to the modification of the electronic properties of the metal particles by the interaction with the support. A shift in the ionization potential of the metal valence orbitals with increase of support alkalinity was proposed to explain the catalytic behavior, in conjunction with IR, XPS and XANES results. Therefore, in this work, exchanging the cation changes the support alkalinity, and directly modifies the nature of Pt – i.e., higher support acidity increases the rate of neopentane hydrogenolysis.

7.4.2.2 n-Hexane Aromatization in a Pulse Reactor

In the pulse mode, the catalytic activity is measured in the absence of deactivation by coke formation. Therefore, the activity represents that of a clean Pt surface. In line with the results of pulse testing of neopentane hydrogenolysis, the hydrogenolysis pathway is more favored with the addition of lithium cation to the support. At 500°C, the Pt/KL TOF of 1.86 s^{-1} was close to that reported in an earlier study of 3.6 s^{-1} [19]. Another work conducted at 425°C presented a result of 1.44 s^{-1} [57]. In that study, the TOF of Pt/NaY, with a more acidic support, was approximately one tenth that observed on Pt/KL. In our work, exchanging K^+ with

Li^+ resulted in a decrease in the aromatization TOF from the value of 1.86 s^{-1} to 0.53 s^{-1}. On the other hand, the Pt/Li/KL hydrogenolysis TOF of 2.12 s^{-1} was much higher than observed for Pt/KL (0.72 s^{-1}), indicating that Pt on the Li/KL support is modified to promote hydrogenolysis.

A wide variation in activation energies has been reported in the literature for aromatization on Pt/KL. For example, in flow mode, Iglesia and Baumgartner [19] determined the activation energy to be around 28 kcal/mol for a 1% Pt/KL catalyst prepared by IWI, while Lane et al. [57], also operating in flow mode, found a much higher value of 54 kcal/mol using a 1% Pt/KL catalyst also prepared by IWI. Our results under pulse testing showed considerably lower activation energy of 17 kcal/mol for the Pt/KL catalyst prepared by VPI. Previous results indicate that deactivation by coking affects the aromatization activity more for IWI catalysts than for VPI catalysts, and these effects are more pronounced under flow mode. This could account for the higher apparent activation energies observed in previous studies. Results indicate that important changes in the activation energy for aromatization occurs with the incorporation of Li^+ to the support. Interestingly, the activation energy barrier for hydrogenolysis is much less affected.

7.4.2.3 n-Hexane Aromatization in a Flow Reactor

The differences in activity and selectivity between both catalysts are remarkable. For the Pt/KL, the main product was benzene whereas the amount of methane and hexane formed were low. Recently, we explained the high aromatization activity of Pt/KL in terms of its ability to convert hexane into benzene

[24]. The KL zeolite plays the important role of inhibiting bimolecular reactions that lead to coke formation [19,20]. By contrast, the Pt/Li/KL catalyst presents a low activity and the main products were hexane and methane. This behavior was very similar to that observed on the nonmicroporous Pt/Mg(Al)O catalyst, where no microporosity is present to protect the Pt clusters, as described in Chapter 3. In that case the results were attributed to the higher formation of coke for Pt/Mg(Al)O and the inhibition of bimolecular encounters for Pt/KL – ensemble effects.

A comparison with our previous results allows us to analyze the selectivities to benzene and hexenes at the same levels of conversion for Pt/KL and Pt/Li/KL (Figure 7.12). As shown in Figure 7.12, the Pt/KL catalyst displays the same selectivity versus conversion pattern as previously observed. The selectivity to hexenes for Pt/Li/KL is less affected than benzene, which is sharply reduced. However, this catalyst presented a high selectivity to hydrogenolysis. Figure 7.12 shows that the selectivity to hydrogenolysis products is relatively constant, while there is obviously interconversion between hexenes and benzene for both catalysts. This suggests that the hydrogenolysis and aromatization pathways are in parallel. The results of neopentane pulse testing, which is metal-catalyzed, demonstrates that the intrinsic nature of the Pt is modified by the presence of Li. In this case, the Pt has a higher propensity to generate hydrogenolysis products in contrast to Pt/KL.

Since we have similar particle size as shown by EXAFS and hydrogen chemisorption and because the platinum clusters are inside the channels of the L-zeolite, as indicated by FTIR, this further suggests that the Pt was affected by the modification of the support alkalinity when lithium was added. The high

hydrogenolysis selectivity could be attributed to the changes in the electronic structure of the metal particle, evidenced by XANES shape resonance spectroscopy.

7.5 CONCLUSIONS

Electronic modification to Pt by exchanging the zeolite cation from potassium to lithium was studied by a combination of methods, including a new shape resonance XANES method, microcalorimetry, pulse neopentane hydrogenolysis, and FTIR of adsorbed CO. The catalysts were also tested for n-hexane aromatization in both flow and pulse modes. Addition of lithium cation has been speculated to increase the acidity of L-zeolite lattice oxygen atoms, causing more rollover of the interatomic potential between Pt and O. The XANES method was based on the different information contained in the L_{III} and L_{II} white lines of the catalyst with and without chemisorbed hydrogen. Addition of lithium resulted in a shift of the Fermi level of Pt away from the antibonding state of Pt-H, strengthening the chemisorption bond of hydrogen. This increased chemisorption bond strength for lithium addition was confirmed by microcalorimetry, and increased hydrogenolysis rates for both neopentane and n-hexane aromatization, to the detriment of benzene production.

SPECIAL ACKNOWLEDGMENTS

I would like to thank our visiting researcher Dr. Fabio Noronha for his help with EXAFS and XANES analysis. Also, I would like to acknowledge Dr. Armando Borgna and Dr. Walter Alvarez for their help with EXAFS.

CHAPTER VIII: CATALYST REGENERATION AND OXIDATION / REDUCTION CYCLES

The regeneration of three different Pt/KL catalysts has been studied after the n-hexane aromatization reaction in the presence of sulfur. It has been found that regeneration in air of poisoned catalysts does not result in recovery of the aromatization activity. After this regeneration, growth of Pt particles outside the channels of the zeolite is observed. By contrast, regeneration with addition of a halo-alcohol results in Pt redispersion and significant recovery of aromatization activity. The preparation method employed and the presence of Tm as a promoter plays an important role in the efficiency of the regeneration procedure.

8.1. INTRODUCTION

It is well known that Pt/KL catalysts have exceptionally high activity and selectivity for the aromatization of n-hexane to benzene. The principal drawback of these catalysts is their high sensitivity to the presence of sulfur even in very low amounts (e.g., ppb). Therefore, development of sulfur-resistant catalysts is a major goal in this area. At the same time, the understanding of the regeneration process is also an issue of great industrial relevance [42-44]. However, only a few papers in the open literature [45] have focused on the effect of different treatments after reaction under clean and sulfur-poisoning conditions. In a previous chapters, we have pointed out that by varying the preparation method of Pt/KL catalysts, one can greatly influence the location and morphology of the Pt particles inside the channels of the zeolite, and these morphological variations may have strong effects on the stability of

the catalysts under both, sulfur-free and sulfur-containing feeds. The vapor-phase impregnation method (VPI) results in catalysts with smaller particles than those in the catalysts prepared by incipient wetness impregnation (IWI). The characteristic morphology produced by the VPI method was found to improve the performance of the catalyst under clean and sulfur poisoned conditions, enhancing the catalyst's resistance to the formation of coke and decreasing the particle agglomeration rate. Similarly, in Chapter 6, we and others [35,36] have observed that the addition of small amounts of thulium resulted in improved performance. We have demonstrated that the addition of Tm (VPI) results in an improvement in metal dispersion. Also the Tm may act as a getter of sulfur, hence delaying the effects of sulfur poisoning on the Pt metal. In this contribution we have investigated different regeneration procedures on three Pt/KL samples, one prepared by IWI, one by VPI, and a third one prepared by VPI containing Tm.

8.2. EXPERIMENTAL

1 wt % Pt/KL catalysts were synthesized by incipient wetness impregnation (IWI) and vapor phase impregnation (VPI). The Tm-promoted catalyst was prepared by sequential vapor phase impregnation, as described in Chapter 6. Briefly, it consists of subliming acetyl-acetonates of Pt and/or Tm in the presence of dry KLTL zeolite in vacuum. Fresh and spent samples were characterized by EXAFS, TEM, and FTIR of adsorbed CO. The aromatization of n-hexane was studied in a pulse reactor in the temperature range of 400°C to 500°C, sending pulses containing around 6.57×10^{-7} moles of n-hexane in a H_2 carrier. The catalysts were studied in the

freshly reduced state, after 9 h under steady state reaction, in the presence of 2 ppm sulfur, and after regeneration. Regeneration procedures were carried out using oxidizing treatments with air and 1,3 dichloro-2-propanol. For both the regeneration treatments, the samples were reduced *in situ* under H_2 for 1 h at 500°C. For the regeneration in air, the temperature was decreased to 400°C and exposed to air for 1.5 h. For the halo-alcohol regeneration procedure, the sample was first treated with 5% O_2/He for 30 min at 400°C. This was followed by an oxychlorination step to obtain the redispersion of Pt particles. The halo-alcohol was saturated with a continuos flow of He through a gas bubbler and then diluted with a stream of 5% O_2/He at 400°C. Then, the sample was exposed to this mixture for 1.5 h. After that step, the halo-alcohol was switched off and the catalyst was allowed to oxidize under 5% O_2/He for another 30 min. The samples were then re-reduced at 500°C for 1 h before the pulse experiments.

8.3. RESULTS

8.3.1. Catalytic Activity Measurements

The conversion of n-hexane was studied in the pulse reactor after the various pretreatments. Fig. 8.1 shows the benzene yields obtained on the three catalysts at 500°C. In agreement with previous results from Chapter 6, the fresh VPI and Tm-VPI catalysts exhibited somewhat higher activity and selectivity than the standard IWI Pt/KL catalyst. However, the greatest differences were observed on the samples aged under sulfur and those regenerated in air alone or with the addition of

chloropropanol. In those samples, the VPI and particularly the Tm-VPI show much better performance than the standard IWI catalyst.

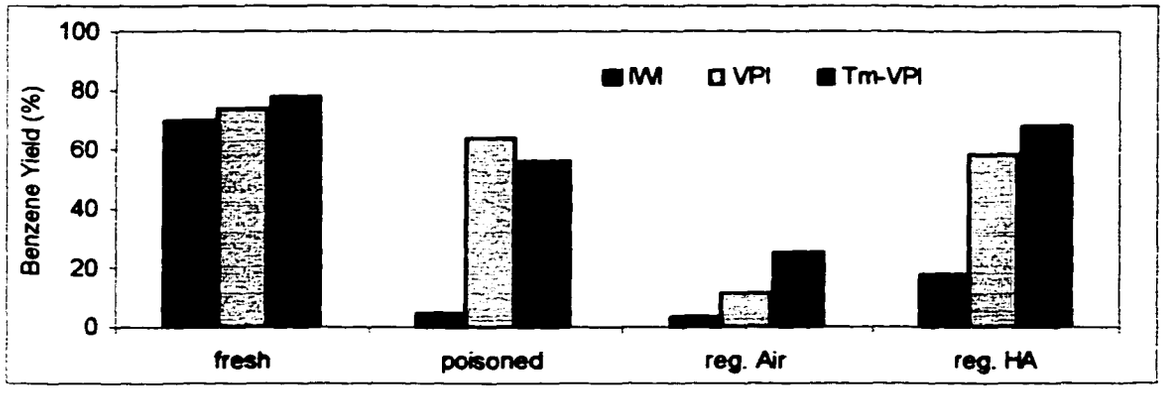

Figure 8.1: Benzene yield for IWI, VPI and Tm-VPI catalysts at 500°C.

8.3.2. Catalyst Characterization

The characterization by EXAFS, TEM and H_2 chemisorption conducted over the three different catalysts indicate that the VPI method leads to the formation of Pt clusters inside the channels of the zeolite much smaller than those prepared by IWI. As summarized in Table 8.1, EXAFS shows lower Pt-Pt coordination numbers, confirming the presence of smaller clusters. At the same time, the coordination of Pt with the lattice oxygen of the zeolite was higher for the VPI catalyst than for the IWI, indicating a greater extent of interaction with the zeolite walls. Similarly, the addition of Tm as a promoter helps to obtain a higher dispersion of Pt, as reflected by lower coordination numbers on the freshly reduced catalyst.

EXAFS has been used to investigate the changes in morphology of the Pt clusters on the three different catalysts after the various treatments. Fig. 8.2 includes

Table 8.1: Structural parameters determined from EXAFS analysis.

	Fresh			Poisoned			Reg-Air			Reg-Haloalcohol		
	Pt-Pt	Pt-O	R (Å)	Pt-Pt	Pt-O	R (Å)	Pt-Pt	Pt-O	R (Å)	Pt-Pt	Pt-O	R (Å)
IWI	7.6	--	2.74	8.2	--	2.75	8.7	--	2.74	3.1	--	2.66
	--	0.25	2.73	--	0.35	2.71	--	0.2	2.70	3.8	--	2.77
										--	0.40	2.68
VPI	2.1	--	2.81	3.1	--	2.77	5.8	--	2.74	2.8	--	2.78
	2.7	--	2.69	2.6	--	2.67	--	0.6	2.66	2.9	--	2.67
	--	0.6	2.67	--	0.5	2.67				--	0.6	2.66
Tm-VPI	2.2	--	2.74	1.9	--	2.8	1.9	--	2.8	2.5	--	2.78
	2.1	--	2.61	2.8	--	2.69	3.3	--	2.69	2.5	--	2.66
	--	1.1	2.39	--	0.95	2.67	--	0.9	2.69	--	0.9	2.64

the Fourier transforms of the EXAFS data obtained on the IWI, VPI, and Tm-VPI samples in the freshly reduced state, after reaction under sulfur (9 h, 2 ppm), after regeneration in air, and after regeneration with addition of chloropropanol. Interesting trends are observed. After reaction for 9 h in the presence of sulfur, a moderate increase in coordination number was observed for all three catalysts. However, it is important to note that, even after this growth, the particles in the VPI and Tm-VPI catalysts are still very small, as indicated by the low coordination numbers.

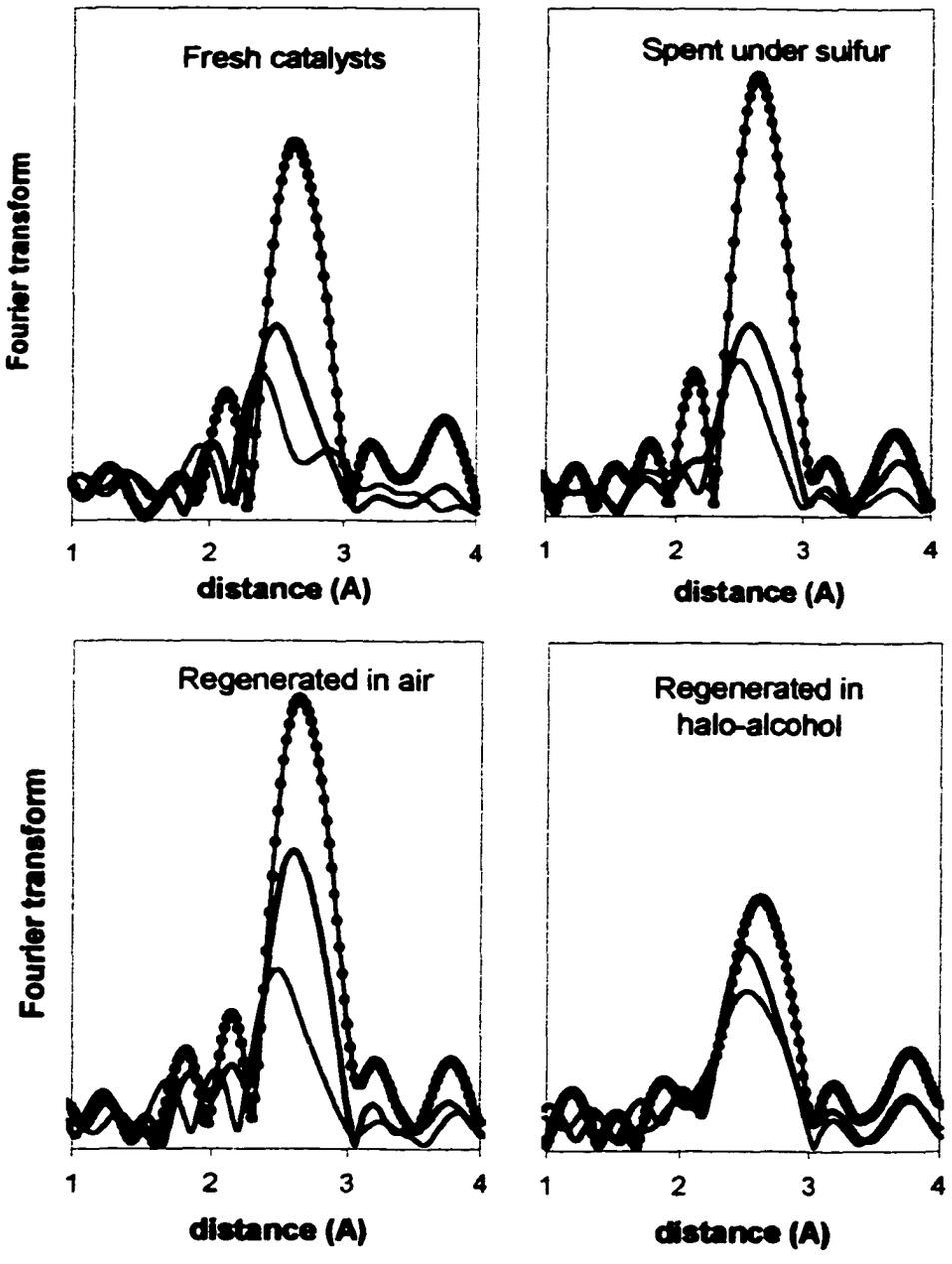

Figure 8.2: Fourier Transform obtained from EXAFS data for fresh, spent and regenerated samples. (line with filled circles-IWI ; thick line-VPI ; thin line-Tm-VPI).

DRIFTS of adsorbed CO helps to further understand what happens with the catalysts after regeneration in air. The fresh catalyst exhibited the typical distribution

of bands in the range 2080 to 1950 cm^{-1}. As discussed in previous chapters, the appearance of the low wavenumber bands are associated with the formation of Pt-carbonyl species, stabilized by the zeolite. Important differences were observed in the spectra of adsorbed CO after exposure to sulfur. While the spectra for the IWI catalyst showed a significant decrease in the region between 2014 and 1970 cm^{-1}, the spectra for the VPI catalyst only showed a modest change in this region. In addition, regeneration in air of the IWI catalyst caused the appearance of a shoulder at about 2084 cm^{-1} on the IWI catalyst that we attribute to large Pt particles that migrated to the outer surface of the zeolite. In contrast, after similar calcination at high temperature, the VPI and Tm-VPI catalysts did not exhibit that high wavenumber shoulder and showed lower decrease in hydrogen chemisorption in comparison with the IWI catalyst.

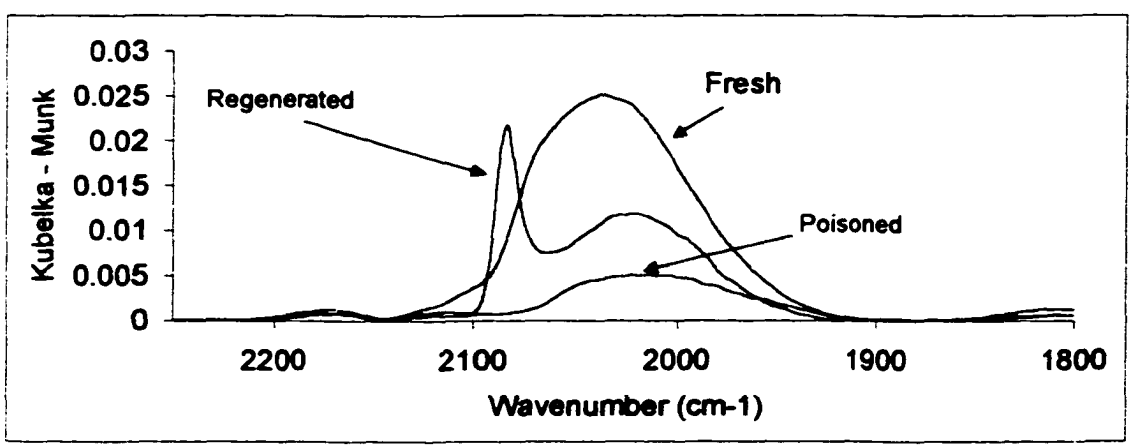

Figure 8.3: DRIFTS spectra for fresh, spent(poisoned) and regenerated(air) IWI samples.

8.4. CONCLUSIONS

This study has demonstrated that both, the catalyst preparation method and the regeneration procedure have important effects on the activity of the catalyst

samples. The VPI and the Tm-VPI catalysts have a better sulfur resistance than the IWI catalysts due to their initial small particle size. Therefore, channel blocking and Pt particle entrapment is delayed. Regeneration in air results in sintering of particles, which causes a drop in the activity of all the samples. The oxychlorination treatment of the poisoned samples result in better Pt dispersion and an increase in the aromatization activity. The increase in the aromatization activity for the IWI sample can be attributed to the redispersion of Pt particles as clearly indicated by EXAFS. For the VPI and Tm-VPI samples, the increase is mainly due to coke and sulfur removal. The addition of Tm as a promoter helps in maintaining the dispersion of Pt particles under the regeneration process.

SPECIAL ACKNOWLEDGMENTS

This was a collaborative work of the OU Heterogeneous Catalysis Group. Special thanks go to Firoz Ghadiali for construction of the pulse system, and for conducting the regeneration treatments and pulse experiments. This was largely his thesis work, and is included here for completeness. Also thanks are due to Dr. Armando Borgna for analysis of the EXAFS data. Finally, I would like to thank Dr. Walter Alvarez and Dr. Adriana Pisanu for their FTIR work.

CHAPTER IX: CONCLUSIONS

Pt/KL was found to be unique in that the microporosity of the KL zeolite has the ability to inhibit bimolecular pathways leading to coke formation on the Pt surface, for those Pt clusters located inside the channels. By catalytic screening of basic supported Pt catalysts, it was demonstrated that Pt/KL has a much higher activity and selectivity than nonmicroporous Pt/Mg(Al)O or Pt/SiO_2 catalysts. It can be concluded that the basicity of the support alone cannot explain the high performance of Pt/KL catalysts for aromatization. The presence of hexenes, products that are generated in the reaction as precursors for benzene, is an indication of the loss of aromatization activity. This loss may be brought about by the presence of a significant fraction of the metal particles outside the zeolite channels or by the partial poisoning of the metal surface, as by sulfur. In most cases, these two phenomena are interconnected since the Pt particles outside the channels of the zeolite are more susceptible to coke formation and are rapidly deactivated. In the presence of sulfur, some accelerated particle growth is observed. However, the pronounced deactivation may also be due to the deposition of small amounts of sulfur on the Pt particles outside and inside the zeolite, which effectively block and deactivate the large ensembles required for aromatization and hydrogenolysis. As a result, the selectivity to hexenes increases as the catalyst deactivates.

Subtle differences in Pt cluster morphology were also studied for Pt/KL catalysts where the majority of Pt was located inside the L-zeolite. The distribution of Pt clusters and their resulting characteristic morphology largely varied with loading and method of preparation. Over a wide range of catalysts studied, we observed three different types of particles that profoundly affected activity, selectivity, stability, and results of catalyst characterization. The different particles included large particles formed outside of the channels, small particles located inside the channels, but large enough to block or partially block them, and clusters that were small enough to reside in the lobes of the L-zeolite channels.

TEM and EXAFS revealed the existence of Pt clusters having very small size located inside the L-zeolite channels for both IWI and VPI preparation methods. In addition, these results were confirmed by FTIR of adsorbed CO, which gave evidence that the particles were small enough to allow for the formation of Pt carbonyls. Furthermore, the increase in coordination of Pt with the oxygen of the L-zeolite framework and the decrease in Pt-Pt coordination observed for the VPI series relative to the IWI series clearly indicated that the particles produced were smaller and of different characteristic morphology. In line with this finding, lower collimation effects were observed for VPI catalysts with respect to IWI catalysts during pulse testing of MCP-RO. This lower collimation strongly suggested that the clusters produced by VPI were small enough to allow for the diffusion of reactants and products around the cluster during the aromatization of n-hexane reaction.

The characteristic location and morphology of the particles produced from the different preparation procedures had important consequences on the conversion,

selectivity, and stability of catalysts under reaction conditions. Under continuous flow conditions, VPI catalysts displayed higher aromatization activity and selectivity, lower production of hydrogenolysis products, lower hexenes, and a significantly lower deactivation rate.

The method of preparation and the choice of either powder or pellet for the support strongly influenced the resulting Pt cluster morphology and location distribution. IE, IWI, and VPI powder catalysts were found to exhibit high H/Pt ratios, all of which were greater than unity. However, FTIR of adsorbed CO showed that, more important than dispersion, it is the distribution of Pt cluster morphology and location that influences the activity and stability of the catalyst for the n-hexane aromatization reaction.

For catalysts reduced at 400°C, FTIR showed that the IE catalyst prepared by the standard method had a large fraction of Pt external to the L-zeolite. In contrast, the IWI and VPI catalysts displayed virtually all of the Pt inside the L-zeolite channels. After reduction at 500°C, the catalysts displayed differences in sensitivity to the treatment. Our standard IE catalysts showed growth in bands at high wavenumbers indicative of Pt migration out of the L-zeolite channels. These catalysts rapidly deactivation by coke formation. An ion exchange catalyst with improved Pt cluster morphology was also prepared using a modified ion exchange procedure found in the patent literature. In that case, an aging step allowed the salt to distribute inside the channels of the L-zeolite, as revealed by DRIFTS of adsorbed CO. IWI catalysts also displayed growth in bands assigned to Pt clusters inside the

channels, but in the near-surface region. The IWI catalysts were found to slowly lose activity, reaching a steady state activity approximately half that of the initial activity. VPI catalysts maintained low wavenumber bands after high temperature reduction, indicating that the small Pt clusters were more evenly distributed, and not localized near the pore mouth. These catalysts displayed the highest activity and selectivity, with long-term stability. The IWI and IE catalysts were found to be less reproducible than the VPI preparation.

Reaction testing and characterization demonstrated that the VPI catalyst could be scaled-up using either a moderate vacuum or a helium flow preparation method. These catalysts displayed very little differences from the high vacuum preparation when probed with FTIR of adsorbed CO. No differences in activity or stability were observed between the catalyst prepared by moderate or high vacuum. The catalyst prepared by the helium flow VPI method showed no differences in band positions, but 10% of the Pt was lost during preparation. Preparation directly on the pellets resulted in a large fraction of Pt external to the pores and likely on the binder for the methods studied in this work – standard IE, IWI, and VPI. However, in light of the results of DRIFTS of adsorbed CO for the powder catalyst, it is likely that the modified IE method could result in a pelletized catalyst with improved characteristics than the one prepared by the standard IE method. Finally, preparation of the pellet directly from extruding the VPI powder catalyst may lead to a good catalyst for commercial use.

The addition of lanthanide promoters was also carried out. When prepared correctly, the addition of Tm has important consequences on the aromatization

performance of Pt/KL catalysts. There are several ways in which Tm affects the activity, selectivity, and stability of Pt/KL:

a) The presence of Tm results in a catalyst with higher Pt dispersion. As demonstrated before, a higher dispersion by itself results in a much better catalyst, even without the addition of any promoter.
c) Tm acts as a sulfur getter, so it delays the poisoning of Pt.
d) The initial activity of the Tm-promoted catalysts is higher than that of unpromoted Pt/KL, even those prepared by VPI. This higher activity would suggest that Tm may directly modify Pt or may even participate in accelerating the aromatization reaction. However, further research is required to make this determination.

However, the amount and method of incorporation of Tm is critical to the catalyst performance. While the sequential vapor phase impregnation method with a small amount of Tm (0.15%) yielded a catalyst with improved catalytic properties, other methods such as coimpregnation of Pt and Tm hindered the dispersion of Pt, causing blocking of the L-zeolite channels and a higher deactivation rate under reaction.

Electronic modification to Pt by exchanging the zeolite cation from potassium to lithium was studied by a combination of methods, including a new shape resonance XANES method, microcalorimetry, pulse neopentane hydrogenolysis, and FTIR of adsorbed CO. The catalysts were also tested for n-hexane aromatization in both flow and pulse modes. Addition of lithium cation has been speculated to increase the acidity of L-zeolite lattice oxygen atoms, causing more rollover of the interatomic potential between Pt and O. The XANES method was based on the different information contained in the L_{III} and L_{II} white lines of the catalyst with and without chemisorbed hydrogen. Addition of lithium resulted in a shift of the Fermi level of Pt away from the antibonding state of Pt-H, strengthening the Pt-H chemisorption bond.

This increased chemisorption bond strength for lithium addition was confirmed by microcalorimetry of adsorbed H_2 and CO, and resulted in increased hydrogenolysis rates for both neopentane and n-hexane aromatization, to the detriment of benzene production.

Finally, the regeneration of Pt/KL catalysts was conducted. Both the catalyst preparation method and the regeneration procedure were found to have important effects on the activity of the catalyst samples. Regeneration in air results in sintering of particles, and a drop in activity for all samples was observed. The oxychlorination treatment of the poisoned samples following air treatment resulted in better Pt dispersion and an increase in the aromatization activity. The increase in the aromatization activity for the IWI sample could be attributed to the redispersion of Pt particles, as revealed by EXAFS. For the VPI and Tm-VPI samples, the increase was mainly due to coke and sulfur removal. The addition of Tm as a promoter helped in maintaining the dispersion of Pt particles under the regeneration process.

LITERATURE CITED

1. Tamm, P. W., Mohr, D. H., and Wilson, C. R., *Stud. Surf. Sci.Catal.* **38**, 335 (1988).
2. Bernard, J. R.; *in* "Proc. 5th Internat. Zeolite Confer.", (L. V. C. Rees, Ed.), p. 686 Heyden, London (1980).
3. Hughes, T.R., Buss, W.C., Tamm, P.W., and Jacobson, R.L., *Stud. Surf. Sci. Catal.*, **28**, 725 (1986).
4. Davis, R. J., *Hetero. Chem. Rev.* **1**, 41 (1994).
5. Kirk and Othmer, *Encyclopedia of Chemical Technology*, **4**, 73 (1991)
6. Milton, R.M., *Molecular Sieves*, Society of Chemical Industry, London, 1968, p. 199.
7. Breck, D.W. and Acara, N.A., U.S. Patent No. 711,565 (1958).
8. Joshi, P.N., Kotasthane, A.N., and Shiralkar, V.P., *Zeolites*, **10**, 598 (1990).
9. Breck, D.W., *Zeolite Molecular Sieves*, New York, John Wiley & Sons, 1974.
10. Barrer, R.M. and Villiger, H., *Z. Kristallogr.*, **128**, 352 (1969)
11. Newell, P.A. and Rees, L.V.C., *Zeolites*, **3**, 22 (1983).
12. Young, D.A. and Yorba, L., U.S. Patent No. 3,867,512 (1975).
13. Lafyatis, D., Froment, G. F., Pasau-Claerbout, A. and Derouane, E. G., *J. Catal.***147**, 552 (1994).
14. Zou, B.S., Dudukovic, M.P., Mills, P.L., *J. Catal.* **145**, 683 (1994).
15. Tauster, S. J., and Steger, J. J., *J. Catal.* **125**, 387 (1990).
16. Derouane, E. G. and Vanderveken, D. J., *Appl. Catal.* **45**, L15 (1988).
17. Larsen, G. and Haller, G.L., *Catal. Lett.* **3**, 103 (1989).
18. Larsen, G. and Haller, G.L., *Catal. Today* **15**, 431 (1992).
19. Iglesia, E., and Baumgartner, J. E., "Proc. X Internat. Congr. Catal, (Guczi L. et al., editors)", p. 993, Elsevier Sci. Publ., New York, (1993).
20. Iglesia, E., and Baumgartner, J. E., Proc. IX Internat. Zeolite Conf., Montreal (1992).
21. Mielczarski, E., Hong, S. B., Davis, R. J., and Davis, M. E., *J. Catal.* **134**, 359 (1992).
22. Hong, S. B., Mielczarski, E., Davis, M. E., *J. Catal.* **134**, 349 (1992).
23. Davis, R. J., and Derouane, E. G., *Nature* **349**, 313 (1991).
24. Jacobs, G., Padro, C. L. and Resasco, D. E., *J. Catal.* **179**, 43 (1998).
25. McVicker, G. B., Kao, J. L., Ziemiak, J. J., Gates, W. E., Robbins, J. L., Treacy, M. M. J., Rice, S. B., Vanderspurt, T. H., Cross, V. R., and Ghosh, A. K., *J. Catal.* **139**, 48 (1993).
26. Jacobs, G., Ghadiali, F., Pisanu, A.P., Borgna, A., Alvarez, W.E. and Resasco, D.E., *Appl. Catal. A* **188**, 79 (1999).
27. Alvarez, W. E., and Resasco, D. E., *J. Catal.* **164**, 467 (1996).
28. Alvarez, W. E., Resasco, D. E., *Catal. Lett.* **8**, 53 (1991).
29. Jacobs, G., Alvarez, W.E., and Resasco, D.E., *Applied Catalysis*, in press.
30. Rotman, D., *Chemical Week* **8** (1992).
31. Vaarkamp, M., Miller, J.T., Modica, F.S., Lane, G.S., Koningsberger, D.C., *J. Catal.* **138**, 675 (1992).

32. Fukunaga, T., and Ponec, V., *J. Catal.* **157**, 550 (1995).
33. Larsen, G., Haller, G. L., Resasco, D. E., and Durante, V. A., U. S. Patent 5,540,833 (1996).
34. Larsen, G., Resasco, D. E., Durante, V. A., Kim, J., and Haller, G. L., *Stud. Surf. Sci. Catal.* **83**, 321 (1994).
35. Fang, X., Li, F., and Luo, L., *Appl. Catal. A*, **146**, 297 (1996).
36. Fang, X., Li, F., Zhou, Q., and Luo, L., *Appl. Catal. A*, **161**, 227 (1997).
37. Jacobs, G., Ghadiali, F., Pisanu, A., Padro, C., Borgna, A., Alvarez, W.E. and Resasco, D.E., *J. Catal.* **191**, 116 (2000).
38. Besoukhanova, C., Guidot, J., and Barthomeuf, D., *J. Chem. Soc. Faraday Trans. I* 77, 1595 (1981).
39. McHugh, B.J., Larsen, G., and Haller, G.L, *J. Phys. Chem* **94**, 8621 (1990).
40. Fukunaga, T. and Ponec, V., *Appl. Catal A*, **154**, 207 (1997).
41. Ramaker, D.E., Mojet, B.L., Oostenbrink, G., Miller, J.T., and Koningsberger, D.C., *Phys. Chem. Chem. Phys.* **1**, 2293. (1999).
42. Burbridge, W. B. and Rees, D. M., US Patent No. 4,192,771 (1980).
43. Bernard, J. R. and Breysse, M., US Patent No. 4,493,901 (1985).
44. Fung, S. C., Tauster, S. J. and Koo, J. Y., US Patent No. 5,726,112 (1998).
45. Sugimoto, M., Katsumo, H., Hayasaka, T., Hirasawa, K. and Ishikawa, N., *Appl. Catal. A: General* **106**, 9 (1993).
46. Che, M. and Bennett, C., *Adv. Catal.*, **36**, 55 (1989).
47. Schweizer, A.E., US Patent 4,992,401 (1991).
48. Dossi, C., Psaro, R., Bartsch, A., Fusi, A., Sordelli, L., Ugo, R., Bellatreccia, M., Zanoni, R. and Vlaic, G., *J. Catal.* **145**, 377 (1994).
49. Bellatreccia, M., Zanoni, R., Dossi, C., Psaro, R., Recchia, S., Vlaic, G., *J. Chem. Soc. Farad. Trans.* **91**, 2045 (1995).
50. Jentoft, R. E., Tsapatsis, M., Davis, M. E., Gates, B. C., *J. Catal.* **179**, 565 (1998).
51. Stohr, J., *NEXAFS Spectroscopy*, Springer-Verlag, Heidelberg, 1992, p. 296.
52. Niemantsverdriet, J.W., *Spectroscopy in Catalysis*, Verlagsgesellschaft, 1993, pp. 150-156.
53. Sayers, D.E., Bunker, B.A., in: Koningsber, D.C., Prins, R. (Eds.), *X-ray Absorption: Principles, Applications, Techniques of EXAFS, SEXAFS, and XANES*, Wiley, 1988, p. 211.
54. Rehr, J.J., Zabinsky, S.I., Albers, R.C., *Phys. Rev. Lett.* **69**, 3397, (1992).
55. Rehr, J.J., Mustre de Leon, J., Zabinsky, S.I., Albers, R.C., *J. Amer. Chem. Soc.* **113**, 5135, (1991).
56. Mustre de Leon, J., Rehr, J.J., Zabinsky, S.I., Albers, R.C., *Phys. Rev. B* **44**, 4146, (1991).
57. Lane, G., Modica, F. S., and Miller, J. T., *J. Catal.* **129**, 145 (1991).
58. Miller, J. T., Agrawal, N. G. B., Lane, G. S., and Modica, F. S., *J. Catal.* **163**, 106 (1996).
59. Schaper, H., Berg-Slot, J.J. and Stork, W.H.J., *Appl. Catal.* **54**, 79 (1989).
60. Cavani, F., Trifirio, F. and Vaccari, A., *Catal. Today* **11**, 173 (1991).
61. Dai, L. X., Sakashita, H., and Tatsumi, T., *Chem. Lett.* **387** (1993).

62. Sugimoto, M., Katsumo, H., Hayasaka, T., Ishikawa, N., and Hirasawa, K., *Appl.Catal. A* **102**, 167 (1993).
63. Sugimoto, M., Murakawa, T., Hirano, T., and Ohashi, H., *Appl. Catal. A* **95**, 257 (1993).
64. Ostgard, D. J., Kustov, L., Poeppelmeier, K. R., and Sachtler, W. M. H., *J. Catal.* **133**, 342 (1992).
65. Vaarkamp, M., van Grondelle, J., Miller, J. T., Sajkowski, D. J., Modica, F. S., Lane, G. S., Gates, G. C., and Koningsberger, D. C., *Catal. Lett.* **6**, 369 (1990).
66. Manninger, I., Zhan, Z., Xu, X. L., and Paal, Z., *J. Mol. Catal.* **66**, 223 (1991).
67. Manninger, I., Zhan, Z., Xu, X. L., Tetenyi, P., and Paal Z, *Appl. Catal.* **51**, L7 (1989).
68. Paal, Z. and Tetenyi, P., *J. Catal.* **30**, 350 (1973).
69. Dautzenberg, F. M. and Plateeuw, J. C., *J. Catal.* **19**, 41 (1970).
70. Sharma, S. B., Ouraipryvan, P., Nair, H. A., Balaraman, P., Root, T. W., and Dumesic, J. A., *J. Catal.* **150**, 234 (1994).
71. Sachtler, J. W. A., and Somorjai, G. A., *J. Catal.* **81**, 77 (1983).
72. Biloen, P., Dautzenberg,, F. M., and Sachtler, W. H., *J. Catal.* **50**, 77 (1977).
73. Paal, Z., Matusek, K., Muhler, M., *Appl. Catal.* **149**, 113 (1997).
74. Zaera, F., and Somorjai, G. A., *J. Catal.* **84**, 375 (1983).
75. Meriaudeau, P., Naccache, C., *Chem. Rev. Sci. Eng.* **39**, 5 (1997).
76. Vaarkamp, M., Mojet, B. L., Kappers, M. J., Miller, J. T., Koningsberger, D. C., *J. Phys. Chem.* **99**, 16067 (1995).
77. Menacherry, P. V., Fernandez-Garcia, M., Haller, G. L., *J. Catal.* **166**, 75 (1997).
78. Ichikuni, N., Iwasawa, Y., *Catal. Lett.* **20**, 87 (1993).
79. Marques, E.C., Sandstroem, D.R., Lytle, F.W., Greegor, R.B.J., *J. Phys. Chem.* 77, 1027 (1982).
80. Brigham, E.O. "The Fast Fourier Transform", Prentice-Hall, Englewood Cliffs, NJ, (1974).
81. Stern, E. A., *Phys. Rev. B* **48**, 9825 (1993).
82. Newville, M., Ravel, B., Haskel, D., Stern, E. A., Yacoby, Y., **Physica B**, **208**, **209**, pp. 154-156. (1995).
83. Koningsberger, D.C., Gates, B.C., *Catal. Lett.* **14**, 271 (1992).
84. Vaarkamp, M., Modica, F.S., Miller, J.T., Koningsberger, D.C., *J. Catal.* **144**, 611 (1993).
85. Cho, S. J., Ahn, W-S, Hong, S. B., Ryoo, R., *J. Phys. Chem.* **100**, 4996 (1996).
86. Han, W-J, Kooh, A. B., Hicks, R. F., *Catal. Lett.* **18**, 193 (1993).
87. Moretti, G., Sachtler, W.M.H., *J. Catal.* **116**, 361 (1989).
88. Bai, X., Sachtler, W.M.H., *J. Catal.* **132**, 165 (1991).
89. Bai, X., Zhang, Z., Sachtler, W.M.H., *Appl. Catal.* **72**, 165 (1991).
90. Kustov, L. M., Ostgard, D. J., Sachtler, W. M. H., *Catal. Lett.* **9**,121 (1991).
91. Stakheev, A. Y., Shpiro, E. S., Jaeger, N. I., Schulz-Ekloff, G., *Catal. Lett.* **32**, 147 (1995).

92. Stakheev, A. Y., Shpiro, E. S., Jaeger, N. I., Schulz-Ekloff, G., *Catal. Lett.* **34**, 293 (1995).
93. Lane, G. S., Miller, J. T., Modica, F. S., and Barr, M. K., *J. Catal.* **141**, 465 (1993).
94. Mojet, B. L. and Koningsberger, D. C., *Catal. Lett.* **39**, 191 (1996).
95. Menacherry, P. V., Haller, G. L., *Catal. Lett.* **44**, 135 (1997).
96. Davis, S. M., Zaera, F., Somorjai, G. A., *J. Catal.* **85**, 206 (1984).
97. Poeppelmeier, K.L., Trowbridge, T.D., Kao, J-L, US Patent 4,568,656 (1986).
98. Fung, S.C., US Patent 5,106,798 (1992).
99. Treacy, M.M.J., *Microporous and Mesoporous Materials* **28**, 271(1999).
100. Larsen, G., Haller, G. L., Resasco, D. E., and Durante, V. A., U. S. Patent 5,540,833 (1996).
101. Larsen, G., Resasco, D. E., Durante, V. A., Kim, J., and Haller, G. L., *Stud. Surf. Sci. Catal.* **83**, 321 (1994).
102. Landau, M. V., Kruglikov, V. Y., Goncharova, N. V., Konoval'chikov, O. D., Chukin, G. D., Smirnov, V. B., and Malevich, V. L., *Kinet. Catal.* **17**, 1104 (1976).
103. Frety, R., Da Silva, P. N., and Guenin, M., *Catal. Lett.* **3**, 9 (1989).
104. Miller, J. T. and Koningsberger, D. C., *J. Catal.* **162**, 209 (1996).
105. Li , F., Lu, W., Wu, G., and Li, J., *J. Alloys and Comp.* **207/208**, 397 (1994).
106. Grau, J. M., Daza, L., Seoane, X. L., and Arcoya, A., *Catal. Lett.* **53**, 161 (1998).
107. Mojet, B.L., Miller, J.T., and Koningsberger, D.C., *J. Phys. Chem.*, **103**, 2724 (1999).
108. Resasco, D.E., Padro, C., Jacobs, G. and Liu, HY, US Patent No. 6,063,724.
109. Mojet, B.L., Miller, J.T., Ramaker, D.E., and Koningsberger, D.C., *J. Catal.* **186**, 373 (1999).
110. Mojet, B.L., Ramaker, D.E., Miller, J.T., and Koningsberger, D.C., *Catal. Lett.* **62**, 15 (1999).
111. Koningsberger, D.C., de Graaf, J., Mojet, B.L., Ramaker, D.E., and Miller, J.T., *Appl. Catal. A* **191**, 205 (2000).
112. Reifsnyder, S.N., Otten, M.M., Sayers, D.E. and Lamb, H.H., *J. Phys. Chem.* **101**, 4972 (1997).
113. Asakura, K., Kubota, T., Ichikuni, N. and Iwasawa, Y., *Stud. Surf. Sci. Catal.* **101**, 911 (1996).
114. Lytle, F.W., Greegor, R.B., Marques, E.C., Sanstrom, D.R., Via, G.H. and Sinfelt, J.H., *J. Catal.* **95**, 546 (1985).
115. Samant, M.G. and Boudart, M., *J. Phys. Chem.* **95**, 4070 (1991).
116. Menacherry, P.V. and Haller, G.L., *J. Catal.* **177**, 175 (1998).
117. Mansour, A.N., Cook, J.W. Jr., Sayers, D.E., *J. Phys. Chem.* **88**, 2330 (1984).
118. Hammer, B. and Norskov, J.K., *Nature* **376**, 238 (1995).
119. Boyanov, B.I. and Morrison, T.I., *J. Phys. Chem.* **100**, 16318 (1996).
120. Soldatov, A.V., Della Longa, S. and Bianconi, A., *Solid State Communications* **85**, 863 (1993).
121. Mojet, B.L., PhD Thesis, 1997.

122. Fano, U., *Phys. Rev.* **124**, 1866 (1961).
123. van Santen, R.A., *J. Chem. Soc., Faraday Trans. I* **83**, 1915 (1987).

PUBLICATIONS, PATENTS, PUBLICATIONS AND POSTERS RESULTING FROM THIS THESIS

PUBLICATIONS (PUBLISHED AND IN PROGRESS)

1. "Comparative Study of n-Hexane Aromatization on Pt/KL, Pt/Mg(Al)O, and Pt/SiO_2 Catalysts: Clean and Sulfur-Containing Feeds" by G. Jacobs, C.L. Padro, and D.E. Resasco, *J. Catal.* **179** (1998) 43.

2. "Characterization of the Morphology of Pt Clusters incorporated in a KL Zeolite by Vapor Phase and Incipient Wetness Impregnation. Influence of Pt Particle Morphology on Aromatization Activity and Deactivation Behavior" by G. Jacobs, F. A. Ghadiali, A.M. Pisanu, A. Borgna, W.E. Alvarez, and D.E. Resasco, *Appl. Catal. A: General*, **188** (1999) 79.

3. "Increased Sulfur Tolerance of Pt/KL Catalysts Prepared by Vapor Phase Impregnation and Containing a Tm Promoter", G. Jacobs, F.A. Ghadiali, C. Padro, A. Borgna, W. Alvarez, and D.E. Resasco, *J. Catal,* **191** *(2000)* 116.

4. "Regeneration and Oxidation-Reduction Cycles of Vapor Phase and Incipient Wetness Impregnation Pt/KL Catalysts" by F.A. Ghadiali, G. Jacobs, A.M. Pisanu, A. Borgna, W.E. Alvarez, and D.E. Resasco, *Stud. Surf. Sci. Catal.*, accepted.

5. "Study of Preparation Parameters of Powder and Pelletized Pt/KL Catalysts for n-Hexane Aromatization", G. Jacobs, W.E. Alvarez, and D.E. Resasco, *Appl.Catal. A*, in press.

6. "*Modification of Pt/KL Catalysts by Addition of Lithium. Electronic Changes in the Fermi Level of Pt*", G. Jacobs, F.B. Noronha, W.E. Alvarez, A. Borgna, and D.E. Resasco, work in progress.

PATENTS (ISSUED AND IN PROGRESS)

1. G. Jacobs, C.L. Padro, H-Y Liu, and D.E. Resasco, "Sulfur-tolerant Aromatization Catalyst", issued May, 2000.
2. P. Cheung, D. Tiedtke, G. Jacobs, and D.E. Resasco, "Method of Platinization", in progress.

PRESENTATIONS AND POSTERS

1. "Deactivation of Pt/KL Catalysts – Clean and Sulfur Containing Feeds", by G. Jacobs (speaker), C.L. Padro, and D.E. Resasco, Environmentally Benign Chemical Processing Workshop, University of Virginia, June, 1998. (oral presentation)

2. "Comparative Study of Aromatization Catalysts Under Clean and Sulfur Poisoned Conditions", by G. Jacobs, C.L. Padro, F.A. Ghadiali, A.M. Pisanu, and D.E. Resasco, AICHE Annual Meeting in Miami, Florida, Nov. 1998. (poster)

3. "Sulfur-tolerant Aromatization Catalysts", by G. Jacobs, F.A. Ghadiali, C.L. Padro, A. Borgna, W.E. Alvarez, and D.E. Resasco (speaker), *Proc. Of 16th North American Catalysis Society Meeting (NAM)* in Boston, Massachusetts, June 1999. (oral presentation)

4. "Characterization of the Morphology of Pt Clusters incorporated in a KL Zeolite by Vapor Phase and Incipient Wetness Impregnation, and Influence of Pt Particle Morphology on n-Hexane Aromatization Activity " by G. Jacobs, F. A. Ghadiali, A.M. Pisanu, A. Borgna, W.E. Alvarez, and D.E. Resasco, AICHE Annual Meeting in Dallas, TX, Nov. 1999. (poster)

5. "Probing Particle Size Effects and Electronic Perturbations of Small Metal Clusters in Zeolite by Shape Resonance X-Ray Absorption and DRIFTS" by G. Jacobs (speaker), W.E. Alvarez, A. Borgna, F. Noronha, and D.E. Resasco,*ACS Meeting, San Francisco, CA (March, 2000).*

6. "Characterization of Pt/LTL Catalysts Prepared by VPI and IWI: Deactivation Study of the Aromatization of n-Hexane Reaction" by G. Jacobs, , F. A. Ghadiali, A.M. Pisanu, A. Borgna, W.E. Alvarez, and D.E. Resasco *Iberoamerican Congress on Catalysis (Portugal, 2000)*, accepted. (poster)

7. "Regeneration and Oxidation-Reduction Cycles of Vapor Phase and Incipient Wetness Impregnation Pt/KL Catalysts" by F.A. Ghadiali, G. Jacobs, A.M. Pisanu, A. Borgna, W.E. Alvarez, and D.E. Resasco, *12th International Congress on Catalysis (Spain, 2000)*, accepted. (poster)

APPENDIX A
XAFS/FTIR Cell

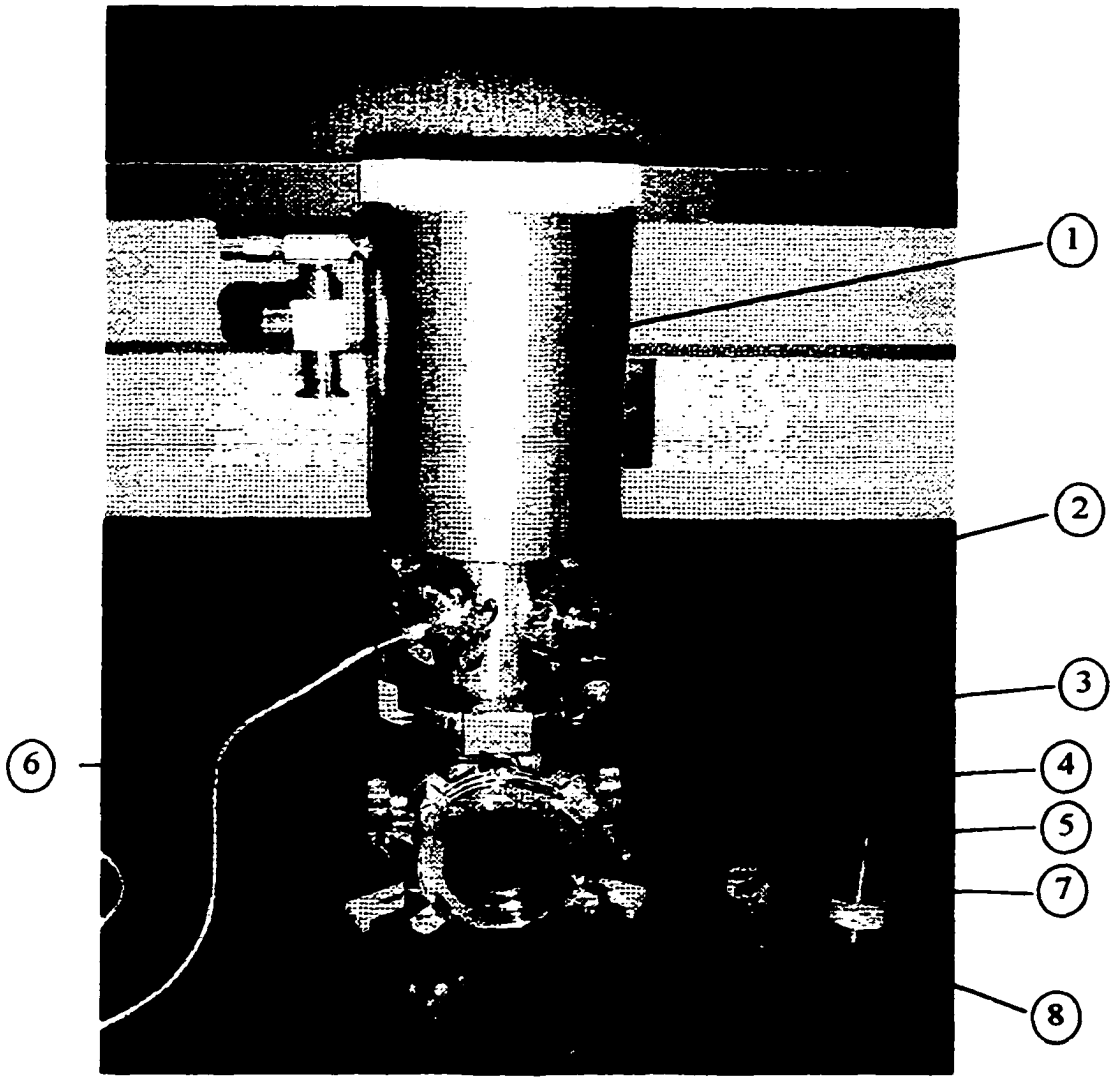

Figure A.1: Front view of cell showing: (1) liquid nitrogen dewar; (2) feedthroughs for inlet/outlet gases, thermocouple, and heater wiring; (3) chain clamp for easy access to sample; (4) transmission windows (5) fluorescence window, (6) inlet for cell water jacket cooling, (7) powder sample press, and (8) sample holder.

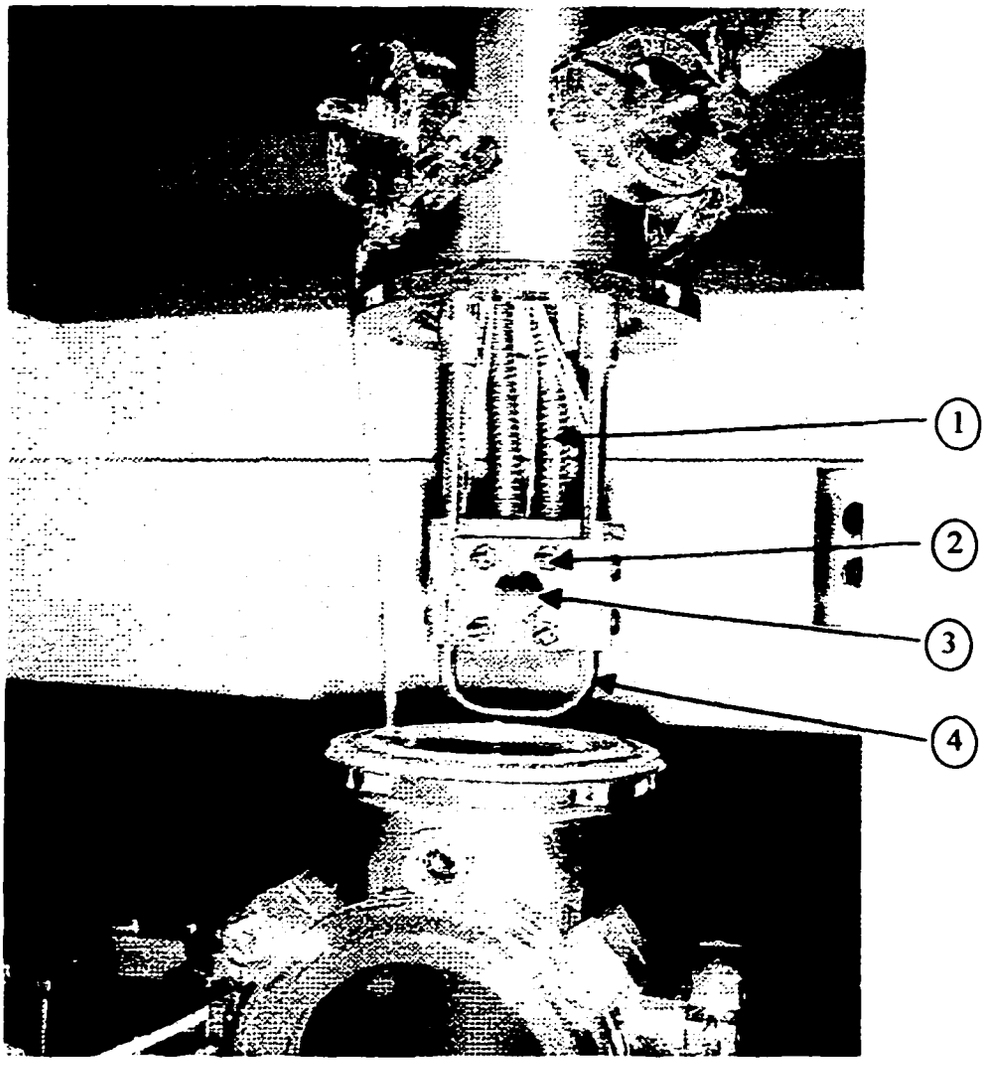

Figure A.2: View of the EXAFS sample block. Note (1) bellowed gas inlet/exhaust lines, (2) 4 screws for mounting sample, bellowed gas lines, (3) bevelled aperture, and (4) liquid nitrogen recirculation line.

APPENDIX B
Sample Calculation and Input

Sample FEFFIT input file

```
title = Fitting of PtKL fresh IWI
title = Fitting N, R, sigma2
%
data   = d:\exafs\ban\ptfrsh.dat %  input data file name
out    = d:\exafs\output\ptkl.dat %  output file name
%  fit R-range and FFT parameters:
  rmax  = 8.0
  dk1   = 3.0   dk2   = 15
  dr1   = 1.88  dr2   = 3.08    kweight = 3
  kspout = true   qspout  = true   rspout = true
  nodegen= true
%-------------------------------------------------------------------
  guess e0        =  0.0
  guess n1        =  4.0
  guess nn3       =  0.01
  set   n3        =  abs(nn3)
  guess ssig21    =  0.004
  set   sig21     =  abs(ssig21)
  guess ssig23    =  0.00019
  set   sig23     =  abs(ssig23)
  guess delR1     =  -0.02
  guess delR3     =  0.0
  set   s02       =  0.9
%-------------------------------------------------------------------
```

Figure B.1: **Sample FEFFIT Input file for EXAFS analysis.**

Sample Chemisorption Calculation

Knowns:
Weight of catalyst is 0.516 g
Pt loading is 1%
Moles of Pt is 2.65 E –5
Dose Volume is 36.91 cc
Dead Volume is 16.79 cc (measured)
Total Volume 53.70 cc
Reduction T of 400°C used

1st isotherm

Po	Pf	To	Tf	H/Pt	H/Pt-tot
35.6	16.1	24	24	1.840	1.840
58.2	44.8	24	25	0.088	1.928
71.9	63.2	24.3	24	0.032	1.959
93.7	84.1	24	24	0.028	1.987

Figure B.2: Sample chemisorption worksheet.

Initial H/Pt = $2 \times [P_0V_{dose}/T_0 - P_fV_{Tot}/T_f]/ [R \times \text{moles Pt}]$
2^{nd} point H/Pt = $2 \times [P_0V_{dose}/T_0 - P_{f,previous}V_{dead}/T_{f,\,previous} - P_fV_{Tot}/T_f]/ [R \times \text{moles Pt}]$

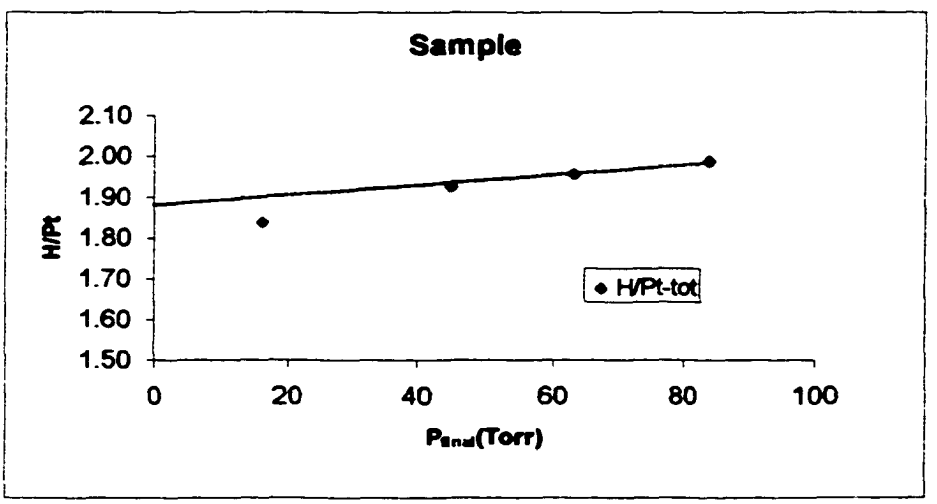

Figure B.3: Sample chemisorption isotherm. Extrapolate to zero pressure to obtain H/Pt of 1.88.

APPENDIX C
n-Heptane Aromatization

Results of n-Heptane Aromatization

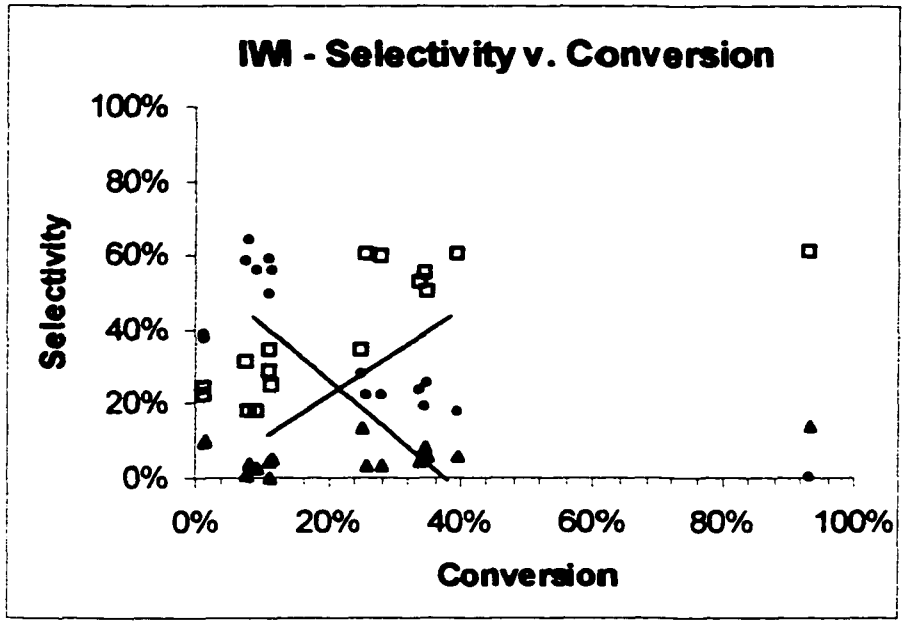

Figure C.1: Similar trends were observed with aromatization of n-heptane. During deactivation, increased production of heptene intermediates was observed. The Pt/KL (above) performed much better than Pt/silica (below), and the crossing of toluene with hexenes is shifted again to higher conversion on the Pt/silica catalysts. Products shown are toluene (open squares); heptenes (closed circles); and methane (open triangles).

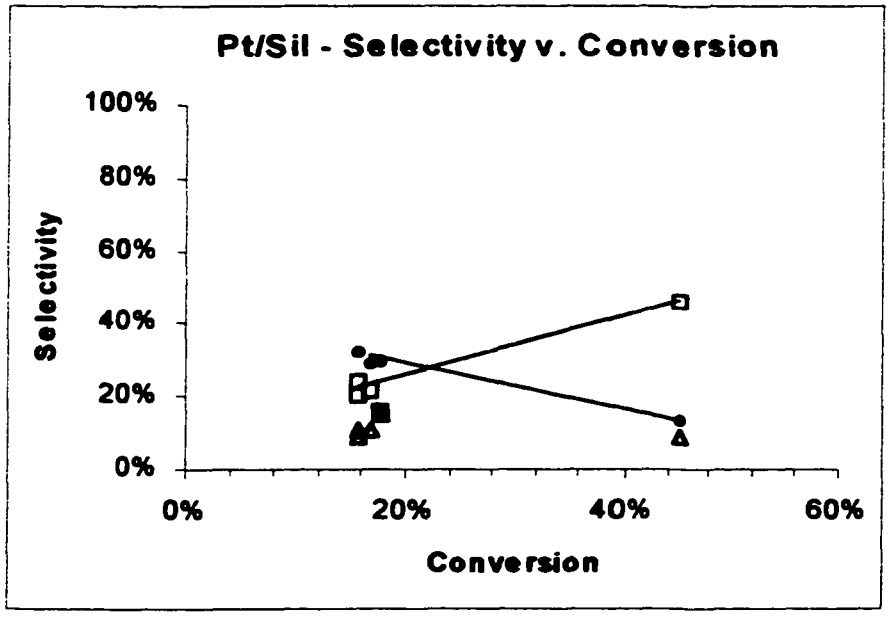

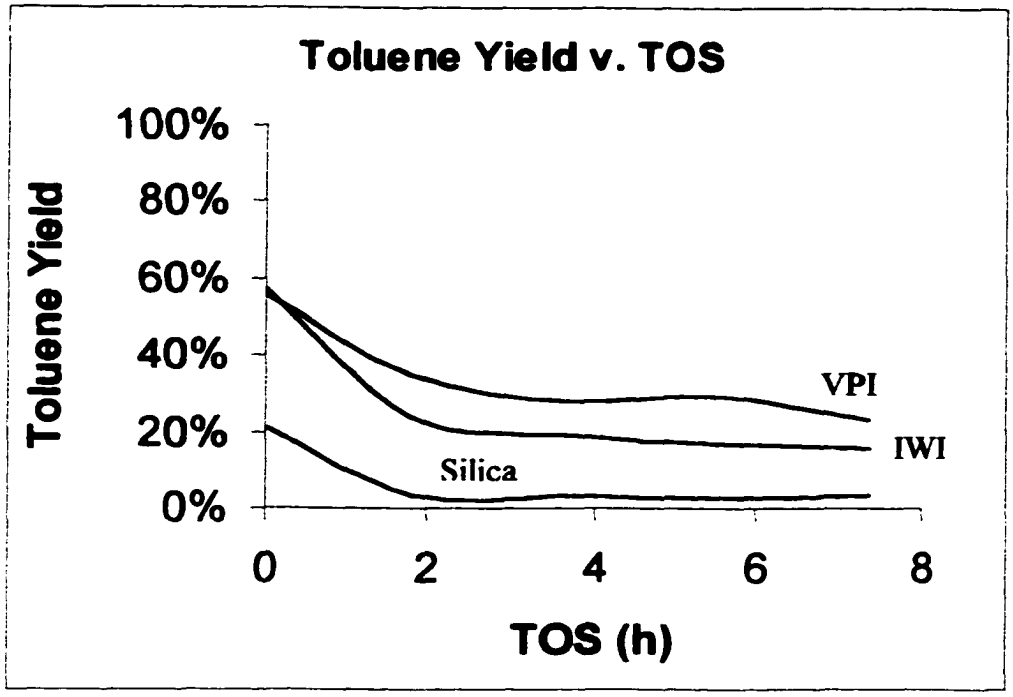

Figure C.2: The VPI catalyst outperformed both the IWI and Pt/Silica catalysts for n-heptane aromatization, as expected.